frontiers | Research Topics

Models in population, community and ecosystem dynamics

Edited by
Mehdi Cherif, Jurek Kolasa and Rui-Wu Wang

Published in
Frontiers in Ecology and Evolution

ISSN 1664-8714
ISBN 978-2-8325-4719-9
DOI 10.3389/978-2-8325-4719-9

About Frontiers

Frontiers is more than just an open access publisher of scholarly articles: it is a pioneering approach to the world of academia, radically improving the way scholarly research is managed. The grand vision of Frontiers is a world where all people have an equal opportunity to seek, share and generate knowledge. Frontiers provides immediate and permanent online open access to all its publications, but this alone is not enough to realize our grand goals.

Frontiers journal series

The Frontiers journal series is a multi-tier and interdisciplinary set of open-access, online journals, promising a paradigm shift from the current review, selection and dissemination processes in academic publishing. All Frontiers journals are driven by researchers for researchers; therefore, they constitute a service to the scholarly community. At the same time, the *Frontiers journal series* operates on a revolutionary invention, the tiered publishing system, initially addressing specific communities of scholars, and gradually climbing up to broader public understanding, thus serving the interests of the lay society, too.

Dedication to quality

Each Frontiers article is a landmark of the highest quality, thanks to genuinely collaborative interactions between authors and review editors, who include some of the world's best academicians. Research must be certified by peers before entering a stream of knowledge that may eventually reach the public - and shape society; therefore, Frontiers only applies the most rigorous and unbiased reviews. Frontiers revolutionizes research publishing by freely delivering the most outstanding research, evaluated with no bias from both the academic and social point of view. By applying the most advanced information technologies, Frontiers is catapulting scholarly publishing into a new generation.

What are Frontiers Research Topics?

Frontiers Research Topics are very popular trademarks of the *Frontiers journals series*: they are collections of at least ten articles, all centered on a particular subject. With their unique mix of varied contributions from Original Research to Review Articles, Frontiers Research Topics unify the most influential researchers, the latest key findings and historical advances in a hot research area.

Find out more on how to host your own Frontiers Research Topic or contribute to one as an author by contacting the Frontiers editorial office: frontiersin.org/about/contact

Models in population, community and ecosystem dynamics

Topic editors

Mehdi Cherif — INRA Centre Bordeaux-Aquitaine, France

Jurek Kolasa — McMaster University, Canada

Rui-Wu Wang — Northwestern Polytechnical University, China

Citation

Cherif, M., Kolasa, J., Wang, R.-W., eds. (2024). *Models in population, community and ecosystem dynamics*. Lausanne: Frontiers Media SA.

doi: 10.3389/978-2-8325-4719-9

Table of contents

frontiers | Frontiers in Ecology and Evolution

TYPE Editorial
PUBLISHED 25 March 2024
DOI 10.3389/fevo.2024.1392926

OPEN ACCESS

EDITED AND REVIEWED BY
Dennis Murray,
Trent University, Canada

*CORRESPONDENCE
Mehdi Cherif
mehdi.cherif@inrae.fr

RECEIVED 28 February 2024
ACCEPTED 18 March 2024
PUBLISHED 25 March 2024

CITATION
Cherif M, Kolasa J and Wang R-W (2024) Editorial: Models in population, community and ecosystem dynamics.
Front. Ecol. Evol. 12:1392926.
doi: 10.3389/fevo.2024.1392926

Editorial: Models in population, community and ecosystem dynamics

Mehdi Cherif[1]*, Jurek Kolasa[2] and Rui-Wu Wang[3]

[1]Aquatic Ecosystems and Global Change Research Unit, National Research Institute for Agriculture, Food and the Environment, Cestas, France, [2]Biology Department, McMaster University, Hamilton, ON, Canada, [3]Center for Ecological and Environmental Sciences, Key Laboratory for Space Bioscience and Biotechnology, Northwestern Polytechnical University, Xi'an, China

KEYWORDS

ecological modelling, uncertainty, stochasticity, evolutionary dynamics, ecosystem processes

Editorial on the Research Topic
Models in population, community and ecosystem dynamics

When first published, the call for this special topic was left very broad, with the aim to "welcome models for all significant aspects of population, community and ecosystem dynamics". The purpose was to obtain —hopefully— an unbiased instantaneous picture of the current directions in the field of ecological modelling. As in most fields of science, the number of publications, methodologies, and models generated in theoretical ecology have inflated in the very recent decades (Rossberg et al., 2019; Zhang and Wang, 2020), so it was an interesting exercise, we thought, to see what a sample of voluntary submissions —self-identified as modelling works by their authors— could provide as a picture of the ongoing trends and research directions in the field.

As expected, the scope of covered topics was very broad, spanning several of the classically-studied processes of interest in ecology, from evolutionary dynamics (Wang and Wang, Fussmann and Kopp) to biogeochemical cycles in ecosystems (Bian and Xia, Zelnik et al.), while several articles concerned the study of interactions of species with their environment or with other species (Guo et al., Hooker et al.) trying to develop novel methods (Lindo et al.), or infuse new paradigms (Dobson et al.).

There was no unifying theme, as expected given the broad scope of the topic. However, we could detect an underlying concern, shared by a majority of the articles. Bian and Xia take an explicit look at the propagation of uncertainty from satellite measurements of leaf area index to estimates of the nitrogen and phosphorus cycles. Dobson et al. speculate whether the specificities of trees (their longevity, and seasonal productivity) could affect the relation between the complexity and stability of the associated food web. Fussmann and Kopp look at populations that witness rapid changes in their environment, questioning the validity of current reciprocal transplant experiments to assess maladaptation. Guo et al. look at spatial heterogeneity and how it affects the stability of competition between species. Hély et al. lay foundation for a novel modelling approach to ecosystem dynamics that incorporates inherent stochasticity and variability to better predict stable and alternative stable states. Hooker et al. start from an extensive dataset to disentangle the drivers of synchrony —and asynchrony— between two species, showing that trophic interactions and

environmental stochasticity interact in yielding synchrony. Lindo et al. tackle the issue of stochasticity, offering practical methods for its inclusion in soil dynamical models. Wang and Wang show how chaotic dynamics may result in unpredictability, despite the deterministic evolution of a phenotypic trait. You may have already understood where we are reaching: all these articles were concerned with one aspect or another of uncertainty. Whether it is background noise, stochasticity, heterogeneity, or dynamic stability (the mirror concept). Only two articles out of the 10, more classically, tried to ascertain the state of the ecological system at equilibrium, whether it was microbial decomposition (Manzoni et al.), or net primary production under nutrient subsidies (Zelnik et al.).

Coincidence or not, we live in times that are perceived by an increasing number of people as uncertain. Incoming challenges are numerous and their complexity hard to fully grasp: the advances of artificial intelligence (Weiser and Von Krogh, 2023), global security challenges (Booth and Wheeler, 2023), pandemics (Batty, 2020), the impending climate breakdown (Barnett, 2023), the absence of clearcut political projects and effective policies (Turk, 2022), the looming prospect of a biodiversity collapse (Maechler and Graz, 2022), economic volatility (Ahir et al., 2022), etc.

We will not enter into the otherwise fascinating debate of the influence of the social context on science (Latour, 1987) or of the effect in return of ecological theory on society (Bosselman and Tarlock, 1994; Scoones, 1999). Nor will we resolve the question of whether ecological paradigms reflect the dominant philosophical ideas in the contemporaneous society (Simberloff, 1980) or whether they are rather shaped by pragmatism reflecting the characteristics of the object they study (Travassos-Britto et al., 2021). What is certain is that all current research efforts aimed at understanding and including uncertainty into ecological theories are welcome and timely.

In conclusion, what have we learnt from the rather limited set of papers published in this Research Topic on ecological modelling? Regarding uncertainty, we will take home the variety of practical methods described that aim at explicitly including e.g., noise and error propagation (Bian and Xia), demographic and environmental stochasticity (Lindo et al.), chaotic dynamics in eco-evolutionary processes (Wang and Wang), and the upscaling of disturbance to a continental scale (Hély et al.). The articles helped us realize as well that, rather than being a nuisance to be reduced, uncertainty and variability is a fundamental component of the functioning of ecological (Lindo et al.) and evolutionary systems (Fussmann and Kopp) to be understood and explained (Guo et al., Wang and Wang, Hooker et al., Dobson et al.). Finally, the works of Manzoni et al. and Zelnik et al. are here to remind us that a mechanistic understanding of ecological processes is as necessary as ever, if only because variability is a process in itself, with mechanisms that generate it. Variability is so intrinsic to complex ecological systems (Roy et al., 2020), and multi-scale that a holistic approach to transcend rather focused studies, such as those included in this Research Topic, might be the next challenge to tackle in ecological modelling (Holyoak and Wetzel, 2020).

We hope that the readers of this special topic will find similar inspiration for their own research from one or several of the published articles in this Research Topic. As editors, we would be gratified if our Research Topic pave the way to future contributions that will help tackle uncertainty in our understanding of the functioning of ecological systems that are put under incomparable strain since the establishment of mankind as a major actor in the biosphere of or planet.

Author contributions

MC: Writing – original draft. JK: Writing – review & editing. RW-W: Writing – review & editing.

Conflict of interest

The authors declare that the research was conducted in the absence of any commercial or financial relationships that could be construed as a potential conflict of interest.

Publisher's note

References

Ahir, H., Bloom, N., and Furceri, D. (2022). "The world uncertainty index," *NBER working papers 29763*. National Bureau of Economic Research, Inc. doi: 10.3386/w29763

Barnett, M. (2023). Climate change and uncertainty: An asset pricing perspective. *Manage. Sci.* 69 (12), 7151–7882. doi: 10.1287/mnsc.2022.4635

Batty, M. (2020). Unpredictability. *Environ. Plann. B.: Urban. Analytics. City. Sci.* 47, 739–744. doi: 10.1177/2399808320934308

Booth, K., and Wheeler, N. J. (2023). "Uncertainty," in *Security Studies* (2 Park Square, Milton Park, Abingdon, Oxon, OX14 4RN, Canada: Routledge), 151–168.

Bosselman, F. P., and Tarlock, A. D. (1994). The influence of ecological science on american law: an introduction. *Chicago-Kent. Law Rev.* 69, 847–873.

Holyoak, M., and Wetzel, W. C. (2020). Variance-explicit ecology: A call for holistic study of the consequences of variability at multiple scales. *Unsolved. Problems. Ecol.*, 25–42. doi: 10.2307/j.ctvs9fh2n

Latour, B. (1987). *Science in action: how to follow scientists and engineers through society* (Cambridge (Mass: Harvard University press).

Maechler, S., and Graz, J.-C. (2022). Is the sky or the earth the limit? Risk, uncertainty and nature. *Rev. Int. Political. Economy.* 29, 624–645. doi: 10.1080/09692290.2020.1831573

Rossberg, A. G., Barabás, G., Possingham, H. P., Pascual, M., Marquet, P. A., Hui, C., et al. (2019). Let's train more theoretical ecologists – here is why. *Trends Ecol. Evol.* 34, 759–762. doi: 10.1016/j.tree.2019.06.004

Roy, F., Barbier, M., Biroli, G., and Bunin, G. (2020). Complex interactions can create persistent fluctuations in high-diversity ecosystems. *PloS Comput. Biol.* 16, e1007827. doi: 10.1371/journal.pcbi.1007827

Scoones, I. (1999). New ecology and the social sciences: what prospects for a fruitful engagement? *Annu. Rev. Anthropol.* 28, 479–507. doi: 10.1146/annurev.anthro.28.1.479

Simberloff, D. (1980). A succession of paradigms in ecology: Essentialism to materialism and probabilism. *Synthese* 43, 3–39. doi: 10.1007/BF00413854

Travassos-Britto, B., Pardini, R., El-Hani, C. N., and Prado, P. I. (2021). Towards a pragmatic view of theories in ecology. *Oikos* 130, 821–830. doi: 10.1111/oik.07314

Turk, M. C. (2022). *A Portfolio Approach to Policymaking Uncertainty*. Florida State University Law Review. 49 (2), 381–446. Availabale at: https://ir.law.fsu.edu/lr/vol49/iss2/4

Weiser, A., and Von Krogh, G. (2023). Artificial intelligence and radical uncertainty. *Eur. Manage. Rev.* 20, 711–717. doi: 10.1111/emre.12630

Zhang, D., and Wang, S. (2020). Theoretical ecology in the 21st century. *Biodiversity. Sci.* 28, 1301–1303. doi: 10.17520/biods.2020471

frontiers | Frontiers in Ecology and Evolution

TYPE Original Research
PUBLISHED 10 November 2022
DOI 10.3389/fevo.2022.1068830

OPEN ACCESS

EDITED BY
Rui-Wu Wang,
Northwestern Polytechnical University, China

REVIEWED BY
Min Su,
Hefei University of Technology, China
Xiaojie Chen,
University of Electronic Science and Technology of China, China

*CORRESPONDENCE
Jinbao Liao
jinbaoliao@163.com

SPECIALTY SECTION
This article was submitted to Models in Ecology and Evolution, a section of the journal Frontiers in Ecology and Evolution

RECEIVED 13 October 2022
ACCEPTED 28 October 2022
PUBLISHED 10 November 2022

CITATION
Guo G, Zhang Z, Zhang H, Bearup D and Liao J (2022) Contrasting effects of dispersal network heterogeneity on ecosystem stability in rock-paper-scissors games. *Front. Ecol. Evol.* 10:1068830. doi: 10.3389/fevo.2022.1068830

Contrasting effects of dispersal network heterogeneity on ecosystem stability in rock-paper-scissors games

Guanming Guo[1], Zeyu Zhang[1], Helin Zhang[1], Daniel Bearup[2] and Jinbao Liao[1]*

[1]Research Center for Theoretical Ecology, Ministry of Education's Key Laboratory of Poyang Lake Wetland and Watershed Research, School of Geography and Environment, Jiangxi Normal University, Nanchang, China, [2]School of Mathematics, Statistics and Actuarial Sciences, University of Kent, Canterbury, United Kingdom

Intransitive competition, typically represented by the classic rock-paper-scissors game, provides an endogenous mechanism promoting species coexistence. As well known, species dispersal and interaction in nature might occur on complex patch networks, with species interacting in diverse ways. However, the effects of different interaction modes, combined with spatial heterogeneity in patch connectivities, have not been well integrated into our general understanding of how stable coexistence emerges in cyclic competition. We thus incorporate network heterogeneity into the classic rock-paper-scissors game, in order to compare ecosystem stability under two typical modes of interaction: species compete to fill empty sites, and species seize each other's colony sites. On lattice-structured regular networks, the two interaction modes produce similar stability patterns through forming conspecific clusters to reduce interspecific competition. However, for heterogeneous networks, the interaction modes have contrasting effects on ecosystem stability. Specifically, if species compete for colony sites, increasing network heterogeneity stabilizes competitive dynamics. When species compete to fill empty sites, an increase in network heterogeneity leads to larger population fluctuations and therefore a higher risk of stochastic extinctions, in stark contrast to current knowledge. Our findings strongly suggest that particular attention should be devoted to testing which mode of interaction is more appropriate for modeling a given system.

KEYWORDS

competitive intransitivity, cyclically competing ecosystems, dispersal network heterogeneity, ecosystem stability, rock-paper-scissors games

Introduction

Understanding the mechanisms of ecosystem stability is a fundamental issue in ecology (May, 1972; Chesson, 2000; Levine and HilleRisLambers, 2009; Allesina and Levine, 2011). Many proposed mechanisms rely heavily on exogenous factors mitigating the effects of competition, such as niche differentiation (Chesson, 2000; Levine and HilleRisLambers, 2009; Chu and Adler, 2015) and intermediate disturbance hypothesis (Connell, 1978; Roxburgh et al., 2004; Liao et al., 2022). In contrast to these exogenous mechanisms, intransitive competition provides an endogenous mechanism promoting coexistence (Laird and Schamp, 2006; Allesina and Levine, 2011; Soliveres et al., 2015; Levine et al., 2017), and, in particular, the simple rock-paper-scissors game has become a typical case to explain ecosystem stability (Huisman and Weissing, 1999; Kerr et al., 2002; Reichenbach et al., 2007). The classic, cyclic game of rock-paper-scissors usually leads to species' abundances neutrally cycling without converging to a stable equilibrium point, which is rarely observed in nature. To overcome this problem, many approaches have been proposed to explain the robust persistence of the cyclically competing system, such as higher-order interactions (Grilli et al., 2017) and spatially structured interactions (Durrett and Levin, 1997; Czárán et al., 2002; Rojas-Echenique and Allesina, 2011; Calleja-Solanas et al., 2021; Zhang et al., 2022). In particular, the latter mechanism of local structured interactions stabilizing coexistence has been documented experimentally (Kerr et al., 2002). Thus, it is widely believed that the inclusion of spatial structure, where the interactions and dispersal of individuals are local, can result in stable coexistence in rock-paper-scissors games. Yet, these conclusions are mostly drawn from lattice-based models, where each individual is assumed to only interact with its surrounding neighbors. This assumption is relatively restrictive, as species dispersal and interactions in nature might occur on complex networks with variation in patch connectivities (i.e., spatial heterogeneity in dispersal networks; Urban and Keitt, 2001; Fortuna et al., 2006; Dale and Fortin, 2010; Galpern et al., 2011; Grilli et al., 2015; Fortin et al., 2021; He et al., 2021; Li et al., 2021; Zhang et al., 2021).

There is abundant evidence that landscape structure, and other factors (e.g., patch quality; Liao et al., 2013), can result in anisotropic (i.e., directionally biased) dispersal behavior and therefore spatial heterogeneity in patch connectivities (Urban and Keitt, 2001; Fortuna et al., 2006; Dale and Fortin, 2010; Galpern et al., 2011; Grilli et al., 2015; Fortin et al., 2021; He et al., 2021). Since different patches in the landscape might be perceived differently by species (Hansbauer et al., 2010; Dondina et al., 2018), and the resulting dispersal network would display diverse patterns of patch connectivity (Yeaton and Bond, 1991; Bunn et al., 2000; Nicholson and Possingham, 2006; Fortuna et al., 2009; Bearup et al., 2013; Hirt et al., 2018; Germain et al., 2019). For instance, species dispersal between sub-reefs within the Great Barrier Reef has been characterized with scale-free networks (Kininmonth et al., 2010), while seed dispersal by birds, as opposed by winds, is better described by an irregular network than a spatially uniform network. In addition, Fortuna et al. (2006) identified a large spatial dispersal network of temporary ponds, which are used as breeding sites for amphibian species, following a power-law degree distribution. As such, there has been an increasing interest in exploring the effects of network heterogeneity on ecosystem stability using graph theory (Szabó et al., 2004; Szolnoki and Szabó, 2004; Masuda and Konno, 2006; Dale and Fortin, 2010; Schütt and Claussen, 2010; Galpern et al., 2011; Laird, 2014; Nagatani et al., 2018; Fortin et al., 2021; He et al., 2021; Zhang et al., 2021). Many studies have found that increasing network heterogeneity (i.e., increasing variation in patch connectivities) can promote stable coexistence in cyclic competition (Masuda and Konno, 2006; Schütt and Claussen, 2010; Nagatani et al., 2018).

Despite these advances, several lattice-based models (Laird and Schamp, 2008; Rojas-Echenique and Allesina, 2011; Zhang et al., 2022) have observed that local intransitive competition can reduce species coexistence compared to long-range competition, in stark contrast to current knowledge of local interactions stabilizing coexistence (Durrett and Levin, 1997; Huisman and Weissing, 1999; Czárán et al., 2002; Kerr et al., 2002; Calleja-Solanas et al., 2021). Rojas-Echenique and Allesina (2011) and Zhang et al. (2022) attributed the opposite outcomes to different interaction modes, which can induce distinct stabilizing mechanisms in lattice-structured models. Indeed, species in diverse natural ecosystems might interact in different ways. For example, there are two typical interaction modes often observed in nature: seedlings of tree species or propagules of grass species compete to fill gaps, while animal species fight directly for colony sites (Rojas-Echenique and Allesina, 2011; Calleja-Solanas et al., 2021; Zhang et al., 2022). However, the effects of these different interaction modes, in combination with spatial heterogeneity in dispersal networks mentioned above, have not been well integrated into our general understanding of how stable coexistence emerges in cyclic competition. In this study, we thus incorporate dispersal network heterogeneity into the classic rock-paper-scissors games, in order to make a comparative analysis of ecosystem stability between the two typical interaction modes.

Materials and methods

Dispersal network heterogeneity

We consider a landscape consisting of a finite number (N) of patches (so-called colony sites), with each accommodating only one individual (or a subpopulation) of a species. In the landscape, individuals can move and interact between patches only along a predefined set of dispersal pathways. This shapes

a dispersal network, with patches and dispersal pathways being represented by network nodes and links, respectively. To model the effect of spatial heterogeneity in dispersal networks (with fixed average patch degree $\bar{k}$ 4), we generate four typical network structures with contrasting heterogeneities (i.e., the extent of variation in patch connectivities):

(1) A lattice-structured regular network with all patches having the same degree (illustrated in **Figure 1A** with each patch linked to other four patches).
(2) A randomly structured network with randomly connected patches (Watts and Strogatz, 1998), yielding small variation in patch degrees (**Figure 1B**).
(3) An exponential network constructed based on the algorithm of random attachment (Barabási and Albert, 1999). This produces a greater variation in patch connectivities than the random network (**Figure 1C**).
(4) A scale-free network structured according to the algorithm of preferential attachment (Barabási and Albert, 1999), producing the highest variation in patch connectivities (**Figure 1D**).

In these networks, species are assumed to use dispersal links in either direction without preference (i.e., undirected dispersal).

Two typical interaction modes

We consider a system of three cyclically competing species on a landscape of size $N = 10{,}000$ patches connected by dispersal networks. Each patch can only accommodate one individual of a species. The competitive relationships between these three species (*i*, *j*, and *k*) follow the rock-paper-scissors game, an example of intransitive competition which usually yields species coexistence with oscillations (Grilli et al., 2017; Li et al., 2020).

To focus solely on the effect of species competition on ecosystem stability, we perform simulations as follows: (i) according to the typical assumption in previous work (Masuda and Konno, 2006; Rojas-Echenique and Allesina, 2011; Grilli et al., 2017; Nagatani et al., 2018; Calleja-Solanas et al., 2021; Zhang et al., 2022), initially all patches are populated with individuals randomly drawn from the three species; (ii) in each time step, we perform a competition event using the two interaction modes specified below; (iii) we repeat step (ii) for a long time, finding that 1,000 generations (1 generation = 10,000 time steps at $N = 10{,}000$ patches) are sufficient for the system to achieve steady state; (iv) at steady state, we record the number of individuals for each species and the spatial patterns at every generation.

In this study, we consider two interaction modes separately in the simulations.

Mode 1: Similar to Grilli et al. (2017) and Calleja-Solanas et al. (2021), in each time step, we randomly select a focal individual (with probability $1/N$ in the whole network) to die, and immediately choose two individuals randomly from its directly linked neighbors for pairwise competition, with the offspring of the winner occupying this empty patch. If the two individuals belong to the same species, then this species directly occupies the empty patch. If there is only one neighbor for the empty patch, then it is occupied directly by this neighbor.

Mode 2: Similar to Rojas-Echenique and Allesina (2011), in each time step, we randomly select two directly linked individuals for competition, with the offspring of the superior competitor substituting the inferior one (otherwise keeping the original state).

Under these two different interaction modes, we firstly explore how increasing network heterogeneity affects ecosystem stability in classic rock-paper-scissors games, and then test whether these outcomes are robust to varying network size.

Results

We begin our analysis by inspecting the temporal evolution of species abundances (**Figure 2**). When species compete to fill an empty patch (Mode 1), increasing network heterogeneity (from lattice-structured regular to scale-free networks) increases the magnitude of population fluctuations and speeds up stochastic species extinctions. In contrast, if the superior competitor directly substitutes the inferior one (Mode 2), all three species can coexist, and the magnitude of population fluctuations around the equilibrium point ($\approx 1/3$) decreases as network heterogeneity increases. In lattice-structured regular networks, both interaction modes yield similar fluctuation size (**Figure 2A** vs. **Figure 2E** with different ranges of *y*-axis). This is more clear when looking at their dynamic trajectories (**Figure 2I** vs. **Figure 2M**). In these dynamic trajectories (**Figures 2I–P**), the abundances of the species at each generation represent a point in the 3-simplex, whose vertices correspond to a monospecific population. Over time, the point follows a trajectory which will reflect the state of the system. If the system is close to the equilibrium abundances, the trajectory eventually occupies a small area near it, whilst larger fluctuations cover larger areas. Similar to **Figures 2A–H**, the interaction mode 1 results in greater fluctuations and ultimately monoculture in more heterogeneous networks (**Figures 2I–L**), as opposed to the interaction mode 2 where ecosystems are more stable in networks with higher heterogeneity.

To test whether these outcomes are robust, we simulate 20 replicates for each case, by regenerating the dispersal network in each replicate (**Figure 3**). In Mode 1, three species can coexist with oscillations around the equilibrium point in the lattice-structured regular network (see **Figure 2A**), unlike other three heterogeneous networks where only one species ultimately

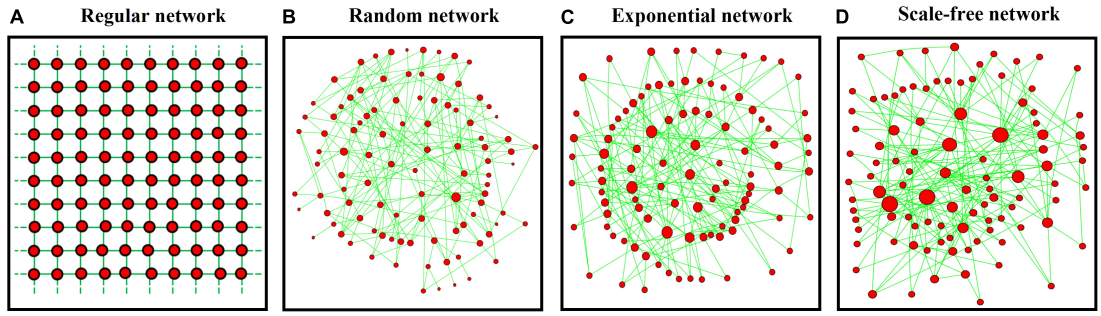

FIGURE 1
Four typical network structures consisting of 100 patches (red nodes) with 200 links (green lines): **(A)** lattice-structured regular, **(B)** randomly connected, **(C)** exponential, and **(D)** scale-free networks. Variation in patch degree (proportional to node size) increases from left to right panels.

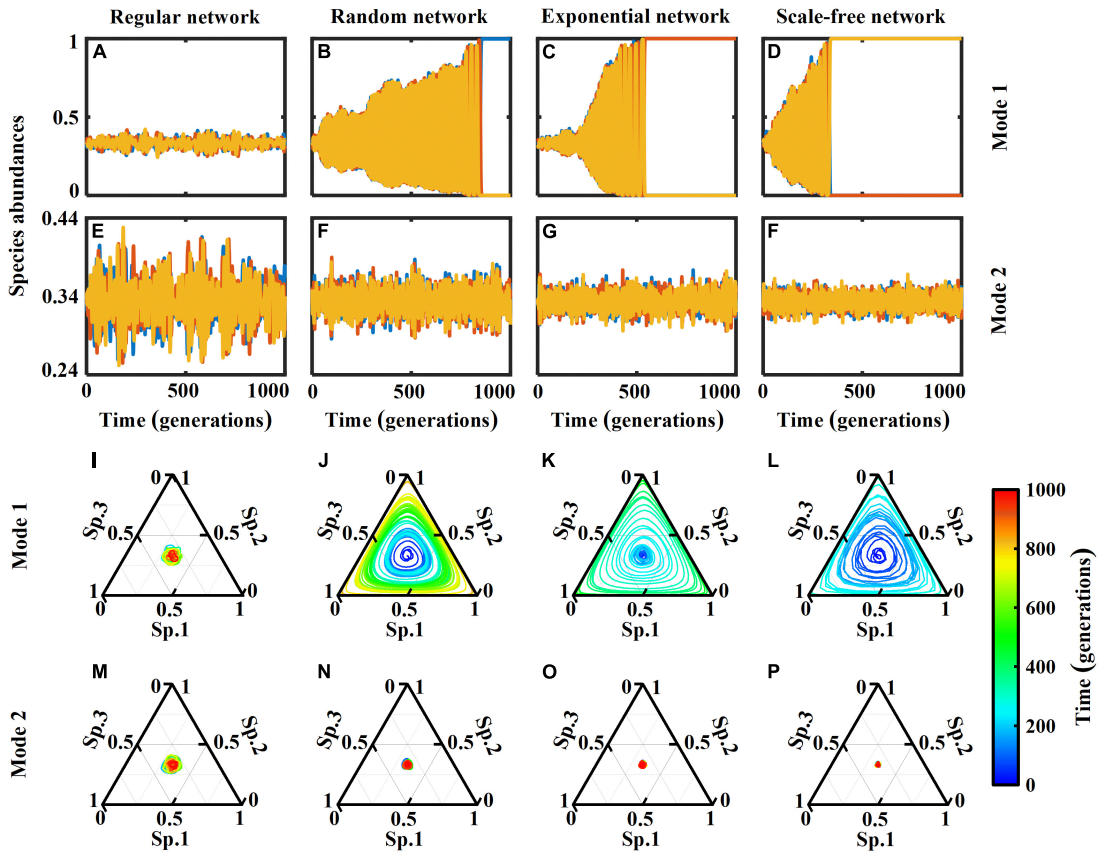

FIGURE 2
(A–H) Dynamics of species abundances of a rock-paper-scissors system (with 1,000 generations = 1×10^7 time steps) in complex networks of size $N = 10^4$ nodes with 2×10^4 links (average patch degree $\bar{k}$ 4), including lattice-structured regular, randomly connected, exponential and scale-free networks. Two interaction modes are considered: (Mode 1) species compete to fill empty patches; and (Mode 2) species seize each other's patches. **(I–P)** Trajectories in the phase space represented by the 3-simplex, corresponding to the dynamics in panels **(A–H)**. The color bar represents time evolution (generations). Oscillations around the equilibrium point cover a smaller area, indicating a more stable ecosystem.

dominates the system (Figure 3A). As such, the outcome in the regular network is absent in Figure 3A. In other three heterogeneous networks, we record the extinction time of the first species in each replicate, with more time required for species extinction implying more stable coexistence. As shown in Figure 3A, increasing network heterogeneity generally leads to species going extinct sooner. In Mode 2, all species can coexist with fluctuations around the equilibrium point in all dispersal networks. Thus, we use variation in fluctuations size (C.V. around the mean species abundances at steady state)

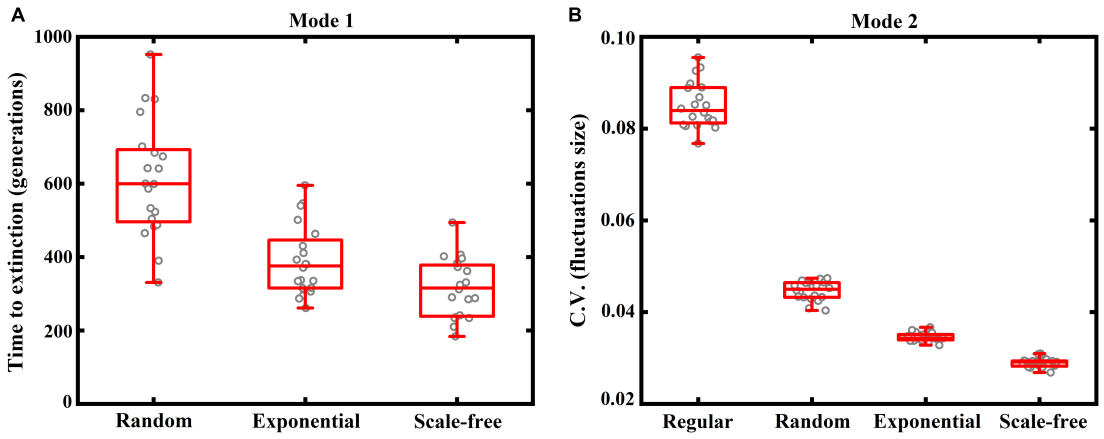

FIGURE 3
Box plots (red) of ecosystem stability (with 20 replicates for each case, indicated by gray cycles), characterized by panel (**A**: Mode 1) the time (generations) required for the first species to go extinct if stochastic extinctions occur, or (**B**: Mode 2) coefficient of variation in fluctuations size (C.V. around the mean species abundances at steady state) if three species can coexist. Again, four typical network structures are included: lattice-structured regular, randomly connected, exponential and scale-free networks. Note that, under Mode 1, three species can coexist in the regular network (see **Figure 2A**), which is thus absent in panel **(A)**. More time required for species extinction or lower values of C.V. implies more stable coexistence. Other settings are the same as in **Figure 2**.

to characterize ecosystem stability, with lower values of C.V. indicating more stable coexistence. As shown in **Figure 3B**, an increase in network heterogeneity generally results in smaller fluctuations in species abundances, yielding a more stable system. These outcomes further confirm our previous conclusions in **Figure 2**.

To better understand the mechanisms behind these dynamic behaviors, we display several snapshots of the spatial patterns of the three competitors in complex networks (**Figure 4**). In the lattice-structured regular network, both interaction modes produce similar conspecific clumping patterns (**Figures 4A,B**). To clearly illustrate the spatial organization in dispersal networks with contrasting heterogeneities, we take a system of $N = 100$ patches for example by displaying their snapshots at the 5th generation in Mode 1 and the 20th generation in Mode 2 (**Figures 4C–J**). In Mode 1 (**Figures 4C–F**), when three species have almost equal abundance in the regular network, increasing network heterogeneity which tends to increase network modularity, enlarges differences in species abundances, most likely accelerating stochastic extinctions. In Mode 2 (**Figures 4G–J**), if three species have unequal abundances in the regular network, dispersal network heterogeneity (i.e., network modularity) acts as a driving force to equalize their abundances, thereby stabilizing the ecosystem. We also observe that species can form self-organized conspecific clusters with the most connected patches at the core in these heterogeneous networks.

Under both interaction modes, we finally focus on how system size (i.e., increasing network size) affects fluctuations in species abundance in networks with contrasting heterogeneities (**Figure 5**). Intuitively, increasing network size promotes ecosystem stability, regardless of interaction mode and network heterogeneity. Specifically, stochastic extinctions in Mode 1 require more time to occur as network size increases, especially in networks with less heterogeneity (**Figure 5A**). This also demonstrates that increasing network heterogeneity greatly destabilizes the system. In Mode 2, the size of population fluctuation declines linearly with increasing network size (with log-log scale in **Figure 5B**), thereby promoting ecosystem stability. Furthermore, increasing network heterogeneity leads to smaller fluctuations, further confirming that network heterogeneity can stabilize the cyclically competing system.

Discussion

Incorporating complex networks into the classic rock-paper-scissors game, we find that whether network heterogeneity can stabilize competitive dynamics depends on the interaction mode. Specifically, if species compete directly for colony sites, increasing spatial heterogeneity in dispersal networks stabilizes the cyclically competing ecosystems, further confirming previous theoretical arguments (Masuda and Konno, 2006; Schütt and Claussen, 2010; Nagatani et al., 2018). In contrast, when species compete to fill an empty site, an increase in network heterogeneity leads to stronger population fluctuations and thus increases the risk of stochastic extinctions. Interestingly, in the lattice-structured regular network, both interaction modes display similar coexistence patterns based on the same mechanism: local interactions allow species to survive by forming conspecific clusters (*via* self-organization) where interspecific competition only takes place at the borders between heterospecific clusters, thereby decreasing the effective

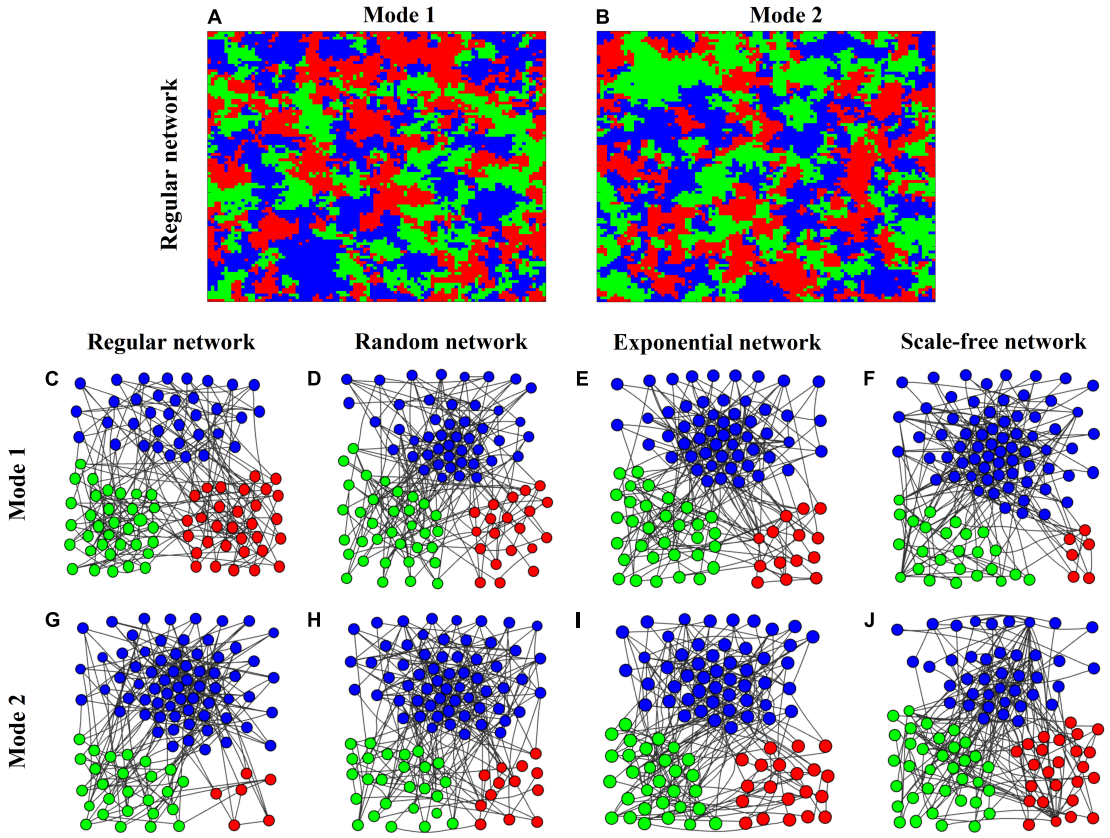

FIGURE 4
(A,B) Snapshots of the spatial organization of a 3-species system in rock-paper-scissors games at the 1000th generation in the lattice-structured regular network of size $N = 10^4$ patches with average degree $\bar{k}$ 4 under Modes 1 & 2. Individuals of each species are painted in a different color. **(C–J)** Snapshots of the spatial patterns of the three species under Modes 1 & 2. **(C–F)** Mode 1 at the 5th generation; **(G–J)** Mode 2 at the 20th generation) in different networks (lattice-structured regular, randomly connected, exponential, and scale-free) of small size $N = 100$ patches (with $\bar{k}$ 4) for clarity.

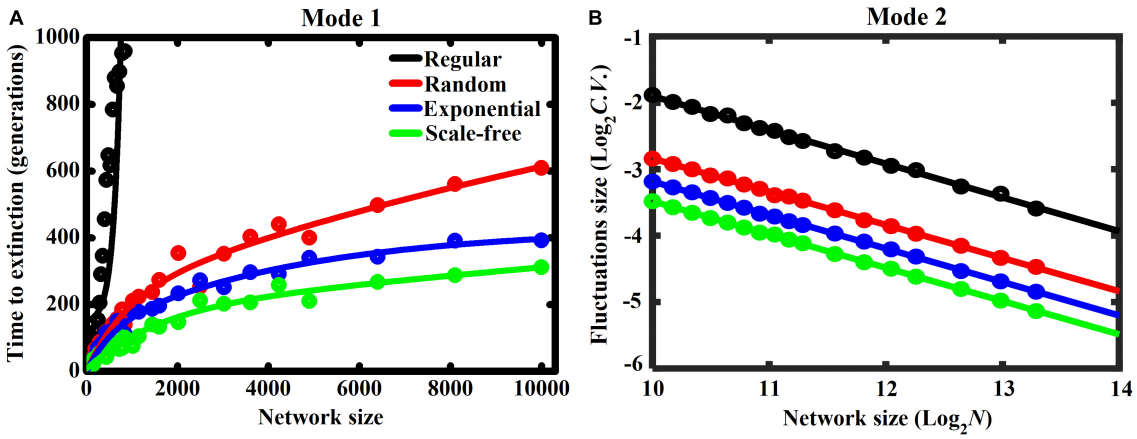

FIGURE 5
Effect of network size (N) on ecosystem stability under Modes 1 & 2 in networks with contrasting heterogeneities, including lattice-structured regular, randomly connected, exponential, and scale-free networks (each dot represents the mean of 20 replicates). Stability is characterized by panel (**A**: Mode 1) the time (generations) required for the first species going extinct, or (**B**: Mode 2) the coefficient of variation (C.V.) in fluctuations size around the mean species abundances at steady state. More time required for species extinction or lower values of C.V. indicates a more stable system.

interspecific competition (by reducing interspecific encounter rate) and therefore population fluctuations (**Figures 4A,B**).

There exist different mechanisms between the two interaction modes that induce contrasting effects of network heterogeneity on ecosystem stability. In our model, the stabilizing role of network heterogeneity is observed when competition occurs through the superior competitor displacing the inferior one in a randomly chosen pair of neighbors. This competition mode has been commonly used and is symmetric in a cyclical way. However, increasing variation in patch connectivities implies that a few patches are highly connected while most have only few connections. A patch with more connections is more likely to be selected as a neighbor, while another neighbor can be sampled from multiple patches that might accommodate any of the three species. As such, which species can occupy this highly connected patch will change more frequently in networks with higher heterogeneity. To some extent, this prohibits the growth of self-organized conspecific clusters with the most connected patches at the core. In fact, increasing network heterogeneity breaks the symmetry in species interactions, that is, those individuals in highly connected patches have a higher chance to participate in competition than other individuals in poorly connected patches. This results in asymmetric interactions that can produce negative frequency dependence (NFD) which is absent in symmetric interactions (Rojas-Echenique and Allesina, 2011). Specifically, the NFD can decrease the average fitness of individuals when they become more common (cf. Zhang et al., 2022). Thus, the NFD, which is more significant in more heterogeneous networks, can suppress the population growth of dominant species but promote the growth of rare species, thereby increasing the frequency of oscillations and stabilizing competitive dynamics.

Network heterogeneity is destabilizing for the interaction mode where species compete for an empty site. This is because, in this mode, each species has the same probability to be selected to die, regardless of patch connectivities, so NFD cannot emerge. As such, conspecific clusters, with highly connected patches at the core, can grow (*via* self-organization) without restriction especially in networks with higher heterogeneity. Within these conspecific clusters, a competition event does not contribute to variation in species abundance, as local competition occurs between conspecific individuals. Thus, changes in species abundances can only take place along the borders between heterospecific clusters. However, the length of these borders increases more rapidly in more heterogeneous networks (i.e., a rapid increase in the number of "active" individuals that can change the state at the borders), promoting interspecific encounter rate and therefore interspecific competition. In addition, these heterospecific clusters can be treated as compartments dominated by different species, but there are lots of links connecting these compartments. If a superior competitor invades a compartment dominated by an inferior one, then it can colonize this compartment *via* the highly connected core. Ultimately, this results in larger population fluctuations and makes stochastic extinction events more likely.

This study incorporates complex networks into the rock-paper-scissors game under two commonly observed modes of interaction. In the lattice-structured regular network, both interaction modes yield similar system stability through forming conspecific clusters to reduce interspecific competition (**Figure 4A** vs. **Figure 4B**). Interestingly, we find that the inclusion of network heterogeneity can induce contrasting coexistence patterns between the two interaction modes, due to different mechanisms as explained above. This strongly suggests that particular attention should be devoted to testing, theoretically and experimentally, which mode of interaction is more appropriate for modeling a given competing system. For example, whereas the death of a tree or grass creates a gap in plant communities (i.e., Mode 1), animal species more typically fight for territory (i.e., Mode 2). Thus, these communities should be modeled with different interaction modes and so can be expected to be affected differently by the structure of the landscape they inhabit. Overall, even if these outcomes are obtained using an extremely simplified model, our findings can help identify different mechanisms to explain the role of different interaction modes in stabilizing competitive dynamics in complex networks with contrasting heterogeneities.

Data availability statement

The original contributions presented in this study are included in the article/supplementary material, further inquiries can be directed to the corresponding author.

Author contributions

GG, ZZ, and HZ built the model, performed simulations, and analyzed the results. JL conceived the study and wrote the manuscript. DB contributed substantially to revisions. All authors contributed to the article and approved the submitted version.

Funding

JL was supported by the National Natural Science Foundation of China (Nos. 32271548 and 31901175).

Conflict of interest

The authors declare that the research was conducted in the absence of any commercial or financial relationships that could be construed as a potential conflict of interest.

Publisher's note

References

Allesina, S., and Levine, J. M. (2011). A competitive network theory of species diversity. *Proc. Natl. Acad. Sci. U.S.A.* 108, 5638–5642. doi: 10.1073/pnas.1014428108

Barabási, A. L., and Albert, R. (1999). Emergence of scaling in random networks. *Science* 286, 509–512. doi: 10.1126/science.286.5439.509

Bearup, D., Petrovskii, S., Blackshaw, R. P., and Hastings, A. (2013). Synchronized dynamics of *Tipula paludosa* metapopulation in a southwestern Scotland agroecosystem: linking pattern to process. *Am. Nat.* 182, 393–409. doi: 10.1086/671162

Bunn, A. G., Urban, D. L., and Keitt, T. H. (2000). Landscape connectivity: a conservation application of graph theory. *J. Environ. Manage.* 59, 265–278. doi: 10.1006/jema.2000.0373

Calleja-Solanas, V., Khalil, N., Hernández-García, E., Gómez-Gardeñes, J., and Meloni, S. (2021). Structured interactions as a stabilizing mechanism for competitive ecosystems. *arXiv* [Preprint]. doi: 10.48550/arXiv.2012.14916

Chesson, P. (2000). Mechanisms of species diversity. *Annu. Rev. Ecol. Syst.* 31, 343–366. doi: 10.1146/annurev.ecolsys.31.1.343

Chu, C., and Adler, P. B. (2015). Large niche differences emerge at the recruitment stage to stabilize grassland coexistence. *Ecol. Monogr.* 85, 373–392. doi: 10.1890/14-1741.1

Connell, J. H. (1978). Diversity in tropical rain forests and coral reefs. *Science* 199, 1302–1310. doi: 10.1126/science.199.4335.1302

Czárán, T. L., Hoekstra, R. F., and Pagie, L. (2002). Chemical warfare between microbes promotes biodiversity. *Proc. Natl. Acad. Sci. U.S.A.* 99, 786–790. doi: 10.1073/pnas.012399899

Dale, M. R. T., and Fortin, M. J. (2010). From graphs to spatial graphs. *Ann. Rev. Ecol. Evol. Syst.* 41, 21–38. doi: 10.1146/annurev-ecolsys-102209-144718

Dondina, O., Orioli, V., Colli, L., Luppi, M., and Bani, L. (2018). Ecological network design from occurrence data by simulating species perception of the landscape. *Landsc. Ecol.* 33, 275—-287. doi: 10.1007/s10980-017-0600-1

Durrett, R., and Levin, S. (1997). Allelopathy in spatially distributed populations. *J. Theor. Biol.* 185, 165–171. doi: 10.1006/jtbi.1996.0292

Fortin, M. J., Dale, M. R. T., and Brimacombe, C. (2021). Network ecology in dynamic landscapes. *Proc. R. Soc. B* 288:20201889. doi: 10.1098/rspb.2020.1889

Fortuna, M., Albaladejo, R., Fernández, L., Aparicio, A., and Bascompte, J. (2009). Networks of spatial genetic variation across species. *Proc. Natl. Acad. Sci. U.S.A.* 106, 19044–19049. doi: 10.1073/pnas.0907704106

Fortuna, M., Gómez-Rodríguez, C., and Bascompte, J. (2006). Spatial network structure and amphibian persistence in stochastic environments. *Proc. R. Soc. B* 273, 1429–1434. doi: 10.1098/rspb.2005.3448

Galpern, P., Manseau, M., and Fall, A. (2011). Patch-based graphs of landscape connectivity: a guide to construction, analysis and application for conservation. *Biol. Conserv.* 144, 44–55. doi: 10.1016/j.biocon.2010.09.002

Germain, R. M., Jones, N. T., and Grainger, T. N. (2019). Cryptic dispersal networks shape biodiversity in an invaded landscape. *Ecology* 100:e02738. doi: 10.1002/ecy.2738

Grilli, J., Barabás, G., and Allesina, S. (2015). Metapopulation persistence in random fragmented landscapes. *PLoS Comput. Biol.* 11:e1004251. doi: 10.1371/journal.pcbi.1004251

Grilli, J., Barabás, G., Michalska-Smith, M. J., and Allesina, S. (2017). Higher-order interactions stabilize dynamics in competitive network models. *Nature* 548, 210–213. doi: 10.1038/nature23273

Hansbauer, M. M., Storch, I., Knauer, F., Pilz, S., Küchenhoff, H., Végvári, Z., et al. (2010). Landscape perception by forest understory birds in the Atlantic Rainforest: black-and-white versus shades of grey. *Landsc. Ecol.* 25, 407–417. doi: 10.1007/s10980-009-9418-9

He, P., Montiglio, P. O., Somveille, M., Cantor, M., and Farine, D. R. (2021). The role of habitat configuration in shaping animal population processes: a framework to generate quantitative predictions. *Oecologia* 196, 649–665. doi: 10.1007/s00442-021-04967-y

Hirt, M. R., Grimm, V., Li, Y., Rall, B. C., Rosenbaum, B., and Brose, U. (2018). Bridging scales: allometric random walks link movement and biodiversity research. *Trends Ecol. Evol.* 33, 701–712. doi: 10.1016/j.tree.2018.07.003

Huisman, J., and Weissing, F. J. (1999). Biodiversity of plankton by species oscillations and chaos. *Nature* 402, 407–410. doi: 10.1038/46540

Kerr, B., Riley, M. A., Feldman, M. W., and Bohannan, B. J. M. (2002). Local dispersal promotes biodiversity in a real-life game of rock-paper-scissors. *Nature* 418, 171–174. doi: 10.1038/nature00823

Kininmonth, S. J., De'ath, G., and Possingham, H. P. (2010). Graph theoretic topology of the great but small barrier reef world. *Theor. Ecol.* 3, 75–88. doi: 10.1007/s12080-009-0055-3

Laird, R. A. (2014). Population interaction structure and the coexistence of bacterial strains playing 'rock–paper–scissors'. *Oikos* 123, 472–480. doi: 10.1111/j.1600-0706.2013.00879.x

Laird, R. A., and Schamp, B. S. (2006). Competitive intransitivity promotes species coexistence. *Am. Nat.* 168, 182–193. doi: 10.1086/506259

Laird, R. A., and Schamp, B. S. (2008). Does local competition increase the coexistence of species in intransitive networks? *Ecology* 89, 237–247. doi: 10.2307/27651526

Levine, J. M., Bascompte, J., Adler, P. B., and Allesina, S. (2017). Beyond pairwise mechanisms of species coexistence in complex communities. *Nature* 546, 56–64. doi: 10.1038/nature22898

Levine, J. M., and HilleRisLambers, J. (2009). The importance of niches for the maintenance of species diversity. *Nature* 461, 254–257. doi: 10.1038/nature08251

Li, C., Feng, T., Zhang, H., Chen, D., Cressman, R., Liao, J., et al. (2021). Multilayer network structure enhances the coexistence of competitive species. *Phys. Rev. E* 104:e024402. doi: 10.1103/PhysRevE.104.024402

Li, Y., Bearup, D., and Liao, J. (2020). Habitat loss alters effects of intransitive higher-order competition on biodiversity: a new metapopulation framework. *Proc. Roy. Soc. B* 287:20201571. doi: 10.1098/rspb.2020.1571

Liao, J., Barabás, G., and Bearup, D. (2022). Competition–colonization dynamics and multimodality in diversity–disturbance relationships. *Ecology* 103:e3672. doi: 10.1002/ecy.3672

Liao, J., Li, Z., Hiebeler, D. E., Iwasa, Y., Bogaert, J., and Nijs, I. (2013). Species persistence in landscapes with spatial variation in habitat quality: a pair approximation model. *J. Theor. Biol.* 335, 22–30. doi: 10.1016/j.jtbi.2013.06.015

Masuda, N., and Konno, N. (2006). Networks with dispersed degrees save stable coexistence of species in cyclic competition. *Phys. Rev. E* 74:e066102. doi: 10.1103/physreve.74.066102

May, R. M. (1972). Will a large complex system be stable? *Nature* 238, 413–414. doi: 10.1038/238413a0

Nagatani, T., Ichinose, G., and Tainaka, K. (2018). Heterogeneous network promotes species coexistence: metapopulation model for rock-paper-scissors game. *Sci. Rep.* 8:7094. doi: 10.1038/s41598-018-25353-4

Nicholson, E., and Possingham, H. P. (2006). Objectives for multiple-species conservation planning. *Conserv. Biol.* 20, 871–881. doi: 10.1111/j.1523-1739.2006.00369.x

Reichenbach, T., Mobilia, M., and Frey, E. (2007). Mobility promotes and jeopardizes biodiversity in rock-paper-scissors games. *Nature* 448, 1046–1049. doi: 10.1038/nature06095

Rojas-Echenique, J., and Allesina, S. (2011). Interaction rules affect species coexistence in intransitive networks. *Ecology* 92, 1174–1180. doi: 10.1890/10-0953.1

Roxburgh, S. H., Shea, K., and Wilson, J. B. (2004). The intermediate disturbance hypothesis: patch dynamics and mechanisms of species coexistence. *Ecology* 85, 359–371. doi: 10.2307/3450202

Schütt, M., and Claussen, J. C. (2010). Stabilization of biodiversity in the coevolutionary rock-paper-scissors game on complex networks. *arXiv* [Preprint]. doi: 10.48550/arXiv.1003.2922

Soliveres, S., Maestre, F. T., Ulrich, W., Manning, P., Boch, S., Bowker, M. A., et al. (2015). Intransitive competition is widespread in plant communities and maintains their species richness. *Ecol. Lett.* 18, 790–798. doi: 10.1111/ele.12456

Szabó, G., Szolnoki, A., and Izsák, R. (2004). Rock-scissors-paper game on regular small-world networks. *J. Phys. A Math. Gen.* 37, 2599–2609. doi: 10.1088/0305-4470/37/7/006

Szolnoki, A., and Szabó, G. (2004). Phase transitions for rock-scissors-paper game on different networks. *Phys. Rev. E* 70, 37102–37102. doi: 10.1103/PhysRevE.70.037102

Urban, D., and Keitt, T. (2001). Landscape connectivity: a graph-theoretic perspective. *Ecology* 85, 1205–1218. doi: 10.2307/2679983

Watts, D. J., and Strogatz, S. H. (1998). Collective dynamics of 'small-world' networks. *Nature* 393, 440–442. doi: 10.1038/30918

Yeaton, R. I., and Bond, W. J. (1991). Competition between two shrub species: dispersal differences and fire promote coexistence. *Am. Nat.* 138, 328–341. doi: 10.2307/2462476

Zhang, H., Bearup, D., Nijs, I., Wang, S., Barabás, G., Tao, Y., et al. (2021). Dispersal network heterogeneity promotes species coexistence in hierarchical competitive communities. *Ecol. Lett.* 24, 50–59. doi: 10.1111/ele.13619

Zhang, Z., Bearup, D., Guo, G., Zhang, H., and Liao, J. (2022). Competition modes determine ecosystem stability in rock–paper–scissors games. *Phys. A* 607:e128176. doi: 10.1016/j.physa.2022.128176

frontiers | Frontiers in Ecology and Evolution

TYPE Original Research
PUBLISHED 16 November 2022
DOI 10.3389/fevo.2022.1064873

OPEN ACCESS

EDITED BY
Mehdi Cherif,
INRA Centre Bordeaux-Aquitaine, France

REVIEWED BY
Xiaoxiao Li,
Guangdong University of Technology, China
Xuan Li,
Fudan University, China

*CORRESPONDENCE
Lin Wang
lwang1253@yeah.net

SPECIALTY SECTION
This article was submitted to Population, Community, and Ecosystem Dynamics, a section of the journal Frontiers in Ecology and Evolution

RECEIVED 08 October 2022
ACCEPTED 31 October 2022
PUBLISHED 16 November 2022

CITATION
Wang L and Wang T (2022) Limited predictability of body length in a fish population.
Front. Ecol. Evol. 10:1064873.
doi: 10.3389/fevo.2022.1064873

Limited predictability of body length in a fish population

Lin Wang[1,2]* and Ting Wang[1]

[1]Ministry of Education's Key Laboratory of Poyang Lake Wetland and Watershed Research, School of Geography and Environment, Jiangxi Normal University, Nanchang, China, [2]School of Ecology and Environment, Northwestern Polytechnical University, Xi'an, China

Recent theoretical studies have identified chaotic dynamics in eco-evolutionary models. Yet, empirical evidence for eco-evolutionary chaos in natural ecosystems is lacking. In this study, we combine analyses of empirical data and an eco-evolutionary model to uncover chaotic dynamics of body length in a fish population (northeast Arctic cod: *Gadus morhua*). Consistent with chaotic attractors, the largest Lyapunov exponent (LE) of empirical data is positive, and approximately matches the LE of the model calculation, thus suggesting the potential for chaotic dynamics in this fish population. We also find that the autocorrelation function (ACF) of both empirical data and eco-evolutionary model shows a similar lag of approximately 7 years. Our combined analyses of natural time series and mathematical models suggest that chaotic dynamics of a phenotypic trait may be driven by trait evolution. This finding supports a growing theory that eco-evolutionary feedbacks can produce chaotic dynamics.

KEYWORDS

eco-evolutionary dynamics, chaos, fish body length, genetic variation, autocorrelation function, predictability

Introduction

One of the main questions in evolutionary biology is how ecological interactions affect the phenotypic trait evolution of species (Thompson, 2005). Variation in phenotypic traits (e.g., body size, behavior, morphology, and physiology) are a common feature in natural populations and phenotypic traits can evolve in natural environments (Coulson et al., 2011; Hanski, 2011; Agrawal et al., 2013). Mutual adaptation induced by ecological interactions; that is, coevolution, can shape the adaptive peaks of pairs of associated species (Guimarães et al., 2017). Moreover, selection caused by ecological interactions can even affect the dynamics of whole ecological systems (Koskella and Brockhurst, 2015) and accelerate the adaptation process of natural population (Galetti et al., 2013). These ecological and evolutionary interactions are critical to the structure and functioning of biodiversity (Ehrlich and Raven, 1964; Thompson, 2005). Hence, understanding how ecological interactions shape biodiversity will determine

how coevolution acts on associated species (Iwao and Rausher, 1997; Parchman and Benkman, 2002; Ridenhour, 2005; Thompson et al., 2013).

The interplay of ecological and evolutionary dynamics has been an increasingly active area of research (Schoener, 2011; Koch et al., 2014). To this end, one of the most important areas of research is the long-term predictability of evolution (Green, 1991; Kauffman and Johnsen, 1991; Ferriere and Fox, 1995), where recent theoretical work has focused on the chaotic properties of ecological and evolutionary processes (Dercole et al., 2010; Schreiber et al., 2011; Gilpin and Feldman, 2017). For example, Dercole et al. (2010) coupled an evolutionary equation to a food chain model and found that coevolution can drive the population size to oscillate at the edge of chaos. Gilpin and Feldman (2017) showed that an even simple two-species predator-prey model could give chaotic dynamics when evolution was included in the model. Schreiber et al. (2011) established an eco-evolutionary model showing how predator trait variation affects the trait value of prey, showing that rapid evolution of a polyphagous predator may generate chaotic dynamics due to eco-evolutionary feedbacks. Some researchers have also explored chaotic dynamics of multidimensional phenotypic traits and considered the effects of high-order interactions (e.g., the rate of phenotype x change with time (dx/dt) is affected by the x^3 term) on the rate of traits change with time, with the aim of analyzing the unpredictability of long-term evolution under high-order coupling (Doebeli and Ispolatov, 2014; Rego-Costa et al., 2018).

It is important to note that proving if eco-evolutionary feedbacks can lead to chaotic dynamics is a daunting task, and the empirical evidence for chaos in phenotypic traits are rare. This lack of evidence may be primarily due to the absence of long time series data on phenotypic traits. Interestingly, body size–a vital phenotypic trait–is also well known to be a major player in the dynamics and stability of interactions and here some longer time series exist (De Roos et al., 2003; Rooney et al., 2010; Heckmann et al., 2012; Delong et al., 2015). For example, Delong et al. (2015) analyzed the interaction between body size and trophic cascades, and found that the loss of larger predators have greater consequences on trophic control and biomass structure than smaller predators. Rooney et al. (2010) systematically analyzed the inner property of two food webs–the Cantabrian Sea Shelf marine and the Central Plains Experimental Range (CPER) shortgrass prairie soil. They found that biomass turnover rates (Production: Biomass ratio) decrease with increasing body size and larger organisms tend to have higher trophic positions. Heckmann et al. (2012) used a bioenergetics approach to analyze the interplay of body-size structure and adaptive foraging of consumers, and they found that stronger body-size structures (i.e., species on higher trophic levels have larger body masses than species on lower levels) and faster adaptation stabilize food webs. De Roos et al. (2003) synthesized research about population dynamics and body size dependence in individual life history, and they found that body size generally leads to population cycles driven by differences in competitiveness of differently sized individuals. Given that body size has been identified as important in mediating dynamical outcomes, it is surprising that no research has investigated eco-evolutionary dynamical properties (e.g., chaos) in the body size.

All of the previously mentioned research has shown that body size affects population dynamics and food web stability. Consistent with this, recent macroecological results found that body size from aquatic ecosystems (composed of smaller body-sized organisms) were less stable (a higher coefficient of variation) than wetland and terrestrial organisms (Rip and McCann, 2011). At the same time, for freshwater fish, recent work showed that the linear correlation between community biomass and mean body mass was not significant (Hatton et al., 2015). However, due to the influence of eco-evolutionary feedbacks (Ferriere and Legendre, 2013), we speculate that there is a non-linear correlation between community biomass and body mass. One well-known mechanism for eco-evolutionary feedbacks that may play a potent role in fish population dynamics is fisheries-induced evolution, which has been significant and ubiquitous in harvested ecosystems (Olsen et al., 2004; Jørgensen et al., 2007). Empirical data of a single fish population has found that body length of different ages can yield cyclic dynamics over time (Eikeset et al., 2016), it remains unknown whether these potentially and rapidly evolution induced evolutionary feedback can have chaotic properties or not.

In practice, the Lyapunov exponent (LE) is a classical method to characterize the chaotic nature of real and model ecosystems (Li et al., 2020; Rogers et al., 2022), and two approaches have been used to compute the LE: direct estimation and Jacobian/indirect estimation. On the one hand, the direct approach uses the definition to estimate LE from the data by measuring the divergence rate of the nearest neighbors over a finite time horizon (Rosenstein et al., 1993). In ecology, this approach is mainly used to describe the results of experimental systems (Becks et al., 2005; Graham et al., 2007; Benincà et al., 2008; Kosuta et al., 2008; Becks and Arndt, 2013; Wang et al., 2019). On the other hand, the Jacobian/indirect approach requires fitting a delayed embedding model (with embedding dimension and lag) to the available time series and calculating the LE from the Jacobian matrix of the model (Nychka et al., 1992). A variety of methods may be used to estimate unknown model frameworks, such as generalized additive models (GAMs) (Benincà et al., 2015), neural networks (Ellner and Turchin, 1995), local linear regression (Sugihara, 1994), and non-linear local LE (Li and Ding, 2022). In particular, to accurately predict the model framework of empirical data, the Jacobian/indirect method usually requires the incorporation of abiotic factors (e.g., temperature) into the system, which inevitably increases the data quality requirements.

In what follows, we use a biologically plausible eco-evolutionary model to study the relationship between a phenotypic trait (body length) and population biomass. We first examine dynamical properties of body length based on the direct LE estimation to reveal evidence of underlying oscillations [*via* autocorrelation function (ACF)] and chaotic dynamics (*via* attractor reconstruction) of the phenotypic trait in a natural time series. Second, we explore a relatively simple, yet plausible, theoretical eco-evolutionary model with body length as a trait, that shows similar dynamical signatures and chaos. Our results suggest that potential for eco-evolutionary dynamics. We answer two vital problems: how phenotypic trait affects population dynamics and system stability; and whether changes in the magnitude of genetic variation in body length can drive eco-evolutionary chaos (chaotic dynamics in ecological and evolutionary processes) in fish population dynamics. Our work supports a growing theory that eco-evolutionary feedbacks can produce chaotic dynamics.

Materials and methods

Time series data

We used a previously published time series data set (Eikeset et al., 2016) on the body length of the northeast Arctic cod (*Gadus morhua*), to study the dynamics of a phenotypic trait. The data set consists of mean body length for different age stages (age 3–12 years) of the population from year 1946 to 2004 (**Supplementary Figure 1**). The original data set includes body length for all 10 age stages. For simplicity, the data set was divided into three broader age classes: age class I (age 3–5), age class II (age 6–9), and age class III (age 10–12). Each class has a different competition (compete for the shared resources) ability and reproductive (egg supply) rate per biomass. We assume that cod of the age class I has the lowest competition ability (characterized by the maximal attack rate) and reproductive rate, the age class II has a moderate level, and the age class III has a high level; we assume that three age classes have low, moderate, and high growth potential in body length (see **Table 1**), respectively. In each age class, means of body length were calculated. Finally, to facilitate data analysis, three time series were transformed by a square-root power transformation to suppress sharp peaks.

Phase space reconstruction of body length

For the empirical data, we employed a state-space reconstruction (i.e., we reconstructed the multidimensional dynamics of each body length class, using the body length time series) (Takens, 1981; Becks et al., 2005; Benincà et al., 2008; Wang et al., 2019; Dakos, 2020). To this end, the C–C method (Kim et al., 1999), which is useful for smaller data sets, was first used to calculate the time delay (τ) of each time series. Second, combined with the time delay (τ), the Grassberger–Procaccia (G–P) method was used to calculate the embedding dimension (m) (Grassberger and Procaccia, 1983). Third, by combining τ and m, the largest LE of each time series was derived (Wolf et al., 1985); moreover, in order to distinguish whether chaos is driven by external environmental noise or endogenous factors, we use *wdencmp* function (Donoho et al., 1995) to filter out the environmental noise of empirical data and re-calculate the largest LE of body length (see **Supplementary Figure 2** and simulation codes in **Supplementary material**). Notably, the system has chaotic dynamics only if the Lyapunov exponent is larger than zero. The Lyapunov exponent quantifies the rate of exponential divergence (or convergence) of nearby trajectories (Strogatz, 1994), and a positive LE indicates chaos where the magnitude of LE effectively measures the system sensitivity to initial conditions.

Eco-evolutionary model

Different with the attractor reconstruction approach, we combine ecological processes (consumer-resource dynamics) with evolutionary processes (phenotypic trait dynamics) to simulate the complex dynamics in fish populations.

The time series data show that fish in the different age stages have different body lengths (**Supplementary Figure 1**). Different with early age-structured consumer-resource models (Schreiber and Rudolf, 2008; Nilsson et al., 2018), in this study, 10 ages are divided into three age classes (mean, body, and length), under the biologically plausible assumptions (i.e., different maximal attack rate and reproductive rate in **Table 1**) of each age class, the system is similar to a multi-species consumer-resource system. Here, we establish a bioenergetic consumer-resource model (McCann, 1998) to include phenotypic representations of quantitative trait evolution (Cortez, 2016, 2018; McPeek, 2017; Yamamichi and Letten, 2021). The model can be written as:

$$\frac{dR}{dt} = R\left(r\left(S_R\right) - \alpha R - \frac{x_1\left(S_R, S_1\right) C_1}{1 + x_1\left(S_R, S_1\right) h_1 R} - \frac{x_2\left(S_R, S_2\right) C_2}{1 + x_2\left(S_R, S_2\right) h_2 R} - \frac{x_3\left(S_R, S_3\right) C_3}{1 + x_3\left(S_R, S_3\right) h_3 R}\right) \quad (1.1)$$

$$\frac{dC_i}{dt} = \left(-d_i\left(S_i\right) - \delta_i a_i\right) C_i + g_i \frac{x_i\left(S_R, S_i\right) C_i R}{1 + x_i\left(S_R, S_i\right) h_i R} + X_i Y_i \quad (1.2)$$

$$\frac{dJ_i}{dt} = b_i C_i - J_i\left(d_{Ji} + d_{JD}\sum_{j=1}^{n=3} J_j\right) \quad (1.3)$$

$$\frac{dS_i}{dt} = V_i\left(-\frac{\partial d_i\left(S_i\right)}{\partial S_i} + g_i \frac{R\frac{\partial x_i\left(S_R, S_i\right)}{\partial S_i}}{\left(1 + x_i\left(S_R, S_i\right) h_i R\right)^2}\right) \quad (1.4)$$

$$\frac{dS_R}{dt} = V_4\left(\frac{\partial r(S_R)}{\partial S_R} - \frac{C_1\frac{\partial x_1(S_R,S_1)}{\partial S_R}}{1+x_1(S_R,S_1)\,h_1R} - \frac{C_2\frac{\partial x_2(S_R,S_2)}{\partial S_R}}{1+x_2(S_R,S_2)\,h_2R} - \frac{C_3\frac{\partial x_3(S_R,S_3)}{\partial S_R}}{1+x_3(S_R,S_3)\,h_3R}\right) \quad (1.5)$$

Where $i = 1, 2, 3$, and

$$X_i = \frac{(W_1 - W_2)\left(1 - e^{-k_i\tau_i}\right)^3 + W_2}{W_2} \quad (1.6)$$

$$Y_i = \frac{e^{-d_{Ji}\tau_i}\delta_i d_{Ji}\sum_{j=1}^{n=3} J_j}{2\left(d_{JD}\left(1 - e^{-d_{Ji}\tau_i}\right)\delta_i\sum_{j=1}^{n=3} J_j + d_{Ji}\right)}. \quad (1.7)$$

The state variable R is the resource biomass; C_i, J_i, and S_i are the biomass, egg biomass and body length of fish in age class i, respectively; S_R is the body length of the resource fish. Equations (1.1–1.3) represent biomass dynamics and Eqs (1.4, 1.5) represent trait dynamics, where $\frac{dS_i}{dt} = V_i\frac{\partial}{\partial S_i}\left[\frac{dC_i/dt}{C_i}\right]$ and $\frac{dS_R}{dt} = V_R\frac{\partial}{\partial S_R}\left[\frac{dR/dt}{R}\right]$. Here we assume that selection is frequency-dependent in both the resource (R) and consumers (C_i). τ_i is the maturation time for all individuals in a consumer population (McCann, 1998). Y_i is Beverton–Holt recruitment of age class i based on reproductive effort τ_i years ago and X_i is the growth of surviving recruits over τ_i, in which growth follows a Bertalanffy function (McCann, 1998). We assume the resource fish shows logistic growth: r is the intrinsic rate of increase of the resource, α is the intraspecific competition coefficient for the resource; Moreover, we use Holling type-II functional response to show predation terms: x_i and h_i are the attack rate and handling time of fish in age class i on the resource, respectively; d_i is the instantaneous rate of mortality of fish in age class i; δ_i is the instantaneous rate of reproductive energy invested into offspring for fish in age class i; a_i is the conversion costs of production of soma to gonadal tissue; g_i is the conversion efficiency of prey biomass into adult biomass; b_i is the egg supply rate of fish in age class i; d_{Ji} is density-independent egg mortality rate; d_{JD} is egg mortality related to egg density dependence; k_i is the rate of fish growth; W_1 is the asymptotic mass; and W_2 is the mass of an individual egg; both V_i and V_4 are the genetic variation of body length S_i and S_R, respectively; a higher value of the genetic variation means a faster speed of evolution. Finally, based on the relationship among resource and fish, similar to the early theoretical approach (Dercole et al., 2010), trait dependencies are modeled using the following functional forms:

$$x_i = x_i(S_i, S_R) = x_{i0}\exp\left[-\left(\frac{S_i - w_{i0}}{e_i}\right)^2 + 2l_i\frac{S_i - w_{i0}}{e_i}\cdot\frac{S_R - w_{40}}{f_i} - \left(\frac{S_R - w_{40}}{f_i}\right)^2\right] \quad (1.8)$$

$$r = r(S_R) = r_0\left(1 - r_1(S_R - w_{40})^2\right) \quad (1.9)$$

$$d_i = d_i(S_i) = d_{i0}\left(1 + m_i(S_i - w_{i0})^2\right) \quad (1.10)$$

Where w_{i0} $(i = 1, 2, 3)$ is the optimal trait values. r_0, r_1, x_{i0}, e_i, l_i, f_i, d_{i0}, and m_i are all positive. The growth rate r is maximum at $S_R = w_{40}$, where the growth of the resource is best adapted to its environment. The attack rate x_i is maximum at $S_i = w_{i0}$ and $S_R = w_{40}$ when the body length of cod matches with the prey fish. The mortality d_i of a fish in age class i is minimum at $S_i = w_{i0}$.

TABLE 1 Parameters used in the eco-evolutionary model.

Par.	Description	Value	Par.	Description	Value
α	Density dependence coefficient	0.35	r_0	Maximal intrinsic rate	1.726
h_i	Handling time	0.06; 0.04; 0.03	w_{i0}	Optimal trait value of S_i	2.3; 2.5; 2.7
δ_i	Instantaneous rate of reproductive energy invested into offspring	0.073; 0.099; 0.2	x_{i0}	Maximal attack rate	15.58; 23.37; 31.16
a_i	Conversion costs	1.326	e_i	Scale coefficient	1
g_i	Conversion efficiency	0.7; 0.924; 0.675	V_i	Genetic variation of S_i	V_1 varies [0, 1]; 0.6; 0.65
b_i	Egg supply rate	0.3; 0.4; 0.5	l_i	Scale coefficient	1; 1.5; 1.2
τ_i	Maturation time	2.5; 2.7; 3.5	d_{i0}	Minimal instantaneous rate of mortality	0.8; 2.5; 3.6
k_i	Growth rate	0.5; 0.3; 0.2	m_i	Scale coefficient	0.03; 0.04; 0.05
d_{Ji}	Density-independent egg mortality	0.24	r_1	Scale coefficient	0.165
d_{JD}	Mortality related to egg density dependence	10	w_{40}	Optimal trait value of S_R	2.1
W_1	Asymptotic mass	40	f_i	Scale coefficient	1
W_2	Individual egg mass	0.29	V_4	Genetic variation of S_R	0.67

For eco-evolutionary model (Thompson, 2005), most of the parameter values were derived from the previous research (McCann, 1998) while the remaining set of parameters were obtained based on the reasonable guess values from parameter space presented in **Supplementary Figure 3**. All parameters can be found in **Table 1**. Similar to early theoretical work (McPeek, 2017; Cortez, 2018), we mainly explore how the speed of evolution in terms of the magnitude of genetic variation (V_i) affects the stability of the eco-evolutionary model (Thompson, 2005). We studied the dynamical properties of the eco-evolutionary model using numerical simulation method. Bifurcation diagrams and LE spectrum can be utilized to find the conditions under which the eco-evolutionary model produced chaotic dynamics (positive LEs). Moreover, we calculated both the ACF and LE of both empirical and theoretical time series to compare model predictions with field data. All simulations were carried out using MATLAB 7.0 (MathWorks, 2004).

Results

Empirical results

The natural time series of body length suggests that chaotic dynamics may be presented in this fish species (**Figure 1**). First, we obtain the time delay $\tau = 2$ (**Figures 1D–F**) and embedding dimension $m = 11$ (the rate of change of $\ln C(m, D)$ with $\ln D$ does not change with the increase of m; **Figures 1G–I**) for the age class I, II, and III, respectively. Then, by combining $\tau = 2$ with $m = 11$, we obtain both of the LE values are greater than zero (**Figures 1G–I**). So, time series of the body length in the fish population exist in the chaotic region. Moreover, a similar result is obtained when the environmental noise of time series is filtered out (**Supplementary Figure 2**), all the LE values are larger than 0 (**Supplementary Figures 2C,F,I**), indicating dynamical chaos. So, the body length dynamics of the fish population present an intrinsic chaotic property.

Theoretical predictions of eco-evolutionary model

As revealed by a theoretical simulation (**Figure 2**), the eco-evolutionary model can give rise to a rich set of potential dynamics. When the genetic variation of body length in the age class I, V_1, is small ($V_1 = 0.03$, LE $= -0.0016$; **Figure 2A**), the dynamics of body length S_1 approaches a simple, regular oscillation (period-2 oscillation). After an increase in the magnitude of genetic variation in body length S_1, V_1 ($V_1 = 0.27$, LE $= -0.0012$; **Figure 2B**), the dynamics of body length S_1 presents a doubling-periodic oscillation. Further, when V_1 is increased even more, the dynamics of body length S_1 appears to enter a chaotic regime ($V_1 = 0.5$, LE $= 0.0643$; **Figure 2C**) as suggested by the Lyapunov exponent (**Figure 2F**). Finally, periodic dynamics (regular oscillation) is observed when V_1 is increased even further ($V_1 = 0.764$, LE $= -0.001$; **Figure 2D**).

Since chaos may occur purely due to ecological dynamics, we did a bifurcation analysis assuming ecological dynamics only (i.e., assuming $V_1 = V_2 = V_3 = V_4 = 0$). Under these purely ecological conditions, the single-parameter bifurcation shows that the ecological process may not produce chaotic dynamics (**Supplementary Figure 3**), and the dynamics of population biomass C_1 is merely represented as a stable equilibrium.

Comparison between theoretical predictions and empirical data

Both theoretical predictions and empirical results show that the dynamics of a phenotypic trait, such as body length, can show chaotic properties. However, if the dynamics of our theoretical model is indeed a plausible representation of the empirical data, other dynamical properties of their respective time series should also be similar.

In this regard, the ACF analysis indeed indicates dynamical similarities among natural (**Figure 3A**) and theoretical (**Figure 3B**) time series. Both theoretical data and empirical data show two major peak lags: short (about 7 years) and long periods (about 24 years). However, due to the limited length of empirical data (in total 59 data points), the long period may be not significant (**Figure 3A**). Moreover, a predictable period (years) of the chaotic timeseries is $1/LE(S_3)$ (i.e., $1/0.1309 = 7.64$ years in body length S_3; **Figure 1I**), which is close to 7 years (calculated by the ACF). Therefore, these results illustrate the eco-evolutionary model can depict the real dynamics of body length in a single fish system.

Discussion

The predictability of long-term evolution has puzzled ecologists for decades (Green, 1991; Kauffman and Johnsen, 1991; Ferriere and Fox, 1995). Although recent theoretical work has analyzed the chaotic properties of eco-evolutionary dynamics (Dercole et al., 2010; Schreiber et al., 2011; Doebeli and Ispolatov, 2014; Gilpin and Feldman, 2017; Rego-Costa et al., 2018), eco-evolutionary chaos has not been shown in empirical data. In this study, we combined an eco-evolutionary model with analyzes of empirical data to uncover chaotic dynamics of body length of a single fish population. Our work may prove the eco-evolutionary chaos in the natural ecological system.

Our work may be treated as a supplementary method to study fish species. In this study, we provided a new mechanism, that is, the genetic variation of phenotypic trait determines chaotic dynamics of body length. The new mechanism revealed

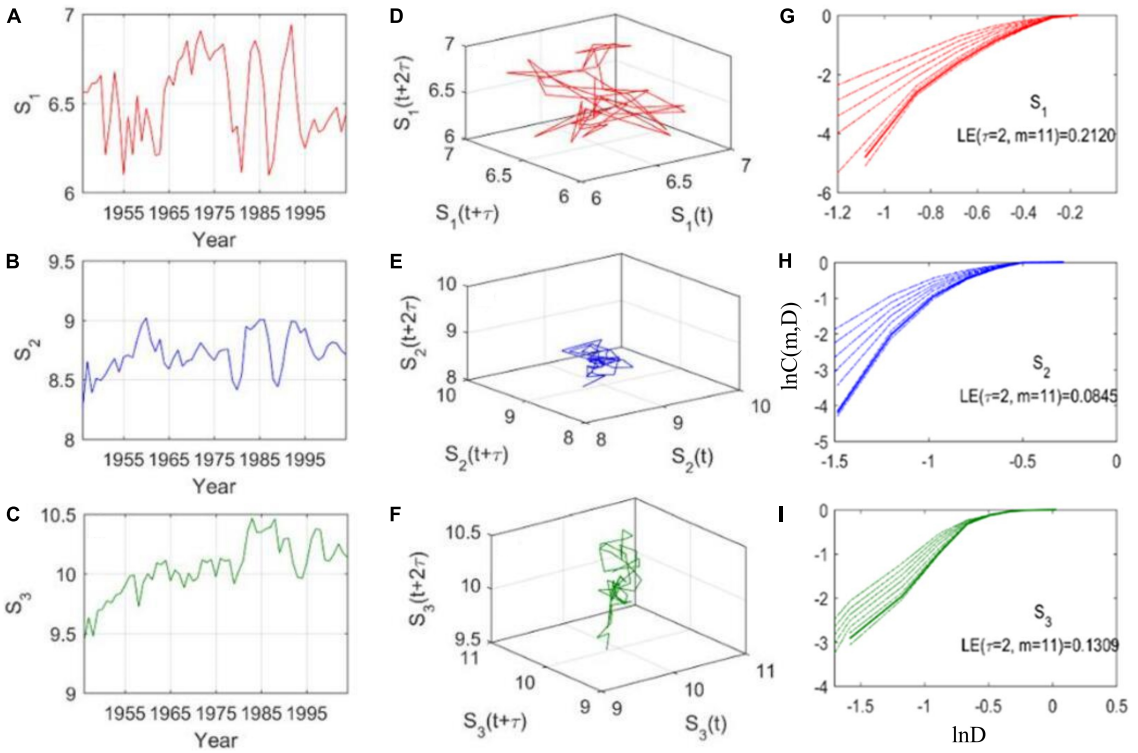

FIGURE 1
Phase space reconstruction of single time series of body length. **(A–C)** Empirical data of body length; **(D–F)** Attractor reconstruction ($\tau = 2$; based on the C–C method) of empirical data with noise; **(G–I)** Lyapunov exponent (LE) of body length: D is the neighborhood radius, m is the embedding dimension, and C is the correlation integral, which is influenced by both D and m. In each rectangle, m varies from 5 to 12 (from top line to bottom line, $m = 11$ can be obtained for each case when the rate of change of $\ln C(m, D)$ with $\ln D$ does not change with the increase of m). Body length S_1 (age class I: age 3–5), S_2 (age class II: age 6–9), and S_3 (age class III: age 10–12) are the mean of each age class. The original data is shown in **Supplementary Figure 1**.

in our work is different from recent studies (Eikeset et al., 2016; Andersen, 2019), which showed many mechanisms could influence population dynamics (stable or oscillatory state) of fish species, such as the change of age structure, life-history parameters, and fishing. Actually, our work involved with above factors. First of all, for different study methods (attractor reconstruction and eco-evolutionary model), different age classes (age 3–12) were divided into three broader age classes, and each class has the different maximal attack rate and reproductive rate (**Table 1**). Moreover, life-history parameters (i.e., individual growth rate k_i and reproduction rate b_i in **Table 1**) indeed influence population dynamics (non-chaos in **Supplementary Figure 3**) of fish species when we neglected the evolutionary dynamics ($V_1 = V_2 = V_3 = V_4 = 0$). Finally, although we do not introduce human harvest (fishing) into the eco-evolutionary model, we infer that fishing will impact the demography and recruitment of a fish stock. Therefore, it is worth trying to analyze how each ecological parameter influence population dynamics of fish. The simulation result showed that non-chaos emerges when we do not consider phenotypic trait evolution in the mechanistic model (**Supplementary Figure 3**).

In short, in this work, the free-equation approach (attractor reconstruction) proved chaos in trait dynamics, and then a plausible interpretation mechanism (regulating the genetic variation of phenotypic trait may result in chaotic dynamics of body length in the eco-evolutionary model) for chaos in body length of fish was suggested, that is, rapid evolution in phenotypic trait may result in chaos in both ecological (population density/biomass) and evolutionary (phenotypic trait) processes.

The road to eco-evolutionary chaos

Early theoretical work found that regulating the magnitude of genetic variation in phenotypic trait can result in periodic oscillations (McPeek, 2017; Cortez, 2018) and chaotic dynamics (Dercole et al., 2010; Gilpin and Feldman, 2017). However, empirical evidence for eco-evolutionary chaos in natural ecosystems is lacking. In this study, we first use the phase space reconstruction method to present the evidence for potential chaos in fish body length. In our eco-evolutionary model, similar to recent theoretical approaches (Cortez, 2018;

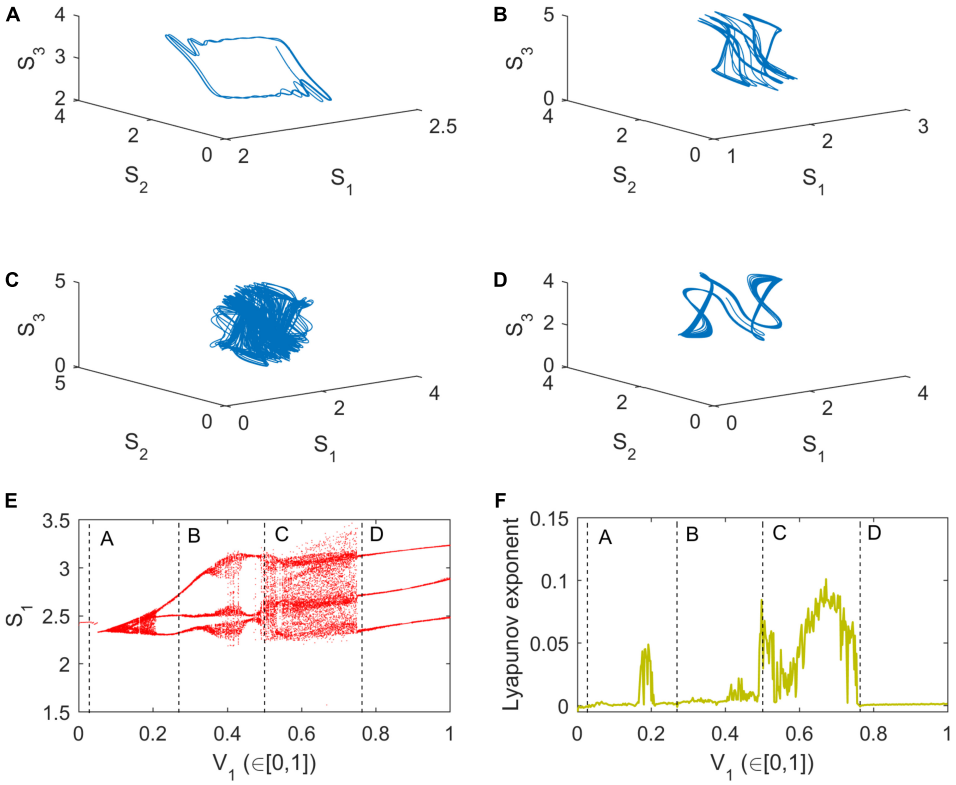

FIGURE 2
Eco-evolutionary dynamical simulations. **(A–D)** Space phase diagrams; **(E)** Bifurcation diagram; **(F)** Lyapunov exponent (LE) spectrum. Model parameters are presented in **Table 1** and V_1 varies in [0, 1]: Panels **(A)** $V_1 = 0.03$, **(B)** $V_1 = 0.27$, **(C)** $V_1 = 0.5$, and **(D)** $V_1 = 0.764$. The simulation time is 1,000 and initial value of Eq. (1) is (0.1, 0.1, 0.03, 0.02, 0.03, 0.01, 0.01, 2.2, 2.4, 2.8, and 3).

Yamamichi and Letten, 2021), we only analyze how system stability varies with the genetic variation (V_1). Our results show the increase of V_1 can generate chaotic dynamics in both phenotypic trait and biomass (LE $>$ 0; **Figure 2F**). However, when we do not consider trait evolution ($V_i = 0$) in the model, population dynamics of the fish population may not present chaos. Then the ACF of both empirical data and simulation data of the eco-evolutionary model show that the predictable period (years) of body length in fish population is about 7 years. Therefore, the eco-evolutionary model can approximately depict and predict the intrinsic dynamic behavior of empirical data.

Moreover, recent theoretical research showed that ecological process (population density/biomass) will produce population oscillation if evolutionary process (phenotypic trait) has the oscillatory dynamics (McPeek, 2017; Cortez, 2018). In our study, we first present chaotic dynamics (irregular periodic oscillation) of the body length (attractor reconstruction), while comparative analyses of the ACF reveal broadly consistent results between experimental data and theoretical models. Therefore, we infer that the eco-evolutionary chaos may be driven by body length evolution (changes in genetic variation of body length) in the cod population.

In the eco-evolutionary model, the chaotic evolutionary trajectories (LE $>$ 0; **Figure 3F**) are intrinsically unpredictable, and strongly dependent on the magnitude of genetic variation in phenotypic trait (V_1). The change switches between the non-chaotic (LE $<$ 0) and chaotic dynamics (i.e., the "edge of chaos") was discussed in earlier work (Ferriere and Fox, 1995; Turchin and Ellner, 2000; Benincà et al., 2015), which may balance the resource-fish system near the "evolutionary sliding" (Dercole et al., 2006). This maybe provide an evolutionary explanation for chaotic dynamics in the nature (Turchin, 2003). Our work identifies eco-evolutionary chaos in a natural ecological system. This empirical finding supports the theory that eco-evolutionary feedbacks can produce chaotic dynamics.

Rapid evolution in body length of fish is limited predictability

The rapid evolution of fish population has caused widespread discussion (Olsen et al., 2004; Jørgensen et al., 2007; Eikeset et al., 2016). In this study, we infer that the change of the body length (chaotic dynamics of

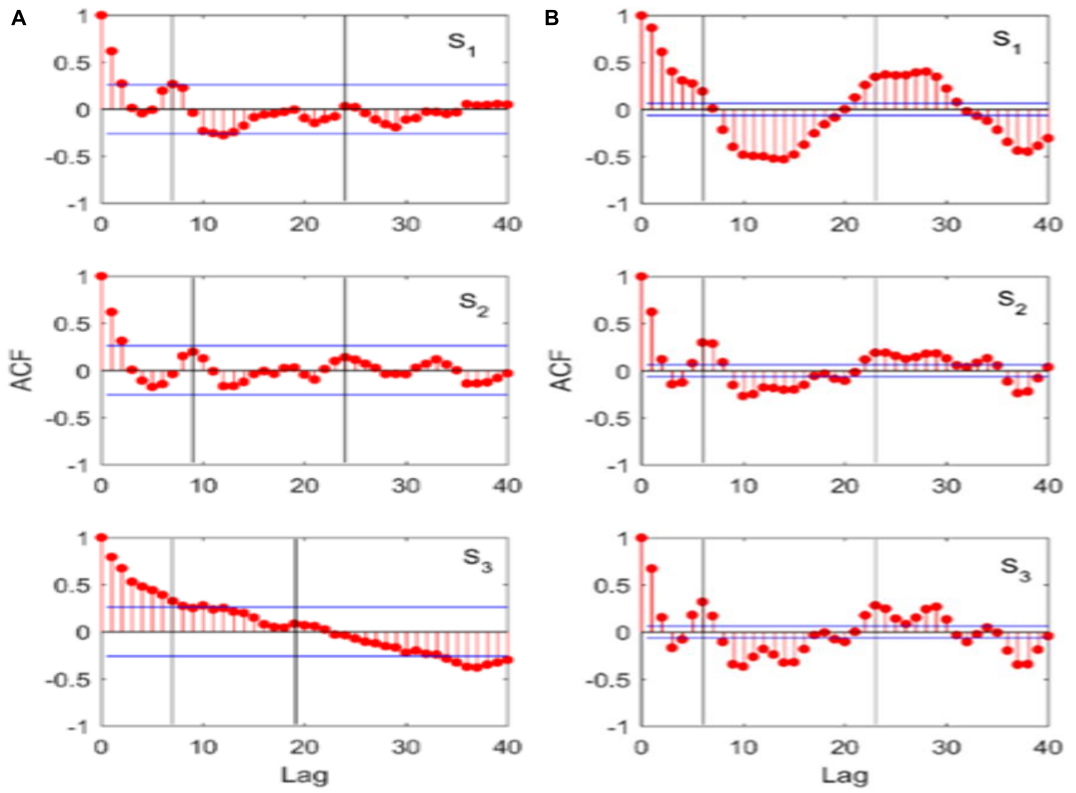

FIGURE 3
Chaotic dynamics is observed for the northeast Arctic cod (*Gadus morhua*) based on empirical data and simulation data analyzes. **(A)** Autocorrelation function (ACF) of empirical data; **(B)** ACF of simulation data; body length class I (S_1), class II (S_2), and class III (S_3). Blue line denotes significance threshold and the value in the middle of two blue lines can be considered not significantly different from 0.

phenotypic trait) is due to evolution. Moreover, the body length evolution has a limited predictability due to its chaotic property.

In the cod population, we checked for chaotic dynamics (positive LE) of body length based on both empirical data and eco-evolutionary model analyses. We found the LE of empirical data [LE(S_3) = 0.1309], which means predictable periods ($1/LE$) of empirical data (i.e., 7.64 years in body length S_3) is also close to 7 years (calculated by the ACF). The eco-evolutionary model can approximately depict and predict the intrinsic dynamic behavior of empirical data, that is, the limited predictable period of rapid evolution ($V_i > 0$) in body length of fish is approach to 7 years. Fish population growth is closely bound up with our daily life, considering the effectively predictable time of body length can help us make a suitable strategy for fishery conservation.

Data availability statement

The original contributions presented in this study are included in the article/**Supplementary material**, further inquiries can be directed to the corresponding author.

Author contributions

LW designed the study, finished model simulations, carried out data analyses, and wrote the first draft of the manuscript. Both authors contributed substantially to revisions and approved the submitted version.

Funding

This research was supported by the National Natural Science Foundation of China (32201259) and Doctor Start-up Fund Project of Jiangxi Normal University (12021105).

Acknowledgments

We thank Kevin McCann, Torbjörn Säterberg, Jennifer Meunier, and Xue-Qi Wang for helpful comments on the manuscript. We also thank two reviewers and editor for many useful suggestions that improved the quality of this manuscript.

Conflict of interest

The authors declare that the research was conducted in the absence of any commercial or financial relationships that could be construed as a potential conflict of interest.

Publisher's note

All claims expressed in this article are solely those of the authors and do not necessarily represent those of their affiliated organizations, or those of the publisher, the editors and the reviewers. Any product that may be evaluated in this article, or claim that may be made by its manufacturer, is not guaranteed or endorsed by the publisher.

Supplementary material

The Supplementary Material for this article can be found online at: https://www.frontiersin.org/articles/10.3389/fevo.2022.1064873/full#supplementary-material

References

Agrawal, A. A., Johnson, M. T., Hastings, A. P., and Maron, J. L. (2013). A field experiment demonstrating plant life-history evolution and its eco-evolutionary feedback to seed predator populations. *Am. Nat.* 181, S35–S45. doi: 10.1086/666727

Andersen, K. H. (2019). *Fish ecology, evolution, and exploitation: A new theoretical synthesis.* Princeton, NJ: Princeton University Press. doi: 10.23943/princeton/9780691192956.001.0001

Becks, L., and Arndt, H. (2013). Different types of synchrony in chaotic and cyclic communities. *Nat. Commun.* 4, 1359. doi: 10.1038/ncomms2355

Becks, L., Hilker, F. M., Malchow, H., Jürgens, K., and Arndt, H. (2005). Experimental demonstration of chaos in a microbial food web. *Nature* 435, 1226–1229. doi: 10.1038/nature03627

Benincà, E., Ballantine, B., Ellner, S. P., and Huisman, J. (2015). Species fluctuations sustained by a cyclic succession at the edge of chaos. *Proc. Natl. Acad. Sci. U.S.A.* 112, 6389–6394. doi: 10.1073/pnas.1421968112

Benincà, E., Huisman, J., Heerkloss, R., Jöhnk, K. D., Branco, P., Van Nes, E. H., et al. (2008). Chaos in a long-term experiment with a plankton community. *Nature* 451, 822–825. doi: 10.1038/nature06512

Cortez, M. H. (2016). How the magnitude of prey genetic variation alters predator-prey eco-evolutionary dynamics. *Am. Nat.* 188, 329–341. doi: 10.1086/687393

Cortez, M. H. (2018). Genetic variation determines which feedbacks drive and alter predator–prey eco-evolutionary cycles. *Ecol. Monogr.* 88, 353–371. doi: 10.1002/ecm.1304

Coulson, T., MacNulty, D. R., Stahler, D. R., Wayne, R. K., and Smith, D. W. (2011). Modeling effects of environmental change on wolf population dynamics, trait evolution, and life history. *Science* 334, 1275–1278. doi: 10.1126/science.1209441

Dakos, V. (2020). Nature's dynamical complexity. *Nat. Ecol. Evol.* 4, 12–13. doi: 10.1038/s41559-019-1077-x

De Roos, A. M., Persson, L., and Mccauley, E. (2003). The influence of size-dependent life-history traits on the structure and dynamics of populations and communities. *Ecol. Lett.* 6, 473–487. doi: 10.1046/j.1461-0248.2003.00458.x

Delong, J. P., Gilbert, B., Shurin, J. B., Savage, V. M., Barton, B. T., Clements, C. F., et al. (2015). The body size dependence of trophic cascades. *Am. Nat.* 185, 354–366. doi: 10.1086/679735

Dercole, F., Ferrière, R., Gragnani, A., and Rinaldi, S. (2006). Coevolution of slow-fast populations: Evolutionary sliding, evolutionary pseudo-equilibria and complex Red Queen dynamics. *Proc. R. Soc. Lond. B Biol. Sci.* 273, 983–990. doi: 10.1098/rspb.2005.3398

Dercole, F., Ferriere, R., and Rinaldi, S. (2010). Chaotic Red Queen coevolution in three-species food chains. *Proc. R. Soc. Lond. B Biol. Sci.* 277, 2321–2330. doi: 10.1098/rspb.2010.0209

Doebeli, M., and Ispolatov, I. (2014). Chaos and unpredictability in evolution. *Evolution* 68, 1365–1373. doi: 10.1111/evo.12354

Donoho, D. L., Johnstone, I. M., Kerkyacharian, G., and Picard, D. (1995). Wavelet shrinkage: Asymptopia. *J. R. Stat. Soc. Ser. B* 57, 301–337. doi: 10.1111/j.2517-6161.1995.tb02032.x

Ehrlich, P. R., and Raven, P. H. (1964). Butterflies and plants: A study in coevolution. *Evolution* 18, 586–608. doi: 10.1111/j.1558-5646.1964.tb01674.x

Eikeset, A. M., Dunlop, E. S., Heino, M., Storvik, G., Stenseth, N. C., and Dieckmann, U. (2016). Roles of density-dependent growth and life history evolution in accounting for fisheries-induced trait changes. *Proc. Natl. Acad. Sci. U.S.A.* 113, 15030–15035. doi: 10.1073/pnas.1525749113

Ellner, S., and Turchin, P. (1995). Chaos in a noisy world: New methods and evidence from time-series analysis. *Am. Nat.* 145, 343–375. doi: 10.1086/285744

Ferriere, R., and Fox, G. A. (1995). Chaos and evolution. *Trends Ecol. Evol.* 10, 480–485. doi: 10.1016/S0169-5347(00)89194-6

Ferriere, R., and Legendre, S. (2013). Eco-evolutionary feedbacks, adaptive dynamics and evolutionary rescue theory. *Philos. Trans. R. Soc. B Biol. Sci.* 368:20120081. doi: 10.1098/rstb.2012.0081

Galetti, M., Guevara, R., Côrtes, M. C., Fadini, R., Von, M. S., Leite, A. B., et al. (2013). Functional extinction of birds drives rapid evolutionary changes in seed size. *Science* 340, 1086–1090. doi: 10.1126/science.1233774

Gilpin, W., and Feldman, M. W. (2017). A phase transition induces chaos in a predator-prey ecosystem with a dynamic fitness landscape. *PLoS Comput. Biol.* 13:e1005644. doi: 10.1371/journal.pcbi.1005644

Graham, D. W., Knapp, C. W., Van Vleck, E. S., Bloor, K., Lane, T. B., and Graham, C. E. (2007). Experimental demonstration of chaotic instability in biological nitrification. *ISME J.* 1, 385–393. doi: 10.1038/ismej.2007.45

Grassberger, P., and Procaccia, I. (1983). Measuring the strangeness of strange attractors. *Physica D* 9, 189–208. doi: 10.1016/0167-2789(83)90298-1

Green, D. M. (1991). Chaos, fractals and nonlinear dynamics in evolution and phylogeny. *Trends Ecol. Evol.* 6, 333–337.

Guimarães, P. R. Jr., Pires, M. M., Jordano, P., Bascompte, J., and Thompson, J. N. (2017). Indirect effects drive coevolution in mutualistic networks. *Nature* 550, 511–514. doi: 10.1038/nature24273

Hanski, I. A. (2011). Eco-evolutionary spatial dynamics in the Glanville fritillary butterfly. *Proc. Natl. Acad. Sci. U.S.A.* 108, 14397–14404. doi: 10.1073/pnas.1110020108

Hatton, I. A., Mccann, K. S., Fryxell, J. M., Davies, T. J., Smerlak, M., Sinclair, A. R., et al. (2015). The predator-prey power law: Biomass scaling across terrestrial and aquatic biomes. *Science* 349:aac6284. doi: 10.1126/science.aac6284

Heckmann, L., Drossel, B., Brose, U., and Guill, C. (2012). Interactive effects of body-size structure and adaptive foraging on food-web stability. *Ecol. Lett.* 15, 243–250. doi: 10.1111/j.1461-0248.2011.01733.x

Iwao, K., and Rausher, M. D. (1997). Evolution of plant resistance to multiple herbivores: Quantifying diffuse coevolution. *Am. Nat.* 149, 316–335. doi: 10.1086/285992

Jørgensen, C., Enberg, K., Dunlop, E. S., Arlinghaus, R., Boukal, D. S., Brander, K., et al. (2007). Managing evolving fish stocks. *Science* 318, 1247–1248. doi: 10.1126/science.1148089

Kauffman, S. A., and Johnsen, S. (1991). Coevolution to the edge of chaos: Coupled fitness landscapes, poised states, and coevolutionary avalanches. *J. Theor. Biol.* 149, 467–505. doi: 10.1016/s0022-5193(05)80094-3

Kim, H. S., Eykholt, R., and Salas, J. D. (1999). Nonlinear dynamics, delay times, and embedding windows. *Physica D* 127, 48–60. doi: 10.1016/s0167-2789(98)00240-1

Koch, H., Frickel, J., Valiadi, M., and Becks, L. (2014). Why rapid, adaptive evolution matters for community dynamics. *Front. Ecol. Evol.* 2:17. doi: 10.3389/fevo.2014.00017

Koskella, B., and Brockhurst, M. A. (2015). Bacteria–phage coevolution as a driver of ecological and evolutionary processes in microbial communities. *FEMS Microbiol. Rev.* 38, 916–931. doi: 10.1111/1574-6976.12072

Kosuta, S., Hazledine, S., Sun, J., Miwa, H., Morris, R. J., Downie, J. A., et al. (2008). Differential and chaotic calcium signatures in the symbiosis signaling pathway of legumes. *Proc. Natl. Acad. Sci. U.S.A.* 105, 9823–9828. doi: 10.1073/pnas.0803499105

Li, X., and Ding, R. (2022). The backward nonlinear local Lyapunov exponent and its application to quantifying the local predictability of extreme high-temperature events. *Clim. Dyn.* 1–15. doi: 10.1007/s00382-022-06469-w

Li, X., Ding, R., and Li, J. (2020). Quantitative study of the relative effects of initial condition and model uncertainties on local predictability in a nonlinear dynamical system. *Chaos Solitons Fractals* 139:110094. doi: 10.1016/j.chaos.2020.110094

MathWorks (2004). *MATLAB*. Natick, MA: MathWorks.

McCann, K. S. (1998). Density-dependent coexistence in fish communities. *Ecology* 79, 2957–2967. doi: 10.2307/176529

McPeek, M. A. (2017). *Evolutionary community ecology*. Princeton, NJ: Princeton University Press.

Nilsson, K. A., McCann, K. S., and Caskenette, A. L. (2018). Interaction strength and stability in stage-structured food web modules. *Oikos* 127, 1494–1505. doi: 10.1111/oik.05029

Nychka, D., Ellner, S., Gallant, A. R., and McCaffrey, D. (1992). Finding chaos in noisy systems. *J. R. Stat. Soc. Ser. B Methodol.* 54, 399–426. doi: 10.1111/j.2517-6161.1992.tb01889.x

Olsen, E. M., Heino, M., Lilly, G. R., Morgan, M. J., Brattey, J., Ernande, B., et al. (2004). Maturation trends indicative of rapid evolution preceded the collapse of northern cod. *Nature* 428, 932–935. doi: 10.1038/nature02430

Parchman, T. L., and Benkman, C. W. (2002). Diversifying coevolution between crossbills and black spruce on Newfoundland. *Evolution* 56, 1663–1672. doi: 10.1554/0014-38202002056[1663:dcbcab]2.0.co;2

Rego-Costa, A., Débarre, F., and Chevin, L. M. (2018). Chaos and the (un)predictability of evolution in a changing environment. *Evolution* 72, 375–385. doi: 10.1111/evo.13407

Ridenhour, B. J. (2005). Identification of selective sources: partitioning selection based on interactions. *Am. Nat.* 166, 12–25. doi: 10.1086/430524

Rip, J. M. K., and McCann, K. S. (2011). Cross-ecosystem differences in stability and the principle of energy flux. *Ecol. Lett.* 14, 733–740. doi: 10.1111/j.1461-0248.2011.01636.x

Rogers, T. L., Johnson, B. J., and Munch, S. B. (2022). Chaos is not rare in natural ecosystems. *Nat. Ecol. Evol.* 6, 1105–1111.

Rooney, N., Mccann, K. S., and Moore, J. C. (2010). A landscape theory for food web architecture. *Ecol. Lett.* 11, 867–881. doi: 10.1111/j.1461-0248.2008.01193.x

Rosenstein, M. T., Collins, J. J., and De Luca, C. J. (1993). A practical method for calculating largest Lyapunov exponents from small data sets. *Physica D* 65, 117–134. doi: 10.1016/0167-2789(93)90009-P

Schoener, T. W. (2011). The newest synthesis: Understanding the interplay of evolutionary and ecological dynamics. *Science* 331, 426–429. doi: 10.1126/science.1193954

Schreiber, S., and Rudolf, V. (2008). Crossing habitat boundaries: Coupling dynamics of ecosystems through complex life cycles. *Ecol. Lett.* 11, 576–587. doi: 10.1111/j.1461-0248.2008.01171.x

Schreiber, S. J., Bürger, R., and Bolnick, D. I. (2011). The community effects of phenotypic and genetic variation within a predator population. *Ecology* 92, 1582–1593. doi: 10.1890/10-2071.1

Strogatz, S. H. (1994). *Nonlinear dynamics and chaos: With applications to physics, biology, chemistry, and engineering*. Cambridge, MA: Perseus Books Publishing.

Sugihara, G. (1994). Nonlinear forecasting for the classification of natural time series. *Philos. Trans. R. Soc. Lond. Ser. A Phys. Eng. Sci.* 348, 477–495.

Takens, F. (1981). Detecting strange attractors in turbulence. *Lect. Notes Math.* 898, 366–381. doi: 10.1007/bfb0091924

Thompson, J. N. (2005). *The geographic mosaic of coevolution*. Chicago, IL: University of Chicago Press.

Thompson, J. N., Schwind, C., Guimarães, P. R. Jr., and Friberg, M. (2013). Diversification through multitrait evolution in a coevolving interaction. *Proc. Natl. Acad. Sci. U.S.A.* 110, 11487–11492. doi: 10.1073/pnas.1307451110

Turchin, P. (2003). *Complex population dynamics: A theoretical/empirical synthesis (MPB-35)*. Princeton, NJ: Princeton University Press.

Turchin, P., and Ellner, S. P. (2000). Living on the edge of chaos: Population dynamics of Fennoscandian voles. *Ecology* 81, 3099–3116. doi: 10.2307/177404

Wang, L., Tang, Y., Wang, R.-W., and Shang, X.-Y. (2019). Re-evaluating the 'plankton paradox' using an interlinked empirical data and a food web model. *Ecol. Model.* 407, 108721.

Wolf, A., Swift, J. B., Swinney, H. L., and Vastano, J. A. (1985). Determining Lyapunov exponents from a time series. *Physica D* 16, 285–317. doi: 10.1016/0167-2789(85)90011-9

Yamamichi, M., and Letten, A. D. (2021). Rapid evolution promotes fluctuation-dependent species coexistence. *Ecol. Lett.* 24, 812–818. doi: 10.1111/ele.13707

frontiers | Frontiers in Ecology and Evolution

TYPE Original Research
PUBLISHED 03 February 2023
DOI 10.3389/fevo.2023.1094269

OPEN ACCESS

EDITED BY
Mehdi Cherif,
INRA Centre Bordeaux-Aquitaine,
France

REVIEWED BY
Robert L. Sinsabaugh,
University of New Mexico,
United States
Jose Murua Royo,
University of California,
United States

*CORRESPONDENCE
Stefano Manzoni
✉ stefano.manzoni@natgeo.su.se

SPECIALTY SECTION
This article was submitted to Models in Ecology and Evolution, a section of the journal Frontiers in Ecology and Evolution

RECEIVED 09 November 2022
ACCEPTED 03 January 2023
PUBLISHED 03 February 2023

CITATION
Manzoni S, Chakrawal A and Ledder G (2023) Decomposition rate as an emergent property of optimal microbial foraging. *Front. Ecol. Evol.* 11:1094269. doi: 10.3389/fevo.2023.1094269

Decomposition rate as an emergent property of optimal microbial foraging

Stefano Manzoni[1]*, Arjun Chakrawal[1] and Glenn Ledder[2]

[1]Department of Physical Geography and Bolin Centre for Climate Research, Stockholm University, Stockholm, Sweden, [2]Department of Mathematics, University of Nebraska-Lincoln, Lincoln, NE, United States

Decomposition kinetics are fundamental for quantifying carbon and nutrient cycling in terrestrial and aquatic ecosystems. Several theories have been proposed to construct process-based kinetics laws, but most of these theories do not consider that microbial decomposers can adapt to environmental conditions, thereby modulating decomposition. Starting from the assumption that a homogeneous microbial community maximizes its growth rate over the period of decomposition, we formalize decomposition as an optimal control problem where the decomposition rate is a control variable. When maintenance respiration is negligible, we find that the optimal decomposition kinetics scale as the square root of the substrate concentration, resulting in growth kinetics following a Hill function with exponent 1/2 (rather than the Monod growth function). When maintenance respiration is important, optimal decomposition is a more complex function of substrate concentration, which does not decrease to zero as the substrate is depleted. With this optimality-based formulation, a trade-off emerges between microbial carbon-use efficiency (ratio of growth rate over substrate uptake rate) and decomposition rate at the beginning of decomposition. In environments where carbon substrates are easily lost due to abiotic or biotic factors, microbes with higher uptake capacity and lower efficiency are selected, compared to environments where substrates remain available. The proposed optimization framework provides an alternative to purely empirical or process-based formulations for decomposition, allowing exploration of the effects of microbial adaptation on element cycling.

KEYWORDS

microbial model, decomposition kinetics, optimization, microbial adaptation, growth-efficiency trade-off

1. Introduction

Organic matter decomposition and its subsequent mineralization by microbial decomposers regulate the flow of carbon and nutrients in both terrestrial and aquatic systems. Two different sets of assumptions have been proposed to describe the kinetics of decomposition in mathematical models. First, based on the observation that the relative mass loss is nearly constant, first-order decay models were initially proposed (Salter and Green, 1933; Olson, 1963). The same concept has been adopted in numerous later biogeochemical models (Manzoni and Porporato, 2009). Second, more recent developments acknowledged the role of microbial biomass as a driver of decomposition and accounted for extra-cellular enzymes in the reaction kinetics. These works assume that the degradation of soil organic matter can be treated as an enzymatic reaction that follows Michaelis–Menten (Michaelis and Menten, 1913) or other nonlinear kinetics laws involving both substrate and enzyme concentrations (Wang and Post, 2013; Tang and Riley, 2019). Even without describing enzymatic reactions *per se*, nonlinear

decomposition models inspired by Monod's results (formally similar to Michaelis–Menten kinetics), or other nonlinear functions, have often been used to include microbial biomass as a driver of decomposition (Monod, 1949; Wutzler and Reichstein, 2008; Manzoni and Porporato, 2009; Abramoff et al., 2018). Despite their differences and contexts of application, linear and nonlinear approaches rely on some *a priori* assumption on the mathematical form of the decomposition kinetics.

Biogeochemical reactions in soils are complicated by chemical and spatial heterogeneities and by the diversity of microbial metabolic strategies. Hence, it is difficult to achieve a theoretically sound representation of macro-scale kinetics laws to interpret experimental data at the field scale, and in ecosystem models at even larger scales. Therefore, one could question whether the underlying kinetics laws should be imposed (as currently done) or regarded as emerging properties of the soil system, and derived based on some physical constrain or ecological consideration. In this contribution, we follow the latter approach by formulating a decomposition model from an optimization perspective, assuming that decomposition should proceed so that decomposers maximize their cumulative growth over the duration of decomposition.

Optimization principles are commonly used in ecology and plant science (Rosen, 1967; Harrison et al., 2021). Their underlying assumption is that evolution leads to optimally-adapted phenotypes by selecting the fittest organisms. The objectives of such evolutionary optimization are typically the maximization of reproductive effort, resource use, or net growth rate. An optimal strategy often exists because resources are limited and therefore need to be used or allocated in particular and timely manners. Moreover, physiological trade-offs and enzymatic capacity constrain the range of possible resource use strategies (Gudelj et al., 2010; Allison, 2012; Waldherr et al., 2015). For example, carbon use efficiency (i.e., the ratio of growth rate over uptake rate) tends to be lower in fast growing organisms (Lipson, 2015; Muscarella et al., 2020). Mathematically, given the optimization objective (fitness maximization) and constraints (resources are limited; physiological trade-offs), and assuming that some traits can be varied thanks to selective pressures, it is possible to formulate organism growth as an optimal control problem.

This is also the case for microbial decomposers, which exploit resources accumulated in organic matter (in soil, litter, sediments, or water) that are not only limited, but also subject to consumption by competing organisms and loss due to physical processes. Therefore, microbes face an inherent dilemma. On the one hand, resources could be consumed rapidly to ensure maximal use, but high rates of consumption are generally achieved over a short period and with low efficiency of conversion to biomass. On the other end, some microbes could aim at consuming resources slowly and efficiently, but in such a case, resources could be lost before they are consumed, because of abiotic processes or other organisms. Finding the optimal foraging strategy and the decomposition kinetics emerging as outcomes of this optimization problem frames the scope of this contribution.

Specifically, we ask:

1. Is there an optimal decomposition rate that maximizes total microbial growth for a given substrate amount?
2. Are the optimal decomposition kinetics consistent with established empirical or theoretical decomposition kinetics?
3. How does the optimal decomposition rate vary with microbial traits?
4. Are any trade-offs between growth rate and carbon-use efficiency emerging from the optimal decomposition strategy?

These questions are addressed by interpreting organic matter decomposition as an optimal control problem, which is solved analytically. The problem is set up in a general way, so that the derived equations can be applied to different decomposition systems, but we illustrate results for terrestrial litter decomposition as a case study.

2. Methods

A simple carbon (C) cycling model with a single substrate mass balance is presented first (Section 2.1), followed by the optimality conditions and the boundary conditions for the optimization (Sections 2.2 and 2.3). The equations describing microbial physiology are presented next (Section 2.4). The following Sections 2.5 and 2.6 detail the derivation of the analytical solution. Finally, the efficiency of the decomposition system is defined in Section 2.7. The model schematic is shown in Figure 1 and the symbols are explained in Table 1.

2.1. Carbon cycling model

We start from the premise that microbial decomposers aim at maximizing their growth rate (g) over a time interval t_τ that is not prescribed, but allowed to emerge as a result of the optimization. Growth is achieved by assimilating organic C, which we assume is the main limiting substrate and energy provider (Figure 1). A single cohort of organic C is denoted by c (expressed as mass of C in the system), and its mass loss during decomposition is described. The C compartment is assumed chemically homogeneous for simplicity (well-mixed approximation). Mass loss is caused by microbial-driven decomposition at rate u, which is not specified *a priori* as typically done in biogeochemical models, but is instead derived as a result of the optimization. We assume that all decomposed C is taken up, so that decomposition and uptake rates are equal to u. Physical processes such as leaching and adsorption, or uptake by other organisms, also contribute to the depletion of substrate C, following first-order kinetics (with rate constant γ). The parameter γ is thus a measure of substrate C availability – higher γ implies faster losses due to abiotic or biotic factors that cannot be controlled by the microbial biomass. Microbial biomass is assumed in quasi-equilibrium, so that mortality equals growth. A fraction μ of microbial necromass production is assumed to be recycled in the substrate compartment. Building on these assumptions, the mass balance equation of the organic matter cohort can thus be written as,

$$\frac{dc}{dt} = -u - \gamma c + \mu g, \quad c(0) = c_0. \tag{1}$$

2.2. Microbial growth as an optimal control problem

The microbial growth optimization problem can be formulated as the maximization of

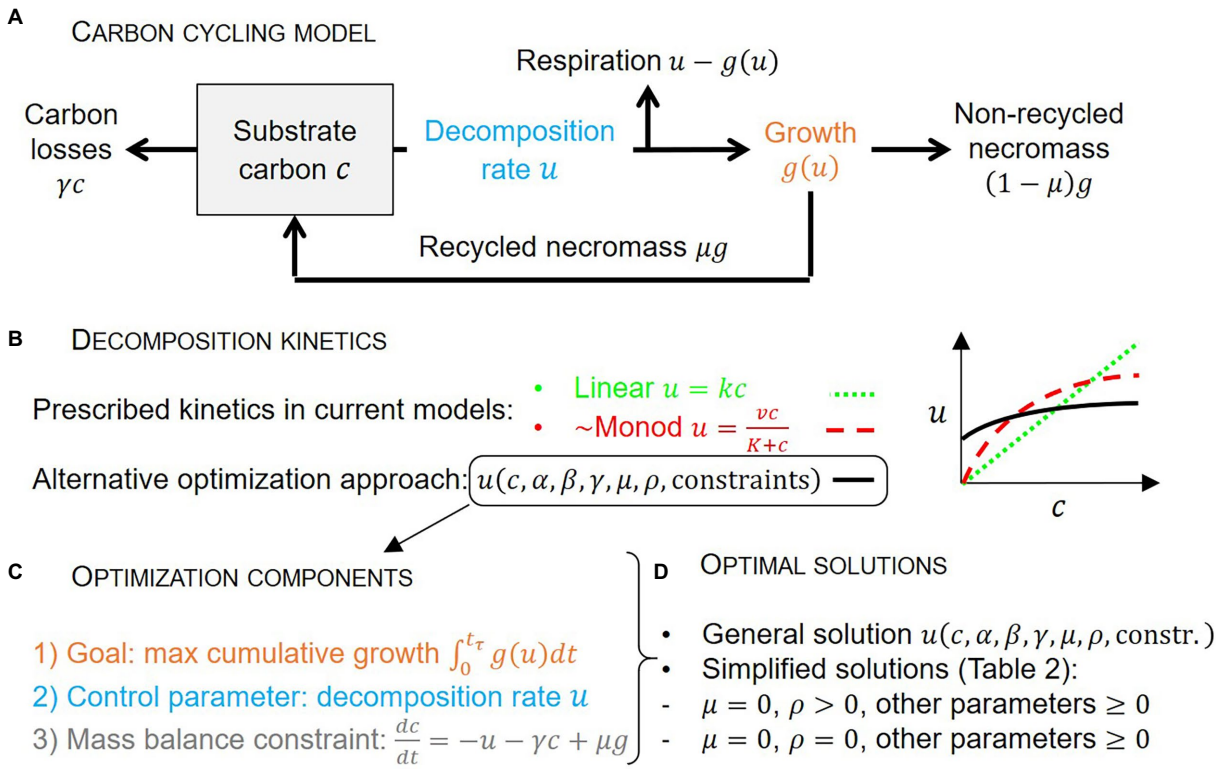

FIGURE 1
Schematic of the carbon cycling model **(A)**, approaches to describe decomposition kinetics **(B)**, main components of the microbial growth optimization problem **(C)**, and optimal solutions **(D)**. Symbols are defined in panel **(A)** and Table 1.

$$J = \int_0^{t_\tau} g(u)\,dt, \tag{2}$$

with free terminal time t_τ and no terminal gain, and subject to the mass-balance constraint in Equation (1). This constitutes an optimal control problem with control u bound to be larger than zero.

Necessary conditions for the optimization can be expressed in terms of the Hamiltonian (H) and a Lagrange multiplier (λ) as (Kirk, 1970; Lenhart and Workman, 2007)

$$H = g + \lambda \frac{dc}{dt} = g + \lambda(-u - \gamma c + \mu g), \tag{3}$$

$$0 = \frac{\partial H}{\partial u} = g' + \lambda(-1 + \mu g'), \tag{4}$$

$$-\frac{d\lambda}{dt} = \frac{\partial H}{\partial c} = -\gamma\lambda, \tag{5}$$

where we use the prime notation exclusively for derivatives with respect to u (e.g., $g' = \partial g / \partial u$, $g'' = \partial^2 g / \partial u^2$) and continue with the Leibniz notation for other derivatives.

These necessary conditions are usually referred to as the Pontryagin Maximum Principle, in honor of the man who first proved the theorem in 1956. While the proof of the theorem is quite theoretical (Kirk, 1970), the basic idea is related to optimization in multivariable calculus. If a point x^* in n-dimensional space maximizes a function $g(x)$ subject to the constraint $f(x) = 0$, the Lagrange multiplier rule says that there exists a number λ such that $\nabla g = \lambda \nabla f$ (where ∇ indicates the gradient of the n-dimensional functions g and f). This can be recast as a statement that x^* maximizes the so-called Hamiltonian function $H = g + \lambda f$ (Equation (3)) for some λ. The simplest proof of the version of the maximum principle we are using is based on elementary calculus (Lenhart and Workman, 2007). Assuming the control variable u is the maximizer of the functional $J[u]$ (Equation (2)), we can choose any allowable variation v and assert that the function value $\epsilon = 0$ is the maximizer of the function $J[u + \epsilon v]$. The conditions (4) and (5) follow from this maximization.

In Equations (4) and (5), the first equalities are the general necessary conditions for optimization, and the second equalities represent the optimization conditions specific to this model. The downward concavity of $g(u)$ (Section 2.4) guarantees that the solution is the maximum of J.

Independent of the specifics of $g(u)$, the temporal evolution of the Lagrange multiplier can be obtained by solving Equation (5),

$$\lambda(t) = \lambda_0 e^{\gamma t}, \tag{6}$$

where λ_0 represents the initial condition, to be determined from the boundary conditions of the optimization problem, as described in the following section.

2.3. Boundary conditions for the optimization problem

Equations (4) and (6) provide two conditions to determine the four unknowns $c(t)$, $u(t)$, λ_0, and t_τ. Therefore, two additional conditions are required to mathematically close the problem. These conditions are specified at the terminal time t_τ. Because the terminal time is free, one of the conditions is given by setting the Hamiltonian to zero at $t = t_\tau$. Moreover, at the terminal time, we assume that the C compartment is completely depleted. Taking $c(t_\tau) = 0$ into $H(t_\tau) = 0$ yields

$$g_\tau = \lambda_\tau (u_\tau - \mu g_\tau), \tag{7}$$

where subscript τ indicates evaluation at the terminal time, so that $u_\tau = u(t_\tau)$, $g_\tau = g(u(t_\tau))$, etc. Next, λ_τ in Equation (7) can be eliminated by using Equation (4) in the form,

$$\lambda = \frac{g'}{1 - \mu g'}. \tag{8}$$

Then after evaluating at the terminal time and simplifying we find,

$$g_\tau = u_\tau g'_\tau. \tag{9}$$

2.4. Growth model

The growth rate is expressed as a saturating function of the uptake rate, which as explained above equals the decomposition rate,

$$g(u) = \alpha \frac{u - \rho}{\beta + u}, \tag{10}$$

where α is the maximum growth rate, β is the half-saturation constant, and ρ the rate of substrate uptake used for cellular maintenance. Because growth rate is by definition equal to the uptake rate times the microbial carbon use efficiency (CUE: ratio of growth rate over uptake rate), and $\mathrm{CUE} \le e_{\max} < 1$, the values of the half-saturation constant and the maximum growth rates must be constrained to satisfy these limits. Specifically, we assume that the slope of the $g(u)$ relation at small u (and for negligible ρ) equals $e_{\max}$, so that $\alpha = \beta e_{\max}$. The function $g(u)$ is shown in Figures 2A,B for various parameter combinations.

The concave shape of the $g(u)$ relation implies declining CUE as the decomposition rate u increases. This decline can be caused by different factors that are not included in this model, but that are surrogated by the $g(u)$ relation: (i) The marginal return on investment in extra-cellular enzymes decreases with increasing u because enzyme synthesis is energetically costly (del Giorgio and Cole, 1998) and hydrogen peroxide required for oxidative enzyme functioning may cause cell damage, thereby reducing CUE (Manzoni et al., 2021). (ii) When the microbial population reaches a steady state, the rate of growth will become limited by the enzymatic capacity in the cell and on cell walls (Waldherr et al., 2015). (iii) At high rates of enzyme release, the substrate binding sites may become saturated (Tang and Riley, 2013). (iv) Diffusion of the reaction products eventually becomes limiting (Vetter et al., 1998). (v) In the case of nitrogen-poor substrates, fast decomposition requires intense nitrogen immobilization, and when inorganic nitrogen sources are unavailable either microbial metabolism slows down due to nutrient limitation, or overflow respiration increases (Manzoni et al., 2021). In all these cases, net growth is expected to stabilize around a maximum value that allows cells to grow within their stoichiometric constraints.

With growth described by Equation (10), we can also define the microbial CUE as,

$$\mathrm{CUE} = \frac{g}{u} = e_{\max} \frac{\beta(u - \rho)}{u(\beta + u)}. \tag{11}$$

Higher values of maintenance respiration ρ decrease CUE, potentially causing it to become negative when $u < \rho$. At high values of u compared to ρ and β (plentiful resources), $\mathrm{CUE} \approx e_{\max}\beta / u$. In general, the maximum CUE is attained at intermediate values of u, but it remains below $e_{\max}$.

2.5. Nondimensionalization

Before beginning the analysis, it is helpful to nondimensionalize the problem, which reduces the number of parameters by two. To that end, we define dimensionless variables (see also Table 1):

$$C = \frac{\gamma c}{\beta} \text{ (and initial condition } C_0 = \frac{\gamma c_0}{\beta}),$$

$$U = \frac{u}{\beta},$$

$$T = \gamma t \text{ (and terminal time } T_\tau = \gamma t_\tau),$$

$$\Lambda = \frac{\beta\lambda}{\alpha}\left(\text{and initial condition } \Lambda_0 = \frac{\beta\lambda_0}{\alpha}\right), \tag{12}$$

growth rate.

$$G = \frac{g}{\alpha}\left(\text{and its derivative } G' = \frac{\beta}{\alpha} g'\right), \tag{13}$$

and parameters

$$R = \frac{\rho}{\beta},$$

$$M = \frac{\alpha\mu}{\beta}, \tag{14}$$

With these changes, the problem consists of an initial value problem in the nondimensional substrate concentration C (from Equation (1))

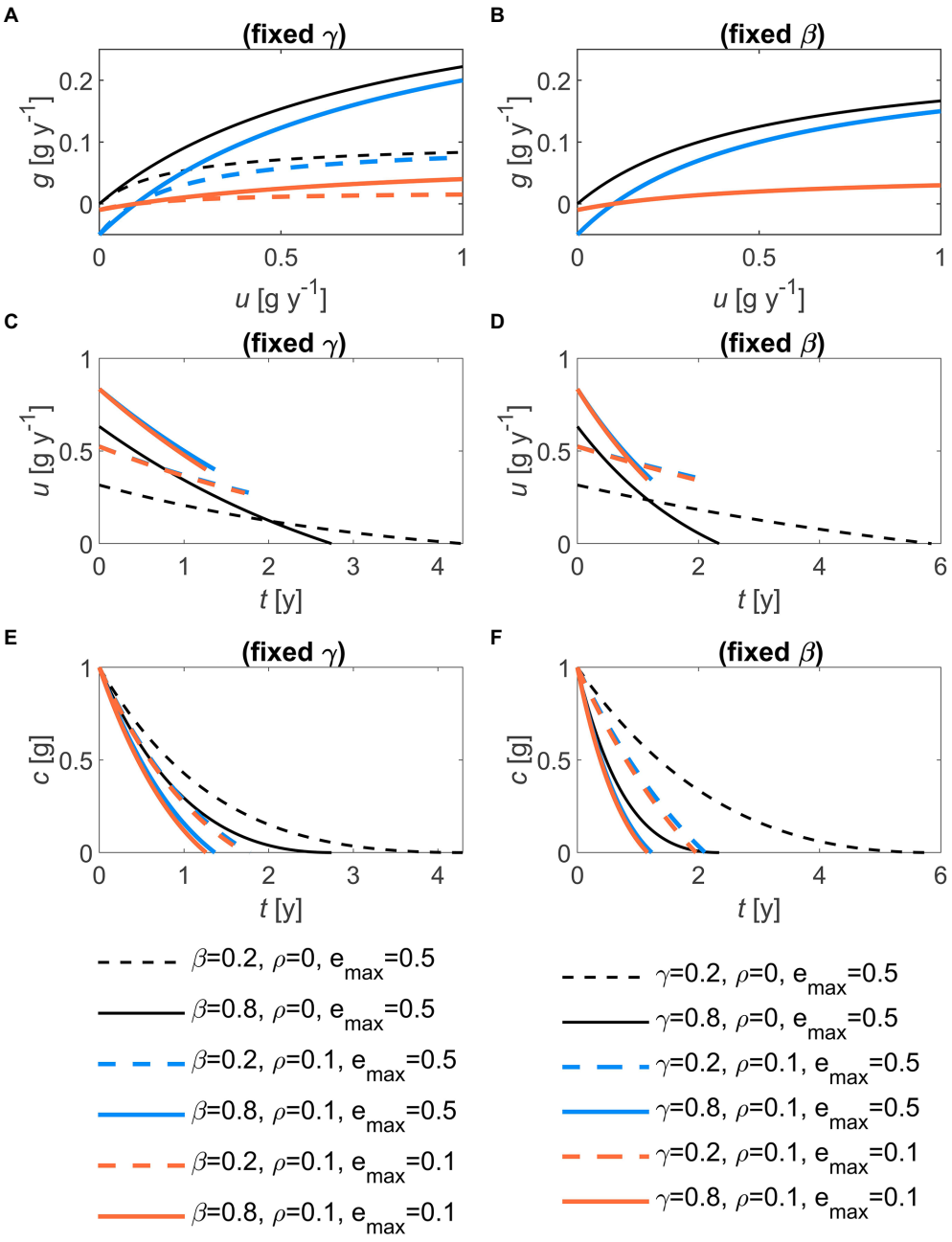

FIGURE 2
Effects of the half saturation constant of the microbial growth rate (β , left panels) and of the first-order decay constant (γ , right panels), for two values of maintenance respiration (ρ) and maximum growth efficiency (e_{max}) on: **(A,B)** the relation between growth rate and decomposition rate, $g(u)$; **(C,D)** the temporal trajectory of the optimal decomposition rate, $u(t)$; and **(E,F)** the temporal trajectory of the substrate carbon, $c(t)$. In all panels: c_0 = 1g, μ = 0.5. In **(B)**, curves with the same γ value overlap, because $g(u)$ does not depend on γ . Parameter units are as in Table 1.

$$\frac{dC}{dT} + C = -U + M\,G, C(0) = C_0, \tag{15}$$

an optimality condition (from Equation (4))

$$G' + L\left(-1 + M\,G'\right) = 0, \tag{16}$$

and terminal conditions (from Equation (9))

$$G_\tau = U_\tau G'_\tau,$$

$$C(T_\tau) = 0, \tag{17}$$

where the subscript τ indicates the terminal time as before. We also define the nondimensional growth rate (from Equation (10)) and its derivative with respect to U,

$$G(U) = \frac{U - R}{1 + U},$$

$$G'(U) = \frac{1 + R}{(1 + U)^2}, \tag{18}$$

TABLE 1 Symbols and units.

Symbol	Explanation	Units	Nondimensional form
Variables and functions			
c, c_0	Substrate C mass	g	$C=\frac{\gamma c}{\beta}$, $C_0=\frac{\gamma c_0}{\beta}$
CUE	C-use efficiency, CUE $=\frac{g}{u}=\frac{G}{U}$	1	
g	Microbial growth rate	g y^{-1}	$G=\frac{g}{\alpha}$
H	Hamiltonian function	g y^{-1}	
S	Reverse nondimensional time, $S=T_\tau-T$	1	
t	Time	y	$T=\gamma t$
u	Decomposition rate	g y^{-1}	$U=\frac{u}{\beta}$
V	Auxiliary variable, $V=1+U$	1	
λ, λ_0	Lagrange multiplier	1	$\Lambda=\frac{\beta\lambda}{\alpha}$, $\Lambda_0=\frac{\beta\lambda_0}{\alpha}$
Parameters			
$e_{\max}$	Maximum microbial growth efficiency	1	
m	Parameter combination, $m=\sqrt{M(1+R)}$	1	
k	Decomposition rate constant in linear kinetics (only used in Figure 7)	y^{-1}	
K	Half saturation constant in monod-type kinetics (only used in Figure 7)	g	
v	Maximum decomposition rate in Monod-type kinetics (only used in Figure 7)	g y^{-1}	
α	Maximum microbial growth rate, $\alpha=\beta e_{\max}$	g y^{-1}	
β	Half saturation constant of the $g(u)$ relation	g y^{-1}	
γ	Rate constant for C losses that are not controlled by the decomposers	y^{-1}	
η	Overall system efficiency	1	
μ	Fraction of necromass production recycled as substrate	1	$M=\frac{\alpha\mu}{\beta}$
ρ	Microbial maintenance respiration rate	g y^{-1}	$P=\frac{\rho}{\beta}$
Subscripts and superscripts			
$'$	Differentiation with respect to u or U		
0	Subscript indicating initial conditions ($t=0$ or $T=0$)		
τ	Subscript indicating evaluation at the terminal time ($t=t_\tau$, $T=T_\tau$, or $S=0$)		

and the nondimensional Lagrange multiplier (from Equation (6))

$$\Lambda(T)=\Lambda_0 e^T. \tag{19}$$

The problem must be solved for parameters U_τ, Λ_0, and T_τ and the variables U and C, after which the dimensional variables and functions can be determined from Equations (12)–(14).

2.6. Analytical solution

We start by substituting the formulas for G and G' (Equation (18)) into the boundary condition in Equation (17) to obtain an equation for decomposition rate at the terminal time,

$$U_\tau=\frac{G_\tau}{G'_\tau}=\frac{(U_\tau-P)(1+U_\tau)}{1+P}. \tag{20}$$

Solving for U_τ we obtain

$$U_\tau = P + \sqrt{P + P^2}, \tag{21}$$

$$G'_\tau = \frac{1+P}{\left(1+U_\tau\right)^2}. \tag{22}$$

The terminal (nondimensional) decomposition rate is therefore only a function of the maintenance respiration rate, and $U_\tau = 0$ when maintenance respiration is negligible. The result $U_\tau > P$ is somewhat surprising, as it means that G does not approach 0 at the end of the decomposition process. This will be a noteworthy feature in graphs of the results. In the subsequent analysis, it is helpful to define an additional function $V = 1 + U$ and parameter $m = \sqrt{M\left(1+P\right)}$. Substituting V into Equation (22) yields the slightly simpler formula

$$G'_\tau = \frac{1+P}{V_\tau^2}, \tag{23}$$

where V_τ is found from the definition of V and Equation (21) as,

$$V_\tau = \sqrt{1+P}\left(\sqrt{1+P} + \sqrt{P}\right). \tag{24}$$

To find Λ_0, we combine the optimality condition of Equation (16) with the solution for Λ of Equation (19), and evaluate at the terminal time,

$$\Lambda_0 = \frac{G'_\tau}{1 - M G'_\tau} e^{-T_\tau} = \frac{1+P}{V_\tau^2 - m^2} e^{-T_\tau}. \tag{25}$$

We now turn to the quantities that are functions of time: G', V, U, and C in turn. These quantities are best understood in reverse time, defined by

$$S = T_\tau - T. \tag{26}$$

G' follows from the optimality condition of Equation (16), since Λ is fully known. After clearing the fractions, we obtain

$$G' = \frac{1+R}{\left(V_\tau^2 - m^2\right)e^S + m^2}. \tag{27}$$

The definition of G' (Equation (18)) then yields

$$V^2 = \left(V_\tau^2 - m^2\right)e^S + m^2, \tag{28}$$

$$U = \sqrt{\left(V_\tau^2 - m^2\right)e^S + m^2} - 1. \tag{29}$$

To obtain the time trajectory of C, we first write the differential equation in reverse time, along with the reverse time initial condition (i.e., applied at $S = 0$, corresponding to $T = T_\tau$). Substituting V for U and simplifying, we have

$$\frac{dC}{dS} = C + V - \left(1+M\right) + \frac{m^2}{V}, C\left(0\right) = 0. \tag{30}$$

This initial value problem has the surprisingly simple solution

$$C = \frac{V^2}{1+P} - 2V + 1. \tag{31}$$

which can be obtained using the integrating factor method and can be confirmed directly from the differential equation by applying the chain rule $\frac{dC}{dS} = \frac{dC}{dV}\frac{dV}{dS}$, with $\frac{dV}{dS}$ from Equation (28).

At this point, we still do not know the terminal time T_τ or the initial value of the decomposition rate U_0. By substituting $V = 1 + U$ into the last result, we can obtain solutions for U and G in turn as functions of C,

$$U = P + \sqrt{\left(1+P\right)\left(C+P\right)}, \tag{32}$$

$$G = \frac{\sqrt{C+P}}{\sqrt{1+P} + \sqrt{C+P}}. \tag{33}$$

From the first of these, we obtain the value of initial U,

$$U_0 = P + \sqrt{\left(1+P\right)\left(C_0+P\right)}. \tag{34}$$

and the corresponding $V_0 = U_0 + 1$,

$$V_0 = \sqrt{1+P}\left(\sqrt{1+P} + \sqrt{C_0+P}\right). \tag{35}$$

Equations (32)–(35) show that the (nondimensional) decomposition rate can be expressed as a function of substrate C and maintenance respiration rate only.

Next, V_τ (Equation (24)) and V_0 (Equation (35)) are substituted into Equation (28), evaluated at $S = T_\tau$, to obtain

$$e^{T_\tau} = \frac{C_0 + 2U_0 + 1 - M}{2U_\tau + 1 - M}. \tag{36}$$

Taking the logarithm yields the terminal time

$$T_\tau = \ln\left(\frac{C_0 + 2U_0 + 1 - M}{2U_\tau + 1 - M}\right). \tag{37}$$

Particularly compact solutions are found when $M = 0$ and/or $P = 0$ (Table 2).

TABLE 2 Analytical solutions of the optimal decomposition problem when $M=0$ or $M=P=0$.

Simplified scenarios:	$M=0,\quad P>0$	$M=0,\quad P=0$
$U(C)$	$P+\sqrt{(1+P)(C+P)}$	$\sqrt{C}$
$u(c)$	$\rho+\sqrt{(\beta+\rho)(\gamma c+\rho)}$	$\sqrt{\beta\gamma c}$
$C(T)$	$(1+2U_\tau)e^{T_\tau-T}-2(1+U_\tau)e^{\frac{T_\tau-T}{2}}+1$	$e^{T_\tau-T}-2e^{\frac{T_\tau-T}{2}}+1$
$U(T)$	$(1+U_\tau)e^{\frac{T_\tau-T}{2}}-1$	$e^{\frac{T_\tau-T}{2}}-1$
T_τ	$\ln\left(\frac{C_0+2U_0+1}{2U_\tau+1}\right)$	$\ln(C_0+2U_0+1)$
η	$\frac{e_{\max}}{C_0}\left[T_\tau-2\frac{1+P}{1+U_\tau}\left(1-e^{-\frac{T_\tau}{2}}\right)\right]$	$\frac{e_{\max}}{C_0}\left[T_\tau-2\left(1-e^{-\frac{T_\tau}{2}}\right)\right]$

2.7. Efficiency of the decomposition system

We define the overall efficiency of the decomposition system as the fraction of initial substrate C that is transferred to other compartments in the form of necromass. This definition is motivated by the argument that stabilized soil organic C is largely composed of microbial necromass (Liang et al., 2017), so that decomposition is efficient from the point of view of C storage when it results in a large net export of necromass. Accordingly, we define

$$\eta=\frac{(1-\mu)J}{c_0}=\frac{e_{\max}(1-\mu)}{C_0}\int_0^{T_\tau}G(U(T))dT, \qquad (38)$$

where J is the cumulative growth rate, which is maximized in the optimization problem (Equation (2)). Using this definition, we find

$$\eta=\frac{e_{\max}(1-\mu)}{C_0}\left\{T_\tau-2\frac{1+P}{m}\ln\left[\frac{V_\tau+m}{\sqrt{V_\tau^2-m^2\left(1-e^{-T_\tau}\right)}+me^{-\frac{T_\tau}{2}}}\right]\right\}. \qquad (39)$$

More compact formulas for η are reported in Table 2 for the simpler cases with $M=0$ and/or $P=0$.

2.8. Model parameters

The model is meant to represent a generic system where decomposers forage on a single cohort of a chemically homogeneous substrate in the absence of additional C inputs. For illustration, we chose parameter values broadly representing the decomposition of 1 g C of plant litter by microbial saprotrophs (for conciseness, in the following we do not specify 'C' in the units).

We expect that litter is decomposed over time scales of years, so that $0<\gamma\le1$ y^{-1} (when studying CUE-growth trade-offs, we allow γ to reach as high as 10^4 y^{-1} for illustration). Consistent with these characteristic timescales and initial substrate C values, β is allowed to vary in the range $0<\beta\le1$ g y^{-1}. The maximum growth efficiency is set to $e_{\max}=0.5$, but we also consider values within the plausible range $0<e_{\max}\le0.8$ (Manzoni et al., 2017). The maintenance respiration rate is varied in the range $0\le\rho\le0.4$ g y^{-1}. There is no consensus on the fraction of decomposer necromass that is recycled as a substrate. Depending on the specific microorganism and environmental context, necromass can be labile or recalcitrant, but can also be stabilized *via* adsorption and occlusion within soil aggregates. For labile necromass that is re-used as substrate, $\mu=1$, whereas for recalcitrant or otherwise not bioavailable necromass, $\mu=0$. Therefore, we explore the full range $0\le\mu\le1$.

Empirical and optimization models for decomposition were compared using a litterbag decomposition time series. To meet the model assumptions, we selected litter of *Swida controversa*, which is characterized by relatively low lignin content (to ensure a relatively homogeneous substrate) and high initial nitrogen content (to avoid nutrient limitation), and that was almost completely degraded by the end of the field incubation (data from "upper site" in Osono and Takeda, 2005). Linear ($u=kc$), Monod-type ($u=\frac{vc}{K+c}$), and optimization-based kinetics were used to fit the time series of remaining litter C. The three models shared the same structure (including respiration and necromass recycling, as in Figure 1A), and only varied by their decomposition kinetics. Parameters k (linear model), v and K (Monod model), and β and ρ (optimization model) were estimated by nonlinear least square fitting. For all models, we set $\gamma=0.8$ y^{-1}, $e_{\max}=0.5$, $\mu=0.5$.

3. Results

In the Results section, the solutions are shown in dimensional form for ease of interpretation, and to illustrate the role of individual parameters on optimal u, and corresponding g and c, during the decomposition process. We start by presenting solutions as a function of time and remaining substrate C (Section 3.1). Next, we illustrate variations in initial decomposition rate and terminal time as microbial traits encoded in model parameters are changed (Section 3.2). Last, we present evidence of

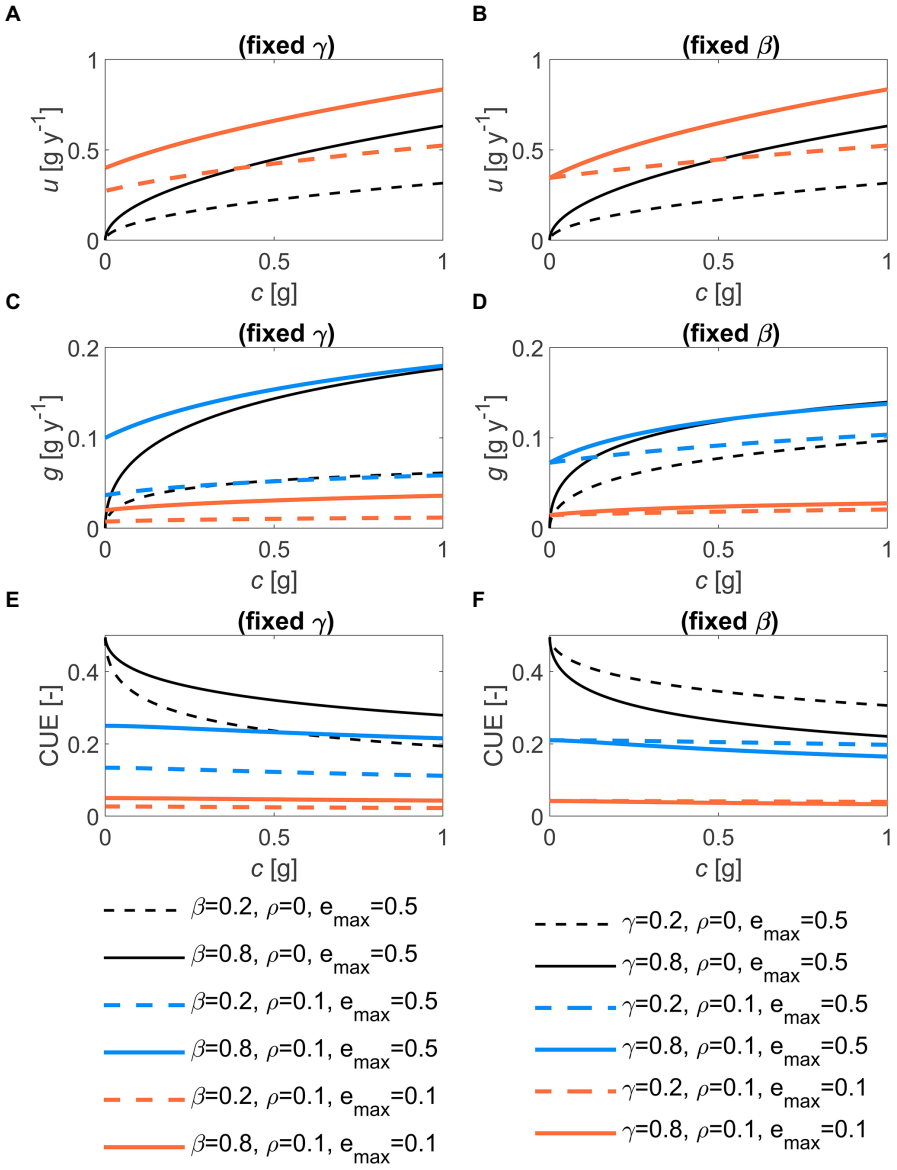

FIGURE 3
Effects of the half saturation constant of the microbial growth rate (β , left panels) and of the first-order decay constant (γ , right panels), for two values of maintenance respiration (ρ) and maximum growth efficiency (e_{max}) on: **(A,B)** the relation between optimal decomposition rate and substrate carbon, $u(c)$; **(C,D)** the relation between optimal growth rate and c, $g(c)$; and **(E,F)** the relation between microbial C-use efficiency (CUE) and c. In all panels: c_0 = 1g, μ = 0.5. Parameter units are as in Table 1.

CUE-growth rate trade-offs and describe patterns in system efficiency when microbes face increasingly large abiotic C losses (Section 3.3).

3.1. Optimal decomposition kinetics and substrate C trajectories

The optimal decomposition rate decreases through time, but it reaches zero at the terminal time only if maintenance respiration is set to zero (Figures 2C,D). Increasing the rate of uncontrolled losses γ or the half saturation constant β (proportional to the maximum growth rate) increases the initial values of u (from dashed to solid lines in Figure 2). However, this more rapid initial depletion of the substrate causes u to decrease faster at higher γ or β. As a direct consequence of the patterns in u in combination with the uncontrolled losses, substrate C decreases faster with higher values of γ or β (Figures 2E,F). Decomposition is also faster at any time point when maintenance respiration is larger than zero, because decomposition is promoted to compensate for maintenance C costs, compared to a scenario without maintenance respiration (compare colored and black lines in Figures 2C,D). Lower maximum growth efficiency (e_{max}) slows down microbial growth, but marginally affects u and substrate C decline (orange vs. blue curves in Figure 2). Notably, necromass recycling does not affect u (Equation (32)), but slightly delays the decline in substrate C thanks to the partial recycling of C that would be otherwise lost from the system (not shown).

The shape of the optimal decomposition kinetics is best illustrated by plotting u as a function of substrate C (with time progressing as c is depleted). The $u(c)$ function is concave downward, scaling approximately as $c^{1/2}$ with an intercept larger than zero at $c = 0$ when maintenance respiration is present (Figures 3A,B). This means that the optimal decomposition rate does not reach zero at the terminal time. Consistent with the time trajectories in Figure 2, increasing γ or β shifts the $u(c)$

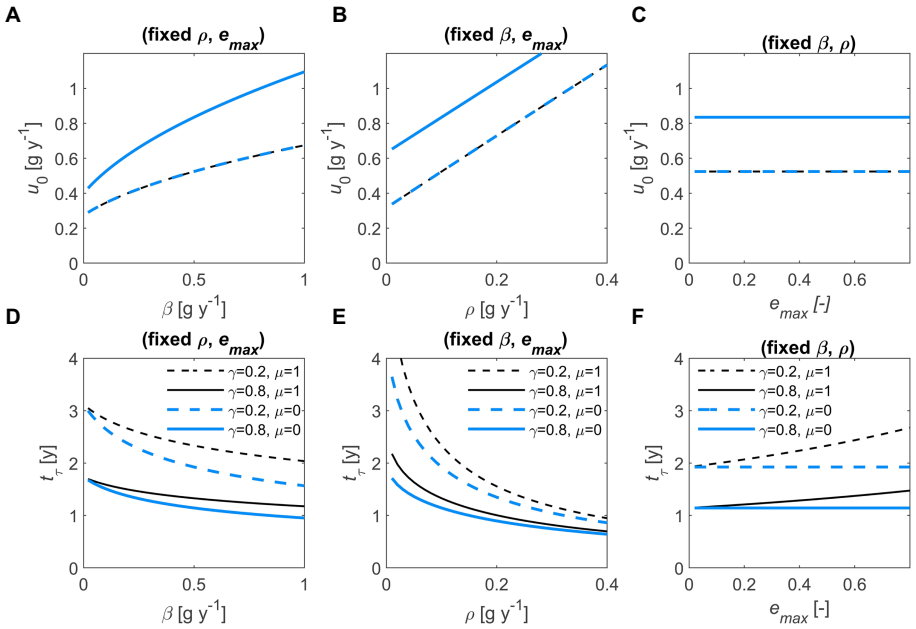

FIGURE 4
Effect of half saturation constant (β , left column), maintenance respiration rate (ρ , central column), and maximum microbial growth efficiency (e_{max} , right column) on initial optimal decomposition rate (u_0 , top row) and terminal time (t_τ , bottom row), for two values of the first-order decay constant (γ , dashed vs. solid) and the necromass recycling fraction (μ , black vs. blue). Other parameters: c_0 = 1g (all panels), ρ = 0.1g y^{-1} **(A,C,D,F)**, β = 0.5g y^{-1} **(B,C,E,F)**, e_{max} = 0.5 **(A,B,D,E)**. In **(A–C)**, lines with different values of μ overlap because u_0 is independent of μ . In all panels: c_0 = 1g. Parameter units are as in Table 1.

curves upwards. The optimal growth rate broadly follows the patterns of u, but the decline of g near $c = 0$ is delayed compared to u (Figures 3C,D). As a result, the CUE increases during decomposition (i.e., with decreasing c) in the absence of maintenance costs, while it remains approximately stable otherwise (Figures 3E,F). Lower e_{max} decreases both g and CUE (orange vs. blue curves in Figure 3).

3.2. Initial decomposition rate and terminal time

The initial u increases with γ and β , whereas it is independent of e_{max} and μ (Figures 4A–C). The terminal time t_τ also depends on γ and β , showing inverse trends compared to u because faster decomposition implies shorter t_τ (Figures 4D–F). When necromass is recycled, the time to consume all the substrate increases (blue vs. black curves in Figures 4D,F). Similarly, higher values of e_{max} – by promoting C retention in the system – lengthen the decomposition process, although this effect appears only when $\mu > 0$ (Figure 4F).

3.3. C-use efficiency-growth trade-offs and system efficiency

Varying the rate of C losses γ drives changes in the initial decomposition rate, growth rate, and CUE. As both these rates increase, initial CUE decreases (Figure 5 shows the relation between CUE and growth rate), implying a rate-efficiency trade-off along environmental gradients where resource losses vary. The trade-off is stronger when $\rho = 0$ (black curves in Figure 5), because maintenance respiration tends to reduce variations in CUE (Figures 3E,F). Moreover, decreasing e_{max} shifts the trade-off relations towards lower CUE values and lower initial growth rates (orange vs. blue curves in Figure 5).

The overall system efficiency (η), decreases as substrate C losses increase (Figure 6). Such a decrease can be compensated by a

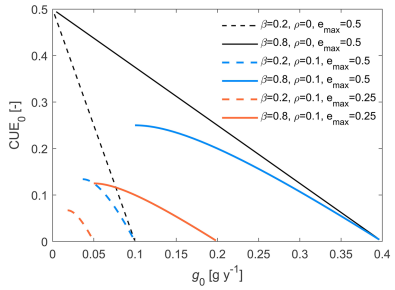

FIGURE 5
Trade-off between initial microbial C-use efficiency (CUE_0) and initial growth rate (g_0), when varying the C loss rate constant (γ , increasing from 10^{-4} to 10^4 y^{-1} left to right along the curves). Line styles refer to different combinations of the half saturation constant (β), maintenance respiration rate (ρ), and maximum microbial growth efficiency (e_{max}). Other parameters: c_0 = 1g, μ = 0.5. Parameter units are as in Table 1.

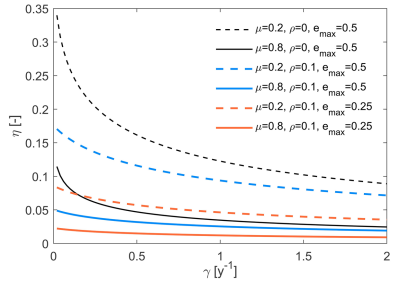

FIGURE 6
Whole system efficiency (g) as a function of the C loss rate constant (γ). Line styles refer to different combinations of the fraction of necromass recycled (μ), maintenance respiration rate (ρ), and maximum microbial growth efficiency (e_{max}). Other parameters: c_0 = 1g, β = 0.5g y^{-1}. Parameter units are as in Table 1.

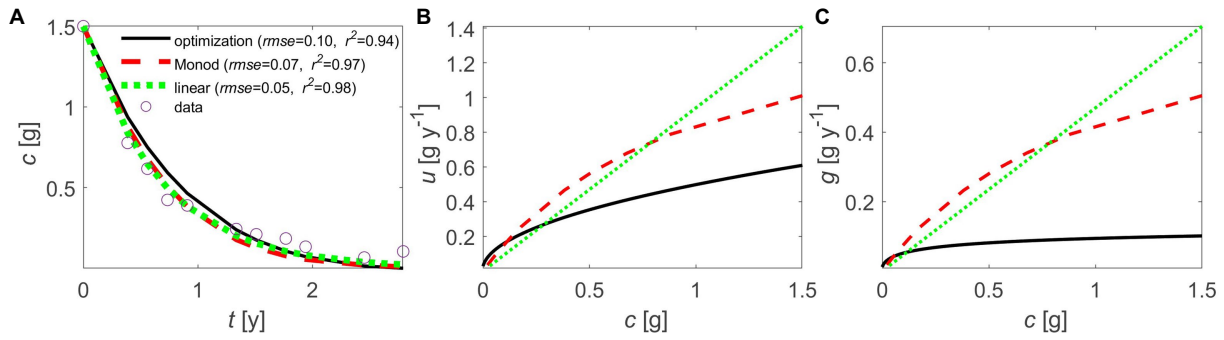

FIGURE 7
Comparison of linear ($u = kc$), Monod-type ($u = \frac{vc}{K + c}$), and optimal decomposition kinetics to describe litter C mass loss: **(A)** temporal trajectory of litter C (c) and model fitting performance (RMSE: root mean square error; R^2: coefficient of determination), **(B)** decomposition rate as a function of litter C ($u(c)$), and **(C)** microbial growth rate as a function of litter C ($g(c)$). Data are from Osono and Takeda (2005); see details on model fitting in Section 2.8 (linear model parameter: k=0.94 y^{-1}; Monod model parameters: v=1.68g y^{-1}, K=1.00g; optimization model parameters: β = 0.3g y^{-1}, ρ = 0.002g y^{-1}).

lower fraction of necromass recycled (dashed vs. solid lines), a lower rate of maintenance respiration (black vs. colored lines), or a higher e_{max} (blue vs. orange curves in Figure 6). The strong effect of necromass recycling is explained by our definition of system efficiency as the fraction of initial C that is transferred to stabilized forms (i.e., that is not recycled as a labile substrate). The latter two parameters (ρ , e_{max}) instead regulate C retention in biomass, and thus how much of the C that microbes take up can be eventually stabilized.

4. Discussion

We proposed an optimization approach to define decomposition kinetics, based on the idea that decomposition is an emergent property of complex microbial dynamics that might be difficult to capture with prescribed kinetics. In our approach, maximum growth is attained by balancing C gains from substrate uptake and C costs for substrate acquisition, maintenance, and growth. This simple principle has already been applied to describe various aspects of decomposition (see a short review of the literature in Section 4.1), but not to our knowledge to define the shape of the decomposition kinetics or changes in decomposition rate through time. The advantage in doing so is that the optimal kinetics structurally account for environmental conditions (resource limitation setting constraints on the optimization) and physiological trade-offs. In contrast, models with prescribed kinetics can only account for these effects through time invariant parameter which might not offer sufficient flexibility to capture microbial adaptations. This advantage might prove particularly important when studying microbial responses to combined climate and land use changes, which challenge microbial communities in ways difficult to replicate in experiments.

4.1. Is there an optimal decomposition rate that maximizes total microbial growth for a given substrate amount?

Describing the decomposition process as an optimal control problem allows for determining the decomposition rate that maximizes microbial growth over the decomposition period. This approach builds on the Darwinian principle that organisms able to maximize their fitness (reproductive success, which translates into biomass growth for soil microbes) should be selected by evolutionary processes (Harrison et al., 2021). This idea has been exploited in previous theoretical works. For example, enzyme synthesis for competing cellular processes (Baloo and Ramkrishna, 1991), cell wall transporter abundance (Casey and Follows, 2020), internal cell composition (Franklin et al., 2011; Maitra and Dill, 2015), allocation to extra-cellular enzymes (Vetter et al., 1998; Averill, 2014; Wutzler et al., 2017; Calabrese et al., 2022), rates of specific metabolic reactions (Vallino et al., 1996), or allocation of C to growth vs. respiratory processes (Manzoni et al., 2017) can be optimized. However, in most of these approaches, the growth rate was maximized at a given time and for given conditions, neglecting an essential feature of decomposition systems – the limiting resources are finite and maximizing growth or consumption rates can lead to a rapid, and suboptimal, resource depletion. Here we approach the problem from the alternative perspective of optimal decomposition rate constrained by limited resource availability.

We found that there is indeed an optimal decomposition rate that allows microbes to effectively 'compete' with biotic or abiotic processes that remove C substrate from the system. Decomposition rates higher than the optimal would result in faster growth, but for a shorter time and at a relatively lower CUE. In contrast, slower rates would leave more substrate to the competitors or to abiotic processes removing resources from the system, leading to lower growth over the whole decomposition period. As substrate losses decrease (lower γ), the optimal decomposition rate is reduced while decomposition time (i.e., terminal time) increases, maximizing the cumulative growth. Notably, the optimal decomposition rate tends to zero in the absence of substrate losses ($\gamma = 0$). This mathematical result suggests that microbes invest energy and nutrients in the production of extra-cellular enzymes as long as there is an evolutionary pressure to do so – if the substrate always remained available through time, microbes would not evolve costly acquisition strategies.

An optimal balance between resource use and time to deplete the resource emerges also in other ecological contexts. For example, plant transpiration rate can be optimized (*via* regulation of stomatal conductance) to maximize plant net C assimilation. This problem has been formulated – as for decomposition models – as an instantaneous maximization problem (e.g., Bassiouni and Vico, 2021 and references therein) or an optimal control problem including the constraint that soil

water is limited (Manzoni et al., 2022). The advantage of formulating resource consumption problems by formally accounting for resource availability constraints (limited substrate C, or soil water in the case of plant growth) is that the optimal solution naturally captures the consumption rate-time trade-off that is inherent in these problems. Approaches based instead on instantaneous maximization can lead to sub-optimal solutions (Feng et al., 2022).

4.2. Are the optimal decomposition kinetics consistent with established empirical or theoretical decomposition kinetics?

Most optimization approaches focused on finding optimal model parameter values for prescribed kinetics of decomposition (Baloo and Ramkrishna, 1991; Averill, 2014; Wutzler et al., 2017; Casey and Follows, 2020; Calabrese et al., 2022). Here instead we do not prescribe any specific kinetics of decomposition, but let that emerge from the optimization. The optimal decomposition rate is in fact obtained analytically as a function of C availability during decomposition.

The optimal kinetics of decomposition scale as the square root of substrate C (Figures 3A,B; Table 2). As a consequence, the optimal growth rate resembles the Monod-type decomposition functions often used in models of microbial growth in cultures (Monod, 1949) and then re-purposed for soil C cycling models (see Manzoni and Porporato, 2009 for a review), although in our optimal solution substrate C appears under square root. The Monod form emerges from the combination of transport and uptake limitations or competing chemical reactions and physical processes (Liu, 2007; Tang and Riley, 2019). In contrast, here the curvature of the optimal decomposition rate vs. C concentration relation is due to two factors: decreasing returns at high decomposition rates (Equation (10)) and higher rates required to compete with other processes removing substrate C from the system.

It is noteworthy that even without prescribing specific mechanisms of C release from the substrate (enzymatic reaction kinetics, extra-cellular enzyme synthesis) and transport from the site of decomposition to the cells (diffusion, advection), we obtain optimal kinetics that have similar downward concavity as previously proposed kinetics laws. This similarity is apparent when fitting empirical and optimal kinetics to the same litter decomposition dataset (Figure 7). The optimal kinetics perform as well as linear or Monod-type kinetics, at least in the case study of a relatively homogeneous and labile litter we selected for illustration (Figure 7A). The optimal and Monod-type $u(c)$ and $g(c)$ relations share some qualitative similarities – e.g., downward concavity and convergence to $u \sim 0$ at low c. However, they both differ from the simpler linear kinetics that do not saturate at high values of c.

In contrast to Monod-type relations, as the substrate concentration decreases, the optimal kinetics tend to zero only when maintenance respiration is negligible, whereas in general they converge to a value larger than zero, and for small values of maintenance respiration, $u \sim \sqrt{\rho}$. This behavior is due to the presence of maintenance costs that require fast decomposition at low substrate to maintain positive growth even at the end of the decomposition process. This result can be contextualized by recalling that our model describes dynamics in homogeneous conditions. We can then consider a collection of homogeneous litter (or soil) patches that are internally homogeneous, but that differ in initial C or environmental conditions. The terminal times in each of these patches will differ, resulting in the superposition of patch-scale $u(c)$ curves that could cause a tapering off of the C decay trajectory at the macroscopic scale when some patches have very long terminal times. Other processes not included here, such as dormancy, could also lengthen the decomposition process. We speculate that these effects could explain why empirical kinetics reach zero at low substrate concentrations and thus appear to be sub-optimal.

Moreover, different from classical microbial growth kinetics, the optimal decomposition rate increases with increasing rate of resource loss. While there is a clear ecological explanation for this effect (Section 4.1), we can also interpret γ from a physical perspective for the case study of terrestrial litter decomposition. Leaching of organic C could be modelled as the product of the medium hydraulic conductance and C concentration, so that γ is interpreted as hydraulic conductivity for a given litter layer thickness. In turn, soil hydraulic conductivity scales as medium water content to a power typically higher than 10 for soils (Rodriguez-Iturbe and Porporato, 2004), suggesting a strong nonlinear control of water content on C losses in moist conditions. Because optimal decomposition scales as the square root of γ, we can expect it to also scale as water content to a power ~ 5. This result suggests that decomposition rates in wet – but still oxic – environments should have evolved in such a way as to increase more than linearly with water content just to contrast hydrological-driven C losses.

The similarities of the optimal and empirical kinetics suggest that the proposed equations could be tested in soil C cycling models as an alternative to currently employed kinetics (Figure 1B). There are major differences between the idealized model structure we adopted and the multi-compartment structures of most C cycling models, and the parameters in our formulation (e.g., β and ρ) are not widely available, hindering a direct application of our solutions in C cycling models. However, it would be interesting to test if kinetics with the same functional form as the optimal solution, but with parameters to be calibrated, perform well once included in the more complex C cycling models. This approach rests on the assumption that each compartment of these models behaves like one substrate-microbial biomass pair as conceptualized here. An application of this approach is illustrated in Figure 7 for a relatively homogeneous litter type.

4.3. How does the optimal decomposition rate vary with microbial traits?

Microbial traits encoded in model parameters affect the optimal decomposition rate mostly *via* the half saturation constant of the growth function (β) and the rate of maintenance respiration (ρ). Higher maximum microbial CUE and the fraction of recycled necromass increase the terminal time of decomposition because they promote C retention in the system, but they do not affect the optimal decomposition rate *per se* (Figure 4).

The effect of β can be explained by recalling first that growth is also rescaled by β to ensure that CUE remains lower than one. This means that β also regulates the maximum growth rate. Therefore, microbes with higher growth capacity should evolve a matching decomposition capacity, even if the relation between these two traits is predicted to be nonlinear, with decomposition rate scaling as the square root of β (Table 2). Higher maintenance costs require an increased decomposition rate to ensure positive net growth (Section 4.2), so increasing ρ promotes faster decomposition (Figure 4B; Table 2), even

though microbial CUE is decreased. Moreover, if both β and ρ exhibit similar sensitivities to environmental conditions, that sensitivity will be retained in the decomposition rate, because u scales linearly with ρ and $\sqrt{\beta\rho}$ (Table 2). For example, physiological responses to warming in terms of changes in ρ and β should be reflected by similar temperature dependence of the overall decomposition rate.

4.4. Are any trade-offs between growth rate and CUE emerging from the optimal decomposition strategy?

It has been hypothesized that CUE could exhibit an inverse relation with decomposition or growth rate when comparing different microbial resource use strategies, due to increasing inefficiencies at high rates (Roller and Schmidt, 2015). The occurrence of such a relation is debated – there is both supporting (Muscarella et al., 2020) and contrasting (Calabrese et al., 2021) evidence of CUE-growth rate trade-offs across isolates grown in laboratory studies. However, this trade-off can occur in whole soil microbial communities (Lipson et al., 2009) that have adapted to a range of competition pressures (Lipson, 2015). High CUE and low resource acquisition are expected to be selected in high-resource environments (high yield strategy, 'Y'), while high resource acquisition and low CUE would be selected in low-resource and highly competitive conditions (acquisition strategy, 'A') (Malik et al., 2020). Consistent with this conceptual understanding, we found that microbial CUE decreases with increasing optimal decomposition or growth rate when the risk of losing C is higher (increasing γ; Figure 5) or when initial C is lower (results not shown) – i.e., when the long-term resource availability decreases.

The tradeoff we found is also consistent with results from another optimization approach, where the allocation of resources to growth (equivalent to our CUE) was the control variable (Frank, 2010). In that framework, microbial populations with lower CUE were selected when the expected survival time of the population was shorter, suggesting that environments with high rate of resource loss (high γ) or subjected to frequent disturbances should select strains with fast, but inefficient, growth.

The shape of the CUE-growth trade-off varies with ρ. Higher maintenance costs, by promoting high optimal decomposition rates, also keep microbes far from the high-efficiency growth that would occur at low decomposition rate and $\rho = 0$. As a result, the CUE-rate inverse relation flattens as ρ is increased. This result is qualitatively consistent with empirical evidence that the CUE-growth rate relation is negative in microbes with high efficiency (low maintenance costs) and relatively flat in microbes with low efficiency (high maintenance costs) (Muscarella et al., 2020).

4.5. Model limitations and extensions

The proposed model, with a single substrate pool and a single microbial pool, is relatively simple to analyze, allowing full analytical tractability. While this 'minimal' model offers clear insights on the optimal kinetics and their consequences on the substrate C balance, it misses potentially important biological, biochemical, and ecological factors. From a biological perspective, we did not study how specific metabolic processes might be optimized, but focused on the macroscopic effect of such processes on decomposition capacity (expressed through the control variable u). As a first step towards improved biological realism, maintenance respiration could be coupled to decomposition capacity by assuming that higher capacity is possible thanks to higher respiratory costs for synthesizing enzymes (as in Calabrese et al., 2022, but in a temporally dynamic context). As an alternative, complex metabolic networks have been analyzed using optimization methods to predict biomass growth and substrate consumption rates (Vallino, 2010; Waldherr et al., 2015; Giordano et al., 2016). While less mechanistic, our approach shows the kinetics of decomposition that would emerge had the decomposers been optimally adapted.

Perhaps the main limitation of our approach is that it postulates that the whole microbial community adapts in the same way. Clearly, competition, mutualism, and predation shape microbial community dynamics (Allison, 2014; Abs et al., 2020; Sokol et al., 2022), providing evolutionary pressures to exploit different niches. However, one could argue that as a first approximation, the (optimal) behavior of a representative organism in the community could be identified and used to characterize the average system dynamics. Studying the aggregated dynamics instead of letting it emerge from the underlying interactions is prone to aggregation errors (Chakrawal et al., 2020), but at least it allows identifying the main controlling factors in a transparent way. For example, CUE at community level varies along nutrient availability gradients as predicted by a community level optimality criterion (Manzoni et al., 2017). In plant communities, most species exhibit traits converging towards the community weighted mean, also suggesting some degree of coordination in the way plants within the community acclimate and adapt (Muscarella and Uriarte, 2016). This evidence supports our assumption that – as a first approximation – optimality criteria can be applied at the community level.

This interpretation, however, can be problematic when investigating long-term processes such as decomposition. In fact, as litter is decomposed, the microbial community undergoes successional dynamics (Berg and McClaugherty, 2003). We incorporated shifts in community composition from low-efficiency, fast-growing organisms (r-strategists) to high-efficiency, slow-growing ones (K-strategists) through the shape of the $g(u)$ relation. Therefore, rather than predicting the outcome of succession, our model is constrained by its occurrence in terms of varying CUE. The optimal u we obtain should then be interpreted as the realized decomposition rate that maximizes the community-level growth over the decomposition process, regardless of the specific actors involved at any particular time during the process.

Previous contributions have explored optimal allocation to enzymes targeting different compounds (Averill, 2014; Wutzler et al., 2017), but not in a dynamic context where the goal function is cumulative biomass growth, as done here. Other efforts focused on the selection process *per se*, by modelling interacting microbial taxa (Allison, 2014; Abs et al., 2020), but translating those results into easily applicable kinetics laws is difficult. Including multiple substrate pools and enzymes targeting specific substrates in our optimal control framework would thus complement these previous works. Moreover, microbial biomass dynamics could be explicitly represented by an additional mass balance constraint. Along these lines, considering also different microbial functional groups would allow addressing the current limitation that optimization is performed at the community level, but would also raise additional questions – should all groups behave optimally given the presence of the other groups? Or should we postulate an 'ecosystem level' optimality criterion (Dewar, 2010)?

5. Conclusion

Starting from the assumption that the decomposition rate is optimized to maximize microbial growth, we have developed an analytical model of organic matter decomposition. When neglecting maintenance respiration, the optimal decomposition kinetics scale as the square root of the substrate C content, so that the growth rate follows a Hill function with exponent ½. In a more general case, including maintenance respiration, optimal kinetics diverge from typical Hill functions, for example by prescribing high decomposition rates even when substrates are nearly exhausted. The evolutionary pressure for performing rapid decomposition is provided here by the risk of losing resources to abiotic processes or other organisms. When such a risk increases, the optimal microbial foraging strategy shifts from high efficiency growth and slow decomposition rates to low efficiency growth and fast rates. Therefore, a growth efficiency-rate trade-off emerges along gradients of increasing pressure to use limiting resources.

Data availability statement

The original contributions presented in the study are included in the article/Supplementary material, further inquiries can be directed to the corresponding authors.

Author contributions

SM designed the study, constructed the model, and drafted the manuscript. AC contributed to the model design and numerical solution. GL derived the analytical solution of the model. All authors contributed to the article and approved the submitted version.

Funding

This project has received funding from the European Research Council (ERC) under the European Union's Horizon 2020 Research and Innovation Programme (grant agreement no 101001608).

Conflict of interest

The authors declare that the research was conducted in the absence of any commercial or financial relationships that could be construed as a potential conflict of interest.

Publisher's note

Supplementary material

The Supplementary material for this article can be found online at: https://www.frontiersin.org/articles/10.3389/fevo.2023.1094269/full#supplementary-material

References

Abramoff, R., Xu, X. F., Hartman, M., O'Brien, S., Feng, W. T., Davidson, E., et al. (2018). The millennial model: in search of measurable pools and transformations for modeling soil carbon in the new century. *Biogeochemistry* 137, 51–71. doi: 10.1007/s10533-017-0409-7

Abs, E., Leman, H., and Ferriere, R. (2020). A multi-scale eco-evolutionary model of cooperation reveals how microbial adaptation influences soil decomposition. *Commun. Biol.* 3:520. doi: 10.1038/s42003-020-01198-4

Allison, S. D. (2012). A trait-based approach for modelling microbial litter decomposition. *Ecol. Lett.* 15, 1058–1070. doi: 10.1111/j.1461-0248.2012.01807.x

Allison, S. D. (2014). Modeling adaptation of carbon use efficiency in microbial communities. *Front. Microbiol.* 5, 1–9. doi: 10.3389/fmicb.2014.00571

Averill, C. (2014). Divergence in plant and microbial allocation strategies explains continental patterns in microbial allocation and biogeochemical fluxes. *Ecol. Lett.* 17, 1202–1210. doi: 10.1111/ele.12324

Baloo, S., and Ramkrishna, D. (1991). Metabolic-regulation in bacterial continuous cultures. 1. *Biotechnol. Bioeng.* 38, 1337–1352. doi: 10.1002/bit.260381112

Bassiouni, M., and Vico, G. (2021). Parsimony vs predictive and functional performance of three stomatal optimization principles in a big-leaf framework. *New Phytol.* 231, 586–600. doi: 10.1111/nph.17392

Berg, B., and McClaugherty, C. A. (2003). *Plant Litter. Decomposition, Humus Formation, Carbon Sequestration*. Berlin: Springer.

Calabrese, S., Chakrawal, A., Manzoni, S., and Van Cappellen, P. (2021). Energetic scaling in microbial growth. *Proc. Natl. Acad. Sci.* 118:e2107668118. doi: 10.1073/pnas.2107668118

Calabrese, S., Mohanty, B., and Malik, A. (2022). Soil microorganisms regulate extracellular enzyme production to maximize their growth rate. *Biogeochemistry* 158, 303–312. doi: 10.1007/s10533-022-00899-8

Casey, J., and Follows, M. (2020). A steady-state model of microbial acclimation to substrate limitation. *PLoS Comput. Biol.* 16:e1008140. doi: 10.1371/journal.pcbi.1008140

Chakrawal, A., Herrmann, A. M., Koestel, J., Jarsjo, J., Nunan, N., Kätterer, T., et al. (2020). Dynamic upscaling of decomposition kinetics for carbon cycling models. *Geosci. Model Dev.* 13, 1399–1429. doi: 10.5194/gmd-2019-133

del Giorgio, P. A., and Cole, J. J. (1998). Bacterial growth efficiency in natural aquatic systems. *Annu. Rev. Ecol. Syst.* 29, 503–541. doi: 10.1146/annurev.ecolsys.29.1.503

Dewar, R. C. (2010). Maximum entropy production and plant optimization theories. *Philos. Trans. R. Soc. B. Biol. Sci.* 365, 1429–1435. doi: 10.1098/rstb.2009.0293

Feng, X., Lu, Y., Jiang, M., Katul, G. G., Manzoni, S., Mrad, A., et al. (2022). Instantaneous stomatal optimization results in suboptimal carbon gain due to legacy effects. *Plant Cell Environ.* 45, 3189–3204. doi: 10.1111/pce.14427

Frank, S. A. (2010). The trade-off between rate and yield in the design of microbial metabolism. *J. Evol. Biol.* 23, 609–613. doi: 10.1111/j.1420-9101.2010.01930.x

Franklin, O., Hall, E. K., Kaiser, C., Battin, T. J., and Richter, A. (2011). Optimization of biomass composition explains microbial growth-stoichiometry relationships. *Am. Nat.* 177, E29–E42. doi: 10.1086/657684

Giordano, N., Mairet, F., Gouze, J. L., Geiselmann, J., and de Jong, H. (2016). Dynamical allocation of cellular resources as an optimal control problem: novel insights into microbial growth strategies. *PLoS Comput. Biol.* 12:e1004802. doi: 10.1371/journal.pcbi.1004802

Gudelj, I., Weitz, J. S., Ferenci, T., Horner-Devine, M. C., Marx, C. J., Meyer, J. R., et al. (2010). An integrative approach to understanding microbial diversity: from intracellular mechanisms to community structure. *Ecol. Lett.* 13, 1073–1084. doi: 10.1111/j.1461-0248.2010.01507.x

Harrison, S. P., Cramer, W., Franklin, O., Prentice, I. C., Wang, H., Brännström, Å., et al. (2021). Eco-evolutionary optimality as a means to improve vegetation and land-surface models. *New Phytol.* 231, 2125–2141. doi: 10.1111/nph.17558

Kirk, D. E. (1970). *Optimal Control Theory. An Introduction*. Englewood Cliffs, NJ: Prentice-Hall Inc.

Lenhart, S., and Workman, J. T. (2007). *Optimal Control Applied to Biological Problems*. New York, NY: Chapman & Hall/CRC.

Liang, C., Schimel, J. P., and Jastrow, J. D. (2017). The importance of anabolism in microbial control over soil carbon storage. *Nat. Microbiol.* 2:17105. doi: 10.1038/nmicrobiol.2017.105

Lipson, D. A. (2015). The complex relationship between microbial growth rate and yield and its implications for ecosystem processes. *Front. Microbiol.* 6:615. doi: 10.3389/fmicb.2015.00615

Lipson, D. A., Monson, R. K., Schmidt, S. K., and Weintraub, M. N. (2009). The trade-off between growth rate and yield in microbial communities and the consequences for under-snow soil respiration in a high elevation coniferous forest. *Biogeochemistry* 95, 23–35. doi: 10.1007/s10533-008-9252-1

Liu, Y. (2007). Overview of some theoretical approaches for derivation of the Monod equation. *Appl. Microbiol. Biotechnol.* 73, 1241–1250. doi: 10.1007/s00253-006-0717-7

Maitra, A., and Dill, K. A. (2015). Bacterial growth laws reflect the evolutionary importance of energy efficiency. *Proc. Natl. Acad. Sci.* 112, 406–411. doi: 10.1073/pnas.1421138111

Malik, A. A., Martiny, J. B. H., Brodie, E. L., Martiny, A. C., Treseder, K. K., and Allison, S. D. (2020). Defining trait-based microbial strategies with consequences for soil carbon cycling under climate change. *ISME J.* 14, 1–9. doi: 10.1038/s41396-019-0510-0

Manzoni, S., Čapek, P., Mooshammer, M., Lindahl, B. D., Richter, A., and Šantrůčková, H. (2017). Optimal metabolic regulation along resource stoichiometry gradients. *Ecol. Lett.* 20, 1182–1191. doi: 10.1111/ele.12815

Manzoni, S., Chakrawal, A., Spohn, M., and Lindahl, B. D. (2021). Modeling microbial adaptations to nutrient limitation during litter decomposition. *Front. For. Glob. Change* 4:686945. doi: 10.3389/ffgc.2021.686945

Manzoni, S., Fatichi, S., Feng, X., Katul, G. G., Way, D., and Vico, G. (2022). Consistent responses of vegetation gas exchange to elevated atmospheric CO2 emerge from heuristic and optimization models. *Biogeosciences* 19, 4387–4414. doi: 10.5194/bg-19-4387-2022

Manzoni, S., and Porporato, A. (2009). Soil carbon and nitrogen mineralization: theory and models across scales. *Soil Biol. Biochem.* 41, 1355–1379. doi: 10.1016/j.soilbio.2009.02.031

Michaelis, L., and Menten, M. L. (1913). Die kinetik der invertinwirkung (translated by Goody R.S., and K.A. Johnson). *Biochem. Z.* 49, 333–369.

Monod, J. (1949). The growth of bacterial cultures. *Annu. Rev. Microbiol.* 3, 371–394. doi: 10.1146/annurev.mi.03.100149.002103

Muscarella, M. E., Howey, X. M., and Lennon, J. T. (2020). Trait-based approach to bacterial growth efficiency. *Environ. Microbiol.* 22, 3494–3504. doi: 10.1111/1462-2920.15120

Muscarella, R., and Uriarte, M. (2016). Do community-weighted mean functional traits reflect optimal strategies? *Proc. R. Soc. B. Biol. Sci.* 283:20152434. doi: 10.1098/rspb.2015.2434

Olson, J. S. (1963). Energy storage and the balance of producer and decomposers in ecological systems. *Ecology* 44, 322–331. doi: 10.2307/1932179

Osono, T., and Takeda, H. (2005). Decomposition of organic chemical components in relation to nitrogen dynamics in leaf litter of 14 tree species in a cool temperate forest. *Ecol. Res.* 20, 41–49. doi: 10.1007/s11284-004-0002-0

Rodriguez-Iturbe, I., and Porporato, A. (2004). *Ecohydrology of Water-Controlled Ecosystems. Soil Moisture and Plant Dynamics*. Cambridge: Cambridge University Press.

Roller, B. R. K., and Schmidt, T. M. (2015). The physiology and ecological implications of efficient growth. *ISME J.* 9, 1481–1487. doi: 10.1038/ismej.2014.235

Rosen, R. (1967). *Optimality Principles in Biology*. New York: Springer.

Salter, R. M., and Green, T. C. (1933). Factors affecting the accumulation and loss of nitrogen and organic carbon in cropped soils. *J. Am. Soc. Agron.* 25, 622–630. doi: 10.2134/agronj1933.00021962002500090010x

Sokol, N. W., Slessarev, E., Marschmann, G. L., Nicolas, A., Blazewicz, S. J., Brodie, E. L., et al. (2022). Life and death in the soil microbiome: how ecological processes influence biogeochemistry. *Nat. Rev. Microbiol.* 20, 415–430. doi: 10.1038/s41579-022-00695-z

Tang, J. Y., and Riley, W. J. (2013). A total quasi-steady-state formulation of substrate uptake kinetics in complex networks and an example application to microbial litter decomposition. *Biogeosciences* 10, 8329–8351. doi: 10.5194/bg-10-8329-2013

Tang, J. Y., and Riley, W. J. (2019). A theory of effective microbial substrate affinity parameters in variably saturated soils and an example application to aerobic soil heterotrophic respiration. *J. Geophys. Res. Biogeosci.* 124, 918–940. doi: 10.1029/2018jg004779

Vallino, J. J. (2010). Ecosystem biogeochemistry considered as a distributed metabolic network ordered by maximum entropy production. *Philos. Trans. R. Soc. B. Biol. Sci.* 365, 1417–1427. doi: 10.1098/rstb.2009.0272

Vallino, J. J., Hopkinson, C. S., and Hobbie, J. E. (1996). Modeling bacterial utilization of dissolved organic matter: optimization replaces Monod growth kinetics. *Limnol. Oceanogr.* 41, 1591–1609. doi: 10.4319/lo.1996.41.8.1591

Vetter, Y. A., Deming, J. W., Jumars, P. A., and Krieger-Brockett, B. B. (1998). A predictive model of bacterial foraging by means of freely released extracellular enzymes. *Microb. Ecol.* 36, 75–92. doi: 10.1007/s002489900095

Waldherr, S., Oyarzun, D. A., and Bockmayr, A. (2015). Dynamic optimization of metabolic networks coupled with gene expression. *J. Theor. Biol.* 365, 469–485. doi: 10.1016/j.jtbi.2014.10.035

Wang, G., and Post, W. M. (2013). A note on the reverse Michaelis–Menten kinetics. *Soil Biol. Biochem.* 57, 946–949. doi: 10.1016/j.soilbio.2012.08.028

Wutzler, T., and Reichstein, M. (2008). Colimitation of decomposition by substrate and decomposers - a comparison of model formulations. *Biogeosciences* 5, 749–759. doi: 10.5194/bg-5-749-2008

Wutzler, T., Zaehle, S., Schrumpf, M., Ahrens, B., and Reichstein, M. (2017). Adaptation of microbial resource allocation affects modelled long term soil organic matter and nutrient cycling. *Soil Biol. Biochem.* 115, 322–336. doi: 10.1016/j.soilbio.2017.08.031

frontiers | Frontiers in Ecology and Evolution

TYPE Original Research
PUBLISHED 24 February 2023
DOI 10.3389/fevo.2023.1105832

OPEN ACCESS

EDITED BY
Rui-Wu Wang,
Northwestern Polytechnical University,
China

REVIEWED BY
Ensheng Weng,
Columbia University,
United States
Jing Peng,
CAS Key Lab of Regional
Climate-Environment for East Asia (TEA),
Institute of Atmospheric Physics,
Chinese Academy of Sciences,
China

*CORRESPONDENCE
Jianyang Xia
✉ jyxia@des.ecnu.edu.cn

SPECIALTY SECTION
This article was submitted to
Models in Ecology and Evolution,
a section of the journal
Frontiers in Ecology and Evolution

RECEIVED 23 November 2022
ACCEPTED 30 January 2023
PUBLISHED 24 February 2023

CITATION
Bian C and Xia J (2023) Uncertainty
propagation in a global biogeochemical model
driven by leaf area data.
Front. Ecol. Evol. 11:1105832.
doi: 10.3389/fevo.2023.1105832

Uncertainty propagation in a global biogeochemical model driven by leaf area data

Chenyu Bian[1,2] and Jianyang Xia[1,2]*

[1]Zhejiang Tiantong Forest Ecosystem National Observation and Research Station, State Key Laboratory of Estuarine and Coastal Research, School of Ecological and Environmental Sciences, East China Normal University, Shanghai, China, [2]Research Center for Global Change and Complex Ecosystems, East China Normal University, Shanghai, China

Satellite-observed leaf area index (LAI) is often used to depict vegetation canopy structure and photosynthesis processes in terrestrial biogeochemical models. However, it remains unclear how the uncertainty of LAI among different satellite products propagates to the modeling of carbon (C), nitrogen (N), and phosphorus (P) cycles. Here, we separately drive a global biogeochemical model by three satellite-derived LAI products (i.e., GIMMS LAI3g, GLASS, and GLOBMAP) from 1982 to 2011. Using a traceability analysis, we explored the propagation of LAI-driven uncertainty to modeled C, N, and P storage among different biomes. The results showed that the data uncertainty of LAI was more considerable in the tropics than in non-tropical regions, whereas the modeling uncertainty of C, N, and P stocks showed a contrasting biogeographic pattern. The spread of simulated C, N, and P storage derived by different LAI datasets resulted from assimilation rates of elements in shrubland and C3 grassland but from the element residence time (τ) in deciduous needle leaf forest and tundra regions. Moreover, the assimilation rates of elements are the main contributing factor, with 67.6, 93.2, and 93% of vegetated grids for the modeled uncertainty of C, N, and P storage among the three simulations. We further traced the variations in τ to baseline residence times of different elements and the environmental scalars. These findings indicate that the data uncertainty of plant leaf traits can propagate to ecosystem processes in global biogeochemical models, especially in non-tropical forests.

KEYWORDS

ecosystem modeling, leaf area index, nitrogen cycle, phosphorus cycle, traceability analysis, uncertainty propagation

1. Introduction

Over the past few decades, terrestrial ecosystems have absorbed nearly one-third of the CO_2 of anthropogenic emissions by vegetation canopy (Friedlingstein et al., 2022). However, the terrestrial carbon uptake by vegetation photosynthetic is widely limited by the availability of essential nutrients, especially nitrogen (N) and phosphorus (P) (Elser et al., 2007; LeBauer and Treseder, 2008; Xia and Wan, 2008; Allen et al., 2020; Hou et al., 2020). The availability of N and P affects vegetation productivity (Elser et al., 2007; Norby et al., 2010), carbon (C) allocation (Hofhansl et al., 2015), litter decomposition (Averill and Waring, 2018), and other processes (Sutton et al., 2008; Melillo et al., 2011). The availability of N and P also constrains soil carbon storage (Crowther et al., 2019), especially under the scenarios of climate change and increasing atmospheric CO_2 (Wang et al., 2020). Thus, global distributions of C, N, and P storages are crucial for modeling the global biogeochemical feedback to future climate change.

Many global biogeochemical models have coupled nutrients processes to provide more realistic simulations of terrestrial ecosystems (Thornton et al., 2007; Wang et al., 2007, 2010; Goll et al., 2012; Yang et al., 2014; Zhu et al., 2019; Sun et al., 2021). Several global models not only incorporated the N cycles (Manzoni and Porporato, 2009; Zaehle et al., 2014; Meyerholt and Zaehle, 2015) but also implemented the P processes, such as ORCHIDEE-CNP (Goll et al., 2017; Sun et al., 2021), QUINCY v1.0 (Thum et al., 2019), GOLUM-CNP (Wang et al., 2018), JSM (Yu et al., 2020), JULES-CNP (Nakhavali et al., 2022), and E3SM (Zhu et al., 2019). The coupled C-N-P cycle reduced the magnitude of disequilibrium in the terrestrial C cycle (Wei et al., 2022a), but how to accurately represent the nutrient cycles and the effects of N and P limitation in biogeochemical models are still challenges (Hungate et al., 2003; Thomas et al., 2015; Wieder et al., 2015; Sun et al., 2017).

Due to the difference in model structure and parameters (Zaehle and Dalmonech, 2011), the increased model complexity further hinders our understanding of the modeling uncertainty. However, most global biogeochemical models share a typical pool-flux structure and follow some fundamental properties of terrestrial element cycling (Xia et al., 2013; Luo et al., 2015). For example, C atoms enter the ecosystem through plant photosynthesis, while plants assimilate N and P mainly from mineral soil. The elements of C, N, and P are allocated among plant pools, then transferred to litter and soil pools, and eventually returned to the atmosphere *via* the decomposition of organic matter (Olson, 1963; Zhang et al., 2008). In biogeochemical models, there are a specific soil inorganic-N pool and a few soil inorganic P pools, which generally separate to distinct pools based on its chemical fractionation (Hedley et al., 1982; Cross and Schlesinger, 1995; Hou et al., 2018). Labile P usually comes from P mineralization, P weathering, and dust deposition (Wang et al., 2010). Some of the labile P can enter the sorbed P pool and subsequently become occluded, but this form is assumed to be unavailable by plants (Wang et al., 2018). Those specific processes of the coupled C-N-P biogeochemical cycles can be found in Figure 1.

Leaf area index (LAI), as a significant uncertainty source of simulated photosynthetic carbon uptake (Li et al., 2018; Cui et al., 2019), is widely used as a critical parameter in the process-based biogeochemical models for depicting vegetation canopy structure (Forzieri et al., 2017; Zeng et al., 2017; Liu et al., 2018; Chen et al., 2019). Many inter-model comparisons on Earth system models (ESMs) have shown a large spread of LAI on a global scale (Zeng et al., 2016), partially leading to their persistent uncertainty in carbon storage projections (Wei et al., 2022b). Recently, many studies have used satellite-based LAI to directly force the models for a more realistic prediction of the global carbon (C) cycle (Zeng et al., 2017; Liu et al., 2018; Chen et al., 2019). However, there are significant discrepancies in different satellite-based LAI products on temporal and spatial scales (Jiang et al., 2017; Xiao et al., 2017; Liu et al., 2018). Therefore, understanding whether and how the data uncertainty in LAI observations propagates to global biogeochemical models helps provide a more accurate prediction of future terrestrial carbon sinks (Heinsch et al., 2006; Liu et al., 2018).

This study introduces a framework to decompose a complex biogeochemical model coupled with C-N-P processes into its traceable components. Considering that the N and P cycles are not a closed cyclic system, we only focused on the organic matter of C, N, and P in this study. Specifically, the framework traces the modeled ecosystem organic C, N, and P storage to the influx of C (i.e., net primary productivity, NPP), N, and P uptake and the corresponding ecosystem residence time [$(i = C,N,P)$]. The τ_i can be further traced to the baseline residence time [$\tau_i^{'}(i = C,N,P)$] and environmental scalars (ξ). The former $\tau_i^{'}$ usually preset in models depends on the soil properties and vegetation characteristics, while the latter usually includes temperature and water scalars and is determined by climate forcings. Based on the framework, we further analyzed the difference among biomes (Supplementary Figure S1) in simulated C, N, and P storage caused by the disagreement of LAI estimates among three satellite-derived products (i.e., GIMMS LAI3g, GLASS, and GLOBMAP) with the Australian Community Atmosphere Biosphere Land Exchange (CABLE) model. The primary goal of this study is to explore the uncertainty propagation of LAI observations to global simulations of C, N, and P storage in the biogeochemical models.

2. Materials and methods

2.1. Satellite-derived leaf area index datasets

Leaf area index is an important parameter that consistently monitors vegetation structure dynamics over large spatial and temporal scales. This study uses three satellite-derived long-term global LAI products: GIMMS LAI3g, GLASS LAI, and GLOBMAP LAI. We re-sampled all three LAI datasets from their native resolution into $0.5° \times 0.5°$ special resolution using the nearest neighbor algorithm and interpolated to the hourly temporal resolution to force the model. All three datasets have been validated and widely used to monitor terrestrial vegetation dynamics (Dardel et al., 2014; Piao et al., 2015; Zhu et al., 2016, 2017; Jiang et al., 2017).

2.1.1. GIMMS LAI3g product

The Global Inventory Modeling and Mapping Studies (GIMMS) LAI3g product (version 01) was generated by the Feed-Forward Neural Network (FFNN) algorithm based on the Advanced Very High Resolution Radiometer (AVHRR) GIMMS Normalized Difference Vegetation Index (NDVI) dataset and Moderate Resolution Imaging Spectroradiometer (MODIS) LAI (Zhu et al., 2013). It provides a global observation at 1/12-degree spatial resolution and 15-day temporal resolution from July 1981 to December 2011. The GIMMS LAI3g dataset was extensively evaluated by comparison with field LAI measurements, other satellite-derived data products, statistical climatic variables, and the simulation results from land models (Mao et al., 2013; Zhu et al., 2013).

2.1.2. GLASS LAI product

The Global LAnd Surface Satellite (GLASS version 03) long-time series LAI product was estimated from MODIS and AVHRR remote sensing data using the General Regression Neural Networks (GRNNs) approach (Xiao et al., 2014). The GRNNs were trained with the fused time-series LAI from MODIS and CYCLOPES products and the MODIS reflectance of the BELMANIP sites. The GLASS LAI product has a temporal resolution of 8 days and spans from 1981 to 2014. For the period of 1981–1999, the data product was generated from AVHRR reflectance data, providing a geographic projection at the spatial resolution of 0.05°. From 2000 to 2014, the LAI product was generated from MODIS surface reflectance data with a spatial resolution of 1 km (Xiao et al., 2014, 2016).

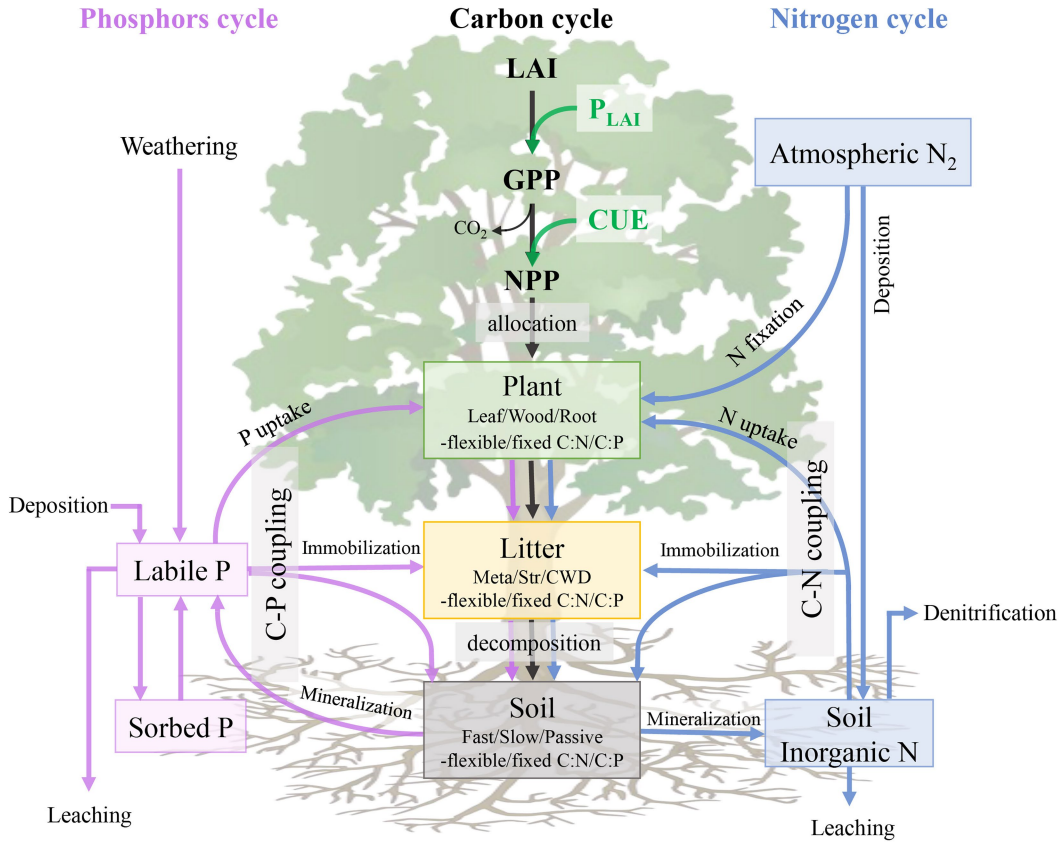

FIGURE 1
Schematic diagram of major carbon (C), nitrogen (N) and phosphorus (P) pools and fluxes in a terrestrial ecosystem. Black, blue and pink arrows indicate the C-cycle processes, N-cycle processes, and P-cycle processes, respectively. Green, yellow, and gray rectangles represent the vegetation, litter and soil pools of organic carbon, nitrogen, and phosphorus. LAI, leaf area index; P_{LAI}, LAI-leval photosynthesis, GPP, gross primary productivity, CUE, carbon use efficiency; NPP, net primady productivity; Meta, metabolic litter; Str, structural litter; CWD, coarse woody debris.

2.1.3. GLOBMAP LAI product

The consistent long-term GLOBMAP LAI product (version 01) was generated by a combination of AVHRR LAI (1981–2000) and MODIS LAI (2000–2011) (Liu et al., 2012). The MODIS LAI time series was generated from MODIS land surface reflectance data based on the GLOBCARBON LAI algorithm (Deng et al., 2006). By establishing a pixel by pixel relationships between AVHRR observations and MODIS LAI data series during the overlapped period (2000–2006), the AVHRR LAI could be retrieved back to 1981. The temporal resolution of this dataset is half a month and 8 days in 1981–2000 and 2001–2011, respectively. The spatial resolution of the AVHRR LAI dataset is 8 km.

2.2. Matrix representation of the carbon, nitrogen, and phosphorus cycle

We developed a theoretical framework for decomposing the terrestrial carbon, nitrogen, and phosphorus stock into some traceable components based on the biogeochemical principles of the terrestrial carbon cycle. For example, the terrestrial carbon cycle can be generally described as the following processes, which includes carbon enters the ecosystem *via* plant photosynthesis; photosynthetic carbon is then allocated among plant pools; part of this carbon is consumed by respiration, and the remainder is further transferred to litter and soil carbon pools; lastly, the carbon in the litter and soil pools is decomposed and back into the atmosphere (Luo and Weng, 2011; Luo et al., 2022). Plants assimilate the nitrogen and phosphorus from mineral soils and then transfer following the same flow with organic matter in terrestrial ecosystems. Therefore, following the approach developed by Xia et al. (2013), the biogeochemical cycle processes can be mathematically represented by three matrix equations:

$$\begin{cases} \dfrac{dX(t)}{dt} = B_C U_C(t) - A\xi(t) C X(t) \\ \dfrac{dN(t)}{dt} = B_N U_N(t) - A\xi(t) C N(t) \\ \dfrac{dP(t)}{dt} = B_P U_P(t) - A\xi(t) C P(t) \end{cases} \quad (1)$$

where $X(t) = (X_1(t), X_2(t), \ldots, X_9(t))^T$, $N(t) = (N_1(t), N_2(t), \ldots, N_9(t))^T$, and $P(t) = (P_1(t), P_2(t), \ldots, P_9(t))^T$ are 9×1 vector, which describes the C, N and P pool size of leaf, root, wood, metabolic litter, structural litter, coarse wood debris (CWD), fast soil, slow soil and passive soil pool at time t in CABLE model. $B_i = (b_1, b_2, b_3, 0, \ldots, 0)^T \ (i = C, N, P)$ is a vector of allocation coefficients of C, N, and P among different plant pools. For the C allocation, the partitioning coefficients from NPP to root and wood carbon pools are equations of availably of light,

nitrogen, and water, respectively. Then the rest of NPP goes to the leaf pool. For the N and P, the allocations of N and P uptake among different plant pools are calculated based on the proportion to each pool's demand of N and P. The inputs of C, N, and P are represented by $U_i(t)(i=C,N,P)$. U_C is the fixed carbon by canopy photosynthesis, i.e., net primary production (NPP). U_N and U_P are the assimilated N and P *via* plant uptake from soil minerals. $\xi(t)$ is a diagonal matrix, the diagonal components representing the environmental scalars (such as temperature and soil moisture) effects on carbon decomposition rate at time *t*. *C* is a 9×9 diagonal matrix with diagonal entries by 9×1 vectors $c=(c_1,c_2,\ldots,c_3)^T$. The diagonal elements indicate the C decay rate for each pool. *A* is a transfer coefficients matrix, which can quantify how much carbon can be transferred among different pools. Therefore, the first term on the right side of Equation (1), $B_iU_i\ (i=C,N,P)$, describes the C, N, and P inputs and allocation among different plant pools, and the second term on the right represents the transfer and exit rates (Xia et al., 2013; Luo et al., 2017).

By letting Equation (1) equal zero, we obtained the C, N, and P pool size at steady-state as the product of ecosystem residence time and influx:

$$\begin{cases} X_{ss}=(A\xi C)^{-1}B_CU_C \\ N_{ss}=(A\xi C)^{-1}B_NU_N \\ P_{ss}=(A\xi C)^{-1}B_NU_P \end{cases} \tag{2}$$

where X_{ss}, N_{ss}, and P_{ss} are vectors that includes all the organic pools at steady state. U_C, U_N, and U_P are the ecosystem C, N, and P influx at steady state. U_C represents NPP in this study, which can be further decomposed to gross primary production (GPP) and carbon use efficiency (CUE) based on some previous studies (Bradford and Crowther, 2013; Xia et al., 2017). The term $(A\xi C)^{-1}B_i\ (i=C,N,P)$ in Equation (2) are vectors of the residence time of individual pools as:

$$\begin{cases} \tau_C=(A\xi C)^{-1}B_C \\ \tau_N=(A\xi C)^{-1}B_N \\ \tau_P=(A\xi C)^{-1}B_P \end{cases} \tag{3}$$

The ecosystem-level residence time of C, N, or P was summed from all the individual pools. The ecosystem residence time can be determined by multiple ecological processes, such as allocation (i.e., the *B* vector), carbon transfer among different pools (i.e., the *A* matrix), decomposition rates (i.e., the *C* matrix), and the environmental scalars (i.e., ξ). The scalar ξ usually consists of the temperature (ξ_T) and water scalars (ξ_W) as:

$$\xi=\xi_T\xi_W \tag{4}$$

Generally, the parameters of *B*, *A*, and *C* matrices are preset in a specific model according to model structure, soil properties, and vegetation characteristics (Zhou et al., 2018). By rearranging Equation (3), we can further decompose the residence time to the environment scalar and the corresponding preset parameters:

$$\begin{cases} \tau_C=\xi^{-1}\times(AC)^{-1}B_C \\ \tau_N=\xi^{-1}\times(AC)^{-1}B_N \\ \tau_P=\xi^{-1}\times(AC)^{-1}B_P \end{cases} \tag{5}$$

The residence time can be further decomposed to environment scalars and baseline residence time vectors. The equation of baseline residence time can be expressed as:

$$\begin{cases} \tau_C'=(AC)^{-1}B_C \\ \tau_N'=(AC)^{-1}B_N \\ \tau_P'=(AC)^{-1}B_P \end{cases} \tag{6}$$

2.3. The Community Atmosphere-Biosphere-Land Exchange (CABLE) model: overview and experiments

The Australian Community Atmosphere Biosphere Land Exchange (CABLE) model version 2 is a global land surface model that can simulate biophysical and biogeochemical processes (Wang et al., 2010, 2011). It includes five submodels: (1) radiation, (2) canopy micrometeorology, (3) surface flux, (4) soil and snow, and (5) ecosystem respiration, and it also incorporates carbon (C), nitrogen (N), and phosphorus (P) cycles. CABLE has been widely evaluated by other global observations (Piao et al., 2015), eddy-flux measurements (Best et al., 2015), and manipulated field experiments (De Kauwe et al., 2014). This model can be applied to attribution analysis (Zhang et al., 2016) or plant feedback effects (Lei et al., 2019) by doing a series of simulation experiments. The default settings of LAI are prognostic in the CABLE model, but a switch can control them. When the switch is turned on, the prognostic LAI can be calculated as the product between specific leaf area (SLA) and leaf biomass. SLA and the phenology phases (used to determine the leaf growth) are prescribed for each plant functional type.

In this study, we turned the switch off and replaced the modeled LAI with data from three satellite-observed products (GIMMS LAI3g, GLASS, and GLOBMAP). Based on the traceability analysis approach, we performed three simulations to diagnose the source of uncertainty in the biogeochemical cycle caused by LAI. The CABLE model was first spun up with the C-N-P coupled schemes to the steady state in 1,900 using a semi-analytical solution (Xia et al., 2012). The forcing data (Zhang et al., 2016) used to spin up the model concludes seven 6-hourly meteorological forcing variables (i.e., temperature, precipitation, downward shortwave radiation, downward longwave radiation, specific humidity, pressure, and wind speed) from the CRUNCEP version 5 (New et al., 1999, 2000, 2002). Using spin-up results as an initial value, we run the model from 1901 to 1981. After that, we performed three simulations by replacing the modeled LAI with three satellite-based LAI products (GIMMS LAI3g, GLASS, GLOBMAP), respectively. Lastly, we spun up CABLE to a steady state forced by the satellite-derived LAI datasets and time-variant CO_2 concentration from 1982 to 2011 (Supplementary Table S1).

3. Results

3.1. Spatial variations of terrestrial carbon, nitrogen, and phosphorus storage

The estimated global mean LAI was 1.24 ± 0.18 m^2 m^{-2} (mean ± SD) across the three data products. The simulated global stocks of C, N, and P were 11.0 ± 1.4 C kg C m^{-2}, 504.3 ± 68.1 g N m^{-2}, and 97.7 ± 13.6 g P m^{-2}, respectively. All three simulations showed the highest mean LAI in tropical regions among the eight biomes (Figure 2A). Furthermore, the variability of LAI across three simulations was also higher in the tropics than in any other area (Figure 2B). However, the simulated element storage (i.e., C, N, and P) showed a divergent spatial pattern in magnitude and variability compared with LAI (Figures 2C–H). Specifically, northern high-latitude regions showed the highest annual mean element storage (12.0 kg C m^{-2} for the C storage, 531.3 g N m^{-2} for the N storage, and 93.1 g P m^{-2} for the P storage) compared with other climate regions. In contrast, tropical regions showed a relatively high C storage (10.0 kg C m^{-2}) but low storage of N (400. 2 g N m^{-2}) and P (78.5 g P m^{-2}) (Figures 2C,E,G). A similar distribution was also found in the spatial variability of elements (Figures 2D,F,H). In addition, it is noted that the high disagreement in P storage across three simulations

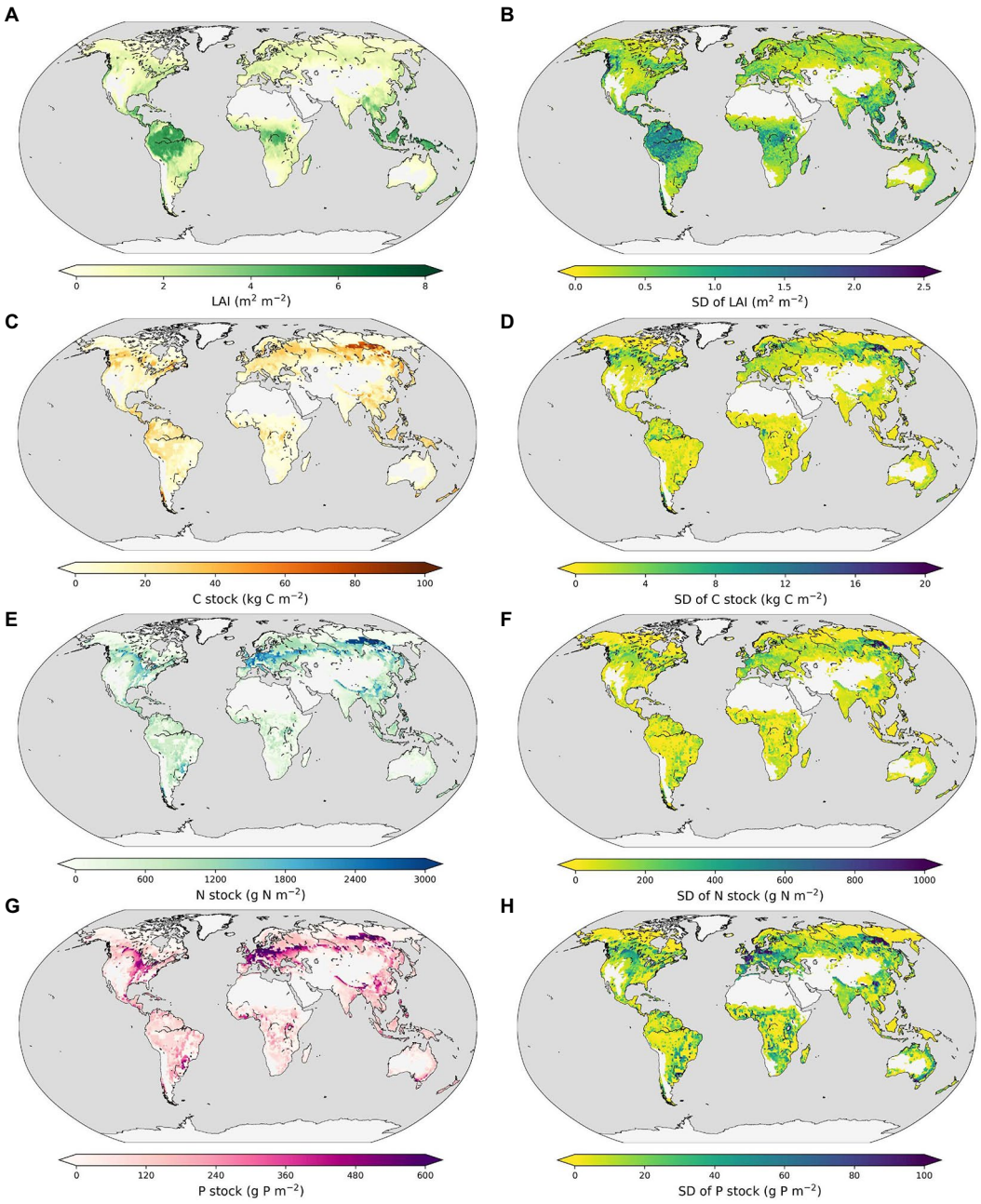

FIGURE 2
Spatial distributions of annual leaf area index (LAI, **A**), carbon **(C)**, nitrogen **(E)** and phosphorus **(G)** storage and the corresponding standard deviation of LAI **(B)**, C **(D)**, N **(F)**, and P **(H)** storage among three satellite-derived simulations. Note that we only consider the organic pools for nitrogen and phosphorus in this study.

is mainly located in the regions covered by herbaceous vegetation, such as eastern Australia, southeastern South America, and southern Africa (Figure 2H).

3.2. Decomposing carbon, nitrogen, and phosphorus storage into ecosystem residence time and the corresponding influx

The ecosystem element storage can be decomposed into the corresponding element residence time (τ_C, τ_N, τ_P) and the influx rate [U_C (NPP), U_N, and U_P] based on the traceability framework according to Equations (2, 3). Deciduous needle leaf forest (DNF) had the largest ensemble annual mean results of ecosystem C (86.0 kg C m^{-2}), N (424.3 g N m^{-2}), and P (24.4 g P m^{-2}) storage among the eight biomes, resulting from its longest residence time (τ_C , 154.3 years; τ_N , 78.4 years; τ_P , 65.5 years) and mediated element input (NPP, 557.4 g C m^{-2} $yr.^{-1}$; U_N, 5.4 g N m^{-2} $yr.^{-1}$; U_P, 0.37 g P m^{-2} $yr.^{-1}$). However, the order of the size in C, N, and P storage was inconsistent in the remaining seven biomes (Supplementary Table S2). Shrubland had the lowest C storage (10.7 kg C m^{-2}) as a result of the smallest NPP (257.6 g C m^{-2} $yr.^{-1}$) and a moderate τ_C (41.4 years). Evergreen needle leaf forest (ENF) had a relatively long τ_N (50.4 years) and low U_N (3.1 g N m^{-2} $yr.^{-1}$). While evergreen broadleaf forest (EBF), deciduous broadleaf forest (DBF), and C3 grassland (C3G) had a short τ_N (~25.0 years) and relatively high U_N (~9.0 g N m^{-2} $yr.^{-1}$), leading to a moderate N storage. For P storage, EBF, DBF, and C3G had a relatively short τ_P (~23.9 years) and relatively high U_P (~0.50 g P m^{-2} $yr.^{-1}$), resulting in a moderate P storage. Although Tundra had a relatively long τ_N (53.0 years) and τ_P (50.9 years), it still has the lowest N (16.5 g N m^{-2}) and P (1.4 g P m^{-2}) storage as the result of the smallest U_N (0.31 g N m^{-2} $yr.^{-1}$) and U_P (0.03 g P m^{-2} $yr.^{-1}$). Additionally, the carbon influx *via* canopy photosynthesis (NPP) can be further decomposed into GPP and CUE (Xia et al., 2017). The results showed that EBF had the highest annual mean GPP (3312.2 g C m^{-2} $yr.^{-1}$), followed by DBF (2103.1), C4 grassland (C4G, 1873.4), C3G (951.3), ENF (912.6), DNF (871.2), Shrubland (511.6) and Tundra (370.8) regions (Supplementary Figure S2 and Supplementary Table S2). The ranges of carbon use efficiency of all eight biomes from 0.37 to 0.71.

The ecosystem element storage derived from three satellite-based LAI differed among the eight biomes. For example, ENF, EBF, and DBF had similar C, N, and P storage for the three simulations (Figure 3). Although Shrubland and C3G had comparable values of element residence time (τ_C , τ_N , and τ_P), their different element uptake rates (NPP, U_N, and U_P) led to variations in element storage across the three simulations. In addition, compared with the simulations derived from GIMMS LAI3g and GLASS, the simulation derived by GLOBMAP LAI had the smallest NPP, U_N, and U_P (Figure 3). Tundra and DNF had comparable C storage across three simulations. However, the N and P storage magnitude varied widely in these regions. The differences in N and P storage across the three simulations are mainly due to τ_N and τ_P (Supplementary Table S2).

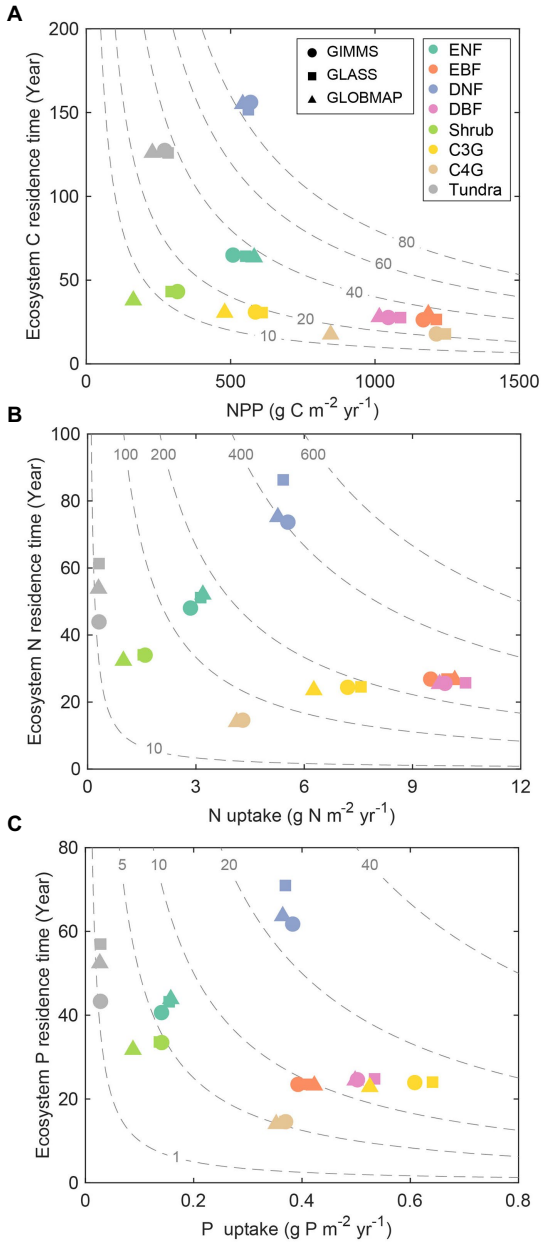

FIGURE 3
Decomposition of ecosystem carbon **(A)**, nitrogen **(B)**, and phosphorus **(C)** storage into its influx and ecosystem residence time in various biomes for each simulation. ENF, evergreen needleleaf forest; EBF, evergreen broadleaf forest; DNF, deciduous needleleaf forest; DBF, deciduous broadleaf forest; Shrub, shrub land; C3G, C_3 grassland; C4G, C_4 grassland.

3.3. Traceability analysis of ecosystem residence time

Ecosystem residence time can be decomposed into baseline residence time and environmental scalars. The baseline residence time is determined by the carbon transfer coefficients matrix (A matrix), decomposition rates (C matrix), and the allocation coefficients (B vector) among different plant element pools based on Equation 6. Considering that the element cycles (C, N, and P) share the same A and C matrix, the difference in baseline element residence time is mainly caused by the element allocation coefficients (B_C, B_N, B_P). The baseline C residence time ($\tau_C^{'}$) is the longest compared with baseline N residence time ($\tau_N^{'}$) and baseline P residence time ($\tau_P^{'}$) (Supplementary Figure S3) in all the eight biomes. Deciduous needle leaf forest has a relatively long $\tau_C^{'}$ (21.8 years), which is almost three times that of $\tau_N^{'}$ (8.2 years) and $\tau_P^{'}$ (6.8 years). Baseline element residence times were similar in C3 grassland ($\tau_C^{'}$, 4.6 years; $\tau_N^{'}$,

3.7 years; τ_P', 3.6 years), C4 grassland (τ_C', 5.6 years; τ_N', 4.3 years; τ_P', 4.3 years), and shrubland (τ_C', 8.7 years; τ_N', 7.1 years; τ_P', 7.1 years) regions. Additionally, τ_C' were similar to each other in three LAI-derived simulations. While τ_N' and τ_P' differed substantially across three simulations, especially in ENF, DNF, and tundra regions (Figure 4).

Environmental scalar (ξ) can regulate ecosystem residence time by limiting the decomposition rates of litter and soil organic pools. By decomposing environmental scalar into temperature (ξ_T) and water scalar (ξ_W), we can found that the multi-year mean of ξ_T ranges from 0.09 for deciduous needle leaf forest to 0.70 for C4 grassland, while ξ_W ranges from 0.60 for tundra and 0.92 for C4 grassland (Figure 5). The global average of ξ_T (0.38) is considerably lower than that of ξ_W (0.82). In general, ξ_T dominates the difference in ξ among eight biomes compared with ξ_W.

3.4. Variation decomposition of the simulated carbon, nitrogen, and phosphorus storage

We decomposed the variations of element storage into several traceable components on each vegetated grid by a traceability analysis approach. Figure 6 shows the dominant traceable component for each grid which explains the greatest contrition to the element storage variation. The results showed that the element influx rates (i.e., NPP, U_N, and U_P) are the primary uncertainty source in 67.6, 93.2, and 93.0% of the vegetated grid cell for the C, N, and P storage, respectively. By further tracing the modeled variation of NPP into GPP and CUE, we found that GPP and CUE explained 91.6 and 8.4% of the variation across simulations, respectively. The baseline residence time has a larger uncertainty contribution than the environmental scalars (Figure 6). Specifically, the contributions of baseline element residence time (i.e., τ_C', τ_N', and τ_P') to the variation of ecosystem element residence time (i.e., τ_C, τ_N, and τ_P) is 75.3, 91.2, and 91.8%, respectively. While the contribution of ξ is 24.7% for the variation of τ_C, 8.8% for τ_N, and 8.2% for τ_P. In addition, the contributions of ξ_T and ξ_W to the variation of element storage are relatively small compared with other contributors, i.e., ξ_T and ξ_W only contribute 3.8 and 4.2% for C storage, 0.32 and 0.28% for N storage, and 0.28 and 0.29% for P storage variation, respectively.

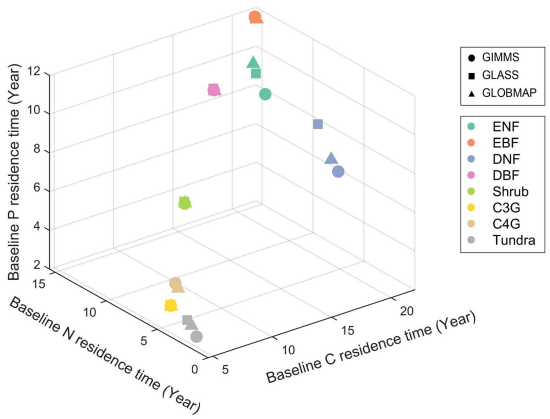

FIGURE 4
Comparison of baseline carbon, nitrogen and phosphorus residence time among different biomes with a three-dimensional scatter plot for each simulation. Abbreviations of biomes are given in Figure 3.

4. Discussion

Several recent studies have compared the differences among the existing satellite-derived LAI products on regional and global scales (Jiang et al., 2017; Liu et al., 2018). However, few studies have explored the influences of data uncertainty on simulated element storage in biogeochemical models. Our study shows that the largest discrepancies in the magnitude and spatial variance among different LAI products are mainly located in the evergreen broadleaf forest (Figure 2B), which is consistent with some previous studies (Camacho et al., 2013; Fang et al., 2013; Xiao et al., 2017; Piao et al., 2020). The significant divergence in different satellite-based LAI observations is due to the saturation effects of LAI in dense vegetation (Goswami et al., 2015; Li et al., 2018), sensor degradation, changes in platforms and sensors, and contamination by clouds and aerosols (Jiang et al., 2017; Liu et al., 2018; Piao et al., 2020). However, the high northern latitudes rather than the tropical regions have the most considerable discrepancies in simulated element storage due to the uncertainty of permafrost processes and the difficulty of spinning the model to equilibrium (Thornton and Rosenbloom, 2005; Xia et al., 2012). The results of the uncertainty pattern in element storage are consistent with that emerged in the current generation of Earth System Models (Arora et al., 2013; Friedlingstein et al., 2014; Zhou et al., 2021; Wei et al., 2022b). The contrast spatial distribution of uncertainty between satellite-derived LAI data and the modeled C-N-P storages indicates a nonlinear propagation of leaf area uncertainty in the biogeochemical models.

Decomposing the modeled element storage to its traceable components can facilitate understanding of inter-biome distributions of terrestrial C, N, and P storage on the globe (Figure 2). For instance, due to the long residence times and the corresponding moderate uptake rate, the deciduous needle leaf forest has the highest C, N, and P storage among all the eight biomes (Figure 3). Although evergreen broadleaf forests have relatively large influxes of C and N, the corresponding short residence time results in intermediate C and N storages. The P storage in the evergreen broadleaf forest regions can be decomposed into the medium P uptake and residence time (Figure 3). The ecosystem element residence time can be further decomposed into the corresponding baseline residence time and environmental scalars. As shown in Figure 4, the evergreen broadleaf forest has almost the longest mean baseline residence times of C (21.9 years), N (15.5 years), and P (11.5 years). However, although deciduous needle leaf forest has a relatively long baseline C residence time (21.8 years), it has only moderate baseline N (8.2 years) and P (6.8 years) residence time (Figure 4). This is because more assimilated N and P than C are allocated to leaves (C: 0.08, N: 0.26, P: 0.38) with faster turnover (Supplementary Figure S4). Previous studies also reported a longer P residence time on soils with low P availability (Tsujii et al., 2020), which can contribute to more efficient P conservation to support plant productivity under nutrient-limited regions (Wang et al., 2018). In addition, environmental scalars can also influence ecosystem residence time by regulating the baseline residence time in the CABLE model. For example, the low temperature decreases the decomposition rates in north-high latitude regions, though the absolute magnitude of

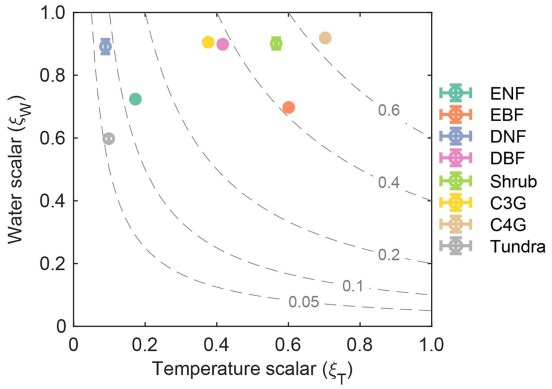

FIGURE 5
Determining of the environmental scalars (ξ) by temperature scalars (ξ_T) and water scalars (ξ_W) among biomes. The dashed line show the constant value of environment scalars. Abbreviations of biomes are given in Figure 3.

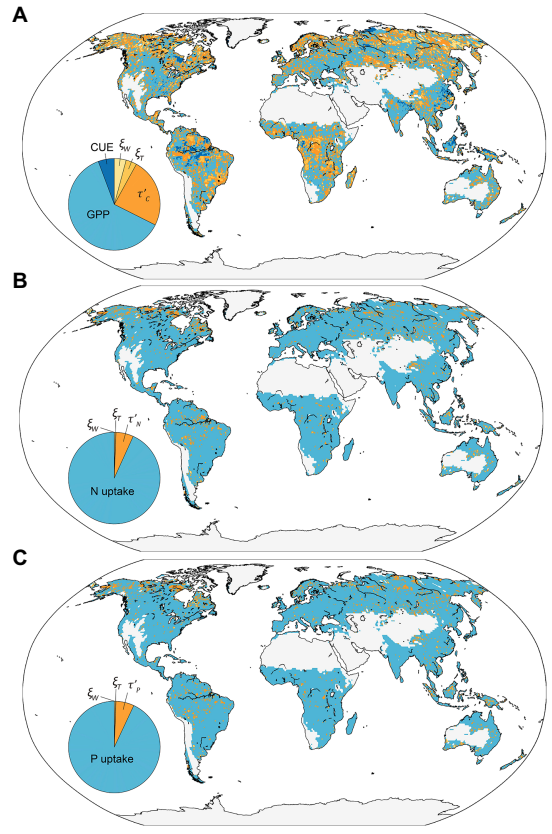

FIGURE 6
The global pattern of the dominant variable for the variation in simulated land carbon **(A)**, nitrogen **(B)**, and phosphorus **(C)** storage among three simulations. The insert panels indicate the proportion of each traceable components in global vegetated grids. GPP, gross primary productivity, CUE, carbon use efficiency; ξ_T , temperature scalars; ξ_W , water scalars; τ'_C , baseline C residence time; τ_N , baseline N residence time; τ_P , baseline P residence time.

discrepancy is large (Figure 5; Koven et al., 2015). Our results indicate that compared with the water scalar, the temperature scaler is the main limiting factor in all eight biomes (Figure 5), which is also supported by the observational datasets in temperate forests on the site levels (Chen et al., 2022).

We diagnosed the uncertainty source of different simulations derived from three satellite-based LAI products based on the traceability framework. We further quantified the dominant traceable component for each grid on a global scale. The results indicate that the uncertainty of element storage across three LAI-derived simulations shows a large spatial variation. Specifically, our study demonstrates that GPP contributes most to the spatial uncertainty of C storage in 61.9% of vegetated grids, mainly located in subtropical and some tropical regions. By contrast, the baseline C residence time was the major contributing factor for northern high-latitude areas (Figure 6). The spatial pattern of the dominant uncertainty components of N and P storage was similar to C storage, with N and P uptake rates dominating >90% of the global vegetated grids.

Although our biogeochemical traceability framework helps trace the uncertainty propagation path, we also acknowledge that it still has some limitations. First, the steady-state assumptions developing the traceability framework in this study are widely used in decomposing the land surface models (Xia et al., 2013; Rafique et al., 2016; Wei et al., 2022b) and developing models (Wang et al., 2018). However, terrestrial ecosystems are not steady (Luo and Weng, 2011) due to increasing atmospheric CO_2, climate warming, nitrogen deposition, and other anthropogenic disturbances (Friedlingstein et al., 2006; Sitch et al., 2015). Second, the plant functional types in each land grid cell are prescribed in the CABLE model. Thus, the uncertainty of LAI data may propagate to different processes in dynamic vegetation models, such as the CLM-FATES (Fisher et al., 2015) and BiomeE (Weng et al., 2015, 2019). Third, we acknowledge that this approach mainly focuses on ecosystems' emergent properties but ignores some understanding of internal ecological mechanisms such as competitive strategies and evolutionary systems. Furthermore, the traceability framework we applied in this study only considered organic pools and ignored soil inorganic N and P pools. The size of soil inorganic N and P pools may enhance or weaken the feedback between vegetation dynamics and climate change (Wei et al., 2019; Wang et al., 2022), calling for a further understanding of the interaction between vegetation and inorganic nutrient pools in biogeochemical models.

5. Conclusion

In summary, this study explored data uncertainty propagation to model uncertainty by decomposing the terrestrial organic element (i.e., C, N, and P) storage into its traceable components. Those components include the element uptake rates, ecosystem baseline residence time, temperature, and water scalars. Such a traceable analytical framework effectively reveals the mechanisms behind the simulation uncertainty and its propagation through ecosystem processes. By applying this framework, we can distinguish the reasons for the difference in simulated element storage caused by LAI among biomes and further diagnose the uncertainty source. It can be applied to other biogeochemical models to help characterize and quantify the uncertainty propagated in element cycles. The nonlinear uncertainty propagation of data to the model explored in this study can help improve biogeochemical models' future prediction ability. The findings in this study also call for more research efforts on the causal

links between leaf area and biogeochemical cycles in terrestrial ecosystems.

Data availability statement

The original contributions presented in the study are included in the article/supplementary material, further inquiries can be directed to the corresponding authors.

Author contributions

CB performed simulations, analyzed the results, and wrote the first draft. JX designed the study and revised the manuscript. All authors approved the submitted version.

Funding

This work was financially supported by the National Natural Science Foundation of China (nos. 31722009 and 41630528).

Conflict of interest

The authors declare that the research was conducted in the absence of any commercial or financial relationships that could be construed as a potential conflict of interest.

Publisher's note

All claims expressed in this article are solely those of the authors and do not necessarily represent those of their affiliated organizations, or those of the publisher, the editors and the reviewers. Any product that may be evaluated in this article, or claim that may be made by its manufacturer, is not guaranteed or endorsed by the publisher.

Supplementary material

The Supplementary material for this article can be found online at: https://www.frontiersin.org/articles/10.3389/fevo.2023.1105832/full#supplementary-material

References

Allen, K., Fisher, J. B., Phillips, R. P., Powers, J. S., and Brzostek, E. R. (2020). Modeling the carbon cost of plant nitrogen and phosphorus uptake across temperate and tropical forests. *Front. For. Glob. Change* 3:43. doi: 10.3389/ffgc.2020.00043

Arora, V. K., Boer, G. J., Friedlingstein, P., Eby, M., Jones, C. D., Christian, J. R., et al. (2013). Carbon–concentration and carbon–climate feedbacks in CMIP5 Earth system models. *J. Clim.* 26, 5289–5314. doi: 10.1175/JCLI-D-12-00494.1

Averill, C., and Waring, B. (2018). Nitrogen limitation of decomposition and decay: How can it occur? *Glob. Chang. Biol.* 24, 1417–1427. doi: 10.1111/gcb.13980

Best, M. J., Abramowitz, G., Johnson, H. R., Pitman, A. J., Balsamo, G., Boone, A., et al. (2015). The plumbing of land surface models: benchmarking model performance. *J. Hydrometeorol.* 16, 1425–1442. doi: 10.1175/JHM-D-14-0158.1

Bradford, M. A., and Crowther, T. W. (2013). Carbon use efficiency and storage in terrestrial ecosystems. *New Phytol.* 199, 7–9. doi: 10.1111/nph.12334

Camacho, F., Cernicharo, J., Lacaze, R., Baret, F., and Weiss, M. (2013). GEOV1: LAI, FAPAR essential climate variables and FCOVER global time series capitalizing over existing products. Part 2: validation and intercomparison with reference products. *Remote Sens. Environ.* 137, 310–329. doi: 10.1016/j.rse.2013.02.030

Chen, J. M., Ju, W., Ciais, P., Viovy, N., Liu, R., Liu, Y., et al. (2019). Vegetation structural change since 1981 significantly enhanced the terrestrial carbon sink. *Nat. Commun.* 10, 4259–4257. doi: 10.1038/s41467-019-12257-8

Chen, Y., Wang, Y. P., Tang, X., Zhou, G., Wang, C., Chang, Z., et al. (2022). Temperature dependence of ecosystem carbon, nitrogen and phosphorus residence times differs between subtropical and temperate forests in China. *Agric. For. Meteorol.* 326:109165. doi: 10.1016/j.agrformet.2022.109165

Cross, A. F., and Schlesinger, W. H. (1995). A literature review and evaluation of the Hedley fractionation: applications to the biogeochemical cycle of soil phosphorus in natural ecosystems. *Geoderma* 64, 197–214. doi: 10.1016/0016-7061(94)00023-4

Crowther, T. W., Van den Hoogen, J., Wan, J., Mayes, M. A., Keiser, A. D., Mo, L., et al. (2019). The global soil community and its influence on biogeochemistry. *Science* 365:eaav0550. doi: 10.1126/science.aav0550

Cui, E., Huang, K., Arain, M. A., Fisher, J. B., Huntzinger, D. N., Ito, A., et al. (2019). Vegetation functional properties determine uncertainty of simulated ecosystem productivity: A traceability analysis in the East Asian monsoon region. *Global Biogeochem. Cy.* 33, 668–689. doi: 10.1029/2018GB005909

Dardel, C., Kergoat, L., Hiernaux, P., Mougin, E., Grippa, M., and Tucker, C. J. (2014). Re-greening Sahel: 30years of remote sensing data and field observations (Mali, Niger). *Remote Sens. Environ.* 140, 350–364. doi: 10.1016/j.rse.2013.09.011

De Kauwe, M. G., Medlyn, B. E., Zaehle, S., Walker, A. P., Dietze, M. C., Wang, Y. P., et al. (2014). Where does the carbon go? A model–data intercomparison of vegetation carbon allocation and turnover processes at two temperate forest free-air CO_2 enrichment sites. *New Phytol.* 203, 883–899. doi: 10.1111/nph.12847

Deng, F., Chen, J. M., Plummer, S., Chen, M., and Pisek, J. (2006). Algorithm for global leaf area index retrieval using satellite imagery. *IEEE T. Geosci. Remote* 44, 2219–2229. doi: 10.1109/TGRS.2006.872100

Elser, J. J., Bracken, M. E., Cleland, E. E., Gruner, D. S., Harpole, W. S., Hillebrand, H., et al. (2007). Global analysis of nitrogen and phosphorus limitation of primary producers in freshwater, marine and terrestrial ecosystems. *Ecol. Lett.* 10, 1135–1142. doi: 10.1111/j.1461-0248.2007.01113.x

Fang, H., Jiang, C., Li, W., Wei, S., Baret, F., Chen, J. M., et al. (2013). Characterization and intercomparison of global moderate resolution leaf area index (LAI) products: Analysis of climatologies and theoretical uncertainties. *J. Geophys. Res. Biogeosci.* 118, 529–548. doi: 10.1002/jgrg.20051

Fisher, R. A., Muszala, S., Verteinstein, M., Lawrence, P., Xu, C., McDowell, N. G., et al. (2015). Taking off the training wheels: the properties of a dynamic vegetation model without climate envelopes, CLM4.5 (ED). *Geosci. Model Dev.* 8, 3593–3619. doi: 10.5194/gmd-8-3593-2015

Forzieri, G., Alkama, R., Miralles, D. G., and Cescatti, A. (2017). Satellites reveal contrasting responses of regional climate to the widespread greening of Earth. *Science* 356, 1180–1184. doi: 10.1126/science.aal1727

Friedlingstein, P., Cox, P., Betts, R., Bopp, L., von Bloh, W., Brovkin, V., et al. (2006). Climate–carbon cycle feedback analysis: results from the C4MIP model intercomparison. *J. Clim.* 19, 3337–3353. doi: 10.1175/JCLI3800.1

Friedlingstein, P., Jones, M. W., O'Sullivan, M., Andrew, R. M., Bakker, D. C., Hauck, J., et al. (2022). Global carbon budget 2021. *Earth Syst. Sci. Data* 14, 1917–2005. doi: 10.5194/essd-14-1917-2022

Friedlingstein, P., Meinshausen, M., Arora, V. K., Jones, C. D., Anav, A., Liddicoat, S. K., et al. (2014). Uncertainties in CMIP5 climate projections due to carbon cycle feedbacks. *J. Clim.* 27, 511–526. doi: 10.1175/JCLI-D-12-00579.1

Goll, D. S., Brovkin, V., Parida, B. R., Reick, C. H., Kattge, J., Reich, P. B., et al. (2012). Nutrient limitation reduces land carbon uptake in simulations with a model of combined carbon, nitrogen and phosphorus cycling. *Biogeosciences* 9, 3547–3569. doi: 10.5194/bg-9-3547-2012

Goll, D. S., Vuichard, N., Maignan, F., Jornet-Puig, A., Sardans, J., Violette, A., et al. (2017). A representation of the phosphorus cycle for ORCHIDEE (revision 4520). *Geosci. Model Dev.* 10, 3745–3770. doi: 10.5194/gmd-10-3745-2017

Goswami, S., Gamon, J., Vargas, S., and Tweedie, C. (2015). Relationships of NDVI, Biomass, and Leaf Area Index (LAI) for six key plant species in Barrow, Alaska. *PeerJ PrePrints* 3:e913v1. doi: 10.7287/peerj.preprints.913v1

Hedley, M. J., Stewart, J. W. B., and Chauhan, B. (1982). Changes in inorganic and organic soil phosphorus fractions induced by cultivation practices and by laboratory incubations. *Soil Sci. Soc. Am. J.* 46, 970–976. doi: 10.2136/sssaj1982.03615995004600050017x

Heinsch, F. A., Zhao, M., Running, S. W., Kimball, J. S., Nemani, R. R., Davis, K. J., et al. (2006). Evaluation of remote sensing based terrestrial productivity from MODIS using regional tower eddy flux network observations. *IEEE T. Geosci. Remote* 44, 1908–1925. doi: 10.1109/TGRS.2005.853936

Hofhansl, F., Schnecker, J., Singer, G., and Wanek, W. (2015). New insights into mechanisms driving carbon allocation in tropical forests. *New Phytologist* 205, 137–146. doi: 10.1111/nph.13007

Hou, E., Luo, Y., Kuang, Y., Chen, C., Lu, X., Jiang, L., et al. (2020). Global meta-analysis shows pervasive phosphorus limitation of aboveground plant production in natural terrestrial ecosystems. *Nat. Commun.* 11, 637–639. doi: 10.1038/s41467-020-14492-w

Hou, E., Tan, X., Heenan, M., and Wen, D. (2018). A global dataset of plant available and unavailable phosphorus in natural soils derived by Hedley method. *Sci. Data* 5:180166. doi: 10.1038/sdata.2018.166

Hungate, B. A., Dukes, J. S., Shaw, M. R., Luo, Y., and Field, C. B. (2003). Nitrogen and climate change. *Science* 302, 1512–1513. doi: 10.1126/science.1091390

Jiang, C., Ryu, Y., Fang, H., Myneni, R., Claverie, M., and Zhu, Z. (2017). Inconsistencies of interannual variability and trends in long-term satellite leaf area index products. *Glob. Chang. Biol.* 23, 4133–4146. doi: 10.1111/gcb.13787

Koven, C. D., Chambers, J. Q., Georgiou, K., Knox, R., Negron-Juarez, R., Riley, W. J., et al. (2015). Controls on terrestrial carbon feedbacks by productivity versus turnover in the CMIP5 Earth System Models. *Biogeosciences* 12, 5211–5228. doi: 10.5194/bg-12-5211-2015

LeBauer, D. S., and Treseder, K. K. (2008). Nitrogen limitation of net primary productivity in terrestrial ecosystems is globally distributed. *Ecology* 89, 371–379. doi: 10.1890/06-2057.1

Lei, L., Zhang, K., Zhang, X., Wang, Y. P., Xia, J., Piao, S., et al. (2019). Plant feedback aggravates soil organic carbon loss associated with wind erosion in Northwest China. *J. Geophys. Res. Biogeosci.* 124, 825–839. doi: 10.1029/2018JG004804

Li, Q., Lu, X., Wang, Y., Huang, X., Cox, P. M., and Luo, Y. (2018). Leaf area index identified as a major source of variability in modeled CO_2 fertilization. *Biogeosciences* 15, 6909–6925. doi: 10.5194/bg-15-6909-2018

Liu, Y., Liu, R., and Chen, J. M. (2012). Retrospective retrieval of long-term consistent global leaf area index (1981-2011) from combined AVHRR and MODIS data. *J. Geophys. Res. Biogeosci.* 117:G04003. doi: 10.1029/2012jg002084

Liu, Y., Xiao, J., Ju, W., Zhu, G., Wu, X., Fan, W., et al. (2018). Satellite-derived LAI products exhibit large discrepancies and can lead to substantial uncertainty in simulated carbon and water fluxes. *Remote Sens. Environ.* 206, 174–188. doi: 10.1016/j.rse.2017.12.024

Luo, Y., Huang, Y., Sierra, C. A., Xia, J., Ahlström, A., Chen, Y., et al. (2022). Matrix approach to land carbon cycle modeling. *J. Adv. Model. Earth Syst.* 14:e2022MS003008. doi: 10.1029/2022MS003008

Luo, Y., Keenan, T. F., and Smith, M. (2015). Predictability of the terrestrial carbon cycle. *Glob. Change Biol.* 21, 1737–1751. doi: 10.1111/gcb.12766

Luo, Y., Shi, Z., Lu, X., Xia, J., Liang, J., Jiang, J., et al. (2017). Transient dynamics of terrestrial carbon storage: mathematical foundation and its applications. *Biogeosciences* 14, 145–161. doi: 10.5194/bg-14-145-2017

Luo, Y., and Weng, E. (2011). Dynamic disequilibrium of the terrestrial carbon cycle under global change. *Trends Ecol. Evol.* 26, 96–104. doi: 10.1016/j.tree.2010.11.003

Manzoni, S., and Porporato, A. (2009). Soil carbon and nitrogen mineralization: theory and models across scales. *Soil Biol. Biochem.* 41, 1355–1379. doi: 10.1016/j.soilbio.2009.02.031

Mao, J., Shi, X., Thornton, P. E., Hoffman, F. M., Zhu, Z., and Myneni, R. B. (2013). Global latitudinal-asymmetric vegetation growth trends and their driving mechanisms: 1982–2009. *Remote Sens.* 5, 1484–1497. doi: 10.3390/rs5031484

Melillo, J. M., Butler, S., Johnson, J., Mohan, J., Steudler, P., Lux, H., et al. (2011). Soil warming, carbon–nitrogen interactions, and forest carbon budgets. *Proc. Natl. Acad. Sci. U.S.A.* 108, 9508–9512. doi: 10.1073/pnas.1018189108

Meyerholt, J., and Zaehle, S. (2015). The role of stoichiometric flexibility in modelling forest ecosystem responses to nitrogen fertilization. *New Phytol.* 208, 1042–1055. doi: 10.1111/nph.13547

Nakhavali, M. A., Mercado, L. M., Hartley, I. P., Sitch, S., Cunha, F. V., di Ponzio, R., et al. (2022). Representation of the phosphorus cycle in the Joint UK Land Environment Simulator (vn5. 5_JULES-CNP). *Geosci. Model Dev.* 15, 5241–5269. doi: 10.5194/gmd-15-5241-2022

New, M., Hulme, M., and Jones, P. (1999). Representing twentieth-century space–time climate variability. Part I: Development of a 1961–90 mean monthly terrestrial climatology. *J. Clim.* 12, 829–856. doi: 10.1175/1520-0442(1999)012<0829:RTCSTC>2.0.CO;2

New, M., Hulme, M., and Jones, P. (2000). Representing twentieth-century space–time climate variability. Part II: Development of 1901–96 monthly grids of terrestrial surface climate. *J. Clim.* 13, 2217–2238. doi: 10.1175/1520-0442(2000)013<2217:RTCSTC>2.0.CO;2

New, M., Lister, D., Hulme, M., and Makin, I. (2002). A high-resolution data set of surface climate over global land areas. *Clim. Res.* 21, 1–25. doi: 10.3354/cr021001

Norby, R. J., Warren, J. M., Iversen, C. M., Medlyn, B. E., and McMurtrie, R. E. (2010). CO_2 enhancement of forest productivity constrained by limited nitrogen availability. *Proc. Natl. Acad. Sci. U. S. A.* 107, 19368–19373. doi: 10.1073/pnas.1006463107

Olson, J. S. (1963). Energy storage and the balance of producers and decomposers in ecological systems. *Ecology* 44, 322–331. doi: 10.2307/1932179

Piao, S., Wang, X., Park, T., Chen, C., Lian, X. U., He, Y., et al. (2020). Characteristics, drivers and feedbacks of global greening. *Nat. Rev. Earth Environ.* 1, 14–27. doi: 10.1038/s43017-019-0001-x

Piao, S., Yin, G., Tan, J., Cheng, L., Huang, M., Li, Y., et al. (2015). Detection and attribution of vegetation greening trend in China over the last 30 years. *Glob. Chang. Biol.* 21, 1601–1609. doi: 10.1111/gcb.12795

Rafique, R., Xia, J., Hararuk, O., Asrar, G. R., Leng, G., Wang, Y., et al. (2016). Divergent predictions of carbon storage between two global land models: attribution of the causes through traceability analysis. *Earth Syst. Dynam.* 7, 649–658. doi: 10.5194/esd-7-649-2016

Sitch, S., Friedlingstein, P., Gruber, N., Jones, S. D., Murray-Tortarolo, G., Ahlström, A., et al. (2015). Recent trends and drivers of regional sources and sinks of carbon dioxide. *Biogeosciences* 12, 653–679. doi: 10.5194/bg-12-653-2015

Sun, Y., Goll, D. S., Chang, J., Ciais, P., Guenet, B., Helfenstein, J., et al. (2021). Global evaluation of the nutrient-enabled version of the land surface model ORCHIDEE-CNP v1. 2 (r5986). *Geosci. Model Dev.* 14, 1987–2010. doi: 10.5194/gmd-14-1987-2021

Sun, Y., Peng, S., Goll, D. S., Ciais, P., Guenet, B., Guimberteau, M., et al. (2017). Diagnosing phosphorus limitations in natural terrestrial ecosystems in carbon cycle models. *Earth's Future* 5, 730–749. doi: 10.1002/2016EF000472

Sutton, M. A., Simpson, D., Levy, P. E., Smith, R. I., Reis, S., Van Oijen, M., et al. (2008). Uncertainties in the relationship between atmospheric nitrogen deposition and forest carbon sequestration. *Glob. Change Biol.* 14, 2057–2063. doi: 10.1111/j.1365-2486.2008.01636.x

Thomas, R. Q., Brookshire, E. N. J., and Gerber, S. (2015). Nitrogen limitation on land: how can it occur in Earth system models? *Glob. Change Biol.* 21, 1777–1793. doi: 10.1111/gcb.12813

Thornton, P. E., Lamarque, J. F., Rosenbloom, N. A., and Mahowald, N. M. (2007). Influence of carbon-nitrogen cycle coupling on land model response to CO_2 fertilization and climate variability. *Global Biogeochem. Cy.* 21:GB4018. doi: 10.1029/2006GB002868

Thornton, P. E., and Rosenbloom, N. A. (2005). Ecosystem model spin-up: estimating steady state conditions in a coupled terrestrial carbon and nitrogen cycle model. *Ecol. Model.* 189, 25–48. doi: 10.1016/j.ecolmodel.2005.04.008

Thum, T., Caldararu, S., Engel, J., Kern, M., Pallandt, M., Schnur, R., et al. (2019). A new model of the coupled carbon, nitrogen, and phosphorus cycles in the terrestrial biosphere (QUINCY v1. 0; revision 1996). *Geosci. Model Dev.* 12, 4781–4802. doi: 10.5194/gmd-12-4781-2019

Tsujii, Y., Aiba, S. I., and Kitayama, K. (2020). Phosphorus allocation to and resorption from leaves regulate the residence time of phosphorus in above-ground forest biomass on Mount Kinabalu. *Borneo. Funct. Ecol.* 34, 1702–1712. doi: 10.1111/1365-2435.13574

Wang, Y., Ciais, P., Goll, D., Huang, Y., Luo, Y., Wang, Y. P., et al. (2018). GOLUM-CNP v1. 0: a data-driven modeling of carbon, nitrogen and phosphorus cycles in major terrestrial biomes. *Geosci. Model Dev.* 11, 3903–3928. doi: 10.5194/gmd-11-3903-2018

Wang, Y. P., Houlton, B. Z., and Field, C. B. (2007). A model of biogeochemical cycles of carbon, nitrogen, and phosphorus including symbiotic nitrogen fixation and phosphatase production. *Global Biogeochem. Cy.* 21:GB1018. doi: 10.1029/2006GB002797

Wang, Y. P., Huang, Y., Augusto, L., Goll, D. S., Helfenstein, J., and Hou, E. (2022). Toward a global model for soil inorganic phosphorus dynamics: dependence of exchange kinetics and soil bioavailability on soil physicochemical properties. *Global Biogeochem. Cy.* 36:e2021GB007061. doi: 10.1029/2021GB007061

Wang, Y. P., Kowalczyk, E., Leuning, R., Abramowitz, G., Raupach, M. R., Pak, B., et al. (2011). Diagnosing errors in a land surface model (CABLE) in the time and frequency domains. *J. Geophys. Res. Biogeosci.* 116:G01034. doi: 10.1029/2010jg001385

Wang, Y. P., Law, R. M., and Pak, B. (2010). A global model of carbon, nitrogen and phosphorus cycles for the terrestrial biosphere. *Biogeosciences* 7, 2261–2282. doi: 10.5194/bg-7-2261-2010

Wang, S., Zhang, Y., Ju, W., Chen, J. M., Ciais, P., Cescatti, A., et al. (2020). Recent global decline of CO_2 fertilization effects on vegetation photosynthesis. *Science* 370, 1295–1300. doi: 10.1126/science.abb7772

Wei, N., Cui, E., Huang, K., Du, Z., Zhou, J., Xu, X., et al. (2019). Decadal stabilization of soil inorganic nitrogen as a benchmark for global land models. *J. Adv. Model. Earth Syst.* 11, 1088–1099. doi: 10.1029/2019MS001633

Wei, N., Xia, J., Wang, Y. P., Zhang, X., Zhou, J., Bian, C., et al. (2022a). Nutrient limitations lead to a reduced magnitude of disequilibrium in the global terrestrial carbon cycle. *J. Geophys. Res. Biogeosci.* 127:e2021JG006764. doi: 10.1029/2021JG006764

Wei, N., Xia, J., Zhou, J., Jiang, L., Cui, E., Ping, J., et al. (2022b). Evolution of uncertainty in terrestrial carbon storage in earth system models from CMIP5 to CMP6. *J. Clim.* 35, 5483–5499. doi: 10.1175/jcli-d-21-0763.1

Weng, E., Dybzinski, R., Farrior, C. E., and Pacala, S. W. (2019). Competition alters predicted forest carbon cycle responses to nitrogen availability and elevated CO_2: simulations using an explicitly competitive, game-theoretic vegetation demographic model. *Biogeosciences* 16, 4577–4599. doi: 10.5194/bg-16-4577-2019

Weng, E. S., Malyshev, S., Lichstein, J. W., Farrior, C. E., Dybzinski, R., Zhang, T., et al. (2015). Scaling from individual trees to forests in an earth system modeling framework using a mathematically tractable model of height-structured competition. *Biogeosciences* 12, 2655–2694. doi: 10.5194/bg-12-2655-2015

Wieder, W. R., Cleveland, C. C., Smith, W. K., and Todd-Brown, K. (2015). Future productivity and carbon storage limited by terrestrial nutrient availability. *Nat. Geosci.* 8, 441–444. doi: 10.1038/ngeo2413

Xia, J., Luo, Y., Wang, Y. P., and Hararuk, O. (2013). Traceable components of terrestrial carbon storage capacity in biogeochemical models. *Glob. Chang. Biol.* 19, 2104–2116. doi: 10.1111/gcb.12172

Xia, J., Luo, Y., Wang, Y.-P., Weng, E., and Hararuk, O. (2012). A semi-analytical solution to accelerate spin-up of a coupled carbon and nitrogen land model to steady state. *Geosci. Model Dev.* 5, 1259–1271. doi: 10.5194/gmd-5-1259-2012

Xia, J., McGuire, A. D., Lawrence, D., Burke, E., Chen, G., Chen, X., et al. (2017). Terrestrial ecosystem model performance in simulating productivity and its vulnerability to climate change in the northern permafrost region. *J. Geophys. Res. Biogeosci.* 122, 430–446. doi: 10.1002/2016JG003384

Xia, J., and Wan, S. (2008). Global response patterns of terrestrial plant species to nitrogen addition. *New Phytol.* 179, 428–439. doi: 10.1111/j.1469-8137.2008.02488.x

Xiao, Z., Liang, S., and Jiang, B. (2017). Evaluation of four long time-series global leaf area index products. *Agric. For. Meteorol.* 246, 218–230. doi: 10.1016/j.agrformet.2017.06.016

Xiao, Z., Liang, S., Wang, J., Chen, P., Yin, X., Zhang, L., et al. (2014). Use of general regression neural networks for generating the GLASS leaf area index product from time-series MODIS surface reflectance. *IEEE T. Geosci. Remote* 52, 209–223. doi: 10.1109/tgrs.2013.2237780

Xiao, Z., Liang, S., Wang, J., Xiang, Y., Zhao, X., and Song, J. (2016). Long-time-series global land surface satellite leaf area index product derived from MODIS and AVHRR surface reflectance. *IEEE T. Geosci. Remote* 54, 5301–5318. doi: 10.1109/tgrs.2016.2560522

Yang, X., Thornton, P. E., Ricciuto, D. M., and Post, W. M. (2014). The role of phosphorus dynamics in tropical forests – a modeling study using CLM-CNP. *Biogeosciences* 11, 1667–1681. doi: 10.5194/bg-11-1667-2014

Yu, L., Ahrens, B., Wutzler, T., Schrumpf, M., and Zaehle, S. (2020). Jena Soil Model (JSM v1. 0; revision 1934): a microbial soil organic carbon model integrated with nitrogen and phosphorus processes. *Geosci. Model Dev.* 13, 783–803. doi: 10.5194/gmd-13-783-2020

Zaehle, S., and Dalmonech, D. (2011). Carbon–nitrogen interactions on land at global scales: current understanding in modelling climate biosphere feedbacks. *Curr. Opin. Env. Sust.* 3, 311–320. doi: 10.1016/j.cosust.2011.08.008

Zaehle, S., Medlyn, B. E., De Kauwe, M. G., Walker, A. P., Dietze, M. C., Hickler, T., et al. (2014). Evaluation of 11 terrestrial carbon–nitrogen cycle models against observations from two temperate Free-Air CO_2 enrichment studies. *New Phytol.* 202, 803–822. doi: 10.1111/nph.12697

Zeng, Z., Piao, S., Li, L. Z., Zhou, L., Ciais, P., Wang, T., et al. (2017). Climate mitigation from vegetation biophysical feedbacks during the past three decades. *Nat. Clim. Chang.* 7, 432–436. doi: 10.1038/nclimate3299

Zeng, Z., Zhu, Z., Lian, X., Li, L. Z. X., Chen, A., He, X., et al. (2016). Responses of land evapotranspiration to earth's greening in CMIP5 earth system models. *Environ. Res. Lett.* 11:104006. doi: 10.1088/1748-9326/11/10/104006

Zhang, D., Hui, D. F., Luo, Y. Q., and Zhou, G. Y. (2008). Rates of litter decomposition in terrestrial ecosystems: global patterns and controlling factors. *J. Plant Ecol.* 1, 85–93. doi: 10.1093/jpe/rtn002

Zhang, X., Rayner, P. J., Wang, Y. P., Silver, J. D., Lu, X., Pak, B., et al. (2016). Linear and nonlinear effects of dominant drivers on the trends in global and regional land carbon uptake: 1959 to 2013. *Geophys. Res. Lett.* 43, 1607–1614. doi: 10.1002/2015GL067162

Zhou, S., Liang, J., Lu, X., Li, Q., Jiang, L., Zhang, Y., et al. (2018). Sources of uncertainty in modeled land carbon storage within and across three MIPs: diagnosis with three new techniques. *J. Clim.* 31, 2833–2851. doi: 10.1175/JCLI-D-17-0357.1

Zhou, J., Xia, J., Wei, N., Liu, Y., Bian, C., Bai, Y., et al. (2021). A traceability analysis system for model evaluation on land carbon dynamics: design and applications. *Ecol. Process.* 10, 1–14. doi: 10.1186/s13717-021-00281-w

Zhu, Z., Bi, J., Pan, Y., Ganguly, S., Anav, A., Xu, L., et al. (2013). Global data sets of vegetation leaf area index (LAI)3g and fraction of photosynthetically active radiation (FPAR)3g derived from global inventory modeling and mapping studies (GIMMS) normalized difference vegetation index (NDVI3g) for the period 1981 to 2011. *Remote Sens.* 5, 927–948. doi: 10.3390/rs5020927

Zhu, Z., Piao, S., Lian, X., Myneni, R. B., Peng, S., and Yang, H. (2017). Attribution of seasonal leaf area index trends in the northern latitudes with "optimally" integrated ecosystem models. *Glob. Chang. Biol.* 23, 4798–4813. doi: 10.1111/gcb.13723

Zhu, Z., Piao, S., Myneni, R. B., Huang, M., Zeng, Z., Canadell, J. G., et al. (2016). Greening of the earth and its drivers. *Nat. Clim. Chang.* 6, 791–795. doi: 10.1038/nclimate3004

Zhu, Q., Riley, W. J., Tang, J., Collier, N., Hoffman, F. M., Yang, X., et al. (2019). Representing nitrogen, phosphorus, and carbon interactions in the E3SM land model: Development and global benchmarking. *J. Adv. Model. Earth Syst.* 11, 2238–2258. doi: 10.1029/2018MS001571

frontiers | Frontiers in Ecology and Evolution

TYPE Original Research
PUBLISHED 20 March 2023
DOI 10.3389/fevo.2023.1106461

OPEN ACCESS

EDITED BY
Mehdi Cherif,
INRA Centre Bordeaux-Aquitaine, France

REVIEWED BY
Shawn James Leroux,
Memorial University of Newfoundland, Canada
Gina Marie Wimp,
Georgetown University, United States

*CORRESPONDENCE
Stefano Manzoni
✉ stefano.manzoni@natgeo.su.se

SPECIALTY SECTION
This article was submitted to Population, Community, and Ecosystem Dynamics, a section of the journal Frontiers in Ecology and Evolution

RECEIVED 23 November 2022
ACCEPTED 09 February 2023
PUBLISHED 20 March 2023

CITATION
Zelnik YR, Manzoni S and Bommarco R (2023) Primary production in subsidized green-brown food webs. *Front. Ecol. Evol.* 11:1106461. doi: 10.3389/fevo.2023.1106461

Primary production in subsidized green-brown food webs

Yuval R. Zelnik[1], Stefano Manzoni[2]* and Riccardo Bommarco[1]

[1]Department of Ecology, Swedish University of Agricultural Sciences, Uppsala, Sweden, [2]Department of Physical Geography and Bolin Centre for Climate Research, Stockholm University, Stockholm, Sweden

Ecosystems worldwide receive large amounts of nutrients from both natural processes and human activities. While direct subsidy effects on primary production are relatively well-known (the green food web), the indirect effects of subsidies on producers as mediated by the brown food web and predators are poorly considered. With a dynamical green-brown food web model, parameterized using empirical estimates from the literature, we illustrate the effect of organic and inorganic nutrient subsidies on net primary production (NPP) (i.e., after removing loss to herbivory) in two idealized ecosystems—one terrestrial and one aquatic. We find that nutrient subsidies increase net primary production, an effect that saturates with increasing subsidies. Changing the quality of subsidies from inorganic to organic tends to increase net primary production in terrestrial ecosystems, but less often so in aquatic ecosystems. This occurs when organic nutrient inputs promote detritivores in the brown food web, and hence predators that in turn regulate herbivores, thereby promoting primary production. This previously largely overlooked effect is further enhanced by ecosystem properties such as fast decomposition and low rates of nutrient additions and demonstrates the importance of nutrient subsidy quality on ecosystem functioning.

KEYWORDS

nutrient subsidy, trophic cascade, primary production, ecosystem function, ecosystem modeling, organic fertilization, food web

1. Introduction

No ecosystem is an island, entirely cut off from external influences. On the contrary, the influx of materials and organisms into ecosystems, known as subsidies, significantly impact the state and functioning of ecosystems (Polis et al., 1997; Palumbi, 2003). The subsidies can take various forms, including mass transport of materials by water and air (Bobbink et al., 2010), animals that move across ecosystems for various activities such as foraging (Marczak et al., 2007; Buendía et al., 2018), and, an increasingly important phenomenon for ecosystems world-wide, input of resources such as nutrients through human activities (Raun and Johnson, 1999; Newsome et al., 2015). Subsidies can have diverse impacts. Adding nutrients in limited supply in the ecosystem often increases primary production (Polis et al., 1997; Montagano et al., 2018), but it can also reduce it when, for instance, adding one nutrient promotes plant–microbe competition for other nutrients (Čapek et al., 2018). The consequences of subsidies depend on the trophic interactions in the ecosystem. Introducing consumers changes ecosystem fluxes which affects biomass distributions across trophic levels (Allen and Wesner, 2016) and thereby how nutrients cycle in the ecosystem. Introduced species can change the behavior of the ecosystem entirely, as they create novel interactions and pathways (Baxter et al., 2004).

Subsidies can move both horizontally between food web compartments at a certain trophic level and vertically across trophic levels within a food web. Horizontal transfer occurs due to nutrient flows and interactions of organisms between food webs, and can occur through physical transfer of material between spatially separated webs in an ecosystem, or through species interactions in linked food webs (Nakano and Murakami, 2001; Baxter et al., 2004). For example, consumer species in green-brown food webs that rely on both primary producers in the green channel and detrital matter in the brown channel connect the two channels and their food webs (Moore et al., 2004; Allen and Wesner, 2016). Subsidies also lead to vertical exchanges between trophic levels within a food web. Subsidies provided from below, by influx of nutrients or direct provision to primary producers, propagates up to consumer species, increasing the overall biomass and altering the shape of biomass distribution in the food web (Hines et al., 2006). Predator subsidies lead to pressure on the herbivores they consume, and can lead to trophic cascades where primary producers are released from herbivory pressure due to predation (Leroux and Loreau, 2008; Newsome et al., 2015; Galiana et al., 2021). Hence, subsidies can cause positive albeit indirect effects on primary production via trophic interactions, but outcomes of such combined horizontal and vertical effects of subsidies in green-brown food webs are poorly explored.

Research on the impact of subsidies has centered on either the horizontal or the vertical flows, without bringing these two perspectives together (Rooney et al., 2006). Studies of landscape ecology and meta-ecosystem theory have focused on horizontal transfer between habitats (Darimont et al., 2009; Gravel et al., 2010), and how it interacts with spatial structure (Jacquet et al., 2022). In contrast, food web ecologists have focused on vertical flows that can change biomass distributions and can lead to trophic cascades (Leroux and Loreau, 2008). However, flow of energy and nutrients due to subsidies can be more nuanced due to the complexity of interactions within ecosystems, intertwining the horizontal and vertical flows. Moreover, research on subsidies has largely focused on green food webs (Nakano and Murakami, 2001; Loreau and Holt, 2004; Bobbink et al., 2010), with more recent interest in brown food webs (Allen and Wesner, 2016; McCary et al., 2020). Linking the two into integrated green-brown food webs has only just begun (Zou et al., 2016).

Nutrient subsidies into the brown channel of the food web has recently been shown to affect plant production (Riggi and Bommarco, 2019; Aguilera et al., 2021). The subsidies provide food for detritivores, which in turn increases predator populations, and lead to a trophic cascade where plants grow more as herbivory pressure is reduced by predators. However, a theoretical understanding of these processes and their relevance has lagged behind. While some theoretical investigations have been conducted on how organic matter subsidies affect primary producers and nutrient recycling (Leroux and Loreau, 2008; Gounand et al., 2014; Spiecker et al., 2016), we know of only two studies in which the full green-brown food web was considered in the context of subsidies (Attayde and Ripa, 2008; McCary et al., 2020). However, they did not consider how the input rate and quality of nutrient subsidies affect the food web.

Here, we develop and use a dynamical model to examine how nutrient subsidies affect primary production in coupled green-brown food webs in terrestrial and aquatic ecosystems. We focus on nitrogen as a key nutrient whose cycle has been widely disrupted by human activities, and measure net primary production (NPP) (i.e., the production remaining after herbivory), as a function of nutrient subsidy. The nutrient subsidy properties we consider are the amounts of inorganic and organic nitrogen in detrital matter (e.g., green or animal manure) and their relative proportions. Inorganic nitrogen is directly taken up by primary producers and fuels the green channel, while organic nitrogen is consumed by decomposers and fuels the brown channel. Combining the model with data from the literature on nitrogen fluxes and stocks we aim to assess, first, how the strength and quality of subsidies affect net primary production. Second, we investigate how food web properties, such as consumption, nitrogen conversion efficiencies, and metabolic rates for consumers, and ecosystem properties, such as nitrogen mineralization rate and primary producer mortality, modify the subsidy effect on primary producers. Our results focus on idealized aquatic and terrestrial ecosystems intended to be representative of widespread conditions on Earth.

2. Methods

We note that we use a similar methodology to another study (Zelnik et al., 2022), with the same model and some of the same sources for parameterizing the model. For clarity, we note a few main differences: (i) We base the parameterization of this model (see below) on fewer studies, as we focus less on the data synthesis aspect of the previous study and more on theoretical analysis. (ii) We use a more general parameter exploration, focusing on two generic ecosystem types rather than six specific types (e.g., forests) as in the previous model, and do not set any parameter to zero throughout, as we did for some parameters in the previous study. (iii) We focus here on net primary production, rather than on general trends of stocks and fluxes, as in the previous study.

2.1. Dynamical model

To model the dynamics of subsidized green-brown food webs, we write six mass balance equations describing the changes in nitrogen stock in units of [gN m^{-2}] (see Table 1). Four compartments are functional groups of organisms: primary producers (P), herbivores (H), detritivores excluding microorganisms (D), and predators (C). The two other compartments are of organic nitrogen including microbial decomposers (S) and inorganic nitrogen (N).

While we focus on nitrogen as a key limiting nutrient in many ecosystems, we keep the model general, to open for the possibility to describe the dynamics of other nutrients as well. We follow Barbier and Loreau (2019) in defining the food web interactions, using a type I functional response for consumption terms, together with self-regulation (Barabás et al., 2017) of each species compartment. A conceptual diagram is given in Figure 1, and the model dynamics

TABLE 1 Definition of variables, fluxes, and metrics used.

Name	Description	Units
P	Primary producer stock	$[\mathrm{gNm^{-2}}]$
H	Herbivore stock	$[\mathrm{gNm^{-2}}]$
S	Detrivore stock	$[\mathrm{gNm^{-2}}]$
C	Predator stock	$[\mathrm{gNm^{-2}}]$
N	Inorganic nitrogen stock	$[\mathrm{gNm^{-2}}]$
S	Organic nitrogen stock	$[\mathrm{gNm^{-2}}]$
I	Subsidy strength	$[\mathrm{gNm^{-2}y^{-1}}]$
I_N	Inorganic subsidy strength	$[\mathrm{gNm^{-2}y^{-1}}]$
I_S	Organic subsidy strength	$[\mathrm{gNm^{-2}y^{-1}}]$
I_0	Nitrogen input from recycling	$[\mathrm{gNm^{-2}y^{-1}}]$
ψ	Fraction of organic subsidy	
$PSOS$	Producer sensitivity to organic subsidies	

Note that $I = I_N + I_S$, $\psi = I_S/I$, and $PSOS = \frac{1}{<P>} \cdot \frac{d}{d\psi} P$.

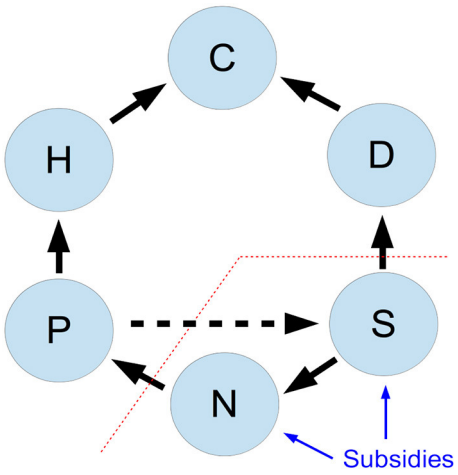

FIGURE 1
Interactions between the six compartments of an ecosystem model with nutrient subsidies. Compartments are: primary producers (P), herbivores (H), detritivores (D), predators (C), inorganic nutrients (N), active organic nitrogen (S). Black lines show nutrient fluxes between compartments; blue lines show the nutrient subsidies that are added to the ecosystem, the red line marks the separation between organism and substrate compartments, and the dashed arrow indicates nutrient recycling from dead primary producers to the organic nitrogen compartment.

are detailed by the coupled ordinary differential equations, given in Equation (1).

$$\frac{d}{dt}P = P\left(\epsilon_P r_P N - r_H H - u_P - q_P P\right) \tag{1a}$$

$$\frac{d}{dt}H = H\left(\epsilon_H r_H P - r_C C - u_H - q_H H\right) \tag{1b}$$

$$\frac{d}{dt}D = D\left(\epsilon_D r_D S - r_C C - u_D - q_D D\right) \tag{1c}$$

$$\frac{d}{dt}C = C\left(\epsilon_C r_C H + \epsilon_C r_C D - u_C - q_C C\right) \tag{1d}$$

$$\frac{d}{dt}N = zS - \ell N - r_P P N + I_N \tag{1e}$$

$$\frac{d}{dt}S = I_0 - zS - r_D D S + I_S \tag{1f}$$

For each of the first four compartments, with i designating the specific compartment, the parameter r_i represents the consumption coefficient of the trophic level below (in units of $[\mathrm{m^2(gN)^{-1}yr^{-1}}]$), ϵ_i is the non-dimensional nutrient conversion efficiency associated with this consumption, u_i is the natural mortality rate (units of $(\mathrm{yr^{-1}})$), and q_i is the self-regulation coefficient (e.g., light limitation for primary producers, or intra-guild predation for predators, in units of $[\mathrm{m^2(gN)^{-1}yr^{-1}}]$). In the two abiotic compartments, z is the rate of nitrogen mineralization, and ℓ is the loss rate of inorganic nitrogen due to mass transport and chemical transformations such as denitrification that remove nitrogen from the N pool, both in units of $(\mathrm{yr^{-1}})$. The latter is assumed independent of the subsidy amount and quality, even though nitrogen loss rates can depend on both amount and quality of the subsidy (e.g., N_2O emissions, Shcherbak et al., 2014). I_N and I_S are the influx rates of nitrogen into the N and S compartments, respectively, which are interpreted as subsidy fluxes of inorganic and organic nitrogen. We define the nutrient subsidy strength as $I = I_N + I_S$. The fraction of organic subsidy, which we call subsidy quality or ψ, is calculated as I_S/I. Thus, $\psi = 0$ for strictly inorganic subsidy and $\psi = 1$ for only organic inputs. I_0 is the input of nutrients from recycled materials from primary producers, given as $I_0 = yu_P P$, with y the recycling rate (the quantitatively smaller recycling from other compartments is neglected for simplicity). The definitions of the different subsidy fluxes are also noted in Table 1.

A few modeling choices require some explanations. By having self-regulation terms (e.g., $q_P P^2$ in the first equation) we can expect more well-behaved dynamics (Barabás et al., 2017), e.g., avoiding oscillatory dynamics observed in previous studies (Attayde and Ripa, 2008). We also make a neutral assumption on predator preference, in which predators are agnostic as to which prey they consume and can switch freely between herbivores and detritivores (i.e., generalist multichannel predators). We focus on a type-I functional response as it is simpler to analyze, and it is not *a priori* clear which type of functional response is the most relevant at the ecosystem level. Beyond type-I functional response, type-II functional response is often used in consumer–resource interactions (Attayde and Ripa, 2008; Wollrab et al., 2012), although its relevance has also been contested Jonsson (2017). Furthermore, it has been previously found that the choice of functional response type does not alter the qualitative outcomes of nutrient enrichment (Wollrab et al., 2012). To assert this also in our model, we test a model with a type-II functional response, and conclude that a type-I functional response is more relevant for our modeling approach, being less likely to lead to extinction of entire functional groups (e.g., no herbivores in the ecosystem) and temporal oscillations (Supplementary material).

Nutrient recycling (I_0), represented by the dashed horizontal arrow in Figure 1, is a main nutrient source in many ecosystems, especially terrestrial and macrophyte-dominated aquatic ecosystems (Manzoni et al., 2018). As we show in the Supplementary material, including recycling has a similar effect as

an increase in subsidy strength I and a decrease in ψ, compared to a scenario without recycling. This effect of recycling can be explained by noticing that even with only the inorganic nitrogen subsidy, the organic nitrogen compartment is fed by nitrogen recycling of primary producer biomass. Therefore, without loss of generality, we focus in the main text on ecosystem dynamics without nutrient recycling, i.e., setting $y = 0$. This assumption allows for a simplified analysis and presentation while retaining the qualitative behavior of the model. We also show that including detritus recycling gives qualitatively similar results (Supplementary material).

2.2. Model parameterization

To analyze the effects of subsidies on primary production, we parameterize the model for two generic ecosystem types: a terrestrial and an aquatic ecosystem. These idealized ecosystems are used as baselines, and we test a wide range of parameters around these baseline values to ensure the generality of our results. We base the model parameterization on two data collections with estimates of nitrogen stocks and flow rates as defined in our model (Cebrian, 1999, 2004). We draw rough estimates of ecosystem properties such as nutrient conversion efficiencies from a dozen additional studies detailed in the Data collection subsection below. All values are converted to units of grams of nitrogen per square meter for stocks, and per year for rates. As explained below in the Parameter derivation subsection, we assume that Equation (1) are in equilibrium, and use the empirically-derived stock and rate estimates to back-calculate the model parameters for the terrestrial and aquatic ecosystem, respectively. We do this by estimating the production fluxes of the four compartments (P, H, D, C), and use these flux values together with values for fraction of production lost to processes such as predation, to estimate the various parameters. Finally, as explained in the Simulations and parameter exploration subsection 2.5, we use two methods to numerically explore the consequences on primary production of a wide range of possible parameter values representing different ecosystems.

2.3. Data collection

We combine the datasets from Cebrian (1999, 2004) according to idealized ecosystem type: terrestrial or aquatic. Terrestrial ecosystems include those labeled as forests, grasslands, savannas, drylands, and boreal ecosystems. Aquatic ecosystems include all marine and freshwater ecosystems, such as oceans, seagrass meadows, coral reefs, and lakes. We exclude data for marshes and swamps from either ecosystem type. With these definitions, we obtain 210 records for the terrestrial and 534 records for the aquatic idealized ecosystem from the datasets. The data types for each record and their associated units are: primary producer nitrogen content (ν_P [gN/gDW]; DW stands for dry weight), primary producer stocks (B_P [gCm^{-2}]), herbivore stocks (B_H [gCm^{-2}]), mineralization rate (z [yr^{-1}]), decomposition flux (f_D [gCyr^{-1}m^{-2}]), detrital production (f_M [gCyr^{-1}m^{-2}]), primary production (f_P [gCyr^{-1}m^{-2}]), herbivory fraction (ρ_{PH}). The geometric average of the available values is calculated for each data type and used in the subsequent estimation of the model parameters for each ecosystem type. The use of a geometric average is appropriate due to the wide range of values for various ecosystems (Bar-On et al., 2018). We use the primary producer average nitrogen content, together with a ratio of carbon to dry-weight ratio of 2.5 (Cebrian and Lartigue, 2004), to convert B_P and all fluxes related to primary producers and detritus from carbon to nitrogen, for instance $P = B_P \cdot (\nu_P/2.5)$. We similarly use a carbon to nitrogen ratio for animals of 5 (Allgeier et al., 2020), to convert B_H from carbon to nitrogen stocks. We estimate S using the ratio between the decomposition flux and mineralization, $D = f_D/z$, where we take S as the effective stock of organic matter.

Beyond the data from Cebrian (1999, 2004), additional estimations of ratios of stocks and process rates are needed to parameterize our model. In absence of a cohesive empirical estimates for terrestrial and aquatic ecosystems, we use representative information from a variety of sources, striving to define plausible values for the model parameters so that nitrogen stocks and fluxes remain within reasonable observed ranges.

We begin by estimating the ratios between compartment stocks, i.e., of predators to herbivores σ_{CH}, detritivores to herbivores σ_{DH}, and of inorganic to organic nitrogen σ_{NS}. From a global estimation of biomass in the oceans (Bar-On et al., 2018), we see that the biomass of fish and large invertebrates is roughly similar to, or slightly smaller than, that of arthropods and protists. This similarity between vertebrates and invertebrates suggests that also the biomass of animals at different trophic levels could be similar because herbivores are mainly planktonic (e.g., protists), predators are mainly vertebrates (e.g., fish), and detritivores span both categories. We therefore assume that their stocks in the aquatic ecosystem to be the same, $\sigma_{CH} = \sigma_{DH} = 1$. Two reports of biomass of different trophic groups in forests (Brockie and Moeed, 1986) and grasslands (Perkins et al., 2018) show that detritivore biomass is an order of magnitude higher than (forest) and similar (grassland) to that of herbivores. Therefore, for terrestrial ecosystems we choose an intermediate value of detritivore biomass as five times the biomass of herbivores, i.e., $\sigma_{DH} = 5$. In the same studies they also find that predator biomass is substantially smaller than herbivore biomass. Hence, we assume for the terrestrial ecosystem that $\sigma_{CH} = 0.2$. These ratios for aquatic and terrestrial ecosystems are also roughly consistent with results for predators and prey across terrestrial and aquatic biomes (Hatton et al., 2015). A study of nitrogen cycling in aquatic ecosystems (Berman and Bronk, 2003) reported ratios between inorganic and organic nitrogen that were both higher and lower than 1. Conversely, Groffman and Rosi-Marshall (2013) found consistently lower inorganic nitrogen levels compared with organic nitrogen in terrestrial ecosystems, even when only considering the active proportion of soil organic material (around 5% of total organic matter; Paul, 2016). Based on this evidence, we assume $\sigma_{NS} = 1$ for the aquatic and $\sigma_{NS} = 0.5$ for the terrestrial ecosystems.

We also estimate fractions of production lost to predation and to self-regulation, which includes intra-guild predation. The fraction of secondary production lost to predation could be high, reaching 90% in forests (Hairston and Hairston, 1993). Because we deem this value to be extremely high, we choose a more moderate value, and assume that $\rho_{HC} = \rho_{HD} = 0.5$ for both the terrestrial and aquatic ecosystems. Estimations for how much

production is lost to self-regulation are basically non-existent. It has been suggested that self-regulation and predation coefficients are roughly proportional for predators (Polis et al., 1989; Galiana et al., 2021). Assuming self-regulation and predation coefficients as equal ($r_C = q_C$), renders self-regulation fractions of $\rho_{CC} = 1.0$ for the aquatic and $\rho_{CC} = 0.067$ for the terrestrial ecosystem (see calculation in the Parameter derivation subsection). However, these values appear extreme and we therefore choose more moderate values, setting $\rho_{CC} = 0.5$ for the aquatic and $\rho_{CC} = 0.1$ for the terrestrial ecosystem. In doing so, we keep a large difference in self-regulation between ecosystem types, as suggested by the predation rates, but refrain from letting this difference be too large, potentially overshadowing other differences between ecosystem types. For other compartments there are no direct means to estimate self-regulation for a representative ecosystem. However, self-regulation for primary producers, e.g., via light limitation (Keddy, 2001), is likely more substantial than for herbivores and detritivores, which are probably more limited by predators and detrital matter, respectively (Hairston et al., 1960). We therefore choose, for both the terrestrial and aquatic ecosystems, small values for self-regulation fractions among herbivores and detritivores $\rho_{HH} = \rho_{DD} = 0.05$, but higher values for primary producers, $\rho_{PP} = 0.2$.

Finally, we estimate loss and leaching rates and nutrient conversion efficiencies. For the terrestrial ecosystem, the ratios between annual loss flux and stocks of inorganic nitrogen are between 0 and 2 (Groffman and Rosi-Marshall, 2013), so that we can assume an annual loss rate of nitrogen $\ell = 1$ [yr^{-1}]. For the aquatic ecosystem, estimates from multiple lakes (Hohener and Gachter, 1993) give a median value of $\ell = 2$ [yr^{-1}], assuming the relevant water column depth is 10 m (Middelboe and Markager, 1997). Next, we estimate nitrogen conversion efficiencies. These are generally higher than carbon conversion efficiencies, but by definition never higher than 1. Nutrient conversion efficiencies for animals have in previous models been assumed to be 0.8 (Zou et al., 2016), 0.5 and 0.25 (Attayde and Ripa, 2008). No loss for primary producer uptake of inorganic nitrogen was assumed. Following these assumptions, we set for primary producers $\epsilon_P = 1$, and for animals an intermediate value of 0.5, i.e., $\epsilon_H = \epsilon_D = \epsilon_C = 0.5$.

2.4. Parameter estimation

The values of all model parameters are estimated by inverting the model equations (Equation 1) for nitrogen fluxes, after setting nitrogen stocks, fluxes, and other ecosystem properties described in the previous subsection (Table 2). This approach is repeated for the terrestrial and aquatic ecosystems.

Since we need values for all six compartments to determine the parameter values, our estimations of stocks are complemented by the ratios between nitrogen stocks in different compartments,

TABLE 2 Parameters values used for simulations.

	Description	Units	Parameter values in:		
			Aquatic	Terrestrial	Wide coexistence
r_P	Production coefficient	[m^{2}gN^{-1}yr^{-1}]	14.6	0.487	0.2
r_H	Herbivory coefficient	[m^{2}gN^{-1}yr^{-1}]	36.0	0.368	0.5
r_D	Detritivory coefficient	[m^{2}gN^{-1}yr^{-1}]	36.0	0.368	0.5
r_C	Predation coefficient	[m^{2}gN^{-1}yr^{-1}]	56.6	24.8	10
u_P	Producer mortality rate	[yr^{-1}]	9.44	0.520	0.5
u_H	Herbivore mortality rate	[yr^{-1}]	9.00	0.477	0.5
u_D	Detritivore mortality rate	[yr^{-1}]	11.6	0.255	0.1
u_C	Predator mortality rate	[yr^{-1}]	4.50	6.44	5
q_P	Producer self-regulation coeff.	[m^{2}gN^{-1}yr^{-1}]	1.89	0.0260	0.02
q_H	Herbivore self-regulation coeff.	[m^{2}gN^{-1}yr^{-1}]	5.66	0.496	0.5
q_D	Detritivore self-regulation coeff.	[m^{2}gN^{-1}yr^{-1}]	7.30	0.0530	0.05
q_C	Predator self-regulation coeff.	[m^{2}gN^{-1}yr^{-1}]	28.3	37.2	15
ϵ_P	Production conversion efficiency		1	1	1
ϵ_H	Herbivory conversion efficiency		0.5	0.5	0.5
ϵ_D	Detritivory conversion efficiency		0.5	0.5	0.5
ϵ_C	Predation conversion efficiency		0.5	0.5	0.5
z	Mineralization rate	[yr^{-1}]	8.40	0.970	0.5
ℓ	Leaching/Loss rate	[yr^{-1}]	2	1	1

In the column labeled "wide-coexistence" a parameter set similar to the terrestrial one is reported, but with values chosen to have a wide region of coexistence. z is the rate of nitrogen mineralization, ℓ is the loss rate of inorganic nitrogen. The 16 other parameters correspond to four compartments (P,H,D,C), noted in the following by i. r_i, consumption coefficient of the trophic level below; ϵ_i, nutrient conversion efficiency associated with consumption; u_i, natural mortality rate; q_i, self-regulation coefficient. Columns of aquatic and terrestrial correspond to the parameter estimations from the literature, as detailed in the section Methods.

as described above: $C = \sigma_{CH}H$, $D = \sigma_{DH}H$, and $N = \sigma_{NS}S$. The values for stocks and fluxes are given in Table S3 in the Supplementary material.

The growth term in Equation (1a), $f_P = \epsilon_P r_P NP$, is essentially the primary production in nitrogen units, so that we can find the consumption rate of nutrients by primary producers as:

$$r_P = f_P/(\epsilon_P NP)$$

Similarly, the loss term due to herbivory is $r_H PH$, which can also be written as $f_P \rho_{PH}$ (recall that ρ_{PH} is the fraction of primary production consumed by herbivores). It follows that the consumption rate by herbivores is:

$$r_H = \rho_{PH} f_P/(PH) = \rho_{PH}\epsilon_P r_P N/H$$

We also assume the detritivory rate to be the same as for herbivores, i.e., $r_D = r_H$, as both herbivores and detritivores are typically mobile animals feeding on sessile material. Finally, the loss term of herbivore biomass due to predation is $r_C HC$, which can also be written as $f_H \rho_{HC}$, where ρ_{HC} is the fraction of herbivore production consumed by predators, and f_H is the flux herbivore gross production. We thus find that:

$$r_C = \rho_{HC} r_H \epsilon_H P/C$$

For primary producers, we use the detrital production flux f_M, to find the natural mortality rate:

$$u_P = f_M/P$$

For the animal compartments we use the fraction left from predation from gross production of the compartment, to estimate the natural mortality:

$$u_H = (1 - \rho_{HC}) r_H \epsilon_H P$$

$$u_D = (1 - \rho_{DC}) r_D \epsilon_D S$$

$$u_C = (1 - \rho_{CC}) r_C \epsilon_C (H + D)$$

We similarly use the fraction of production lost to self-regulation, normalized by the compartment's stock, to estimate the self-regulation coefficients:

$$q_P = \rho_{PP} r_P \epsilon_P N/P$$

$$q_H = \rho_{HH} r_H \epsilon_H P/H$$

$$q_D = \rho_{DD} r_D \epsilon_D S/D$$

$$q_C = \rho_{CC} r_C \epsilon_C (H + D)/C$$

The values of the other parameters, namely the nutrient conversion efficiencies and the parameters describing losses from the organic nitrogen compartment (z and ℓ), are taken directly from their empirical estimates (Table 2). These derivations yield two parameter sets of 18 parameters for each ecosystem (Table 2). Furthermore, we construct an additional parameter set, based on the terrestrial parameters noted as "wide coexistence" in Table 2. These parameter values are chosen with a wide range of ψ within the coexistence range when $I = 10$ [gN m^{-2}yr^{-1}] (i.e., with all compartments extant), while remaining closely similar to the terrestrial ecosystem parameter set. While the choice of the "wide coexistence" parameter values is arbitrary, it is done in order to visually demonstrate the effect of food web properties in Figure 1. We show in the Supplementary material that the specific parameter value choice does not effect the qualitative results, and thus emphasize that our choices of this "wide coexistence" parameter values are only for presentation purposes, and do not affect the conclusions.

2.5. Simulations and parameter exploration

In all simulations and calculations we focus on the equilibrium of the ecosystem model. We find this equilibrium by integrating in time, until the maximal change in stocks per year, calculated for all nutrient input options, is less than 10^{-5} [gN m^{-2}], or until the simulation reached 1,000 years, whichever comes first. We note that most simulations reach equilibrium in less than 100 years, and very few reach the 1,000 years mark (Table S1).

To answer our questions on how (1) subsidy strength and quality affect net primary production (NPP) and (2) consumer rates and other ecosystem properties modify the subsidy effect on primary producers, we assess how NPP changes as the subsidy strength I and quality ψ are varied. The former is assumed to range between 1 and 100 [gN m^{-2}yr^{-1}], and the latter across all possible values, between 0 (only inorganic nitrogen) and 1 (only organic nitrogen).

Besides varying the external inputs, we also explore the effect of other parameters: (i) the effects of food web properties are assessed by changing several parameters in conjunction, and (ii) an uncorrelated random parameter exploration of all parameters is performed to confirm the generality of the results.

First, we test the effect on ecosystem dynamics of three overarching properties of the food web: consumption, conversion efficiency, and metabolic rates. We vary the baseline values of the parameters by a factor γ, so that the parameters change together in a perfectly coordinated manner. For consumption, we change consumption coefficients for the animal compartment i as: $\tilde{r}_i = \gamma r_i$. For conversion, we change nutrient conversion for the animal compartment i as $\tilde{\epsilon}_i = \frac{1}{4}\gamma\epsilon_i$, noting that the smaller range of nutrient conversion efficiencies is due to the constraint $\epsilon_i \leq 1$. For metabolic rates, we change the consumption coefficients, natural mortality and self-regulation coefficients in the three animal compartments as $\tilde{a}_i = \gamma a_i$, where a stands for r, u, and q, and i identifies the animal compartment.

In these analyses, we vary the control parameter γ on a logarithmic scale between 0.1 and 10. Our focus on variations in the properties of the animal compartments is motivated by our interest in how primary production is altered in the food web.

However, we also test if concurrently changing the parameters for the primary producers, P, changes the qualitative results (see Supplementary material). To present the dependence of NPP on ψ (Figure 3), we calculate the average value of NPP across the range of I-values for each ψ, and only show ψ-values where compartments coexist, i.e., where all compartments have non-zero values at equilibrium for at least some value of I. To present the NPP dependence on I, we do the same, but now averaging over the range of ψ values for each I.

Second, to robustly test the effect of changing each parameter, we perform a random parameter exploration. We take each of 18 model parameters: all parameters except I and ψ. We change their values relative to the baseline values of terrestrial or aquatic ecosystems (Table 2), without any correlation between parameters (in contrast to the first analysis). For each parameter, we assume a log-normal distribution, such that the base-10 logarithm values have a standard-deviation of 1, except for nutrient conversion efficiencies, for which we assume a standard-deviation of 0.25 and we cap the values at 1. We repeat the sampling to create 20,000 sets of randomly chosen parameters, and explore subsidy scenarios by considering a range of ψ values between 0 and 1, and seven values of I (1, 2, 5, 10, 20, 50, 100 [gN $m^{-2}yr^{-1}$]).

2.6. Ecosystem metrics for subsidy impact assessment

We focus on estimating NPP, and its dependence on nutrient subsidies. The effect of herbivory is included in our definition of NPP, motivated by our aim to describe variations in net biomass production increments, that is, primary production left after the herbivory fraction has been removed. This amounts to the term $u_P P$ in Equation (1), which is also directly proportional to the producer biomass P (as opposed to the term $r_{P \in P} NP$, which includes the production lost to herbivory). Since production is strongly dependent on input levels I, and we change I across two orders of magnitude, it is useful to normalize NPP by I. We thus use a measure of normalized production, given by $u_P P/I$. We note that this normalized production term is dimensionless, representing an ecosystem-level nitrogen use efficiency if we assume that mortality is due to harvesting in analogy to agricultural ecosystems (Scaini et al., 2020). As we show in the results, it is also useful to examine how P changes when the subsidies are more organic, i.e., $\frac{d}{d\psi}P$ (u_P and I are constant along the ψ axis, and we can therefore ignore them here). We normalize this term by the average primary producer biomass for a given level of subsidy strength I, and call this metric "Producer Sensitivity to Organic Subsidy" (PSOS): $\frac{1}{<P>} \cdot \frac{d}{d\psi}P$.

3. Results

3.1. General responses of primary production to changes in subsidy strength and quality

We begin by examining how subsidies, and in particular their strength I and their organic fraction ψ, affect NPP as given by the term $u_P P$ for our two representative ecosystems, terrestrial (Figure 2, left) and aquatic (Figure 2, right). In each ecosystem, all parameters are constant except the subsidy parameters I and ψ. In general, NPP increases with subsidy strength, as more nutrients are converted into biomass. To highlight the effect of subsidies on the efficiency of nutrient conversion to biomass, in Figure 2 and in the following we focus on the normalized production $u_P P/I$. When nitrogen inputs are low (the lower region in subsidy parameter space), normalized production is also low (dark blue). At high inputs, normalized production levels saturate as more biomass is lost to top consumers in the aquatic ecosystem, or to inefficiencies related to primary producer self-regulation such as light limitation in the terrestrial ecosystem. Eventually, these effects will cause normalized production to decrease at very high subsidy strength, as seen on top of each panel in Figure 2.

As we increase the organic fraction of nitrogen inputs, i.e., moving left to right in the subsidy parameter space, NPP consistently decreases in the aquatic ecosystem. In contrast, NPP can also increase in the terrestrial ecosystem within certain ranges of organic fraction. This increase only occurs within the coexistence range where all compartments have non-zero values (marked by gray lines Figure 2). The positive trend in the terrestrial ecosystem occurs because organic nitrogen supports a large detritivore community, which feeds the predators that in turn reduce the herbivores, thereby allowing plants to grow more. At higher organic fractions outside the coexistence range, NPP decreases when larger amounts of nitrogen flow into the brown food web instead of being used by primary producers.

The behavior outside the coexistence region can be explained as follows. When $D = 0$ (due to low ψ), net nitrogen mineralization equals the input of organic nitrogen ($zS = I_S$). Hence, all nitrogen inputs reach the N compartment at equilibrium, with ψ playing no further role. When $H = 0$ (due to high ψ) the only effect of detritivores on primary producers is competition over nitrogen, leading to a decrease of P with ψ. Here, the detritivores have opportunities to consume organic nitrogen before it is mineralized and consumed by the primary producers. Finally, when $C = 0$ (low I) no top-down control of the herbivores can occur, and hence D only exerts a negative effect via resource competition, similarly to the case where $H = 0$. Hereafter, we will focus on how nutrient subsidies determine NPP within the coexistence region, which changes depending on parameter selection because we expect the species groups represented in our model—primary producers, herbivores, predators, and detritivores—to all be extant in most ecosystems.

3.2. Effects of food web properties on production-subsidy relations

Focusing on the coexistence region, we can now assess how food web properties determine how NPP is affected by subsidy strength and quality. We consider three food web properties encoded in parameters describing the three animal compartments (H, D, C): consumption, conversion efficiency, and metabolic rates.

Net primary production, normalized by subsidy strength, is affected jointly by subsidy quality ψ (top of Figure 3) and strength

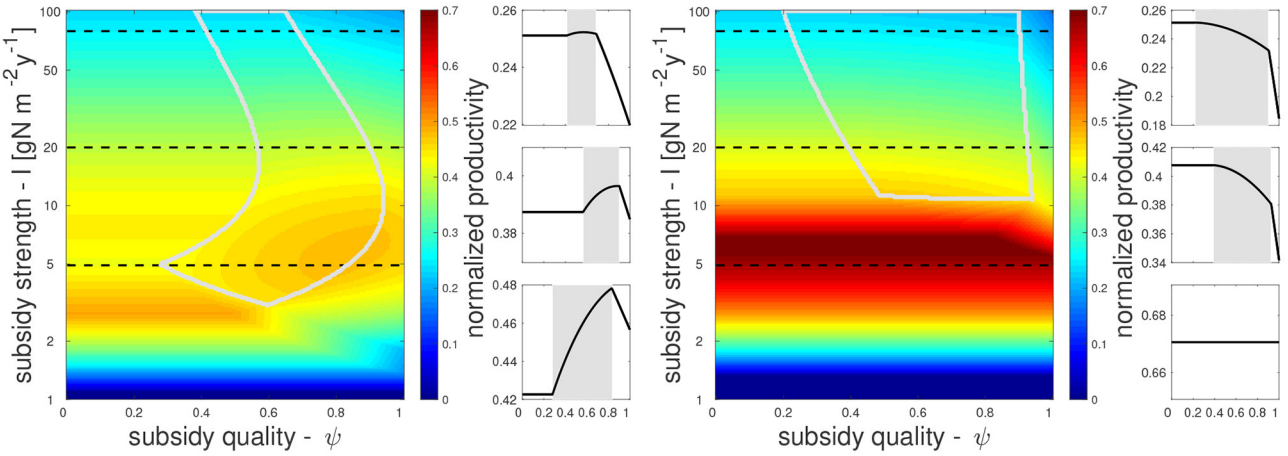

FIGURE 2
Normalized production $u_P P/I$ as a function of nitrogen subsidy strength (I) and quality (organic nitrogen fraction, ψ), in terrestrial **(left)** and aquatic **(right)** ecosystems. Besides I and ψ, other parameters are kept constant; gray lines enclose the coexistence region where all food web compartments (P,H,D,C) are extant. Small panels on the right of each parameter-space show normalized production at a constant value of I (gray background shows coexistence region), corresponding to the three horizontal dashed lines in each parameter-space.

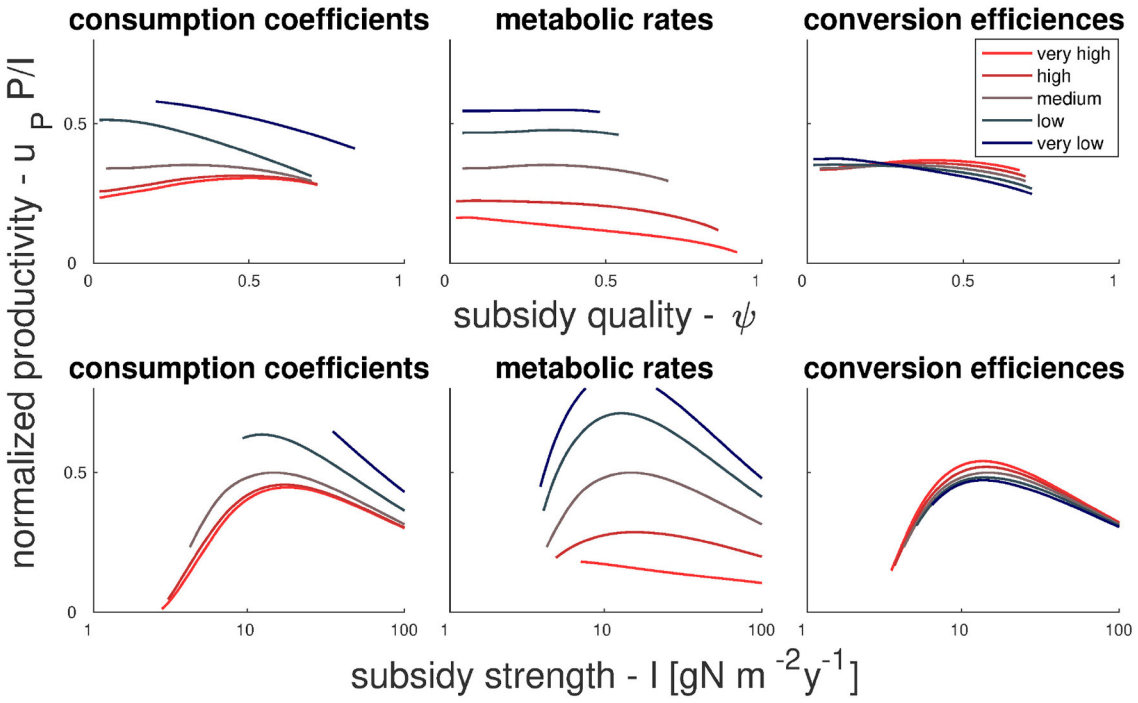

FIGURE 3
Effect of food web properties and subsidies on net primary production. Top and bottom panels show normalized production as a function of subsidy quality **(top)** and subsidy strength **(bottom)**. Left, middle, and right panels show sensitivities to food web properties as described by the parameters characterizing the animal compartments H, D, and C [**(left)** consumption coefficients; **(middle)** consumption coefficients, mortality rates, and self-regulation coefficients; **(right)** nutrient conversion efficiencies]; shades from blue to red (light to dark) correspond to increasing values of model parameters. These changes are done relative to baseline parameters defined in Table 2 (column labeled "wide-coexistence"), corresponding to a terrestrial ecosystem with a large coexistence range. Results for other baseline parameter values are summarized in Figure S10.

I (bottom of Figure 3), and by food web properties (indicated by different colors). This is shown for a specific set of initial ecosystem parameters (denoted as "wide-coexistence" in Table 2), but we conduct a sensitivity analysis to test that the reported trends are consistent for a wide range of parameter sets, including parameters for aquatic ecosystems, as well as with internal recycling (see Supplementary material).

Overall, the response of NPP is stronger when subsidy strength is varied than when varying subsidy quality, and it is often hump-shaped with a maximum at intermediate I. These responses vary in

shape depending on the food web properties considered, indicating interactions between these properties and subsidies strength and quality. Net primary production decreases mildly with increasing consumption coefficients and strongly with increasing metabolic rates. In contrast, NPP varies less (and generally increases) with increasing nutrient conversion efficiency. Increasing metabolic rates causes a shift from mild positive dependency of NPP on subsidy quality to a mild negative dependency, whereas trends turn to positive when increasing consumption or conversion. The most notable interaction of food web properties with subsidy strength occurs when increasing metabolic rate, which causes a shift from hump-shaped to weakly negative relation between NPP and subsidy strength.

3.3. Analytical exploration of ecosystem processes driving production-subsidy relations

As we have seen in the results so far, a higher fraction of organic subsidies can increase NPP, in particular in terrestrial ecosystems and under scenarios of strong consumption and more efficient nutrient conversion by animals. Beside these food web properties, we now assess which model parameters and thus which associated ecosystem processes that play a role for the relationship between production and subsidy quality. We do this using both an analytical (this section) and a numerical approach (Section 3.4).

Starting from analytical arguments, it is useful to consider a simplified scenario where predator self-regulation is negligible (i.e., $q_C C \approx 0$). Not only is this approximation mathematically convenient, but this term is also indeed substantially smaller than other terms in terrestrial ecosystems: with our estimated C stock, we have $q_C C = 0.714 \ll 6.44 = u_C$ [yr^{-1}]. Under this approximation, solving Equation (1d) at equilibrium yields

$$H + D = \frac{u_C}{\epsilon_C r_C}, \tag{2}$$

which means that increases in H are balanced by decreases in D and *vice versa* as ψ is increased, because their total is fixed. It is therefore natural to ask how P changes between the low ψ value where $D = 0$ and the high ψ value where $H = 0$. Note that D and H do not necessarily span this whole range for $0 < \psi < 1$, but answering the question remains useful to clarify the role of model parameters. At low ψ and with $D = 0$, all nitrogen subsidies flow into N, and from Equation (1)a we have at equilibrium:

$$q_P P_L = \frac{\epsilon_P r_P I}{\ell + r_P P_L} - \frac{r_H u_C}{\epsilon_C r_C} - u_P, \tag{3}$$

where $P_L = P(\psi \approx 0)$. At high ψ and with $H = 0$, we have no herbivory term in Equation (1a), so that at equilibrium:

$$q_P P_H = \frac{\epsilon_P r_P I}{\ell + r_P P_H} \cdot (1 - \psi + \psi\phi) - u_P, \tag{4}$$

where $P_H = P(\psi \approx 1)$ and we defined the parameter group $\phi = (1 + \frac{r_D u_C}{\epsilon_C r_C z})^{-1}$, associated with nutrient uptake by detritivory. Equations (3) and (4) can be directly solved to find P, but it is more instructive to study the difference between their right hand sides, where state variables and parameters affecting stocks P, and hence also production, appear. Using these equations, we can estimate the sensitivity of production to changes in ψ because Equations (3) and (4) represent P at low and high ψ, respectively, and the derivative $\frac{d}{d\psi}P$ scales as $P_H - P_L = P(\psi \approx 1) - P(\psi \approx 0)$. Subtracting the two equations, we find the difference between P stocks between $\psi \approx 1$ and $\psi \approx 0$,

$$\Delta_P = P_H - P_L = \frac{1}{q_P}\left[\epsilon_P r_P I\left(\frac{1}{\ell + r_P P_H} - \frac{1}{\ell + r_P P_L}\right) + \frac{r_H u_C}{\epsilon_C r_C} - \psi(1-\phi)\frac{\epsilon_P r_P I}{\ell + r_P P_H}\right]. \tag{5}$$

We can largely disregard the first term in round brackets, because it only decreases the difference Δ_P, but does not affect the direction of the ψ effect: if $P_H = P_L$ this whole term vanishes, if $P_H > P_L$ it is negative, and if $P_H < P_L$ it is positive. The second term, $\frac{r_H u_C}{\epsilon_C r_C}$, shows that herbivory increases Δ_P. Similarly, the third and last term in the square brackets shows the effect of nutrient competition by detritivory, with a decrease in Δ_P as ϕ decreases from its maximal value of 1.

The formulation of Δ_P reveals how NPP is affected by larger fractions of organic inputs, seen by the changes in the second and third term of the equation. For instance, fast rates of organic nitrogen dynamics (large ℓ and z) lead to a more positive effect of ψ on P (positive $\frac{d}{d\psi}P$), since ℓ occurs in the denominator of the third term, and large z keeps ϕ closer to 1. For both ℓ and z, less nitrogen is lost due to resource competition with detritivores, and hence NPP gains due to lower herbivory become more important. Decreasing subsidy strength I or production coefficient r_P has the same qualitative effect as increasing ℓ (i.e., decreasing the relative importance of the growth term), and hence also leads to a more positive $\frac{d}{d\psi}P$.

Focusing on the second term that captures herbivory effects, a higher herbivory rate r_H also leads to a more positive $\frac{d}{d\psi}P$: if herbivory pressure is high, increase in ψ leads to larger P-values due to lower herbivore densities. Finally, higher r_D decreases nutrient availability for producers by routing nutrients to decomposers (decreasing ϕ), thus also lowering $\frac{d}{d\psi}P$. Effects of other parameters on production are harder to predict—for example, u_C occurs in both the herbivory term and in ϕ, makings its effect less straight-forward.

3.4. Numerical exploration of ecosystem processes driving production-subsidy relations

We corroborate these analytical relationships with an extensive numerical exploration using randomly chosen parameter sets. In this exploration, we show how the metric PSOS, which represents the average sensitivity of producer biomass P on subsidy quality ψ, varies as a function of parameter values (Figure 4). We focus here on parameters characterizing the terrestrial ecosystem (see Table 2). A similar exploration of parameters for aquatic ecosystems shows overall comparable results (see

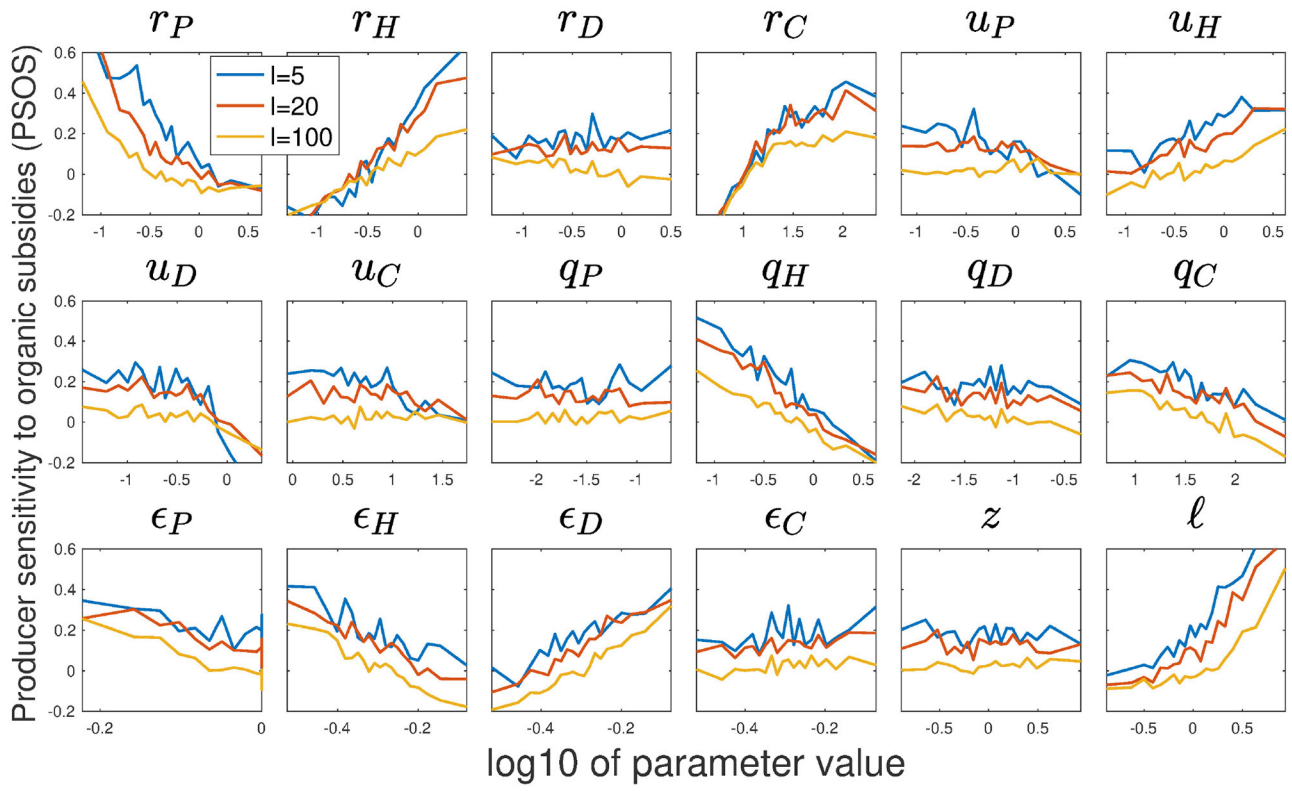

FIGURE 4
Producer sensitivity to organic subsidies (PSOS) as a function of variation in model parameters, averaged over 1,000 random parameter sets per point shown. Median parameter values for the terrestrial ecosystem are used to construct the random parameter space (see Table 2). Results are shown for varying subsidy strength I, as indicated by different colors: blue ($I = 5$), red ($I = 20$), and yellow ($I = 100$). PSOS is defined as: $\frac{1}{<P>} \cdot \frac{d}{d\psi} P$.

Supplementary material), with a few exceptions, notably that in aquatic ecosystems organic additions have a more negative effect on NPP.

Producer sensitivity to organic subsidy increases with higher r_H and ℓ, and decreases with I and r_P, consistent with our analytical analysis (Figure 4). However, r_D and z show the predicted trends only for parameters of aquatic ecosystems (and even then with weak trends, see Supplementary material). This suggests that herbivory (mediated by r_H) and nutrient loss (ℓ, but also I and r_P) play a significant role in determining the sensitivity of NPP on subsidy quality, while resource competition with detritivores (r_D and z) does not. Moreover, PSOS increases with u_H, ϵ_D, and r_C, and decreases with ϵ_H and u_D. Additionally, self-regulation of all animal compartments causes a weak negative trend, which virtually disappears in the aquatic ecosystems (see Supplementary material). The effect of r_C and the animal self-regulation coefficients could not be seen using our analytical approach, since they are at odds with negligible predator self-regulation. r_C is mainly relevant in relation to q_C (Barbier and Loreau, 2019), and hence neglecting q_C takes away our ability to see this effect. The other self-regulation coefficients can become important only when q_C is large, as otherwise top-down control is too dominant—This is indeed evidenced by their minimal effect in the aquatic ecosystems where predator self-regulation is weak.

4. Discussion

4.1. Subsidy effects on net primary productivity

Our main results can be summarized along four main points. First, as expected, increasing (strengthening) nitrogen inputs leads to higher Net Primary Production (NPP), but this effect saturates as nutrients inputs increase, as can be seen by the decreasing normalized NPP values at higher subsidy strength (Figure 2). Second, we predict that increasing the fraction of nitrogen subsidies in organic form (higher ψ) will lead to higher NPP in many terrestrial ecosystems, but more often to lower NPP in aquatic ecosystems (Figure 2, Figure S6). Third, the slope of the production—subsidy quality relation increases with higher consumption coefficients, but decreases substantially with higher metabolic rates (Figure 3, Figure S10). Fourth, we find that several ecosystem properties mediate the effect of subsidy quality on NPP (Figure 4). For example, increasing the herbivory coefficient (r_H), predation coefficient (r_C), detritivory conversion efficiency (ϵ_D), and loss rate (ℓ), consistently and strongly increases the positive effect of an increasing fraction nitrogen in organic form (ψ) on NPP.

All these relationships between subsidy and NPP depend on the ecosystem in question, and we confirm that terrestrial

and aquatic ecosystems respond differently to subsidies (Nakano and Murakami, 2001; Shurin et al., 2006; Leroux and Loreau, 2008). The finding that in terrestrial ecosystems NPP is more positively affected by organic additions than in aquatic ecosystems may seem surprising, given that this effect is driven by trophic cascades of predators suppressing herbivores—a process that is typically associated with aquatic ecosystems. One explanation could be that metabolic rates of herbivores are often higher in aquatic ecosystems (Cebrian and Lartigue, 2004), and, as we have seen (Figure 3), high metabolic rates lead to a more negative effect of organic inputs on NPP. We also find that increasing the mineralization rate (z), production coefficient (r_P), herbivore mortality rate (u_H), and herbivore self-regulation coefficient (q_H) lead to a more positive relationship between ψ and NPP in aquatic ecosystems (Figure S5). This in turn implies that in aquatic systems primary producers are nutrient limited, so that increasing the mineralization rate (z) or production coefficient (r_P) allows them to take up more nitrogen. In contrast, herbivores are already predator-controlled as increasing herbivore mortality rate (u_H) or herbivore self-regulation coefficient (q_H) decreases the predator control over herbivores. Hence, we predict that subsidizing aquatic ecosystems is less likely to increase NPP via the indirect effect of predator control, compared with terrestrial ecosystems. Finally, we note that aquatic ecosystems often receive substantial subsidies from nearby terrestrial ecosystems (Shurin et al., 2006; Leroux and Loreau, 2008), and high subsidy strength (I) weakens the importance of subsidy quality (ψ) (Figure 4). Therefore, aquatic ecosystems with high subsidy strength (I) are not likely to exhibit higher NPP due to higher fractions of organic subsidies.

From a theoretical perspective, the positive effect of organic subsidies on primary production can be understood as a particular case of apparent competition (Holt, 1977; Abrams et al., 1998), in which consumers are suppressed by predators that in turn benefit from the subsidies. In this light, the switch from positive to negative effects of subsidies on NPP, for instance when comparing terrestrial to aquatic systems (Figure S6), is conceptually similar to the switch between apparent competition and apparent mutualism (Montagano et al., 2018), since in both cases indirect effects on consumers due to predation pressure can have negative or positive effects, respectively. However, unlike the competition-mutualism switch that centers on predation alone, in our case it is the interplay between predation pressure and resource competition that determines the effect of subsidies. A similar situation may occur in meta-ecosystems where flows of abiotic resources and animals are often very different, highlighting the importance of incorporating high trophic levels into theoretical meta-ecosystem studies (Gounand et al., 2018).

Our numerical exploration (Figure 4) largely confirms our analytical results [using Equations (3) and (4)] where low subsidy strength (I) and high loss rate of inorganic nitrogen (ℓ) lead to a positive relationship between the fraction of organic subsidies and net primary production. However, our analytical analysis did not allow for identifying effects of other ecosystem parameters on the relationship between subsidy quality and NPP. The numerical analysis instead pointed to the negative impact of herbivory conversion efficiency (ϵ_H) and detritivore mortality rate (u_D) and the positive impact of detritivory conversion efficiency (ϵ_D) and herbivore mortality rate (u_H). Both high herbivore mortality rate (u_H) and low herbivory conversion efficiency (ϵ_H) decrease herbivore biomass, whereas low detritivore mortality rate (u_D) and high detritivory conversion efficiency (ϵ_D) increase detritivore biomass. All these changes lead to higher NPP when increasing organic subsidies. We thus find an asymmetry between the impacts on NPP of herbivores (which directly decrease NPP) and detritivores (which indirectly increase NPP by promoting predators).

4.2. Nitrogen recycling and other model assumptions

To ease the analysis and presentation, we chose not to include nitrogen recycling from producers and other compartments to the organic nitrogen compartment, which are often considered in theoretical analyses of ecosystem dynamics (De Mazancourt et al., 1998; Attayde and Ripa, 2008; Cherif and Loreau, 2009). However, as we show in the Supplementary material, the qualitative results are similar with and without nitrogen recycling, with three notable exceptions. Adding nitrogen recycling in the model results in higher production due to the increased efficiency of the system, leads to a slight shift left of coexistence boundaries on the ψ axis, as recycled material feeds the organic nutrient compartment and weakens the positive link between ψ and NPP. This last aspect implies that in ecosystems where nutrient recycling is minimal, such as in agricultural crop fields, switching from inorganic to organic nutrient inputs is more likely to increase NPP. It is also difficult to find a simple explanation to this last aspect, but it can be partially attributed to the increased effective inputs, which play the role of higher subsidy strength (I) (see, e.g., Figure 4).

Beyond nutrient recycling, we have made some other notable simplifying assumptions. We chose to use linear kinetics for the organic nitrogen compartment (as in most soil biogeochemical models, Manzoni and Porporato, 2009) and a type I functional response for species interactions. While converting literature data to the nitrogen stock units, constant carbon-to-nutrient ratios were assumed within each compartment. This assumption of stoichiometric homeostasis is supported by evidence for animals, but less so for primary producers (Elser et al., 2000). We also used a neutral assumption on predation choice, assuming that predators can predate on both herbivores and detritivores, and show no preference in the matter. This choice was used to highlight the distinct nature of green-brown food webs, where herbivores and detritivores compete for resources in an inherently non-equal way, leading to an interesting interplay between resource competition and apparent competition due to predation pressure. This is in contrast to previous research which has focused more on green food webs, and has considered both apparent competition and prey switching in detail (Abrams et al., 1998; Chase et al., 2002; Leroux and Loreau, 2012). While all these simplifications affect the results, we expect them to make second-order corrections, and they should affect the quantitative but not the qualitative outcomes. Since we focus here on the qualitative response of production to

subsidies, we believe that, much like for nutrient recycling, these other simplifications will not impact our general conclusions.

Finally, the proposed model focuses on nitrogen flows and stocks, neglecting interactions of nitrogen and other elements that can modify the rates and efficiencies of nitrogen transfers among compartments, depending on the most limiting element (Sterner and Elser, 2002; Cherif and Loreau, 2013; Manzoni et al., 2017). This assumption has also implications for the interpretation of subsidy quality. Here, we have defined quality in terms of relative amounts of inorganic and organic N in the subsidy, but other measures of quality could be considered, including the elemental composition of the organic subsidy. For example, inputs of organic matter with high C:N ratio would cause C:N in the *S* compartment to increase, eventually resulting in inorganic nitrogen immobilization (Cherif and Loreau, 2013). In our framework, net immobilization is a nitrogen transfer from *N* to *S*, which we have not considered but that would reduce the amount of *N* available for primary producers. Thus, high C:N organic subsidies would be of "lower quality" compared to low C:N organic subsidies. In the long term, as carbon is removed from organic matter via respiration, nitrogen mineralization would be restored, but lower inorganic nitrogen and higher organic matter C:N ratio resulting from this low quality subsidies might lower the nitrogen content in primary producers, and increase the nitrogen assimilation efficiencies while decreasing the growth rates at higher trophic levels (due to lower efficiency of carbon conversion to biomass, Manzoni et al., 2017). However, a stoichiometric explicit model [building on Cherif and Loreau (2013) and Buchkowski et al. (2019)] would need to be used to assess these consequences on the food web as a whole.

By focusing on the nitrogen cycle only, our model did not include non-linear feedback mechanisms involving other variables partly controlled by nitrogen stocks. For example, subsidies can lead to nutrient accumulation in water bodies that promote NPP, but eventually can lead to eutrophication and a dramatic change in ecosystem function. This type of regime shifts (Scheffer and Carpenter, 2003) require a modeling approach that includes also state variables outside the nitrogen cycle, such as light and oxygen availability in the case of eutrophication.

4.3. Implications and future directions

An understanding of which parts of the parameter space that are relevant to real ecosystems will be useful for applied purposes. For instance, the model predicts that introducing organic fertilization in agriculture improves regulation of herbivores, which are potential pests on crop plants. Indeed, empirical work has shown that organic fertilization can suppress herbivores (Settle et al., 1996; Riggi and Bommarco, 2019), but does not always increase primary production (Halaj and Wise, 2002), emphasizing that benefits of organic subsidies to primary production are context dependent. Further, in conjunction with site-specific parameter estimates, the model we present with linked green and brown resource channels can be used to predict the effects of anthropogenic subsidies on specific natural ecosystems such as grasslands or forests. The model can indicate which ecosystems are more sensitive to nutrient enrichment. Furthermore, climate change affects various ecosystem properties such as metabolic rates and the kinetics of soil nutrient cycling, which in turn affect the impacts of nutrient subsidies on NPP.

It is difficult to extrapolate on the overall effect of climate change, given the range of positive and negative effects of different parameters (Figure 4, Figure S5), and the difficulty in estimating the effect of warming on model parameters (Bideault et al., 2021). However, if we assume that metabolic rates are more sensitive to warming than other ecosystem properties such as consumption coefficients, we can speculate from Figure 3 that warming will lead to a more negative impact of organic subsidies on NPP. This highlights the importance of exploring how ecosystems respond to compound climatic changes and perturbations in the subsidy strength and quality. These changes lead ecosystems toward conditions not previously experienced, which are therefore also harder to predict. Our approach of developing theory for subsidized ecosystems using dynamical models, parameterizing these models for a wide range of ecosystem and testing confounding effects of model parameters, is a step toward understanding how ecosystems respond to human influence. Importantly, it is clearly essential to consider the green and brown food webs in concert.

While useful for qualitative predictions, testing our theoretical predictions empirically in specific case studies is likely to be challenging. There are recent investigations of nutrient quality and quantity subsidy effects on primary producers in conjunction with food-web dynamics (Riggi and Bommarco, 2019; Aguilera et al., 2021), but it is difficult to directly connect their results to our theoretical findings. A particular problem is to normalize results by subsidy strength, i.e., empirically disentangling the effects of subsidy strength (I) and subsidy quality (ψ). This is of interest since the subsidy effect in the context of green-brown food webs should be most striking along the ψ axis, given that the effect of I on production is a more straightforward bottom-up one. Indeed, despite clear results showing that detritus additions increase primary producer stocks (Hagen et al., 2012), it is not possible to attribute subsidy effects to bottom-up vs. top-down mechanisms, because experiments typically manipulate both ψ and I, and increases in I may overshadow the top-down effects of higher ψ. A practical solution may be to compare ecosystems with and without herbivory and/or predation (e.g., due to pesticide use), where the effect of ψ for different parameter regimes should be most evident.

Here, we explored how two aspects of nutrient subsidies—strength and quality—impact primary production in green-brown food webs. Subsidy strength has a direct positive impact, mainly as a bottom-up direct effect on producers. The effect of subsidy quality truly connects the green and brown channels in food webs—organic subsidies can indirectly promote production via predator control on herbivores. This aspect of nutrient enrichment has been largely overlooked, and as we have seen here can play a major role in determining ecosystem functioning. These results show that the impact of nutrient enrichment depends on more than its strength, and that human overloading of ecosystems with inorganic nutrients is consequential not only because of its large amounts, but also due to higher proportions of inorganic nutrients, which promote production at the cost of losing the ecological function of the brown channel.

Data availability statement

Publicly available datasets were analyzed in this study. This data can be found here: Cebrian (1999, 2004) and Cebrian and Lartigue (2004); model scripts are included as Supplementary material.

Author contributions

YZ, SM, and RB conceived the study and developed the model. YZ performed the data collection, analysis, and simulations. All authors interpreted the results. YZ led the writing, which SM and RB commented on and revised. All authors contributed to the article and approved the submitted version.

Funding

This research was funded by the Swedish University of Agricultural Sciences, the Swedish Research Council for Sustainable Development FORMAS (grant no. 2022-00928), and by the European Research Council (ERC) under the European Union Horizon 2020 Research and Innovation Programme (grant agreement no. 101001608). Open access publication fees were covered by Stockholm University.

Acknowledgments

A previous version of this manuscript was uploaded as a preprint to the bioRxiv repository (Zelnik et al., 2021).

Conflict of interest

The authors declare that the research was conducted in the absence of any commercial or financial relationships that could be construed as a potential conflict of interest.

Publisher's note

Supplementary material

The Supplementary Material for this article can be found online at: https://www.frontiersin.org/articles/10.3389/fevo.2023.1106461/full#supplementary-material

References

Abrams, P. A., Holt, R. D., and Roth, J. D. (1998). Apparent competition or apparent mutualism? Shared predation when populations cycle. *Ecology* 79, 201–212. doi: 10.1890/0012-9658(1998)079[0201:ACOAMS]2.0.CO;2

Aguilera, G., Riggi, L., Miller, K., Roslin, T., and Bommarco, R. (2021). Organic fertilization suppresses aphid growth via carabids in the absence of specialist predators. *J. Appl. Ecol.* 58, 1455–1465. doi: 10.1111/1365-2664.13862

Allen, D. C. and Wesner, J. S. (2016). Synthesis: comparing effects of resource and consumer fluxes into recipient food webs using meta-analysis. *Ecology* 97, 594–604. doi: 10.1890/15-1109

Allgeier, J. E., Wenger, S., and Layman, C. A. (2020). Taxonomic identity best explains variation in body nutrient stoichiometry in a diverse marine animal community. *Sci. Rep.* 10, 13718. doi: 10.1038/s41598-020-67881-y

Attayde, J. L., and Ripa, J. (2008). The coupling between grazing and detritus food chains and the strength of trophic cascades across a gradient of nutrient enrichment. *Ecosystems* 11, 980–990. doi: 10.1007/s10021-008-9174-8

Barabás, G., Michalska-Smith, M. J., and Allesina, S. (2017). Self-regulation and the stability of large ecological networks. *Nat. Ecol. Evol.* 1, 1870–1875. doi: 10.1038/s41559-017-0357-6

Barbier, M., and Loreau, M. (2019). Pyramids and cascades: a synthesis of food chain functioning and stability. *Ecol. Lett.* 22, 405–419. doi: 10.1111/ele.13196

Bar-On, Y. M., Phillips, R., and Milo, R. (2018). The biomass distribution on earth. *Proc. Natl. Acad. Sci. U.S.A.* 115, 6506–6511. doi: 10.1073/pnas.1711842115

Baxter, C. V., Fausch, K. D., Murakami, M., and Chapman, P. L. (2004). Fish invasion restructures stream and forest food webs by interrupting reciprocal prey subsidies. *Ecology* 85, 2656–2663. doi: 10.1890/04-138

Berman, T., and Bronk, D. (2003). Dissolved organic nitrogen: a dynamic participant in aquatic ecosystems. *Aquat. Microb. Ecol.* 31, 279–305. doi: 10.3354/ame031279

Bideault, A., Galiana, N., Zelnik, Y. R., Gravel, D., Loreau, M., Barbier, M., et al. (2021). Thermal mismatches in biological rates determine trophic control and biomass distribution under warming. *Glob. Change Biol.* 27, 257–269. doi: 10.1111/gcb.15395

Bobbink, R., Hicks, K., Galloway, J., Spranger, T., Alkemade, R., Ashmore, M., et al. (2010). Global assessment of nitrogen deposition effects on terrestrial plant diversity: a synthesis. *Ecol. Appl.* 20, 30–59. doi: 10.1890/08-1140.1

Brockie, R. E., and Moeed, A. (1986). Animal biomass in a New Zealand forest compared with other parts of the world. *Oecologia* 70, 24–34. doi: 10.1007/BF00377108

Buchkowski, R. W., Leroux, S. J., and Schmitz, O. J. (2019). Microbial and animal nutrient limitation change the distribution of nitrogen within coupled green and brown food chains. *Ecology* 100, e02674. doi: 10.1002/ecy.2674

Buendía, C., Kleidon, A., Manzoni, S., Reu, B., and Porporato, A. (2018). Evaluating the effect of nutrient redistribution by animals on the phosphorus cycle of lowland Amazonia. *Biogeosciences* 15, 279–295. doi: 10.5194/bg-15-279-2018

Čapek, P., Manzoni, S., Kaštovská, E., Wild, B., Diáková, K., Bárta, J., et al. (2018). A plant–microbe interaction framework explaining nutrient effects on primary production. *Nat. Ecol. Evol.* 2, 1588–1596. doi: 10.1038/s41559-018-0662-8

Cebrian, J. (1999). Patterns in the fate of production in plant communities. *Am. Nat.* 154, 449–468. doi: 10.1086/303244

Cebrian, J. (2004). Role of first-order consumers in ecosystem carbon flow: carbon flow through first-order consumers. *Ecol. Lett.* 7, 232–240. doi: 10.1111/j.1461-0248.2004.00574.x

Cebrian, J., and Lartigue, J. (2004). Patterns of herbivory and decomposition in aquatic and terrestrial ecosystems. *Ecol. Monogr.* 74, 237–259. doi: 10.1890/03-4019

Chase, J. M., Abrams, P. A., Grover, J. P., Diehl, S., Chesson, P., Holt, R. D., et al. (2002). The interaction between predation and competition: a review and synthesis. *Ecol. Lett.* 5, 302–315. doi: 10.1046/j.1461-0248.2002.00315.x

Cherif, M., and Loreau, M. (2009). When microbes and consumers determine the limiting nutrient of autotrophs: a theoretical analysis. *Proc. Roy. Soc. B Biol. Sci.* 276, 487–497. doi: 10.1098/rspb.2008.0560

Cherif, M., and Loreau, M. (2013). Plant–herbivore–decomposer stoichiometric mismatches and nutrient cycling in ecosystems. *Proc. Roy. Soc. B Biol. Sci.* 280, 20122453. doi: 10.1098/rspb.2012.2453

Darimont, C. T., Paquet, P. C., and Reimchen, T. E. (2009). Landscape heterogeneity and marine subsidy generate extensive intrapopulation niche diversity in a large terrestrial vertebrate. *J. Anim. Ecol.* 78, 126–133. doi: 10.1111/j.1365-2656.2008.01473.x

De Mazancourt, C., Loreau, M., and Abbadie, L. (1998). Grazing optimization and nutrient cycling: when do herbivores enhance plant production? *Ecology* 79, 2242–2252. doi: 10.1890/0012-9658(1998)079[2242:GOANCW]2.0.CO;2

Elser, J. J., Fagan, W. F., Denno, R. F., Dobberfuhl, D. R., Folarin, A., Huberty, A., et al. (2000). Nutritional constraints in terrestrial and freshwater food webs. *Nature* 408, 578–580. doi: 10.1038/35046058

Galiana, N., Arnoldi, J.-F., Barbier, M., Acloque, A., Mazancourt, C., and Loreau, M. (2021). Can biomass distribution across trophic levels predict trophic cascades? *Ecol. Lett.* 24, 464–476. doi: 10.1111/ele.13658

Gounand, I., Harvey, E., Little, C. J., and Altermatt, F. (2018). Meta-ecosystems 2.0: rooting the theory into the field. *Trends Ecol. Evol.* 33, 36–46. doi: 10.1016/j.tree.2017.10.006

Gounand, I., Mouquet, N., Canard, E., Guichard, F., Hauzy, C., and Gravel, D. (2014). The paradox of enrichment in metaecosystems. *Am. Nat.* 184, 752–763. doi: 10.1086/678406

Gravel, D., Guichard, F., Loreau, M., and Mouquet, N. (2010). Source and sink dynamics in meta-ecosystems. *Ecology* 91, 2172–2184. doi: 10.1890/09-0843.1

Groffman, P. M., and Rosi-Marshall, E. J. (2013). "The nitrogen cycle," in *Fundamentals of Ecosystem Science*, eds K. C. Weathers, D. L. Strayer, and G. E. Likens (New York, NY: Elsevier), 137–158. doi: 10.1016/B978-0-08-091680-4.00007-X

Hagen, E. M., McCluney, K. E., Wyant, K. A., Soykan, C. U., Keller, A. C., Luttermoser, K. C., et al. (2012). A meta-analysis of the effects of detritus on primary producers and consumers in marine, freshwater, and terrestrial ecosystems. *Oikos* 121, 1507–1515. doi: 10.1111/j.1600-0706.2011.19666.x

Hairston, N. G., and Hairston, N. G. (1993). Cause-effect relationships in energy flow, trophic structure, and interspecific interactions. *Am. Nat.* 142, 379–411. doi: 10.1086/285546

Hairston, N. G., Smith, F. E., and Slobodkin, L. B. (1960). Community structure, population control, and competition. *Am. Nat.* 94, 421–425. doi: 10.1086/282146

Halaj, J., and Wise, D. H. (2002). Impact of a detrital subsidy on trophic cascades in a terrestrial grazing food web. *Ecology* 83, 3141–3151. doi: 10.1890/0012-9658(2002)083[3141:IOADSO]2.0.CO;2

Hatton, I. A., McCann, K. S., Fryxell, J. M., Davies, T. J., Smerlak, M., Sinclair, A. R. E., et al. (2015). The predator-prey power law: biomass scaling across terrestrial and aquatic biomes. *Science* 349, aac6284. doi: 10.1126/science.aac6284

Hines, J., Megonigal, J. P., and Denno, R. F. (2006). Nutrient subsidies to belowground microbes impact aboveground food web interactions. *Ecology* 87, 1542–1555. doi: 10.1890/0012-9658(2006)87[1542:NSTBMI]2.0.CO;2

Hohener, P., and Gachter, R. (1993). Prediction of dissolved inorganic nitrogen (DIN) concentrations in deep, seasonally stratified lakes based on rates of DIN input and N removal processes. *Aquat. Sci.* 55, 112–131. doi: 10.1007/BF00877440

Holt, R. D. (1977). Predation, apparent competition, and the structure of prey communities. *Theor. Popul. Biol.* 12, 197–229. doi: 10.1016/0040-5809(77)90042-9

Jacquet, C., Carraro, L., and Altermatt, F. (2022). Meta-ecosystem dynamics drive the spatial distribution of functional groups in river networks. *Oikos* 2022, e09372. doi: 10.1111/oik.09372

Jonsson, T. (2017). Conditions for Eltonian pyramids in Lotka-Volterra food chains. *Sci. Rep.* 7, 10912. doi: 10.1038/s41598-017-11204-1

Keddy, P. (2001). *Competition, 2nd Edn.* Population and Community Biology Series 26. Louisiana, LA: Springer Science & Business Media.

Leroux, S. J., and Loreau, M. (2008). Subsidy hypothesis and strength of trophic cascades across ecosystems: subsidies and trophic cascades. *Ecol. Lett.* 11, 1147–1156. doi: 10.1111/j.1461-0248.2008.01235.x

Leroux, S. J., and Loreau, M. (2012). Dynamics of reciprocal pulsed subsidies in local and meta-ecosystems. *Ecosystems* 15, 48–59. doi: 10.1007/s10021-011-9492-0

Loreau, M., and Holt, R. D. (2004). Spatial flows and the regulation of ecosystems. *Am. Nat.* 163, 606–615. doi: 10.1086/382600

Manzoni, S., Čapek, P., Mooshammer, M., Lindahl, B. D., Richter, A., and Santruckova, H. (2017). Optimal metabolic regulation along resource stoichiometry gradients. *Ecol. Lett.* 20, 1182–1191. doi: 10.1111/ele.12815

Manzoni, S., Čapek, P., Porada, P., Thurner, M., Winterdahl, M., Beer, C., et al. (2018). Reviews and syntheses: carbon use efficiency from organisms to ecosystems–definitions, theories, and empirical evidence. *Biogeosciences* 15, 5929–5949. doi: 10.5194/bg-15-5929-2018

Manzoni, S., and Porporato, A. (2009). Soil carbon and nitrogen mineralization: theory and models across scales. *Soil Biol. Biochem.* 41, 1355–1379. doi: 10.1016/j.soilbio.2009.02.031

Marczak, L. B., Thompson, R. M., and Richardson, J. S. (2007). Meta-analysis: trophic level, habitat, and productivity shape the food web effects of resource subsidies. *Ecology* 88, 140–148. doi: 10.1890/0012-9658(2007)88[140:MTLHAP]2.0.CO;2

McCary, M. A., Phillips, J. S., Ramiadantsoa, T., Nell, L. A., McCormick, A. R., and Botsch, J. C. (2020). Transient top-down and bottom-up effects of resources pulsed to multiple trophic levels. *Ecology* 102, e03197. doi: 10.1002/ecy.3197

Middelboe, A. L., and Markager, S. (1997). Depth limits and minimum light requirements of freshwater macrophytes. *Freshw. Biol.* 37, 553–568. doi: 10.1046/j.1365-2427.1997.00183.x

Montagano, L., Leroux, S. J., Giroux, M.-A., and Lecomte, N. (2018). The strength of ecological subsidies across ecosystems: a latitudinal gradient of direct and indirect impacts on food webs. *Ecol. Lett.* 22, 265–274. doi: 10.1111/ele.13185

Moore, J. C., Berlow, E. L., Coleman, D. C., Ruiter, P. C., Dong, Q., Hastings, A., et al. (2004). Detritus, trophic dynamics and biodiversity: detritus, trophic dynamics and biodiversity. *Ecol. Lett.* 7, 584–600. doi: 10.1111/j.1461-0248.2004.00606.x

Nakano, S., and Murakami, M. (2001). Reciprocal subsidies: dynamic interdependence between terrestrial and aquatic food webs. *Proc. Natl. Acad. Sci. U.S.A.* 98, 166–170. doi: 10.1073/pnas.98.1.166

Newsome, T. M., Dellinger, J. A., Pavey, C. R., Ripple, W. J., Shores, C. R., Wirsing, A. J., et al. (2015). The ecological effects of providing resource subsidies to predators: resource subsidies and predators. *Glob. Ecol. Biogeogr.* 24, 1–11. doi: 10.1111/geb.12236

Palumbi, S. R. (2003). Ecological subsidies alter the structure of marine communities. *Proc. Natl. Acad. Sci. U.S.A.* 100, 11927–11928. doi: 10.1073/pnas.2335832100

Paul, E. A. (2016). The nature and dynamics of soil organic matter: plant inputs, microbial transformations, and organic matter stabilization. *Soil Biol. Biochem.* 98, 109–126. doi: 10.1016/j.soilbio.2016.04.001

Perkins, M. J., Inger, R., Bearhop, S., and Sanders, D. (2018). Multichannel feeding by spider functional groups is driven by feeding strategies and resource availability. *Oikos* 127, 23–33. doi: 10.1111/oik.04500

Polis, G. A., Anderson, W. B., and Holt, R. D. (1997). Toward an integration of landscape and food web ecology: the dynamics of spatially subsidized food webs. *Annu. Rev. Ecol. Syst.* 28, 289–316. doi: 10.1146/annurev.ecolsys.28.1.289

Polis, G. A., Myers, C. A., and Holt, R. D. (1989). The ecology and evolution of intraguild predation: potential competitors that eat each other. *Annu. Rev. Ecol. Syst.* 20, 297–330. doi: 10.1146/annurev.es.20.110189.001501

Raun, W. R., and Johnson, G. V. (1999). Improving nitrogen use efficiency for cereal production. *Agron. J.* 91, 357–363. doi: 10.2134/agronj1999.00021962009100030001x

Riggi, L. G., and Bommarco, R. (2019). Subsidy type and quality determine direction and strength of trophic cascades in arthropod food web in agro-ecosystems. *J. Appl. Ecol.* 56, 1982–1991. doi: 10.1111/1365-2664.13444

Rooney, N., McCann, K., Gellner, G., and Moore, J. C. (2006). Structural asymmetry and the stability of diverse food webs. *Nature* 442, 265–269. doi: 10.1038/nature04887

Scaini, A., Zamora, D., Livsey, J., Lyon, S. W., Bommarco, R., Weih, M., et al. (2020). Hydro-climatic controls explain variations in catchment-scale nitrogen use efficiency. *Environ. Res. Lett.* 15, 094006. doi: 10.1088/1748-9326/ab9691

Scheffer, M., and Carpenter, S. R. (2003). Catastrophic regime shifts in ecosystems: linking theory to observation. *Trends Ecol. Evol.* 18, 648–656. doi: 10.1016/j.tree.2003.09.002

Settle, W. H., Ariawan, H., Astuti, E. T., Cahyana, W., Hakim, A. L., Hindayana, D., et al. (1996). Managing tropical rice pests through conservation of generalist natural enemies and alternative prey. *Ecology* 77, 1975–1988. doi: 10.2307/2265694

Shcherbak, I., Millar, N., and Robertson, G. P. (2014). Global metaanalysis of the nonlinear response of soil nitrous oxide (N_2O) emissions to fertilizer nitrogen. *Proc. Natl. Acad. Sci. U.S.A.* 111, 9199–9204. doi: 10.1073/pnas.1322434111

Shurin, J. B., Gruner, D. S., and Hillebrand, H. (2006). All wet or dried up? Real differences between aquatic and terrestrial food webs. *Proc. Roy. Soc. B Biol. Sci.* 273, 1–9. doi: 10.1098/rspb.2005.3377

Spiecker, B., Gouhier, T. C., and Guichard, F. (2016). Reciprocal feedbacks between spatial subsidies and reserve networks in coral reef meta-ecosystems. *Ecol. Appl.* 26, 264–278. doi: 10.1890/15-0478

Sterner, R. W., and Elser, J. J. (2002). *Ecological Stoichiometry: The Biology of Elements from Molecules to the Biosphere*. Princeton, NJ: Princeton University Press. doi: 10.1515/9781400885695

Wollrab, S., Diehl, S., and De Roos, A. M. (2012). Simple rules describe bottom-up and top-down control in food webs with alternative energy pathways. *Ecol. Lett.* 15, 935–946. doi: 10.1111/j.1461-0248.2012.01823.x

Zelnik, Y. R., Manzoni, S., and Bommarco, R. (2021). Primary productivity in subsidized green-brown food webs. *bioRxiv*. doi: 10.1101/2021.12.22.473860

Zelnik, Y. R., Manzoni, S., and Bommarco, R. (2022). The coordination of green–brown food webs and their disruption by anthropogenic nutrient inputs. *Glob. Ecol. Biogeogr.* 31, 2270–2280. doi: 10.1111/geb.13576

Zou, K., Thébault, E., Lacroix, G., and Barot, S. (2016). Interactions between the green and brown food web determine ecosystem functioning. *Funct. Ecol.* 30, 1454–1465. doi: 10.1111/1365-2435.12626

frontiers | Frontiers in Ecology and Evolution

TYPE Original Research
PUBLISHED 24 April 2023
DOI 10.3389/fevo.2023.1151283

OPEN ACCESS

EDITED BY
Rui-Wu Wang,
Northwestern Polytechnical University, China

REVIEWED BY
Mauro Santos,
Autonomous University of Barcelona, Spain
Pietro Landi,
Stellenbosch University, South Africa

*CORRESPONDENCE
Gregor F. Fussmann
✉ gregor.fussmann@mcgill.ca

RECEIVED 25 January 2023
ACCEPTED 03 April 2023
PUBLISHED 24 April 2023

CITATION
Fussmann GF and Kopp M (2023) Apparent evolutionary maladaptation and inference from reciprocal transplants.
Front. Ecol. Evol. 11:1151283.
doi: 10.3389/fevo.2023.1151283

Apparent evolutionary maladaptation and inference from reciprocal transplants

Gregor F. Fussmann[1]* and Michael Kopp[2]

[1]Department of Biology, McGill University, Montreal, QC, Canada, [2]Aix-Marseille Université, CNRS, Centrale Marseille, I2M, UMR 7373, Marseille, France

In rapidly changing environments populations and species face a challenge to remain adapted and avoid extinction or replacement by fitter types. If evolutionary adaptation cannot keep pace with the speed of environmental change populations will exhibit varying degrees of maladaptation with respect to the current environmental state. Reciprocal transplant experiments are an established method for comparatively assessing the relative fitness of multiple populations in their respective environments. Here we use a quantitative-genetics model to show that inference from reciprocal transplants can be misleading when applied to populations that are in the process of adapting to environmental change. Specifically, we analyze (a) the case of two populations adapting to two different fitness optima starting from a suboptimal initial state and (b) the case of two populations attempting to adapt to changing trait targets that move at different speeds. We find that, in both scenarios, populations can undergo transitional fitness states that, if reciprocal transplant experiments were performed, would lead to the conclusion of (local) non-adaptation or maladaptation. This signature of apparent maladaptation occurs although both populations strictly follow an evolutionary trajectory dictated by the principle of fitness increase over time. Our results have implications for potential patterns of latitudinal replacement of populations/species with ongoing global change and might help shed light on the surprising finding (based on reciprocal transplants) that many populations in the wild fail to show a strong signature of adaptation to their local environments.

KEYWORDS

evolutionary dynamics, maladaptation, local adaptation, reciprocal transplant, relative fitness, quantitative genetics model, adaptive divergence, invasion success

1. Introduction

Evolutionary biologists and ecologists have based their work on the premise that the evolutionary response to environmental change in nature should be adaptive. That is, when populations face changing conditions that make them less adapted, they are expected to evolve in a way that strives to restore the fitness they have lost in the process. Yet, studies conducted in natural ecosystems as well as in the laboratory frequently fail to show evidence of local adaptation. A sizeable number of studies report the absence of adaptation, insufficient adaptation or even an evolutionary response that is worse, from a fitness perspective, than no change at all would have been. A meta-analysis of reciprocal transplant

experiments estimated that the signature of local adaptation (where resident populations have higher fitness than foreign populations) occurred in 70% of cases (Hereford, 2009). This means that in 30% of cases populations were found to be maladapted to their environment, a result that might be an underestimate given that there is likely a reporting bias in favor of studies that "prove" adaptation. In the same vein, another meta-analysis focusing on selection coefficients found that in 64% of cases the mean trait value displayed by the studied populations was more than one phenotypic standard deviation away from the optimal trait value (Estes and Arnold, 2007). The perplexing ubiquity of populations in maladaptive states has led to two recent special issues on the topic of "maladaptation" in the journals *American Naturalist* and *Evolutionary Applications*. In addition to rallying papers with new case studies of maladaptation (Brady et al., 2019c; Fraser et al., 2019; Loria et al., 2019), the introductory articles of these special issues provide insightful analyses on the potential causes and mechanisms (Brady et al., 2019a,b).

In the present theoretical study we perform a closer investigation of a phenomenon labeled "apparent maladaptation", where a population appears to be maladapted when in fact it is in the process of adapting to a changed or changing environment (Brady et al., 2019b). This type of maladaptation can occur when the time scale of observation is insufficient so that snapshots (or a single snapshot) of the dynamical process of adaptation show maladaptive states. More precisely, on their trajectory to an adaptive state, populations undergo transient states that are (or appear) maladaptive. A simple case of this phenomenon would be a population that adapts to its changing environment but lags behind the optimal adaptive state. Depending on the relation of the speed of environmental change and the adaptive potential of the population, the gap between the realized and fitness-optimizing trait values (i.e., the degree of maladaptation) could narrow, widen or stay the same over time (Kopp and Matuszewski, 2014). Here, we will use a simple, established evolutionary model that can explain how evolutionary dynamics that follow fitness gradients in a changed (or changing) environment can (transiently or permanently) result in apparently maladaptive outcomes. Our analysis reveals patterns of transient maladaptation that are far more diverse and surprising than the gradual changes in adaptation expected under the lagging-behind-the-optimum scenario.

Our study obtains an empirical and application-related dimension in the context of reciprocal transplant experiments, which are often considered the "gold standard" for assessing the degree of local adaptation (Kawecki and Ebert, 2004; Hereford, 2009; Blanquart et al., 2013; Brady et al., 2019b). In reciprocal transplant experiments the fitness of a population *A*, supposedly adapted to environmental conditions *a*, is compared with the fitness of a (or several) population(s) *B*, adapted to environmental conditions *b*. Individuals (and their genotypes) from both populations are transplanted to the other environment to enable a direct fitness comparison between populations in their respective local vs. foreign environments. To a first degree, local adaptation can be concluded from a pattern of higher fitness of the resident populations in their respective environments and lower fitness of foreign/introduced populations in the environments foreign to them. However, as we will discuss, appropriate inference from the results of reciprocal transplant experiments is somewhat disputed (Kawecki and Ebert, 2004; Blanquart et al., 2013). We use the predictions of our evolutionary model to simulate the results of hypothetical reciprocal transplant experiments performed at different time points of transient evolutionary dynamics. We will show that transient evolutionary states can lead to varying inferences arising from reciprocal transplant outcomes. Depending on the timing of the experiment and the criteria for local adaptation adopted, strong, weak, or no support for adaptation can be found when resident and foreign populations are evolving.

Finally, the results of our model can also be interpreted in the context of global change, where evolution might be able to make up for the loss of fitness of populations or species due to rapid environmental change (Diamond, 2018). However, the prevailing opinion is that populations/species become less and less fit in their local environments because the speed of global change outpaces the populations' adaptive potential (Somero, 2010). In response, populations might migrate and reestablish themselves in environments that allow them to be fit without the need for rapid evolutionary adaptation. As a result, global warming is expected to lead to major latitudinal range shifts of species (Deutsch et al., 2008; Sunday et al., 2012; Bennett et al., 2021). Despite the vast differences in spatial and temporal scales, it can be argued that the same ecological and evolutionary principles apply to reciprocal transplant experiments and global change-induced species range shifts. Our model also informs the latter process by highlighting the temporal succession of two distinct checkpoints that might occur during colonization of and adaptation to the new environment: a better fit to the new than to the old environment and becoming fitter than the resident populations in the new environment.

2. Materials and methods

2.1. Evolutionary model

Our analysis is based on a classical model of quantitative trait evolution (Lande, 1976; Estes and Arnold, 2007) and largely relies on previously established realistic parameter values (Bürger and Lynch, 1995). The model describes the stochastic evolution of the mean phenotype in a randomly mating, finite population with discrete generations (t). Trait phenotypes are normally distributed with mean trait value $\bar{z}_t$ and phenotypic variance σ^2. Traits are under stabilizing selection on viability (either with or without a moving trait optimum) and the average fitness of individuals in the population with mean trait value $\bar{z}$ is determined by the Gaussian adaptive landscape function

$$\overline{W}_z = \overline{W}_{\max} \exp\left(-\frac{(\bar{z}-\theta)^2}{2\left(\omega^2+\sigma^2\right)}\right), \quad (1)$$

where θ is the optimum phenotypic trait value, ω^2 characterizes the width of the adaptive landscape and $\overline{W}_{\max}$ is the maximum attainable average fitness (arbitrarily set to one in this study).

Adaptive evolution can be imagined as the trait mean climbing the slope of the adaptive landscape function toward the fitness maximum. Direction and speed of evolution are determined by the position of the trait mean relative to the optimum trait value, the shapes of the adaptive landscape and the phenotypic trait distribution, and the heritability of the trait. It is possible to find

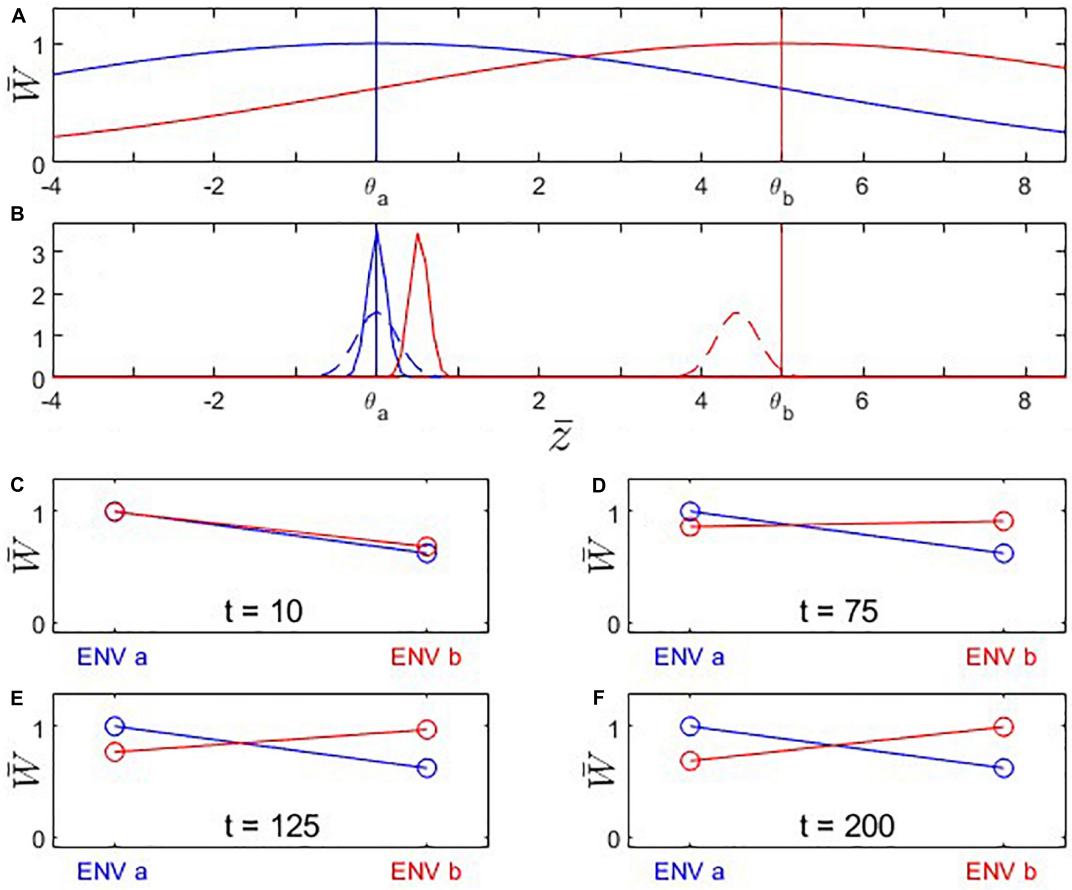

FIGURE 1
Fitness landscapes, trait evolution, and reciprocal-transplant experiments under Scenario 1: Trait optima are stationary; initial trait value $\bar{z}_0$ is located at the fitness optimum for environment *a*. Population *B* branches off from population *A* at time t_0 and adapts to the new environmental conditions dictated by the changed fitness landscape. **(A)** Fitness landscapes for environment *a* (blue) and *b* (red); vertical lines indicate the location of the fitness optima. **(B)** Probability distributions for phenotypic means after t = 10 (solid) and 200 (dashed) generations of evolution. Note that population *A*'s (blue) mean trait value remains in place while population *B* evolves toward the new trait optimum $\theta_b = 5$. Also note that the width of the distribution shown is the variance of the mean phenotype across hypothetical replicated populations (arising due to genetic drift), not the genetic variance of a single population (which is assumed to remain constant). **(C–F)** Fitness plots for hypothetical reciprocal transplant experiments performed at t = 10, 75, 125, 200 (Left side of each panel: fitness of populations *A* (blue) and *B* (red) in environment *a*; right side: fitness of populations *A* and *B* in environment *b*). Parameters: $\bar{z}_{0,a} = \bar{z}_{0,b} = 0$; $\theta_a = 0$; $\theta_b = 5$; $\overline{W}_{\max,a} = \overline{W}_{\max,b} = 1$; $\omega_a = \omega_b = 5$; $\sigma_a = \sigma_b = 1.135$; $h_a^2 = h_b^2 = 0.224$; $N_a = N_b = 200$.

a solution (Lande, 1976; Estes and Arnold, 2007) for the probability distribution of the mean phenotype $\Phi(\bar{z}_t)$ after t generations of trait evolution, which, again, is a normal distribution characterized by its mean $\bar{z}_\Phi(t)$ and variance $\sigma_\Phi^2(t)$

$$\begin{aligned} &\Phi(\bar{z}_t) = \frac{1}{\sqrt{2\pi\sigma_\Phi^2(t)}} \exp\left(-\frac{(\bar{z}_t - \bar{z}_\Phi(t))^2}{2\sigma_\Phi^2(t)}\right), \\ &\text{with}: \quad \bar{z}_\Phi(t) = (\bar{z}_0 - \theta)\exp\left(-\frac{h^2\sigma^2}{\omega^2+\sigma^2}t\right) + \theta, \\ &\text{and}: \quad \sigma_\Phi^2(t) = \frac{\omega^2+\sigma^2}{2N}\left(1 - \exp\left(-2\frac{h^2\sigma^2}{\omega^2+\sigma^2}t\right)\right) \end{aligned} \tag{2}$$

where $h^2$is the realized heritability and N the effective population size. In addition to our analyses based on this deterministic model we also performed individual-based stochastic simulations. These simulations were done to verify that our results from the deterministic analyses also hold up when populations experience demographic stochasticity and the associated risk of extinction (Bürger and Lynch, 1995). We found that the model predictions between the two approaches are in very good agreement and present the methodology and results of the individual-based simulations in the **Supplementary material**.

2.2. Adaptive scenarios

2.2.1. Stationary trait optima

We first consider the scenario of a population *A* under environmental conditions *a* from which a part branches off to colonize a different environment *b* as a new population *B* (**Figures 1–4**). Natural circumstances under which such a scenario might happen are emigration or the splitting of the population by a catastrophic event. The scenario is also comparable to those conducive to allopatric speciation. We follow the evolutionary trajectory of the same fitness-determining trait in both populations in their respective environments. We do not make specific assumptions about the nature of the trait (and assign arbitrary trait values), but possible cases are organisms

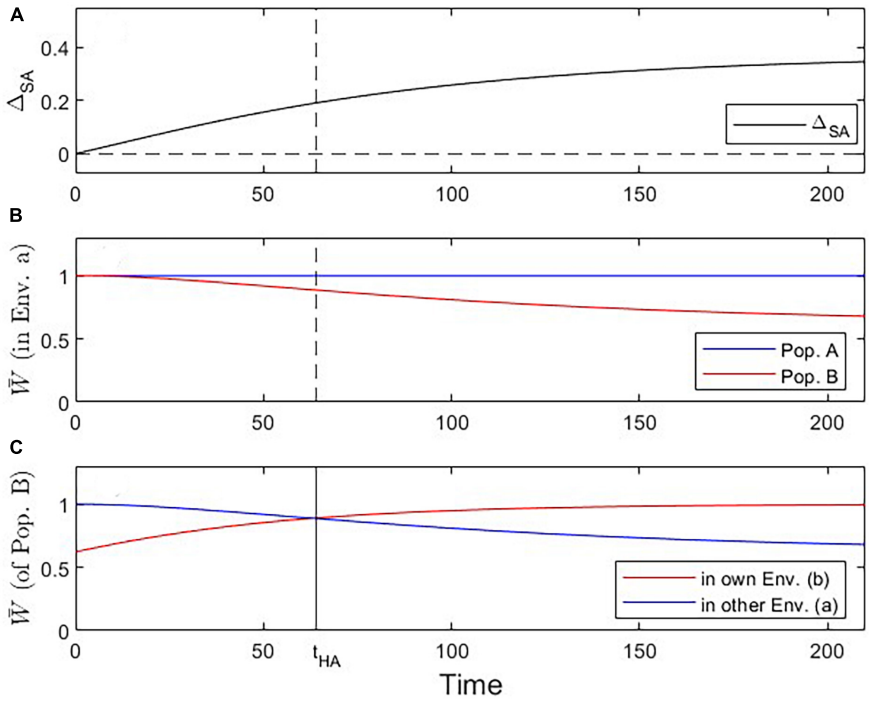

FIGURE 2
Visualization of three critical checkpoints during the evolutionary dynamics under Scenario 1. **(A)** Evidence for local adaptation by the Δ_{SA} contrast criterion (satisfied for all $t > 0$). **(B)** Fitness of population *A* vs. *B* in environment *a* (addressing the Local vs. Foreign criterion; satisfied for all $t > 0$). **(C)** Fitness of population *B* in own vs. other environment (addressing the Home vs. Away criterion; $t_{crit} = 64$; solid vertical line in this panel; dashed vertical line in other panels).

facing different temperature regimes or gape-limited predators encountering differently sized prey in environments *a* and *b*. We also put ourselves in the shoes of an evolutionary biologist who performs reciprocal transplant experiments to assess the degree of adaptation of populations *A* and *B* to their respective environments, without necessarily knowing their evolutionary history. We produce the typical reciprocal transplant plots that would arise from experiments conducted at different time points (**Figures 1C–F**, **3C–F**). We start by analyzing the special case where the original population (i.e., population *A* before population *B*'s split-off) has a trait value that maximizes fitness in environment *a* (Scenario 1; **Figures 1**, **2**). Subsequently, however, we will be particularly interested in cases where the original population has not yet reached the optimal trait value (Scenario 2; **Figures 3**, **4**), for example, because it is itself a recent colonizer of environment *a*.

2.2.2. Moving trait optima

Secondly, we analyze the more general case where the trait optima are gradually shifting over time in one direction (Scenario 3; **Figures 5–7**). Here, fitness differences will arise because, starting from the branching point, the two populations are facing environmental change that progresses at different speeds. The scenario is closely related to global-change phenomena (such as increasing temperatures), which are nearly ubiquitous but differ in magnitude regionally.

Under this scenario, the trait optima of populations *A* and *B* start at the identical initial value θ_0 and move over time in the same direction, according to $\theta_t = kt$, but at different rates k_a and k_b. The expected mean trait value $\bar{z}_\Phi(t)$ of a population adapting to such a moving optimum is given by Estes and Arnold (2007):

$$\bar{z}_\Phi(t) = (z_0 + kt) - k\left(\frac{\omega^2 + \sigma^2}{h^2\sigma^2}\right)\left(1 - \exp\left(-\frac{h^2\sigma^2}{\omega^2 + \sigma^2}t\right)\right), \quad (3)$$

with the same variance as in Equation 2.

2.3. Inference from reciprocal transplants

Different measures have been proposed to estimate local adaptation from the results of reciprocal transplant experiments (Kawecki and Ebert, 2004; Blanquart et al., 2013). A straightforward approach is to rely on estimates of the average local adaptation. For this measure, the Δ_{SA} ***contrast*** (i.e., sympatric vs. allopatric contrast), one calculates the difference between the average fitness in sympatric combinations of populations and sites and the average fitness in allopatric combinations (Blanquart et al., 2013), i.e., for our case of two populations *A*, *B* in two environments *a*, *b*:

$$\Delta_{SA} = \frac{1}{2}\left(\overline{W}_{A\ in\ a} + \overline{W}_{B\ in\ b}\right) - \frac{1}{2}\left(\overline{W}_{A\ in\ b} + \overline{W}_{B\ in\ a}\right), \quad (4)$$

where $\overline{W}_{J\ in\ i}$ is the average fitness of population $J = A,B$ evaluated in environment $i = a,b$, respectively. Local adaptation would be indicated if $\Delta_{SA} > 0$.

In contrast, the ***Local vs. Foreign criterion (L–F)*** emphasizes the comparison between populations within environments (Kawecki and Ebert, 2004). Under local adaptation, the local population is expected to show higher fitness than the foreign

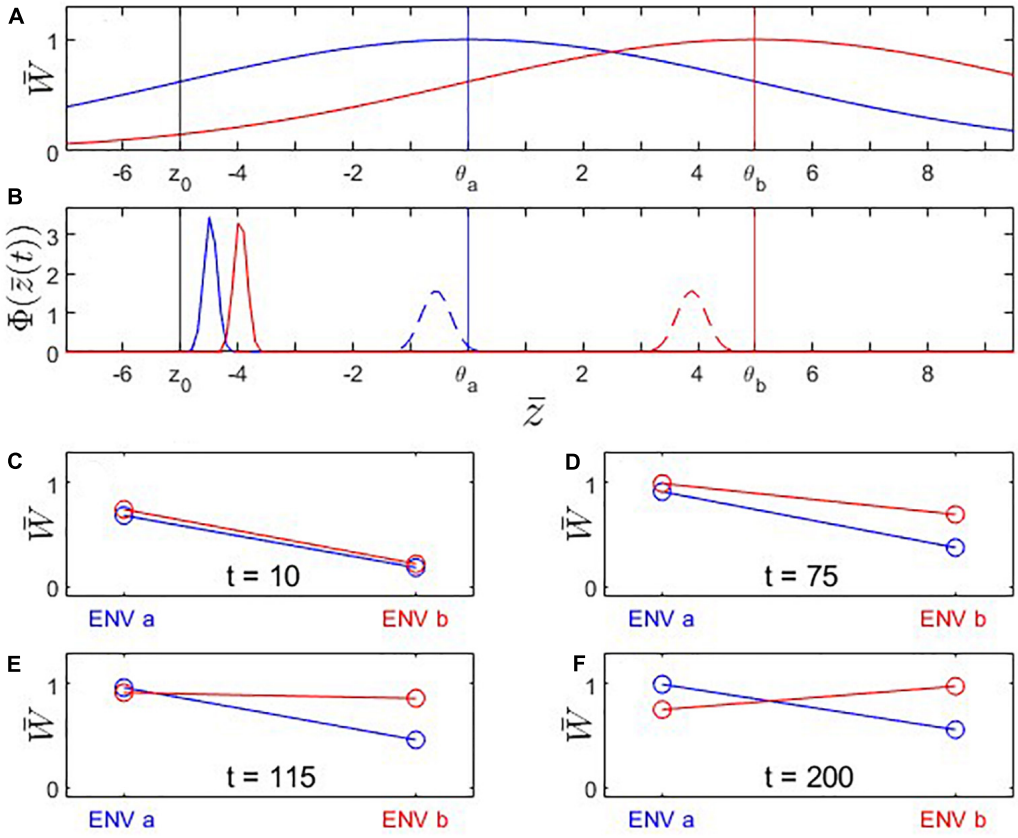

FIGURE 3
Fitness landscapes, trait evolution and reciprocal transplant experiments under Scenario 2: Trait optima are stationary; initial trait value $\bar{z}_0$ is located at a suboptimal value to the left of the fitness optimum for environment *a*. Both populations adapt to new environmental conditions but population *B*'s (red) fitness optimum is farther to the right than population *A*'s (blue). **(A)** Fitness landscapes for population *A* (blue) and population *B* (red); vertical lines: fitness optima (blue, red) and initial trait value $\bar{z}_0$ (black). **(B)** Distributions of phenotypic mean after t = 10 (solid) and t = 200 (dashed) generations of evolution. Note that population *A*'s (blue) mean trait value changes less than population *B*'s. **(C–F)** Fitness plots for hypothetical reciprocal transplant experiments performed at t = 10, 75, 115, 200. Parameters: $\bar{z}_{0,a} = \bar{z}_{0,b} = -5$; other parameters as in Figure 1.

population in both environments. This means that, in a classical reciprocal transplant plot, with environments on the x-axis and fitness on the y-axis, the lines connecting the fitness values of a given population in the two environments need to cross (as, e.g., in Figure 3E) (We note that, while it is also possible for the lines to cross if, in each environment, it is the foreign population that has higher fitness, such a case of complete maladaptation did not occur in our present study).

Finally, the ***Home vs. Away criterion (H-A)*** emphasizes the comparison between populations across environments (Kawecki and Ebert, 2004). Under this criterion, local adaptation exists if each population has higher fitness in its own environment than in the alternative environment. With respect to a reciprocal transplant plot, this means that local adaptation occurs if the line connecting the two fitness values for a population has a negative slope for population *A* and a positive slope for population *B* (assuming that environment *a* is placed to the left of environment *b* on the plot's x-axis; as, e.g., in Figure 5D). Note that, under this criterion, no direct comparison is made between the fitness values of the two populations, however it is possible that one population is locally adapted to its environment while the other one is not.

3. Results

3.1. Stationary trait optima

We first analyze the most basic case (Scenario 1 above) where population *A* is perfectly adapted to its environment *a*, and population *B* branches off from population *A* and shows steady evolutionary adaptation toward a new optimal trait value in environment *b* (Figure 1). Reciprocal transplant experiments performed at different time points would show accumulating evidence of local adaptation (Figures 1C–F, 2). At $t > 0$, blue and red lines cross over, indicating that each population is fitter in its own environment than the other population (L-F criterion satisfied; Figure 2B). Once the mean trait value of Population *B* has evolved to be closer to the optimal trait value for environment *b* than the one for environment *a*, each population has higher fitness in its own environment than in the other environment (blue line has negative slope, red line has positive slope; H-A criterion satisfied; Figure 2C). Signal strength in support for both the L-F and H-A criteria increases with time, and so does the estimate of the average local adaptation, the Δ_{SA} contrast, which has a positive value at all times $t > 0$ (Figure 2A).

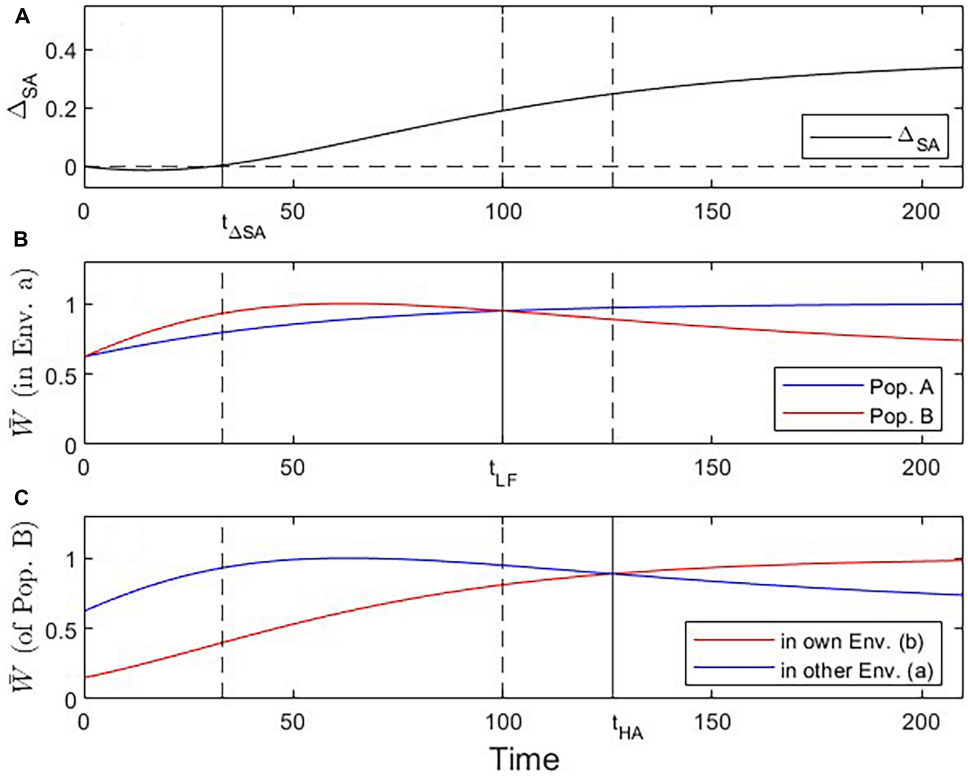

FIGURE 4
Visualization of three critical checkpoints (vertical lines) during the evolutionary dynamics under Scenario 2. **(A)** Evidence for adaptation by the Δ_{SA} contrast criterion (at $t \geq 33$). **(B)** Fitness of population *A* vs. *B* in environment *a* (addressing the Local vs. Foreign criterion; t_{crit} = 100). **(C)** Fitness of Population *B* in own vs. other environment (addressing the Home vs. Away criterion; t_{crit} = 126).

Under Scenario 2, both populations start the evolutionary process at a trait value displaced to the left of the optimal trait value for environment *a* (Figure 3A). Because population *B*'s trait optimum lies further to the right than that of population *A*, its evolutionary trajectory moves across high-fitness regions of population *A*'s fitness landscape. As a result, population *B* encounters periods where it is better adapted to environment *a* than population *A*, as well as periods where population *B* is better adapted to environment *a* than to environment *b*. Initially, none of the criteria for local adaptation is satisfied; with progressing evolution, however, the Δ_{SA} contrast, the L-F criterion, and the H-A criterion become consecutively fulfilled (Figure 4). Due to these periods of apparent maladaptation, hypothetical reciprocal transplant experiments would only reveal an unequivocal signature of local adaptation about 126 generations after the split of populations *A* and *B* (with the current parameterization; Figures 3F, 4C).

3.2. Moving trait optima

The phenomenon of apparent maladaptation also arises under Scenario 3 (moving trait optima with different speed). Because the conditions are assumed to be changing more rapidly in environment *a* than in environment *b*, population *A* is trailing the optimal trait value more than population *B* is. Starting from an initial state of complete local adaptation (Figures 5B, C), population *B* first gains fitness superiority over population *A* in environment *a* (loss of local adaptation according due to the L-F criterion; Figures 5D, 6B, 7), then population *B* becomes the universally more fit population (Figure 5E), and finally, population *A* becomes better adapted to environment *b* than to environment *a*, (loss of local adaptation according to the H-A criterion; Figures 5F, 6C, 7). If environmental and evolutionary change continue for a sufficiently long period, both populations will trail their environmental fitness optima by a constant gap (Figure 7), and the signature of relative (yet, not complete) local adaptation becomes reinstated ($t \approx 300$).

4. Discussion

In this theoretical study we analyzed realistic evolutionary scenarios during which populations can display transitional fitness states that carry the signature of non-adaptation or maladaptation. Before discussing the implications of our findings in more detail, we feel that it is useful to evoke two conceptual perspectives: the concept of adaption as a process vs. adaptation as a state; and the concept of relative vs. absolute fitness.

Unlike evolution, which always refers to a process, adaptation can either refer to the process of adapting or to the state of being adapted. This distinction is very much at the core of our seemingly paradoxical observations, where populations strictly obey the laws of quantitative genetics by displaying monotonous

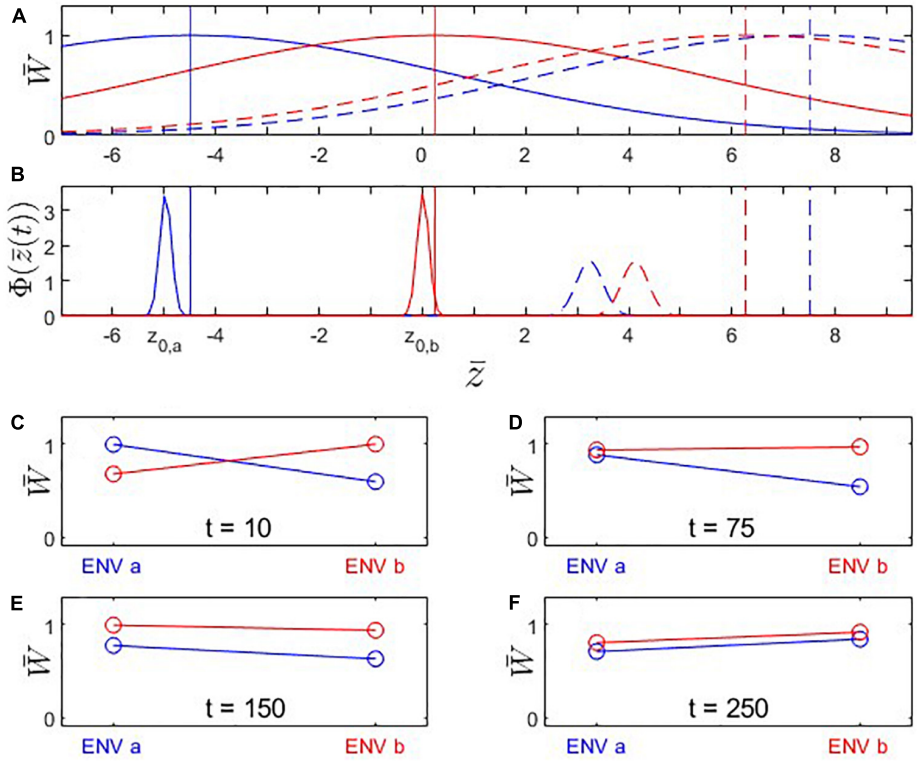

FIGURE 5
Fitness landscapes, trait evolution and reciprocal transplant experiments under Scenario 3: Trait optima are moving (from left to right along the x-axis); initial trait values $\bar{z}_{0,a}$ and $\bar{z}_{0,b}$ are located at the fitness optima for their environments. Both populations adapt to the shifting environmental conditions but population *A*'s (blue) fitness optimum moves faster than population *B*'s (red). **(A)** Fitness landscapes for population *A* (blue) and population *B* (red) at t = 10 (solid) and t = 250 (dashed); vertical lines: fitness optima. **(B)** Distributions of phenotypic means at t = 10 (solid) and t = 250 (dashed). Note that both populations are trailing their respective fitness optima. **(C–F)** Fitness plots for hypothetical reciprocal transplant experiments performed at t = 10, 75, 150, 250. Parameters: $k_a = 0.050$; $k_b = 0.025$; $\bar{z}_{0,a} = -5$; $\bar{z}_{0,b} = 0$; other parameters as in **Figure 1**.

adaptive evolution [i.e., they climb their respective adaptive hills, leading to "adaptive divergence" (Hendry, 2017)] yet undergo transient maladaptive states. Keeping the two views on adaptation straight is key when interpreting the kind of evolutionary dynamics that occurred in our study. However, we believe that we are dealing with a problem that runs deeper than merely a semantic issue. The reason is that nearly all practical methods of assessing adaptation in nature (such as reciprocal transplant or common garden experiments) implicitly quantify adaptive states, but the results are often interpreted as evidence for the process of evolutionary adaptation (or the lack thereof).

In a similar vein, distinguishing between relative and absolute fitness is crucial when discussing (mal)adaptation (Holt and Gomulkiewicz, 1997; Brady et al., 2019b). Specifically, evolutionary biologists tend to emphasize relative fitness while ecologists focus on absolute fitness (Hendry and Gonzalez, 2008; Brady et al., 2019b). This means that, to an evolutionary biologist who strictly applies the relative fitness concept, a population is maladapted if it has lower fitness than a relevant reference population. By contrast, an ecologist might score the same population as well adapted if it displays a positive growth rate in its local environment, and particularly so if the population has evolved toward this state from a previous state of lower absolute fitness. In our study, populations always increase their local absolute fitness in the environment they are adapting to (in Scenarios 1 and 2), except in cases where environmental change outpaces the capacity for evolutionary change (in some instances of Scenario 3). Relative fitness of a population, however, depends on the comparison with a reference population, either within (L-F criterion) or across (H-A criterion) environments.

Equipped with this background it should be straightforward to understand the evolutionary dynamics presented in Scenarios 2 and 3 for what they are, namely adaptive trajectories that, on their way to an adaptive steady state, pass through transient states of maladaptation (in the evolutionary sense above, that is in terms of relative fitness). This phenomenon can only occur while the evolutionary process is not at a (stable or dynamic) equilibrium, either because the populations are not initially at their fitness optima (Scenario 2) or because the fitness optima themselves are moving targets (Scenario 3; we also have analyzed the combination of these two causes of steady-state divergence but omitted the results from this paper as they did not provide any additional insights to what is presented here). The phenomenon necessarily implies change in relative fitness and may (Scenario 3) or may not (Scenario 2) be accompanied by intermittent loss of absolute fitness of one or both populations. The label "apparent maladaptation" (Brady et al., 2019b) tries to reconcile the facts that the underlying process is truly adaptive yet produces snapshots of true maladaptive states.

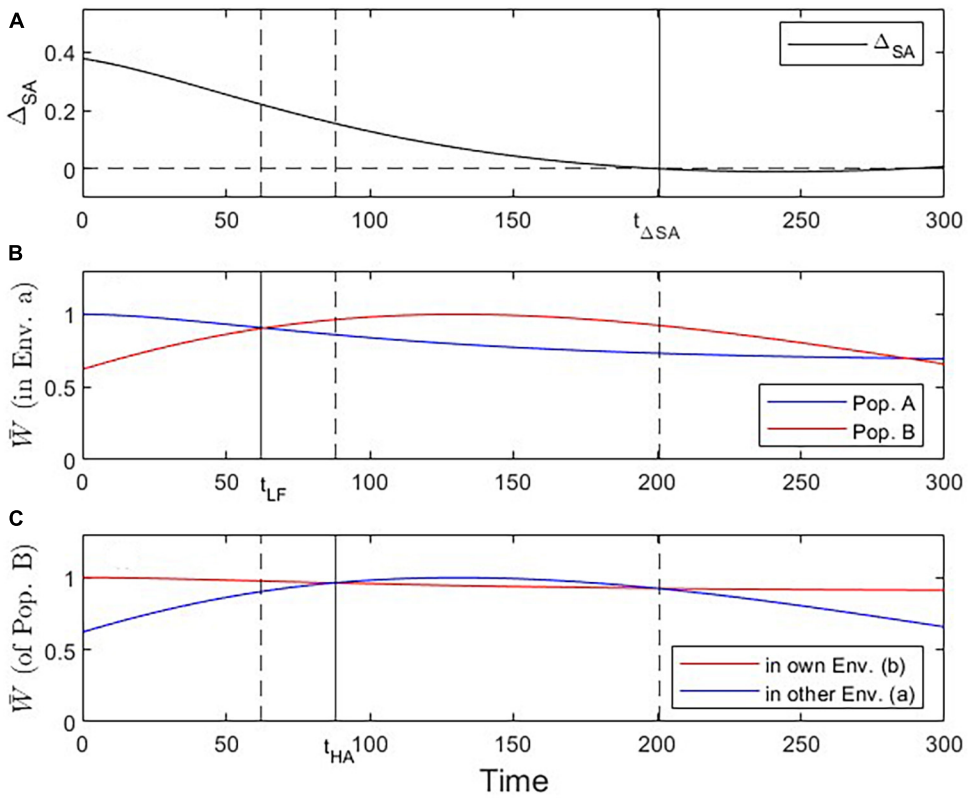

FIGURE 6
Visualization of three critical checkpoints (vertical lines) during the evolutionary dynamics under Scenario 3. **(A)** Evidence for local adaptation by the Δ_{SA} contrast criterion (at $t \leq 201$). **(B)** Fitness of population *A* vs. *B* in environment *a* (addressing the Local vs. Foreign criterion; $t_{crit} = 62$). **(C)** Fitness of population *B* in own vs. other environment (addressing the Home vs. Away criterion; $t_{crit} = 88$).

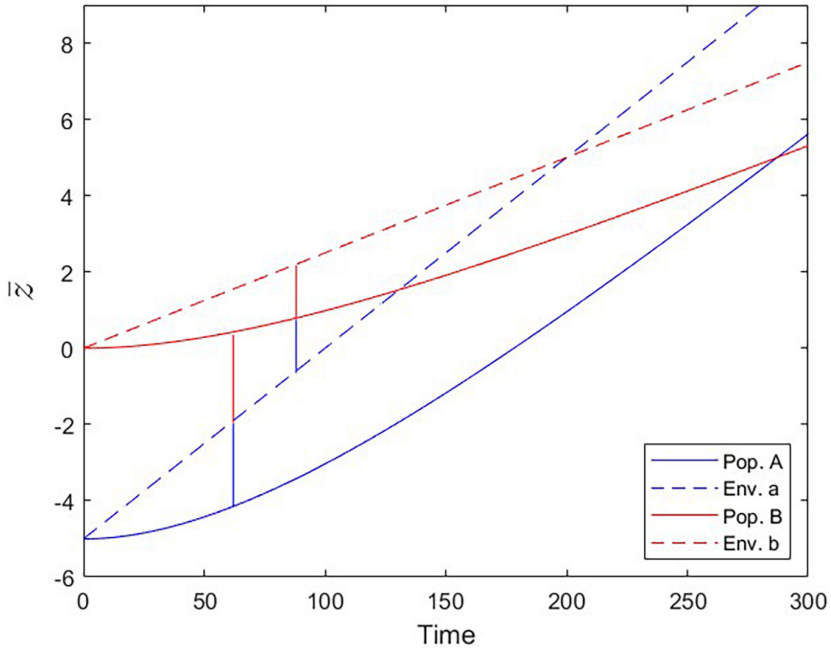

FIGURE 7
Populations trailing the moving fitness optima over time (Scenario 3). Optimal trait values set by the environmental conditions (dashed lines) and trait values realized by populations *A* and *B* (solid lines). At the Local vs. Foreign criterion checkpoint ($t_{crit} = 62$), population *B* is as fit in environment *a* as population *A* is. At the Home vs. Away criterion checkpoint ($t_{crit} = 88$), population *B* is equally fit in environments *a* and *b*.

Our study has some implications for the interpretation of reciprocal transplant experiments, one of the primary methods for detecting and quantifying adaptive divergence (Kawecki and Ebert, 2004; Hendry, 2017). While many such experiments have detected clear patterns of local adaptation (Nagy, 1997; Hargreaves and Eckert, 2019), other studies have reported a nearly complete lack of adaptation (Low-Decarie et al., 2013; Rolshausen et al., 2015); indeed, meta-analyses have revealed that about 30% of experiments failed to detect the classical signature of local adaptation, i.e., higher relative fitness of local types in each environment (i.e., the L-F criterion) (Leimu and Fischer, 2008; Hereford, 2009). Part of these results are likely due to a lack of adaptive dynamics per se (e.g., due to lack of genetic variation). In addition, however, our study points to a variety of cases that fail to produce adaptive signatures even in the presence of adaptive dynamics, leading to apparent maladaptation. These cases include examples of one population being relatively better locally adapted than the other, no matter what the environment (e.g., **Figures 3C, D, 5D–F**); or examples of one environment leading to lower absolute fitness of both populations than the other environment (e.g., **Figures 3C–E**), even with the identity of the low-fitness environment switching over time (**Figures 5E, F**). That said, we did not find any instances of complete maladaptation, where each population has the highest fitness in the non-native environment. In a real experimental situation, maladaptive patterns of the kind we observed may arise due to a multitude of factors such as constraints on evolution, genotype-by-environment interaction, co-evolution, unaccounted traits under selection or phenotypic plasticity (Bjorklund, 1996; Hendry, 2017). We would like to add to this list as a possible factor "transient adaptive dynamics," given that our results demonstrate that these trajectories do not just amount to a delayed approach to the adaptive state (as in Scenario 1) but may cross through truly maladaptive transition states (Scenarios 2, 3). This realization is very much in line with the idea and recent experimental demonstration of an "adaptational lag" (akin to our Scenario 3) that leads to fitness superiority of non-native populations because local populations failed to keep evolutionary pace with rapid environmental climate change (Kooyers et al., 2019). Reciprocal transplants are often labor-intensive experiments, replication in time (as simulated in our purposefully placed snapshots presented in panels C through F of **Figures 1**, **3**, **5**) is rarely possible, and the evolutionary history of the populations chosen for the experiment is often scarcely known. As such, we advise against taking the absence of evidence for adaptation (based on results from a single reciprocal transplant or common garden experiment) as hard evidence for the absence of adaptive divergence.

Over the course of the adaptive divergence observed in our model simulations, we were able to track certain measures commonly used as indicators of local adaptation (see Section 2.3). Among these measures, the Local vs. Foreign criterion (L-F) adopts the most "evolutionary" perspective, in that it emphasizes the comparison of relative fitness among populations, and some authors maintain that it should be used as the only diagnostic for establishing local adaptation (Kawecki and Ebert, 2004). An implicit consequence of the L-F criterion is that overall local adaptation can only be concluded from a reciprocal transplant experiment if all populations tested are locally adapted. Other authors found this criterion overly strict and impractical and have advocated for adopting the Δ_{SA} contrast, which is satisfied if, on average, populations have higher fitness in their native than in their non-native environments (Blanquart et al., 2013). Which criterion a researcher decides to use when interpreting their experiment probably depends ultimately on the experimental design and the type and strength of inference they wish to draw from their experiment. We feel, that, in our study, the Δ_{SA} contrast proved to be an unacceptably lenient benchmark. For instance, this criterion would have led us to conclude local adaptation in the cases depicted in **Figures 3D** or **5E**, simply based on the fact that the adaptation of population *B* to environment *b* slightly exceeds the clear maladaptation of Population *A* to environment *a*. In situations like ours, where only few populations and environments are compared with one another, the L-F and H-A criteria appear to be the more useful diagnostics. In all our simulations, both diagnostics were far more restrictive in assigning local adaptation to results of a reciprocal transplant experiment than the Δ_{SA} contrast; however, which of the two measures (L-F or H-A) were satisfied during a longer period of the simulated evolutionary dynamics depended on the concrete parameterization.

We framed our study around populations that face different adaptive challenges for a certain period of time and whose local fitnesses are compared afterwards in the context of a reciprocal transplant experiment. One could argue that this scenario has similarities with the process of species invasions that occur on a global scale, even more so because it is becoming increasingly clear that climate change can be a crucial factor determining the introduction and establishment of non-native species (Hulme, 2017; Ricciardi et al., 2021). Hence, our Scenario 3 could also be interpreted from an invasion biological perspective, where trait optima shift due to the regionally different intensity and speed of climate change. Our current approach is certainly too generic in parameterization as well as too low-dimensional in trait space to be able to make useful predictions for concrete invasion scenarios. However, we would like to point out the possibility that the L-F and H-A checkpoints might serve as invasion criteria. Over the course of adaptation to climate change a potentially invasive species would likely increase its invasion potential in two steps. It would (*a*) develop higher relative fitness than the resident species and (*b*) become better adapted to the foreign environment than to its native environment (**Figure 7**). Checkpoint *a* aligns with the L-F criterion and gives the invader the competitive edge, whereas checkpoint *b* (= H-A) would increase the incentive to migrate out of the native environment (provided there are individuals that are able to probe both environments as, for instance, in migratory birds). Our simulations revealed that the order in which these two events occur is not fixed and depends on the specific conditions (i.e., parameterizations, in the model), but they always occurred in temporal succession. It would be premature to decide if one of the two criteria can serve as a more significant predictor for invasion success than the other, but in many real-life scenarios the invasion probability will likely be higher when both criteria are met.

In this theoretical study we have elaborated on the phenomenon of apparent maladaptation that previously has been sketched out in Brady et al. (2019b). We have shown that our results have potentially important implications in applied areas that reach beyond theoretical evolutionary biology. However, we also decided to keep things simple, traceable and generic by using

a very simple evolutionary model that was not parameterized for any concrete real eco-evolutionary scenario. We consider our contribution a first step toward investigating this interesting phenomenon of apparent maladaptation. We can envision many realistic model alterations, such as multiple evolving traits, evolutionary constraints, alternatively shaped fitness functions (Osmond and Klausmeier, 2017), eco-evolutionary scenarios in multi-species communities (Govaert et al., 2019; Hui et al., 2021), and so on, and invite other researchers to evaluate the validity of our conclusions under model realizations that mirror more concrete scenarios than we were able to analyze.

Data availability statement

The original contributions presented in this study are included in the article/**Supplementary material**, further inquiries can be directed to the corresponding author.

Author contributions

GF conceived the study, performed the modeling, and wrote the first draft of the manuscript. MK performed the analyses presented in the **Supplementary material**. Both authors analyzed and interpreted the results, discussed the scope of the manuscript, edited the manuscript, and approved the final version.

Funding

GF was supported by NSERC Discovery Grant RGPIN/04780-2020.

Acknowledgments

GF is grateful for a sabbatical leave granted by McGill University, which promoted the research collaboration leading to this publication.

Conflict of interest

The authors declare that the research was conducted in the absence of any commercial or financial relationships that could be construed as a potential conflict of interest.

Publisher's note

Supplementary material

The Supplementary Material for this article can be found online at: https://www.frontiersin.org/articles/10.3389/fevo.2023.1151283/full#supplementary-material

References

Bennett, J. M., Sunday, J., Calosi, P., Villalobos, F., Martinez, B., Molina-Venegas, R., et al. (2021). The evolution of critical thermal limits of life on earth. *Nat. Commun.* 12:1198. doi: 10.1038/s41467-021-21263-8

Bjorklund, M. (1996). The importance of evolutionary constraints in ecological time scales. *Evol. Ecol.* 10, 423–431. doi: 10.1007/Bf01237727

Blanquart, F., Kaltz, O., Nuismer, S. L., and Gandon, S. (2013). A practical guide to measuring local adaptation. *Ecol. Lett.* 16, 1195–1205. doi: 10.1111/ele.12150

Brady, S. P., Zamora-Camacho, F. J., Eriksson, F. A. A., Goedert, D., Comas, M., and Calsbeek, R. (2019c). Fitter frogs from polluted ponds: The complex impacts of human-altered environments. *Evol. Appl.* 12, 1360–1370. doi: 10.1111/eva.12751

Brady, S. P., Bolnick, D. I., Angert, A. L., Gonzalez, A., Barrett, R. D. H., Crispo, E., et al. (2019a). Causes of maladaptation. *Evol. Appl.* 12, 1229–1242. doi: 10.1111/eva.12844

Brady, S. P., Bolnick, D. I., Barrett, R. D. H., Chapman, L., Crispo, E., Derry, A. M., et al. (2019b). Understanding maladaptation by uniting ecological and evolutionary perspectives. *Am. Nat.* 194, 495–515. doi: 10.1086/705020

Bürger, R., and Lynch, M. (1995). Evolution and extinction in a changing environment - a quantitative-genetic analysis. *Evolution* 49, 151–163. doi: 10.2307/2410301

Deutsch, C. A., Tewksbury, J. J., Huey, R. B., Sheldon, K. S., Ghalambor, C. K., Haak, D. C., et al. (2008). Impacts of climate warming on terrestrial ectotherms across latitude. *Proc. Natl Acad. Sci. U.S.A.* 105, 6668–6672. doi: 10.1073/pnas.0709472105

Diamond, S. E. (2018). Contemporary climate-driven range shifts: Putting evolution back on the table. *Funct. Ecol.* 32, 1652–1665. doi: 10.1111/1365-2435.13095

Estes, S., and Arnold, S. J. (2007). Resolving the paradox of stasis: Models with stabilizing selection explain evolutionary divergence on all timescales. *Am. Nat.* 169, 227–244. doi: 10.1086/510633

Fraser, D. J., Walker, L., Yates, M. C., Marin, K., Wood, J. L. A., Bernos, T. A., et al. (2019). Population correlates of rapid captive-induced maladaptation in a wild fish. *Evol. Appl.* 12, 1305–1317. doi: 10.1111/eva.12649

Govaert, L., Fronhofer, E. A., Lion, S., Eizaguirre, C., Bonte, D., Egas, M., et al. (2019). Eco-evolutionary feedbacks-theoretical models and perspectives. *Funct. Ecol.* 33, 13–30. doi: 10.1111/1365-2435.13241

Hargreaves, A. L., and Eckert, C. G. (2019). Local adaptation primes cold-edge populations for range expansion but not warming-induced range shifts. *Ecol. Lett.* 22, 78–88. doi: 10.1111/ele.13169

Hendry, A. P. (2017). *Eco-evolutionary dynamics*. Princeton, NJ: Princeton University Press.

Hendry, A. P., and Gonzalez, A. (2008). Whither adaptation? *Biol. Philos.* 23, 673–699. doi: 10.1007/s10539-008-9126-x

Hereford, J. (2009). A quantitative survey of local adaptation and fitness trade-offs. *Am. Nat.* 173, 579–588. doi: 10.1086/597611

Holt, R. D., and Gomulkiewicz, R. (1997). How does immigration influence local adaptation? A reexamination of a familiar paradigm. *Am. Nat.* 149, 563–572. doi: 10.1086/286005

Hui, C., Richardson, D. M., Landi, P., Minoarivelo, H. O., Roy, H. E., Latombe, G., et al. (2021). Trait positions for elevated invasiveness in adaptive ecological networks. *Biol. Invas.* 23, 1965–1985. doi: 10.1007/s10530-021-02484-w

Hulme, P. E. (2017). Climate change and biological invasions: Evidence, expectations, and response options. *Biol. Rev.* 92, 1297–1313. doi: 10.1111/brv.12282

Kawecki, T. J., and Ebert, D. (2004). Conceptual issues in local adaptation. *Ecol. Lett.* 7, 1225–1241. doi: 10.1111/j.1461-0248.2004.00684.x

Kooyers, N. J., Colicchio, J. M., Greenlee, A. B., Patterson, E., Handloser, N. T., and Blackman, B. K. (2019). Lagging adaptation to climate supersedes local adaptation to herbivory in an annual monkeyflower. *Am. Nat.* 194, 541–557. doi: 10.1086/702312

Kopp, M., and Matuszewski, S. (2014). Rapid evolution of quantitative traits: Theoretical perspectives. *Evol. Appl.* 7, 169–191. doi: 10.1111/eva.12127

Lande, R. (1976). Natural selection and random genetic drift in phenotypic evolution. *Evolution* 30, 314–334. doi: 10.2307/2407703

Leimu, R., and Fischer, M. (2008). A Meta-Analysis of Local Adaptation in Plants. *PLoS One* 3:e4010. doi: 10.1371/journal.pone.0004010

Loria, A., Cristescu, M. E., and Gonzalez, A. (2019). Mixed evidence for adaptation to environmental pollution. *Evol. Appl.* 12, 1259–1273. doi: 10.1111/eva.12782

Low-Decarie, E., Jewell, M. D., Fussmann, G. F., and Bell, G. (2013). Long-term culture at elevated atmospheric CO_2 fails to evoke specific adaptation in seven freshwater phytoplankton species. *Proc. R. Soc. B Biol. Sci.* 280:20122598. doi: 10.1098/rspb.2012.2598

Nagy, E. S. (1997). Selection for native characters in hybrids between two locally adapted plant subspecies. *Evolution* 51, 1469–1480. doi: 10.2307/2411199

Osmond, M. M., and Klausmeier, C. A. (2017). An evolutionary tipping point in a changing environment. *Evolution* 71, 2930–2941. doi: 10.1111/evo.13374

Ricciardi, A., Iacarella, J. C., Aldridge, D. C., Blackburn, T. M., Carlton, J. T., Catford, J. A., et al. (2021). Four priority areas to advance invasion science in the face of rapid environmental change. *Environ. Rev.* 29, 119–141. doi: 10.1139/er-2020-0088

Rolshausen, G., Phillip, D. A. T., Beckles, D. M., Akbari, A., Ghoshal, S., Hamilton, P. B., et al. (2015). Do stressful conditions make adaptation difficult? Guppies in the oil-polluted environments of southern Trinidad. *Evol. Appl.* 8, 854–870. doi: 10.1111/eva.12289

Somero, G. N. (2010). The physiology of climate change: How potentials for acclimatization and genetic adaptation will determine 'winners' and 'losers'. *J. Exp. Biol.* 213, 912–920. doi: 10.1242/jeb.037473

Sunday, J. M., Bates, A. E., and Dulvy, N. K. (2012). Thermal tolerance and the global redistribution of animals. *Nat. Clim. Change* 2, 686–690. doi: 10.1038/Nclimate1539

frontiers | Frontiers in Ecology and Evolution

TYPE Systematic Review
PUBLISHED 09 May 2023
DOI 10.3389/fevo.2023.1055336

OPEN ACCESS

EDITED BY
Mehdi Cherif,
INRA Centre Bordeaux-Aquitaine, France

REVIEWED BY
Massimo Migliorini,
University of Siena, Italy
César Marín,
Santo Tomás University, Chile
Elizabeth M. Bach,
The Nature Conservancy, United States

*CORRESPONDENCE
Zoë Lindo
✉ zlindo@uwo.ca

RECEIVED 27 September 2022
ACCEPTED 10 April 2023
PUBLISHED 09 May 2023

CITATION
Lindo Z, Bolger T and Caruso T (2023) Stochastic processes in the structure and functioning of soil biodiversity.
Front. Ecol. Evol. 11:1055336.
doi: 10.3389/fevo.2023.1055336

Stochastic processes in the structure and functioning of soil biodiversity

Zoë Lindo[1]*, Thomas Bolger[2,3] and Tancredi Caruso[2,3]

[1]Department of Biology, The University of Western Ontario, London, ON, Canada, [2]School of Biology and Environmental Science, University College Dublin, Dublin, Ireland, [3]Earth Institute, University College Dublin, Dublin, Ireland

Ecologists are increasingly recognizing the importance of stochastic processes in generating spatial and temporal variation in biological communities. This variation is very high in soil, which hosts not <¼ of all biodiversity on Earth and is central to how terrestrial ecosystems respond to perturbations. Measurement errors, demographic stochasticity (individual variability in traits such as birth and death rates), and environmental stochasticity (fluctuations in environmental properties) are the three main sources of stochasticity in ecology. Here, we synthesize how these three sources of stochasticity are quantified and incorporated in the study of soil biodiversity, highlighting current limits, possible solutions, and future research needs. We stress the relevance of all these factors to our future understanding of terrestrial ecosystems via plant-soil and soil-climate interactions and feedbacks. In soil, measurement errors are due to the small size, high abundance, and broad distributions of soil organisms, which limit sampling in space and especially over time. We argue that positive autocorrelation is a main characteristic of soil environmental properties, which may have important consequences on the response of soil biota to perturbations. At a local scale, large populations of soil organisms also imply a minor role of demographic stochasticity. Despite demographic stochasticity being a less significant source of variability than environmental stochasticity, we show that demographic stochasticity can be sizeable, but that within soil systems, stochasticity of environmental conditions must be accounted for. Explicit consideration of stochastic processes in soil biodiversity research is essential to our future understanding of the processes that control soil biodiversity. In classical ecology, stochasticity implies probabilistic predictions in terms of population growth, extinction, species coexistence, and community diversity. In soil, stochasticity implies very variable responses to climate change and the soil-climate feedback. Future studies will have to identify the major sources of environmental stochasticity with a particular focus on the interaction between multiple global change factors.

KEYWORDS

stochasticity, soil biodiversity, terrestrial ecology, global change, time serial data

1. Introduction

Individuals, populations, and ecological communities display very large variability over space and time. Since a fully deterministic description of all the factors that control this variability is not feasible, ecologists have developed a large number of models that explicitly incorporate stochastic processes in modeling this variability (May, 1973; Caswell, 2000; Lande et al., 2003; Vellend, 2010).

Shoemaker et al. (2020) have recently clarified many of the misconceptions and confusions on stochastic processes in ecology, highlighting the importance of an integrative framework to make the study of ecological communities more robust and predictive. In fact, a major misconception is that stochastic approaches imply uncertainty and unpredictability while, instead, they simply imply that predictions are probabilistic, and that there are different sources of variance that contribute to the outcome of an ecological process. Stochastic ecological processes can thus be quantified in terms of probability distributions and expectations (Lande et al., 2003). In other words, models that incorporate stochastic processes make "the unpredictable" predictable, if we accept that most predictions in ecology will be of a probabilistic nature. There is a misconception that a stochastic process implies total ignorance of a process, which is rarely the case. In most cases, there is information available to us that allows for predictions while calculating some degree of uncertainty around the mean. More generally, modeling a process using a stochastic approach does not mean that the process is intrinsically random and has no deterministic causes. Rather that the complexity of the factors that determine the trajectory of the measured variables is so high that a probability description of the possible trajectories is tractable while a deterministic one is not (Karlin and Taylor, 1975).

Soil is one of the most variable and diverse components in terrestrial ecosystem and hosts not <¼ of all biodiversity on earth (Bardgett and Van der Putten, 2014; FAO, 2020). The variability of soil biodiversity over space and time is enormous and observed from very small (a few mm) to global scales (e.g., Ettema and Wardle, 2002; Bardgett et al., 2005; Delgado-Baquerizo et al., 2018; Phillips et al., 2019; White et al., 2020; Caruso and Bardgett, 2021). Many studies have clarified the roles of the abiotic and biotic factors that control the distribution of soil organisms from global (Delgado-Baquerizo et al., 2018; Phillips et al., 2019; Van Den Hoogen et al., 2019) to intermediate and local scales (Lindo and Winchester, 2009; Caruso et al., 2019). But the abiotic and biotic factors that control soil organism distribution, and the ecosystem functions that these organisms mediate, vary over space and time, and stochastic processes offer the quantitative framework to link fluctuations in abiotic and biotic factors to variation in population and communities (Lande et al., 2003). This is particularly important for soil communities, that are central to ecosystem functioning, especially biogeochemical cycles (Bardgett and Wardle, 2010; Crowther et al., 2019), which are connected via plants and the atmosphere to global climate change dynamics (Bardgett et al., 2008), and are subjected to a complex interaction of multiple global change factors (e.g., warming, changes in soil moisture, nitrogen deposition) (Rillig et al., 2019; Bardgett and Caruso, 2020). Interactions with multiple factors imply important temporal and spatial fluctuations in populations, biomass, microbial and faunal traits, and biological rates, including energy fluxes. Given that a fully deterministic description of all these interactions is not feasible, we argue that stochastic approaches offer a solution to conceptualize and model this complexity. We thus offer a synthesis and perspective on how stochastic processes have been considered in past soil biodiversity research, highlighting some important aspects of the state-the-of-the-art, current limitations in terms of data availability, and solutions that will boost, in our view, a deeper understanding of the response of terrestrial ecosystems to environmental variation and perturbation regimes.

2. Sources of stochasticity in soil biodiversity

Over the last 15 years, the factors and processes that structure soil biodiversity have been studied intensively and over multiple spatial scales. For example there have been some general literature reviews and synthesis papers on different biodiversity theory and methods as applied to soil biota (e.g., Vályi et al., 2016; Thakur et al., 2020; White et al., 2020), large scale studies investigating the factors that control the distribution of soil organisms (e.g., Delgado-Baquerizo et al., 2018; Crowther et al., 2019; Phillips et al., 2019; Tedersoo et al., 2022), and studies that have tested the predictions of competing community assembly models (e.g., Lekberg et al., 2007, 2011; Lindo and Winchester, 2009; Dumbrell et al., 2010; Caruso et al., 2011, 2012). Much of this work was meta-analyzed by Guerra et al. (2020). In many of these studies, and also as recently summarized in Vályi et al. (2016), Thakur et al. (2020), and White et al. (2020), there is a relatively large proportion of the variance in the data that cannot be attributed to the factors analyzed. There is typically variance observed in the abundance of organisms, but also in relative species abundance and species composition, as well as in ecosystem functions (for example, total soil respiration). Much of this variance is typically spatial because most studies have focused on the spatial dimension, and time series of soil biota are rare. Caruso et al. (2020) recently reviewed the literature for soil animals and highlighted the rarity of time series for soil biota. For example, in the BioTIME database (Dornelas et al., 2018) the only time series for soil organisms are the two we recently submitted.

Depending on the specific context of the different research, various authors have offered multiple explanations on the sources underlying this "unexplained" variance, but in general there are three main sources in ecology (Figure 1): measurement errors, environmental, and demographic stochasticity (Shoemaker et al., 2020). The term "unexplained" is thus not really appropriate in our view, because the sources of variances are known, but what it is not known are their relative contributions.

2.1. Measurement errors

The process of measurement in science is best modeled using probability distributions, given that measurements are subjected to a myriad of sources of error that together affect the accuracy and precision of measurements (Taylor, 1997). In this sense, measurement errors can be measured and accounted for (e.g., through instrument calibration, detection limits), such that, in principle we should always be able to quantify them. In ecology, at a theoretical level, measurement errors are perhaps the least interesting source of stochastic variation, but in soil research this type of error represents an important source of variance for two reasons: firstly, soil biota are very small sized and patchily distributed from local to broad scales (Ettema and Wardle, 2002), meaning the sampling regime should be very intense at multiple

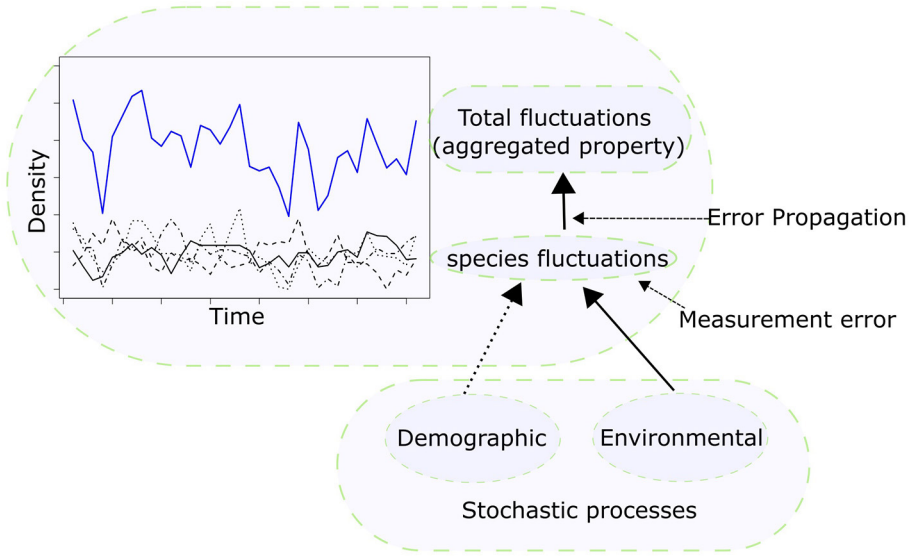

FIGURE 1
Stochastic processes affect population fluctuations (black lines of different types), and so species intraspecific and interspecific interaction and eventually fluctuations in any properties emerging from these interactions (for example, the simple total density as the sum of individual species density, blue solid line). The two key types of stochastic processes are demographic stochasticity and environmental stochasticity. A third source of variance is measurement errors, which propagates when variable measured with uncertainty (species fluctuation) are combined into an aggregated properties (for example, total sum of species densities).

scales in order to provide precise estimates of ecological variables such as population density and biomass; secondly, basically all taxonomic groups in soil are sampled destructively, meaning that repeated measurements on the "same object" are not possible, and that measurements at one particular spatial scale must be based on either a composite sample from multiple samples or technical replicates later pooled or averaged to represent the community at the chosen spatial scale (Caruso and Bardgett, 2021). While this is well-known in the practice of soil ecology, we propose that there are also other sources of measurement errors that are underestimated in soil biodiversity research, and that soil ecologists and ecologists in general, rarely apply the rules of error propagation in their estimates of measurement errors. In ecology this topic has been considered explicitly only in a few works mostly related to the estimate of the biomass of plants (Deutschman et al., 1999; Lo, 2005; Molto et al., 2013).

We propose that there are two major areas where error propagation can become an important approach to estimating the contribution of measurement error to the total variance observed in soil ecological systems. One is the estimate of population biomass, which is usually based on compounding information on body size with information on population density (Turnbull et al., 2014). The other is the related estimate of energy fluxes (e.g., Potapov et al., 2016) that is based on the allometric scaling of metabolism with body size and temperature. This latter case is particularly important, given that an energetic description of soil food webs potentially allows the estimation of matter fluxes and so, for example, rates of CO_2 emissions (Moore and de Ruiter, 2012). In energetic food webs estimated through allometric metabolic scaling (Barnes et al., 2018), the total metabolic loss of a trophic species is the sum of the losses of each individual within that species population. The metabolic loss I of one individual of biomass M is typically estimated with an equation of the type: $I \propto M^b$. There is a measurement error σ_M in M, which is often due to estimating individual biomass M by body size, with uncertainty both in length measurements and the parameters that link body size to body dry or wet weight. But, even more fundamentally, there is also uncertainty in the scaling exponent b. The exact value of the scaling exponent, and the implication of this value, have been a subject to heated discussion in the more general debate on the metabolic scaling theory of ecology (Enquist et al., 2003; Brown et al., 2004; Makarieva et al., 2006, 2008; Glazier, 2010). Regardless of the different theories and predictions on the exact value of the scaling exponent, experimentally there is a well-known systematic variation in the scaling exponent, which varies between taxa and phylogenetic lineages (Ehnes et al., 2011). For example, Ehnes et al. (2011) estimated (mean ± SE) b as 0.68 (± 0.4) for oribatid mites and 0.69 (± 0.09) for mesostigmatid mites. Our point is that the experimental error σ_b around b as well as the error σ_M around M are both needed to assess the measurement error of I, which is a combination of the two errors.

This can be demonstrated through an equation of the type $I \propto M^b$ to estimate I, given uncertainty σ_b and σ_M in b and M, respectively. From error propagation theory (Taylor, 1997), the uncertainty in I would then be $\sigma_I \approx I^2 \left[\left(\frac{M}{b}\,\sigma_M\right)^2 + \left(\ln(M)\,\sigma_b\right)^2\right]$ under the assumption that there is no correlation in the error structure of M and b. If there was some non-negligible correlation between the two measurements, one more term should be added to the error of I, with the general effect of further increasing measurement uncertainty. Even more, usually the general equation used to estimate I is $I = i0\, M^b\, exp(-\frac{E}{kT})$ where k is the Boltzman constant, T is temperature, E activation

energy, and *i0* is a taxon-specific constant. The latter two parameters (*E* and *i0*) are estimated experimentally with some errors, which should also be incorporated in the estimate of σ_I. Given that the I_j of each individual j is estimated with an error σ_I, and that the total metabolism of a trophic species is the sum of all individual metabolisms, that is $I_{tot} = \sum I_j$, the error of I_{tot} will be obtained by propagating the errors from the sum of all I_j. That would simply be $\sigma_{tot} = \sum \sigma_I$ assuming no correlation between the measurements of the metabolic loss of each individual (a correlation would further increase the combined error for the total).

These estimates of individual biomass based on allometric scaling become compound errors with calculations into population level biomass, which are then used in calculations of flux in food web models. The estimate of the energy fluxes between two trophic species finally requires the knowledge of other coefficients, which express the efficiency of energetic transfers between trophic levels. Arguably, these coefficients are known with some errors and the errors should thus propagate to the estimate of the energy flux together with the error of the metabolic loss. All these errors are rarely, if ever, taken into account, and are (implicitly) assumed to be negligible (Barnes et al., 2014, 2018; Potapov et al., 2019, 2021), or are not taken into account (Gauzens et al., 2019). Similar issues apply to conversions from abundance to biomass data, assignment of species into trophic groups (see Buchkowski and Lindo, 2021), extrapolation of density data across scales, and in general any conversion based on measurements and coefficients that, being based on experimental measurements, are necessarily known with a degree of uncertainty intrinsic to the measurement process. We thus recommend that future soil biodiversity studies explicitly consider the issue of error propagation in the quantification of error measurements, as this is important to estimate lower and upper bounds for key ecosystem level quantities such as respiration and fluxes of C and N.

2.2. Demographic stochasticity

Individuals within a species differ in vital rates, especially survival and fecundity, that together determine individual fitness (Caswell, 2000; Lande et al., 2003). In very small populations (typically < 100), this variability in vital rates is the source of demographic stochasticity, and can be measured by following cohorts of individuals, their survival and reproduction output (Lande et al., 2003). This is relatively straightforward, while time consuming, for vertebrates such as birds (Engen and Sæther, 1998; Sæther et al., 2000; Engen et al., 2001, 2003) but much more challenging for soil organisms, apart from laboratory studies on soil animals (Siepel, 1994; Søvik and Leinaas, 2003; Stamou, 2012). Despite the fact that direct measurements of demographic stochasticity are difficult to obtain for soil biota, there is theoretical ground to expect demographic stochasticity plays a minor role in structuring soil biodiversity. For example, following Lande et al. (2003), in simple, unstructured density independent stochastic models, the total variance σ^2_λ of the finite rate of population growth λ equals $\sigma^2_e + \frac{\sigma^2_d}{N}$, where σ^2_e is environmental variance (defined in the next section), σ^2_d is demographic variance, and N is total population size. Density independence is appropriate because demographic stochasticity applies to small populations, which are arguably far away from their carrying capacity. In large populations, population size $N \gg \frac{\sigma^2_d}{\sigma^2_e}$ and demographic stochasticity plays a much smaller role than environmental stochasticity. A critical population size $N_c = 10\frac{\sigma^2_d}{\sigma^2_e}$ can be defined, above which demographic stochasticity can be ignored. In birds, this critical population size can range from a few tens to various hundreds of individuals (Lande et al., 2003). Clearly, the issue is that we do not know the magnitude of environmental and demographic variance in soil organisms. However, it is textbook knowledge that the density per square meter of most soil organisms is typically well above 100 or 1,000 units for animals and up to 1 billion bacterial cells and 200 m of fungal hyphae per gram of soil microbes (Coleman et al., 2004).

It is thus unlikely that demographic stochasticity plays any role at all for most species at scales larger than 1 m^2 (see also Section 3). At scales smaller than 1 m^2, however, various soil animal species, such as Collembola and mites, can have population sizes of a few tens of individuals, making demographic variance a likely source of stochasticity. If we assume a small population size at this scale, and thus a density independent model following Lande (1998), and the formulation in Lande et al. (2003), we can also formulate an unstable stochastic equilibrium for population size that establishes a critical threshold below which the probability of extinction approaches unity. This critical equilibrium value can be calculated as $N_* = \frac{\frac{\sigma^2_d}{4}}{\lambda - 1 - \frac{\sigma^2_e}{2}}$. For example, if $\sigma^2_d = 1$ and $\sigma^2_e = 0.04$, and the average $\lambda = 1.03$, the critical population size would be 25 individuals. This is a likely scenario at some spatial scales (1–100 m) for some groups of soil fauna given existing estimates of population size and finite rates of increases (e.g., Caruso et al., 2020). However, at this scale interactions between individuals in soil become very likely, as also shown by highly aggregated distribution of soil fauna and microbes at small scales (Ettema and Wardle, 2002). The implication is that other biological mechanisms will potentially contribute to population fluctuations, especially Allee effects, which makes again pure demographic stochasticity unlikely to be a large and only source of fluctuations in soil biota.

These considerations are very relevant to the large body of literature that has investigated the relative roles of stochastic and deterministic determinants of soil biodiversity. A recent synthesis has been offered by Thakur et al. (2020), who found about 100 papers explicitly testing community ecology assembly theory in soil communities, and concluded that theory such as the neutral theory, which has demographic stochasticity as the core process, are generally not well-supported suggesting niche-based explanations underly community composition, and the high levels of unexplained variance are likely due to other stochastic processes described here (see next section). This conclusion is consistent with the general consideration that for most soil species, large population sizes over relatively broad scale (>100 m) imply a small role of demographic stochasticity. It is, however, important to remark that in many of the papers reviewed in Thakur et al. (2020) there is, in our opinion, very often confusion between the assumption of neutrality in certain models and the role of stochastic processes. As made clear by Adler (2007), demographic

stochasticity is just a demographic process that may be at play both in neutral and niche community dynamics (see also the simple niche stochastic model example by Tilman, 2004). This means that the rejection of a neutral model does not imply that community fluctuations are not affected by demographic stochasticity, but only that the assumption of neutrality is not sufficient to explain the tested community patterns (Vellend, 2010).

2.3. Environmental stochasticity

Besides individual-level variability in vital rates such as birth and survival rate, the average expression of rates in the population also depends on the environment, which fluctuates. Sometimes conditions are favorable, sometimes they are not. After removing structural, periodic fluctuations due to, for example, the day and night cycle, or the seasonal cycle, or trends due, for example, to global warming, many environmental fluctuations are best modeled as probability distributions (Figures 2, 3), that is, stochastic fluctuations. The implication is that the vital rates, too, will fluctuate stochastically. A simple density independent model for this type of stochastic fluctuations is $N_t = N_0 \prod_{i=1}^{t} \lambda_i$ where the population size N grows geometrically from time 0 to time t according to the finite rate of increase λ, but at each time step the value of λ changes, because the environment changes (Botsford et al., 2019). This implies fluctuations in the rate of growth and so population size over time. It will also imply fluctuations in interspecific interactions, and all the ecosystem processes that depends on these interactions (Figure 1).

The first population level implication of environmental stochasticity is that the long-term growth rate of the population will be smaller than the expected average growth rate, and the higher the environmental variance the smaller the rate will be (Caswell, 2000; Lande et al., 2003). This also applies to populations structured by age and stages (Caswell, 2000; Tuljapurkar, 2013), which is the case with many soil animals (Walter and Proctor, 1999). However, while this is generally true for so called "white noise", which is fluctuations without temporal autocorrelation (Figure 3), many time series of environmental variables display autocorrelation in their random component (Figures 3, 4). This is the so called "color" of noise, which has been shown to have different types and sometimes contrasting effects on the long-term rate of population growth (Ripa and Lundberg, 1996; Ruokolainen et al., 2009)—we argue this is particularly important in soil properties such as soil moisture. For example, in the time series we show in Figure 4, soil moisture and temperature, but especially soil moisture, clearly show fluctuations due to the day-night cycle and pulses of rain. After removing these fluctuations, the remaining random noise is positively autocorrelated, with highest variance displayed over short period of times. This is relatively easy to interpret: if soil becomes dry, it will stay so for a certain time until it rewets. As well as the rewetted soil may be subjected to another bout of drought but with loss of moisture that will take a certain time, meaning that the closer in time any two soil moisture measurements are, the more similar the measurements are likely to be (i.e., red noise). The implication is that both wet and dry conditions may persist longer than under purely white noise, and certain population models imply that red noise may reduce the risk of extinction (Ripa and Lundberg, 1996).

Regardless of the particular population model, however, an important tool to describe the structure of environmental stochasticity in time series analysis is the Fourier transformation (Bloomfield, 2004; Bush et al., 2017). The Fourier transform of a time series moves data from the time domain (x-axis) to the frequency domain (new x-axis); in the original time series, the y-axis is simply the measured variable (Figure 3), and in the Fourier transform the y-axis becomes variance (Figure 3). In practice, the Fourier transform allows detection of the frequencies or, conversely, time period mostly expressed in the data (i.e., that shows more variance). If all the frequencies are equally expressed, the pattern (or spectrum) of the Fourier transform is flat (white noise), and there is no relationship between frequency and variance. If low frequencies show more variance than high frequency there will be a negative correlation between frequency and variance (i.e., there will be positive autocorrelation in the time domain referred to as red noise). Fourier analysis of soil time series can thus quantify the autocorrelation structure of environmental stochasticity in soil, thereby elucidating the effect of this stochasticity on soil biota population and communities. This analysis is straightforward for abiotic variables especially for data collected from data loggers that allow the collection of time series of desired length and resolution (see example in Figure 4).

Unfortunately, the same is not possible for soil biota (Caruso and Bardgett, 2021). Yet, future modeling studies (see example in Figure 2) still benefit from incorporating forms of environmental stochasticity, that reflect the random structure observed in soil abiotic environments. For example, energetic food webs incorporate temperature as a key parameter via the fundamental metabolic scaling equation $I = i0\, M^b\, exp(-\frac{E}{kT})$. There are now soil food web models parameterized on field data (Potapov et al., 2021; Pettit et al., 2023) using the energetic approach (Moore and de Ruiter, 2012). Thus, *in silico* soil food web models (i.e., computer model estimations) can explore the effect of environmental stochasticity on energy fluxes using information on the stochastic structure that can be revealed by a Fourier analysis of soil temperature time series (Figure 4). These models could also simulate the impact of perturbation regimes, that changes the temporal structure of fluctuations in environmental variables.

3. Community level estimate of stochasticity

One major limitation in the study of stochastic fluctuations in soil biodiversity is the lack of time series (Bardgett and Caruso, 2020; Caruso and Bardgett, 2021). However, many ecological processes that happen over time potentially leave their signature in the spatial distribution of organisms, and there are some models that may allow estimate of environmental and stochastic variance from combined spatial and temporal time series (Lande et al., 2003; Botsford et al., 2019). We offer an example here, based on a publicly available time series of soil oribatid mites (https://doi.org/10.5061/dryad.tmpg4f4vt), which was the subject of previous work of ours (Caruso et al., 2020). The dataset consists of several 9-year time series replicated over multiple sampling locations. We

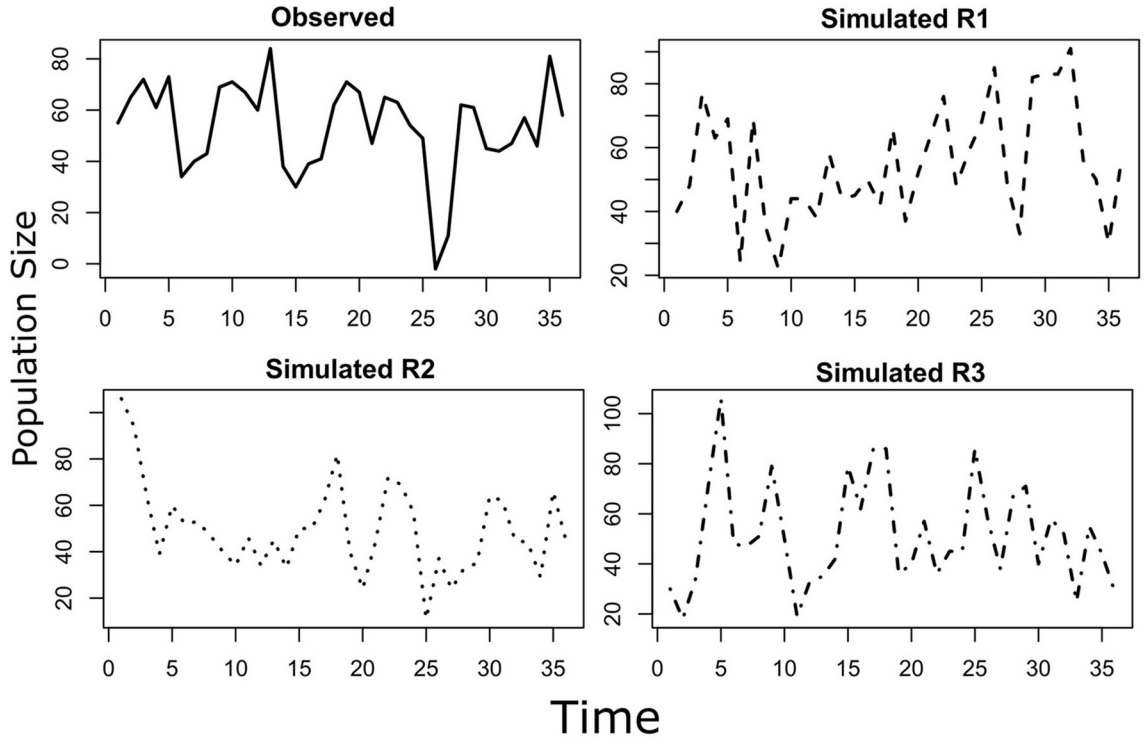

FIGURE 2
The "observed" population stochastically fluctuate around an equilibrium. The fluctuation follows a normal distribution with autocorrelation parameter "phi". The parameter phi and the mean and variance of the observed population can be estimated from a sample of the population. The estimate of the mean, variance and autocorrelation parameter can be used to draw a desired number of "simulated" populations. In this example, three simulated populations (Simulated R1, R2, and R3) are shown together with the originally observed population. The three simulated population and the observed one represents four realizations of the same stochastic process, with the probability distribution of the process been estimated from the observed population. This time series displays positive autocorrelation, that is "red" noise.

fitted the model by Engen et al. (2002) to this dataset, and we provide an R script (see Data Availability Statement) that displays all the key step of the model fitting procedure. The key output of the model is a partitioning of the total community variance in terms of environmental variance, and a term that is the sum of demographic variation and overdispersion (which is relative to the underlying Poisson distribution assumed by the model). The environmental variance is further decomposed into two sources: general environmental variance, which is a forcing component that applies to all species, and species-specific environmental variance. The model takes the relative abundance of species, location and sampling time as input. It is fitted in stages: first, a bivariate Poisson distribution is fitted to the combined species relative abundance of all pairs of possible samples. Second, the variance and correlation parameters of each fit are combined with the spatial and temporal distance between each pair of samples. Third, an estimate is obtained for the parameters that control the dependency of the correlation parameter on the spatial and temporal distance between any two samples.

These parameters contain the main output, that is the estimate of environmental and demographic variance. Note however, as outlined in the previous section, because measurement errors are generally not well-incorporated into models and analyses, estimates of environmental and demographic stochasticity are likely overestimated. This model is based on the following main stochastic model, where the logarithm X of the abundance of any species i in the community has the following forms: $\frac{dX_i}{dt} = r_i - mX_i - \mathbf{A}(\mathbf{X}) + \frac{\sigma_d}{\sqrt{N_i}}D_i + \sigma_e S_i + \sigma_E E$. Where the subscript i indicates a certain species, D, S, and E are Brownian motions and, respectively, represents demographic (D), species specific (S) environmental, and general environmental (E) effects. The sigma coefficient of each of this term (D, S, and E) is the variance we aim to estimate in order to quantify the relative importance of environmental (e+E) vs. demographic (d) stochasticity. The model is not neutral with respect to intrinsic growth rate r and the species level stochastic effect D and E, and it includes interactions between species $\mathbf{A}(\mathbf{X})$ as well as density dependence controlled by parameter m. With these simple assumptions, a crude but field-based estimate of environmental and demographic stochasticity is possible from the type of community data sets available to soil ecologists. Our calculations (see R script, Sup. Info.) show that for an old conifer forest (>100 yrs), the total variance observed in the temporal and spatial fluctuation of oribatid species could be partitioned as 85% environmental variance ($\sigma_e + \sigma_E$) and 15% demographic variance + overdispersion (that is $\sigma_d + o$). However, the method does not allow separation of demographic variance from overdispersion (the deviation in the relationship between mean and variance of the underlying Poisson distribution of the model), which is likely due to spatial aggregation observed at small scales (Engen et al., 2002). Regardless, the results empirically confirm the

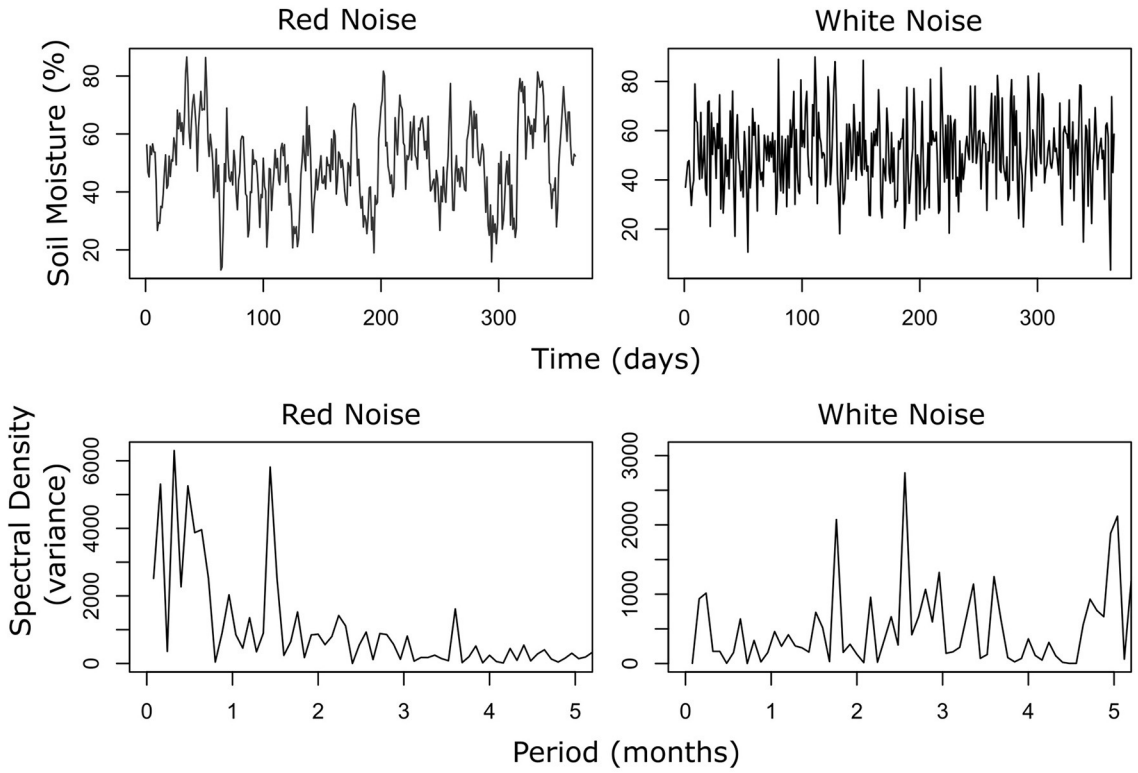

FIGURE 3
A Fourier transformation decomposes the overall pattern of the time series to reveal the underlying frequencies present in the original function. As such, the Fourier transformation can be used to provide information on seemingly stochastic processes. Environmental variables typically display "red" noise or positive autocorrelation over time. In this figure, a time series of soil moisture with red and white noise (no autocorrelation) are simulated. A Fourier transformation of the two timeseries (top panels, red and white noise) demonstrates that in the spectrum of the red noise most of the variance is displayed over short time scales, with a negative correlation between variance and periods. The spectrum of the white noise is flat, with all periods displaying similar variance.

theoretical expectation for the main source of stochastic variation as environmental, but also non-neutral. Following, the 85% of total environmental variance can be partitioned into interspecific differences in the response to the general environmental variance (82% of the 85%, or 70% of the total) and local, species-specific response (18% of the 85%, or 15% of the total). The variance values were ${\sigma_e}^2 = 0.36$; ${\sigma_E}^2 = 1.37$; ${\sigma_{d+o}}^2 = 0.29$. Assuming no overdispersion we would have ${\sigma_e}^2 = 0.36$ and ${\sigma_d}^2 = 0.29$, which we use to estimate an average critical population density of 12 individuals (using $N_c = 10\frac{\sigma_d^2}{\sigma_e^2}$).

Most oribatid mite species in forest soils have densities above 50 individual m^{-2}. Using the formula for the critical equilibrium value N_c with a long-term stochastic rate $\lambda = 1.6$, ${\sigma_e}^2 = 0.36$ and ${\sigma_d}^2 = 0.29$ (see Caruso et al., 2020), N_c is < 1, suggesting the risk of extinction is negligible. Although crude, the example shows that relatively short time series (9 years) with some spatial replication and community level data allows an estimate of environmental and demographic stochasticity in soil communities. The time scale of the time series might be tuned to the biological groups under consideration. For example, for bacteria a time series could occur over a single season. In the northern hemisphere at temperate latitudes, bacterial communities could be sequenced molecularly at 10 intervals from May to August (the growing season) in multiple locations with relatively affordability.

4. Emerging concepts and way forward

Stochasticity can be fully embraced in the study of the factors that control the structure and functions of soil biodiversity and aboveground-belowground linkages. Through modeling stochastic processes, we can better predict and identify populations, communities or ecosystems that are vulnerable to stochasticity in terms of fluctuations that can make soil biological activities uncertain and unstable (Bardgett and Caruso, 2020). This is important because instability in soil biological activities cause uncertainty and instability in fluxes that link aboveground and belowground components, and functions such as nutrient cycling. To obtain this goal, we need to improve data in terms of a quantification of measurement errors based on the theory of error propagation, and produce more time series of different soil biota across multiple locations. Experimental time series are the main tool to elucidate potential divergent (i.e., alternative stable state) soil-climate feedbacks through examining the resistance and resilience of soil biodiversity and function (Bardgett and Caruso, 2020). However, experimental tests and empirical data of this are lacking. In terms of new data and models, we need a quantification of the relative roles of different sources of stochasticity and explicit incorporation of stochastic autocorrelation structure into

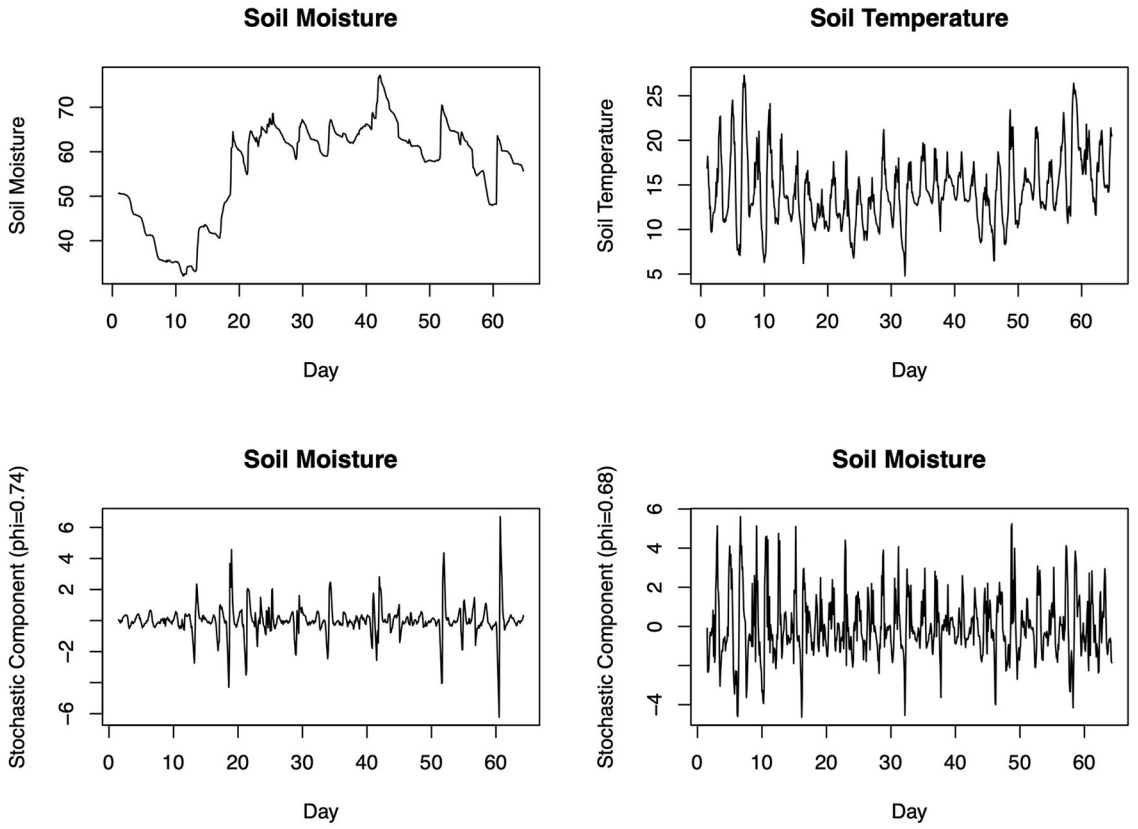

FIGURE 4
Two real world time series of soil moisture and temperature. In the time domain (top panels) both variables, but especially soil moisture, displays clear positive autocorrelation (over short time scales values tend to be similar). After detrending linear and periodic trends and isolating the stochastic component, the calculation of the autocorrelation coefficient phi confirms the presence of positive autocorrelation (i.e., red noise). With these parameters, one can now draw a desired number of stochastic trajectories, which can inform the modeling of population, community, and ecosystem level (e.g., energy fluxes and soil respiration) processes.

soil models (at population, community, and ecosystem levels). Improved experimental designs, theory and practical methods are already available to quantify and propagate measurement errors (for example see Caruso and Rillig, 2022). It is just a matter of applying them more extensively and critically, acknowledging errors at the various levels at which they occur (e.g., in energetic soil food webs). Time series remain challenging to obtain but there is an increasing number of contributions toward a temporal description of soil biota (e.g., Barreto et al., 2021), and especially for microbial groups the collection of time series within a single year or season is both feasible and informative of short terms dynamics.

We demonstrate that even a modest time series replicated over space allows a crude but reliable quantification of demographic and environmental stochasticity in soil communities and the quantification of the joint spatial and temporal autocorrelation observed both in biota and the environment, while a Fourier analysis of the stochastic components of time series can reveal the type of autocorrelation that characterizes stochastic fluctuations both in biota and the environment. We believe this approach will be very useful in future manipulative experiments, such as global change experiments that manipulate the intensity, frequency, and type of multiple perturbations (Rillig et al., 2019), which generate complex fluctuations.

Data availability statement

Publicly available datasets were analyzed in this study. This data can be found here: https://doi.org/10.6084/m9.figshare.22654375.v1.

Author contributions

TC, TB, and ZL all developed the ideas in this manuscript. TC coded and ran models and wrote the first version of the manuscript with ZL. All authors contributed to drafts and the final version of the manuscript with approval for publication.

Funding

Funding was provided by European Commission to TC (Structure and Ecological Niche in the Soil Environment; EC FP7-631399-SENSE) and by the Natural Sciences and Engineering Research Council of Canada (NSERC) Discovery Grants program to ZL (#418241-2012 and #05901-2019).

Conflict of interest

The authors declare that the research was conducted in the absence of any commercial or financial relationships that could be construed as a potential conflict of interest.

Publisher's note

All claims expressed in this article are solely those of the authors and do not necessarily represent those of their affiliated organizations, or those of the publisher, the editors and the reviewers. Any product that may be evaluated in this article, or claim that may be made by its manufacturer, is not guaranteed or endorsed by the publisher.

References

Adler, P. B. (2007). A niche for neutrality. *Ecol. Lett.* 10, 95–104. doi: 10.1111/j.1461-0248.2006.00996.x

Bardgett, R. D., Bowman, W. D., Kaufmann, R., and Schmidt, S. K. (2005). A temporal approach to linking aboveground and belowground ecology. *Trends Ecol. Evol.* 20, 634–641. doi: 10.1016/j.tree.2005.08.005

Bardgett, R. D., and Caruso, T. (2020). Soil microbial community responses to climate extremes: resistance, resilience and transitions to alternative states. *Philos. Trans. R. Soc. B Biol. Sci.* 375, 20190112. doi: 10.1098/rstb.2019.0112

Bardgett, R. D., Freeman, C., and Ostle, N. J. (2008). Microbial contributions to climate change through carbon cycle feedbacks. *ISME J.* 2, 805–814. doi: 10.1038/ismej.2008.58

Bardgett, R. D., and Van der Putten, W. H. (2014). Belowground biodiversity and ecosystem functioning. *Nature* 515, 505–511. doi: 10.1038/nature13855

Bardgett, R. D., and Wardle, D. A. (2010). *Aboveground-Belowground Linkages: Biotic Interactions, Ecosystem Processes, and Global Change*. San Diego, CA: Oxford University Press.

Barnes, A. D., Jochum, M., Lefcheck, J. S., Eisenhauer, N., Scherber, C., O'Connor, M. I., et al. (2018). Energy flux: the link between multitrophic biodiversity and ecosystem functioning. *Trends Ecol. Evol.* 33, 186–197. doi: 10.1016/j.tree.2017.12.007

Barnes, A. D., Jochum, M., Mumme, S., Haneda, N. F., Farajallah, A., Widarto, T. H., et al. (2014). Consequences of tropical land use for multitrophic biodiversity and ecosystem functioning. *Nat. Commun.* 5, 1–7. doi: 10.1038/ncomms6351

Barreto, C., Branfireun, B. A., McLaughlin, J., and Lindo, Z. (2021). Responses of oribatid mites to warming in boreal peatlands depend on fen type. *Pedobiol. J. Soil Ecol.* 89, 150772. doi: 10.1016/j.pedobi.2021.150772

Bloomfield, P. (2004). *Fourier Analysis of Time Series: An Introduction*. New York, NY: John Wiley and Sons.

Botsford, L. W., White, J. W., and Hastings, A. (2019). *Population Dynamics for Conservation*. Oxford: Oxford University Press. doi: 10.1093/oso/9780198758365.001.0001

Brown, J. H., Gillooly, J. F., Allen, A. P., Savage, V. M., and West, G. B. (2004). Toward a metabolic theory of ecology. *Ecology* 85, 1771–1789. doi: 10.1890/03-9000

Buchkowski, R., and Lindo, Z. (2021). Stoichiometric and structural uncertainty in soil food web models. *Func. Ecol.* 35, 288–300. doi: 10.1111/1365-2435.13706

Bush, E. R., Abernethy, K. A., Jeffery, K., Tutin, C., White, L., Dimoto, E., et al. (2017). Fourier analysis to detect phenological cycles using long-term tropical field data and simulations. *Methods Ecol. Evol.* 8, 530–540. doi: 10.1111/2041-210X.12704

Caruso, T., and Bardgett, R. D. (2021). Variance, locality and structure: three experimental challenges in the study of the response of soil microbial communities to multiple perturbations. *Pedobiologia* 87–88, 150741. doi: 10.1016/j.pedobi.2021.150741

Caruso, T., Hempel, S., Powell, J. R., Barto, K., and Rillig, M. C. (2012). Compositional divergence and convergence in arbuscular mycorrhizal fungal communities. *Ecology* 93, 1115–1124. doi: 10.1890/11-1030.1

Caruso, T., Melecis, V., Kagainis, U., and Bolger, T. (2020). Population asynchrony alone does not explain stability in species-rich soil animal assemblages: the stabilizing role of forest age on oribatid mite communities. *J. Anim. Ecol.* 89, 1520–1531. doi: 10.1111/1365-2656.13203

Caruso, T., and Rillig, M. C. (2022). A general stochastic model shows that plant-soil feedbacks can buffer plant species from extinction risks in unpredictable environments. *Plant Soil*. doi: 10.1007/s11104-022-05698-6

Caruso, T., Schaefer, I., Monson, F., and Keith, A. M. (2019). Oribatid mites show how climate and latitudinal gradients in organic matter can drive large-scale biodiversity patterns of soil communities. *J. Biogeogr.* 46, 611–620. doi: 10.1111/jbi.13501

Caruso, T., Taormina, M., and Migliorini, M. (2011). Relative role of deterministic and stochastic determinants of soil animal community: a spatially explicit analysis of oribatid mites. *J. Anim. Ecol.* 81, 214–221. doi: 10.1111/j.1365-2656.2011.01886.x

Caswell, H. (2000). *Matrix Population Models*, Vol. 1. Sunderland, MA: Sinauer.

Coleman, D. C., Crossley, D. A., and Hendrix, P. F. (2004). *Fundamentals of Soil Ecology*. San Diego, CA: Elsevier Academic Press.

Crowther, T. W., Van den Hoogen, J., Wan, J., Mayes, M. A., Keiser, A., Mo, L., et al. (2019). The global soil community and its influence on biogeochemistry. *Science* 365, eaav0550. doi: 10.1126/science.aav0550

Delgado-Baquerizo, M., Oliverio, A. M., Brewer, T. E., Benavent-González, A., Eldridge, D. J., Bardgett, R. D., et al. (2018). A global atlas of the dominant bacteria found in soil. *Science* 359, 320–325. doi: 10.1126/science.aap9516

Deutschman, D. H., Levin, S. A., and Pacala, S. W. (1999). Error propagation in a forest succession model: the role of fine-scale heterogeneity in light. *Ecology* 80, 1927–1943. doi: 10.2307/176669

Dornelas, M., Antao, L. H., Moyes, F., Bates, A. E., Magurran, A. E., Adam, D., et al. (2018). BioTIME: a database of biodiversity time series for the Anthropocene. *Glob. Ecol. Biogeogr.* 27, 760–786. doi: 10.1111/geb.12729

Dumbrell, A. J., Nelson, M., Helgason, T., Dytham, C., and Fitter, A. H. (2010). Relative roles of niche and neutral processes in structuring a soil microbial community. *ISME J.* 4, 337–345. doi: 10.1038/ismej.2009.122

Ehnes, R. B., Rall, B. C., and Brose, U. (2011). Phylogenetic grouping, curvature and metabolic scaling in terrestrial invertebrates. *Ecol. Lett.* 14, 993–1000. doi: 10.1111/j.1461-0248.2011.01660.x

Engen, S., Lande, R., and Sæther, B.-E. (2003). Demographic stochasticity and Allee effects in populations with two sexes. *Ecology* 84, 2378–2386. doi: 10.1890/02-0123

Engen, S., Lande, R., Walla, T., and DeVries, P. J. (2002). Analyzing spatial structure of communities using the two-dimensional Poisson lognormal species abundance model. *Am. Nat.* 160, 60–73. doi: 10.1086/340612

Engen, S., Sæther, B., and Møller, A. P. (2001). Stochastic population dynamics and time to extinction of a declining population of barn swallows. *J. Anim. Ecol.* 70, 789–797. doi: 10.1046/j.0021-8790.2001.00543.x

Engen, S., and Sæther, B.-E. (1998). Stochastic population models: some concepts, definitions and results. *Oikos* 83, 345–352. doi: 10.2307/3546848

Enquist, B. J., Economo, E. P., Huxman, T. E., Allen, A. P., Ignace, D. D., and Gillooly, J. F. (2003). Scaling metabolism from organisms to ecosystems. *Nature* 423, 639–642. doi: 10.1038/nature01671

Ettema, C. H., and Wardle, D. A. (2002). Spatial soil ecology. *Trends Ecol. Evol.* 17, 177–183. doi: 10.1016/S0169-5347(02)02496-5

FAO, ITPS, GSBI, SCBD, and EC (2020). *State of Knowledge of Soil Biodiversity - Status, Challenges and Potentialities: Report 2020*. FAO.

Gauzens, B., Barnes, A., Giling, D. P., Hines, J., Jochum, M., Lefcheck, J. S., et al. (2019). fluxweb: an R package to easily estimate energy fluxes in food webs. *Methods Ecol. Evol.* 10, 270–279. doi: 10.1111/2041-210X.13109

Glazier, D. S. (2010). A unifying explanation for diverse metabolic scaling in animals and plants. *Biol. Rev.* 85, 111–138. doi: 10.1111/j.1469-185X.2009.00095.x

Guerra, C. A., Heintz-Buschart, A., Sikorski, J., et al. (2020). Blind spots in global soil biodiversity and ecosystem function research. *Nat. Commun.* 11, 3870. doi: 10.1038/s41467-020-17688-2

Karlin, S., and Taylor, H. M. (1975). *A First Course in Stochastic Processes*. San Diego, CA: Academic Press.

Lande, R. (1998). Demographic stochasticity and Allee effect on a scale with isotropic noise. *Oikos* 83, 353–358. doi: 10.2307/3546849

Lande, R., Engen, S., and Saether, B.-E. (2003). *Stochastic Population Dynamics in Ecology and Conservation*. Oxford: Oxford University Press. doi: 10.1093/acprof:oso/9780198525257.001.0001

Lekberg, Y., Koide, R. T., Rohr, J. R., Aldrich-Wolfe, L., and Morton, J. B. (2007). Role of niche restrictions and dispersal in the composition of arbuscular mycorrhizal fungal communities. *J. Ecol.* 95, 95–105. doi: 10.1111/j.1365-2745.2006.01193.x

Lekberg, Y., Schnoor, T., Kjøller, R., Gibbons, S. M., Hansen, L. H., Al-Soud, W. A., et al. (2011). 454-sequencing reveals stochastic local reassembly and high disturbance tolerance within arbuscular mycorrhizal fungal communities. *J. Ecol.* 100, 151–160. doi: 10.1111/j.1365-2745.2011.01894.x

Lindo, Z., and Winchester, N. (2009). Spatial and environmental factors contributing to patterns in arboreal and terrestrial oribatid mite diversity across spatial scales. *Oecologia* 160, 817–825. doi: 10.1007/s00442-009-1348-3

Lo, E. (2005). Gaussian error propagation applied to ecological data: post-ice-storm-downed woody biomass. *Ecol. Monogr.* 75, 451–466. doi: 10.1890/05-0030

Makarieva, A., Gorshkov, V., Li, B., and Chown, S. (2006). Size-and temperature-independence of minimum life-supporting metabolic rates. *Func. Ecol.* 20, 83–96. doi: 10.1111/j.1365-2435.2006.01070.x

Makarieva, A. M., Gorshkov, V. G., Li, B.-L., Chown, S. L., Reich, P. B., and Gavrilov, V. M. (2008). Mean mass-specific metabolic rates are strikingly similar across life's major domains: evidence for life's metabolic optimum. *Proc. Natl. Acad. Sci. U.S.A.* 105, 16994–16999. doi: 10.1073/pnas.0802148105

May, R. M. (1973). *Stability and Complexity in Model Ecosystems.* Princeton, NJ: Princeton University Press. doi: 10.2307/1935352

Molto, Q., Rossi, V., and Blanc, L. (2013). Error propagation in biomass estimation in tropical forests. *Methods Ecol. Evol.* 4, 175–183. doi: 10.1111/j.2041-210x.2012.00266.x

Moore, J. C., and de Ruiter, P. C. (2012). *Energetic Food Webs: An Analysis of Real and Model Ecosystems*. Oxford: Oxford University Press. doi: 10.1093/acprof:oso/9780198566182.001.0001

Pettit, T., Faulkner, K. J., Buchkowski, R. W., Kamath, D., and Lindo, Z. (2023). Changes in peatland soil fauna biomass alter food web structure and function under warming and hydrological changes. *Eur. J. Soil Bio. Spec. Issue Soil Food Webs*.

Phillips, H. R., Guerra, C. A., Bartz, M. L., Briones, M. J., Brown, G., Crowther, T. W., et al. (2019). Global distribution of earthworm diversity. *Science* 366, 480–485. doi: 10.1126/science.aax4851

Potapov, A. A., Semenina, E. E., Korotkevich, A. Y., Kuznetsova, N. A., and Tiunov, A. V. (2016). Connecting taxonomy and ecology: trophic niches of collembolans as related to taxonomic identity and life forms. *Soil Biol. Biochem.* 101, 20–31. doi: 10.1016/j.soilbio.2016.07.002

Potapov, A. M., Klarner, B., Sandmann, D., Widyastuti, R., and Scheu, S. (2019). Linking size spectrum, energy flux and trophic multifunctionality in soil food webs of tropical land-use systems. *J. Anim. Ecol.* 88, 1845–1859. doi: 10.1111/1365-2656.13027

Potapov, A. M., Rozanova, O. L., Semenina, E. E., Leonov, V. D., Belyakova, O. I., Bogatyreva, V., et al. (2021). Size compartmentalization of energy channeling in terrestrial belowground food webs. *Ecology* 102, e03421. doi: 10.1002/ecy.3421

Rillig, M. C., Ryo, M., Lehmann, A., Aguilar-Trigueros, C. A., Buchert, S., Wulf, A., et al. (2019). The role of multiple global change factors in driving soil functions and microbial biodiversity. *Science* 366, 886–890. doi: 10.1126/science.aay2832

Ripa, J., and Lundberg, P. (1996). Noise colour and the risk of population extinctions. *Proc. R. Soc. Lond. Ser. B Biol. Sci.* 263, 1751–1753. doi: 10.1098/rspb.1996.0256

Ruokolainen, L., Lindén, A., Kaitala, V., and Fowler, M. S. (2009). Ecological and evolutionary dynamics under coloured environmental variation. *Trends Ecol. Evol.* 24, 555–563. doi: 10.1016/j.tree.2009.04.009

Sæther, B.-E., Tufto, J., Engen, S., Jerstad, K., Røstad, O. W., and Skåtan, J. (2000). Population dynamical consequences of climate change for a small temperate songbird. *Science* 287, 854–856. doi: 10.1126/science.287.5454.854

Shoemaker, L. G., Sullivan, L. L., Donohue, I., Cabral, J. S., Williams, R. J., Mayfield, M. M., et al. (2020). Integrating the underlying structure of stochasticity into community ecology. *Ecology* 101, e02922. doi: 10.1002/ecy.2922

Siepel, H. (1994). Life-history tactics of soil microarthropods. *Biol. Ferti. Soils* 18, 263–278. doi: 10.1007/BF00570628

Søvik, G., and Leinaas, H. P. (2003). Adult survival and reproduction in an arctic mite, Ameronothrus lineatus (Acari, Oribatida): effects of temperature and winter cold. *Can. J. Zool.* 81, 1579–1588. doi: 10.1139/z03-113

Stamou, G. P. (2012). *Arthropods of Mediterranean-Type Ecosystems*. Berlin: Springer Science and Business Media.

Taylor, J. (1997). *Introduction to Error Analysis, the Study of Uncertainties in Physical Measurements*. Sausalito: University Science Books.

Tedersoo, L., Mikryukov, V., Zizka, A., Bahram, M., Hagh-Doust, N., Anslan, S., et al. (2022). Global patterns in endemicity and vulnerability of soil fungi. *Glob. Change Biol.* 28, 6696–6710. doi: 10.1111/gcb.16398

Thakur, M. P., Phillips, H. R. P., Brose, U., De Vries, F. T., Lavelle, P., Loreau, M., et al. (2020). Towards an integrative understanding of soil biodiversity. *Biol. Rev.* 95, 350–364. doi: 10.1111/brv.12567

Tilman, D. (2004). Niche tradeoffs, neutrality, and community structure: a stochastic theory of resource competition, invasion, and community assembly. *Proc. Natl. Acad. Sci. U.S.A.* 101, 10854–10861. doi: 10.1073/pnas.0403458101

Tuljapurkar, S. (2013). *Population Dynamics in Variable Environments*. Berlin: Springer-Verlag.

Turnbull, M. S., George, P. B., and Lindo, Z. (2014). Weighing in: size spectra as a standard tool in soil community analyses. *Soil Biol. Biochem.* 68, 366–372. doi: 10.1016/j.soilbio.2013.10.019

Vályi, K., Mardhiah, U., Rillig, M. C., and Hempel, S. (2016). Community assembly and coexistence in communities of arbuscular mycorrhizal fungi. *ISME J.* 10, 2341–2351. doi: 10.1038/ismej.2016.46

Van Den Hoogen, J., Geisen, S., Routh, D., Ferris, H., Traunspurger, W., Wardle, D. A., et al. (2019). Soil nematode abundance and functional group composition at a global scale. *Nature* 572, 194–198. doi: 10.1038/s41586-019-1418-6

Vellend, M. (2010). Conceptual synthesis in community ecology. *Q. Rev. Biol.* 85, 183–206. doi: 10.1086/652373

Walter, D. E., and Proctor, H. C. (1999). *Mites: Ecology, Evolution, and Behaviour*. Wallingford: CABI Publishing. doi: 10.1079/9780851993751.0000

White, H. J., León-Sánchez, L., Burton, V. J., Cameron, E. K., Caruso, T., Cunha, L., et al. (2020). Methods and approaches to advance soil macroecology. *Glob. Ecol. Biogeogr.* 29, 1674–1690. doi: 10.1111/geb.13156

frontiers | Frontiers in Ecology and Evolution

TYPE Original Research
PUBLISHED 18 July 2023
DOI 10.3389/fevo.2023.1159464

OPEN ACCESS

EDITED BY
Jurek Kolasa,
McMaster University, Canada

REVIEWED BY
William Harrower,
Government of British Columbia, Canada
Sungwoo Ahn,
East Carolina University, United States

*CORRESPONDENCE
Katie R. Hooker
Tta4@cdc.gov

RECEIVED 06 February 2023
ACCEPTED 27 June 2023
PUBLISHED 18 July 2023

CITATION
Hooker KR, Conner LM, Jack SB, Morris G, Palmer WE, Rutledge BT, Sisson DC, Terhune TM, Wellendorf SD and McCleery RA (2023) Trophic interactions between primary consumers appear to weaken during periods of synchrony. *Front. Ecol. Evol.* 11:1159464. doi: 10.3389/fevo.2023.1159464

Trophic interactions between primary consumers appear to weaken during periods of synchrony

Katie R. Hooker[1]*, L. Mike Conner[2], Steven B. Jack[2], Gail Morris[2], William E. Palmer[3], Brandon T. Rutledge[2], D. Clay Sisson[3], Theron M. Terhune[3], Shane D. Wellendorf[3] and Robert A. McCleery[1]

[1]Department of Wildlife Ecology and Conservation, University of Florida, Gainesville, FL, United States, [2]The Jones Center at Ichauway, Newton, GA, United States, [3]Tall Timbers Research Station and Land Conservancy, Tallahassee, FL, United States

Our understanding of synchrony between populations from different taxonomic groups has been centered on predator–prey dynamics in simple systems but has rarely been examined in complex predator–prey systems. In addition to trophic interactions such as predator–prey dynamics, there is some evidence that exogenous factor such as climatic variation may facilitate synchrony between different taxonomic groups. Using three longitudinal datasets on quail (*Colinus virginianus*) and cotton rats (*Sigmodon hispidus*) we examined 1) the consistency of synchrony across time and space, 2) the relative influence of trophic interactions vs. exogenous factors on synchrony and 3) if trophic interactions were positively associated with synchrony between populations. We found evidence of consistent synchrony in cotton rat and bobwhite populations at both the site and regional levels. We found that trophic interactions between cotton rats and bobwhite were associated with relative synchrony between these populations, but these interactions appeared to weaken in years of greater synchrony. We did not find evidence that exogenous factors influenced relative synchrony at the regional level. Given the lack of a clear mechanistic explanation of the patterns observed in our data, we propose an alternative climate-mediated predation framework to explain synchrony in complex predator–prey systems. This framework includes both classic bottom-up theories of regulation while integrating trophic interactions via components of the shared predator hypothesis.

KEYWORDS

climate, *Colinus virginianus*, Moran's theorem, shared predator hypothesis, *Sigmodon hispidus*

Introduction

Wildlife populations that co-vary in time and space have been investigated by scientists since the birth of ecology (Chapman, 1928; Elton, 1949; Andrewartha and Birch, 1954; Krebs, 1985; Brewer, 1988). Synchronous population dynamics, defined as coincident changes in abundance (Liebhold et al., 2004), have been observed across taxonomic groups, including invertebrates (Sutcliffe et al., 1996), fish (Myers et al., 1997), birds (Michel et al., 2016), and mammals (Ims and Steen, 1990). Despite its historical foundation, the patterns, causes, and consequences of synchronous population fluctuations are still not well understood (Liebhold et al., 2004). Most examples of synchrony come from disjunct populations of the same species (Burrows et al., 2002; Post and Forchhammer, 2002; Bellamy et al., 2003; Krebs et al., 2013) or closely related species (Raimondo et al., 2004a; Raimondo et al., 2004b; Robertson et al., 2015).

Synchrony between populations from different taxonomic groups is thought to be driven by exogenous factors such as environmental stochasticity (Moran, 1953) and trophic interactions such as competition and predation (Liebhold et al., 2004). There is considerable evidence that exogenous factors can cause synchrony in closely related species (Cavanaugh and Marshall, 1972; Ranta et al., 1997; Kendall et al., 2000; Koenig and Liebhold, 2016). Two sympatric populations may co-occur without synchronizing until a catalyst, such as changes in weather patterns, creates conditions for synchrony (Moran, 1953). Additionally, factors such as changes in habitat quality and weather patterns (i.e., the North Atlantic Oscillation) can alter the amount of synchrony found among populations across space and time (Hurrell, 1995; Ranta et al., 1997; Ranta et al., 1998; Koenig, 2001; Allstadt et al., 2015). While these patterns appear to be clear for closely related species, they are unclear when synchrony occurs in populations of different taxonomic groups.

Much of our understanding of synchrony between populations from different taxonomic groups has centered on trophic interactions, *via* predator–prey dynamics (Ims and Steen, 1990; De Roos et al., 1991; Gurney et al., 1998; Spiller et al., 2016) that occur in relatively simple communities of predators and prey (Lack, 1954; Angelstam et al., 1984). While the concepts generated from simple systems have been broadly applied (Davenport and Chalcraft, 2012; Nordberg and Schwarzkopf, 2019), rarely have they been examined in complex predator–prey systems. Meanwhile, other trophic mechanisms like competition for resources (Koenig, 2001; Jones et al., 2003) and similarity in species' reproductive strategies may also increase the opportunity for synchrony (Moran, 1953; Liebhold et al., 2004). Additionally, there is some evidence (Liebhold et al., 2004) but little understanding of how trophic interactions and exogenous factors may interact to influence synchrony between populations from different taxonomic groups (Bjørnstad et al., 1999).

Two species that may allow us to better understand the influence of the synergies of exogenous factors and trophic interactions in a complex food web are hispid cotton rats (*Sigmodon hispidus*) and northern bobwhite (*Colinus virginianus*; hereafter bobwhite; Staller et al., 2005; Morris et al., 2011). Cotton rats and bobwhite are dominant primary consumers in ecosystems throughout the southeastern United States. Both species serve as an important food source to several shared generalist avian, mammalian, and reptilian secondary consumers (Schnell, 1968; Barrett et al., 2001). Anecdotal evidence of synchronous population fluctuations in cotton rat and bobwhite populations have been observed, leading some to hypothesize a trophic interaction mechanism of synchrony (Errington and Stoddard, 1938; Schnell, 1968; Barrett et al., 2001; Staller et al., 2005). However, environmental conditions can also influence both populations, for example, bobwhite chick survival can be sensitive to rainfall during their restricted breeding season (Terhune et al., 2019). Alternatively, variation in seasonal temperatures has been correlated with cotton rat reproductive activity (Goertz, 1965) and abundance (Rehmeier et al., 2005).

Our objective was to understand the patterns and drivers of synchrony for two sympatric primary consumers in a complex food web. Specifically, we wanted to address the following questions: 1) Do bobwhite and cotton rats synchronize consistently across space and time? 2) What is the relative influence of trophic interactions vs. exogenous factors on the amount of synchrony between populations, and 3) does the strength of trophic interactions increase with increasing synchrony between populations? Using datasets from sites in their southeastern geographic ranges, we predicted that bobwhite and cotton rats would exhibit punctuated but inconsistent periods of synchrony because the species' reproductive potential is influenced differently by environmental variation. In support of Moran's theorem of synchrony (Moran, 1953; Stien et al., 2012), we predicted that periods of synchronous fluctuations would be more closely associated with exogenous factors because populations of these species can be sensitive to climatic variation (Eifler and Slade, 1999; Perez et al., 2002; Hernández et al., 2005; Rehmeier et al., 2005). Finally, we predicted that trophic interactions (e.g., predation and competition) would not vary with the relative amount of synchrony between populations because empirical evidence (Miller and Epstein, 1986; Post and Forchhammer, 2002; Raimondo et al., 2004a) and theory suggest that exogenous factors drive synchrony in unrelated species (Moran, 1953; Royama, 1992; Koenig, 2001).

Materials and methods

Study species

Cotton rat and bobwhite distributions overlap in the southern United States and Mexico. Both species are ~160 g as adults (cotton rat range: 100 to 225 g; bobwhite range: 140 to 170 g; Cameron, 1999; Brennan et al., 2014) and primarily herbivorous, consuming grass and forb seeds, fruits, leafy vegetation, and sometimes invertebrates (Fleharty and Olson, 1969; Campbell-Kissock et al., 1985). Although they share similar resources, cotton rats and bobwhite select different vegetation structure. Cotton rat density generally increases with grass height and density (Goertz, 1964) whereas bobwhite prefer bunchgrasses and shrubs for cover and nesting (Wells, 2008). They also differ in life history strategies.

Cotton rats can breed year-round if environmental conditions are favorable (Linzey, 1998), while bobwhite reproduction is restricted to a defined breeding season, primarily May–August (DeVos and Mueller, 1993).

Both bobwhite and cotton rat populations can be sensitive to environmental variation. Bobwhite abundance and survival have been linked to climatic conditions (Speake and Haugen, 1960; Jackson, 1962; Perez et al., 2002; Hernández et al., 2005). Although deviations from average seasonal environmental conditions can influence populations of both species, extreme weather events (e.g., extreme heat and drought) during the bobwhite breeding season can have a greater relative impact on their demographics (Perez et al., 2002; Tri et al., 2012). Similarly, extreme summer temperatures and cold winters have been shown to reduce cotton rat reproduction and abundance (Eifler and Slade, 1999; Rehmeier et al., 2005).

Study sites

To investigate the patterns of cotton rat and bobwhite population fluctuations, we used long-term data from three study sites: Tall Timbers Research Station (TT) in Leon County, Florida, the Jones Center at Ichauway (JC) in Baker County, Georgia, and a private property (Private) in Baker County, Georgia (Private; Figure 1).

Tall Timbers is a 1,600-ha forest in Leon County, Florida, USA, approximately 33.3 km north of Tallahassee, Florida. Tall Timbers' landscape is dominated by sparsely distributed pine trees and a diverse understory of forbs and grasses. Characterized by a humid, subtropical climate and summer rainy season, TT has an average air temperature of 19.78°C and an average annual precipitation of 1.50 m.

The Jones Center at Ichauway is a 12,000-ha research facility in Baker County, Georgia, USA, approximately 20 km southwest of Newton, Georgia. The Jones Center is dominated by longleaf pine (*Pinus palustris*) and a diverse understory of grasses, forbs, and shrubs. The climate at JC is characterized by long, hot summers and cool, short winters (Lynch et al., 1986) with an average annual temperature of 18.11°C and average annual precipitation of 1.41 m.

The private property in Baker County, Georgia is a 6,000-ha forest approximately 24 km southwest of Albany, Georgia. In the Upper Coastal Plain physiographic region, this property is characterized by sandy-loam soils with low natural fertility (Palmer et al., 2012). The temperate, subtropical climate receives an average of 1.41 m of annual precipitation and has an average annual air temperature of 18.11°C. The dominant vegetation community is defined by low density upland pines, predominantly slash (*P. elliottii*), longleaf, and loblolly (*P. taeda*) and a diverse understory of forbs, legumes, and native warm season grasses (Yates et al., 1995).

Population data collection

Cotton rats

At TT, we established eight 1.82-ha plots, made up of 100 Sherman live traps (7.62 × 8.89 × 22.86 cm, H. B. Sherman Traps, Inc., Tallahassee, FL) arranged in a 10 × 10 grid. We placed traps 15 m apart and baited them with oats. At JC, in late July to mid-August each year from 2003 to 2017, we also trapped on eight plots with 144 Sherman live traps in 12 × 12 grids with 15 m spacing (2.72-ha). At the private property, each August from 2008 to 2017, we established four 1.82-ha plots made up of 100 Sherman live traps arranged in a 10 × 10 grid spaced 15 m apart. We trapped at each of these locations annually in late July–August (TT: 2002–2017, JC: 2003–2017, Private: 2008–2017), for four consecutive nights. We trapped cotton rats in August based on the within-year cycles of cotton rat populations observed in the region, which include annual peak densities in August each year (Hannon, 2006). We marked

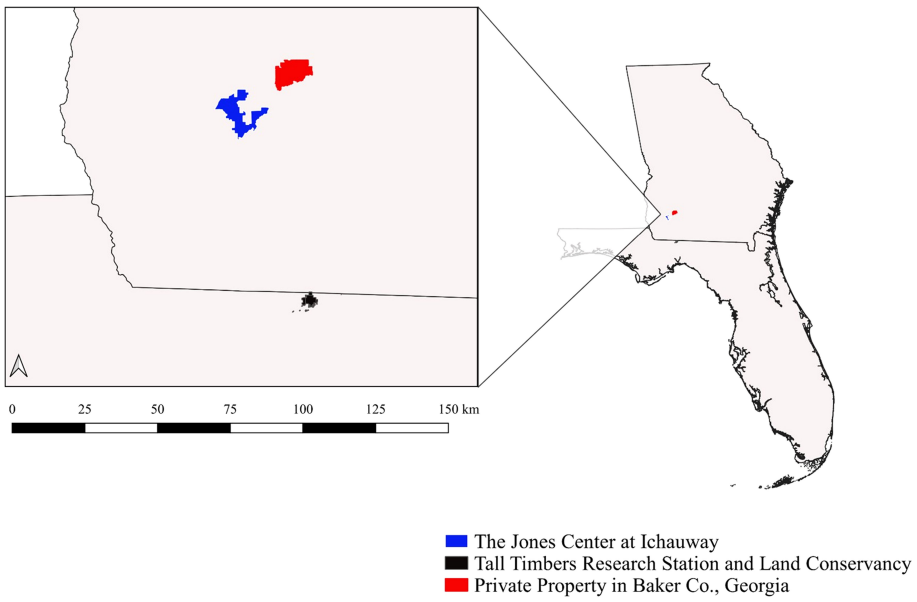

FIGURE 1
Study sites including the Jones Center at Ichauway, Baker Co., GA, a private property in Baker Co., GA, and Tall Timbers Research Station, Leon Co., FL.

individuals with a unique numeric ear tag (Style 1005-1, National Band and Tag Co., Newport, KY) and collected data on location. We released marked animals at place of capture. Our trapping and handling methods followed the recommendations of the Animal Care and Use Committee of the American Society of Mammalogists (Sikes and Animal Care and Use Committee of the American Society of Mammalogists, 2016). Our methods were approved by Tall Timbers Research Station under (IACUC permit GB-2001-01-15), at the Jones Center at Ichauway under the Georgia Department of Natural Resources (scientific collecting permit 1000528068), and at the private property under the Georgia Department of Natural Resources (scientific collecting permit 1000650622).

Bobwhite

We conducted annual autumn covey counts at TT between September and November from 2002 to 2017 based on the methodology of Wellendorf and Palmer (2005). Each year, we randomly established twelve 25-ha quadrants. We placed a trained observer at the midpoint of each side of the quadrant (4 observers/quadrant). During the 45 minutes before sunrise, we recorded the estimated distance, bearing, and location of all calling coveys on a map of the quadrant and surrounding areas. We determined calling covey locations *via* triangulation based on observers' bearings and distances. We grouped estimated distances from observer to covey into four categories: 0–100 m, 101–250 m, 251–500 m, and > 500 m. We estimated covey size based on flush counts conducted following point counts. We used this same methodology at the private property, where we conducted annual autumn (September–November) covey counts on four randomly established 25-ha quadrants from 2008 to 2017.

At JC, we conducted point count covey call surveys on a 92-station grid covering 6,997-ha from mid-October to early-November from 2003 to 2017. Beginning 45 minutes before sunrise, we recorded each covey heard until all calling had ceased. We grouped estimated distances from observer to covey into five distance bands: 0–25 m, 25–50 m, 50–100 m, 100–250 m, and 250–500 m. We assumed 12 bobwhite/covey based on published average covey size (Janke et al., 2013).

Environmental data collection

We selected a suite of environmental variables to determine the influence of exogenous factors on patterns of cotton rat and bobwhite population fluctuations. Enhanced vegetation index (EVI) is an optimized index that quantifies the "greenness" of vegetation based on the difference between the visible and near-infrared light reflected by vegetation (Huete et al., 2006). We chose EVI over the traditionally used NDVI (normalized difference vegetation index) because EVI has improved sensitivity to high biomass regions and is less influenced by cloud cover compared to NDVI (Huete et al., 2006). We downloaded EVI data from NASA's MODIS platform (Didan, 2015) using product MOD13Q1 at a 250 m spatial resolution and 16-day temporal scale. We averaged these data for seasonal (spring: March–May, summer: June–August, autumn: September–November, winter: December–February) EVI measurements at all sites. Additionally, we focused on seasonal climatic variation due to the well-established links with both bobwhite and cotton rat population growth. Specifically, we obtained seasonal mean precipitation (cm) and temperature (°C) from NOAA's National Centers for Environmental Information (NCEI, 2020) closest to each study site (mean distance ~21 km from study sites) from 2001 to 2017. We paired environmental data from the winter and spring prior to animal capture, the summer concurrent with cotton rat and prior to bobwhite capture, and the autumn after cotton rat and concurrent with bobwhite capture.

Statistical analyses

Animal density estimation

We estimated cotton rat density at TT, JC and the private property using annual August capture data. We calculated density based on a subset of Otis' closed capture models (null (M_0), time-varying (M_t), behavioral response (M_b); Otis et al., 1978; SI 1) using a conditional likelihood approach of two parameters: capture probability (p) and recapture probability (c; Huggins, 1989; Cooch and White, 2012). We chose a closed capture framework due to the single trapping session each year. We grouped each capture by "Plot" and "Year." We used both ΔAIC_C and model weight to identify the most parsimonious model (AIC_C; Akaike, 1973; Burnham and Anderson, 2002; Burnham and Anderson, 2004). We derived plot-level abundance estimates from the most parsimonious model using the package RMark (Laake, 2013) in Program R (R Core Team, 2021). We averaged estimated abundance across plots within each year to provide a single annual cotton rat abundance estimate for each site.

We estimated bobwhite density at TT and the private property based on a global distance function from a subset of available detection functions in Program DISTANCE (Thomas et al., 2010) using an information theoretic criterion (AIC; Akaike, 1973) and model fit using chi-square model fit statistics (Burnham and Anderson, 1998). We estimated bobwhite density at JC based on an annual calling rate calculated given daily weather conditions (Wellendorf and Palmer, 2005), the assumed covey size, and the number of coveys heard. Different methodologies were used to estimate density at TT and JC due to differences in data collection methods across organizations/sites.

Synchrony of cotton rats and bobwhite

To determine if bobwhite and cotton rats consistently synchronize at each site, across the region, and through time we used concordance as a proxy for relative synchrony or the coincident population fluctuations (Gouhier and Guichard, 2014; Borgmann-Winter et al., 2021) of bobwhite and cotton rats. We measured concordance with a Kendall's W test of concordance (*kendall.global* function) in the vegan package (Oksanen et al., 2013) in R (R Core Team, 2021). Kendall's W is a non-parametric test of agreement among independent measures (i.e., judges) of same attributes which provides a concordance estimate ranging from 0 (no concordance) to 1 (full concordance), an F statistic, and probability (p). We treated cotton rat and bobwhite

densities from each site as judges to measure relative synchrony at the site level. Then we treated cotton rat and bobwhite densities in each year as judges to test regional relative synchrony across years. The magnitude of agreement among judges can be interpreted as slight ($0 < W < 0.20$), fair ($0.20 < W < 0.40$), moderate ($0.40 < W < 0.60$), substantial ($0.60 < W < 0.80$), or almost perfect ($0.80 < W < 1.0$; Landis and Koch, 1977). We used the default 999 permutations and a Holm probability correction (Legendre, 2005) with $\alpha = 0.05$ level of significance. We conducted *post-hoc* testing *(kendall.post* function) of the results to determine which judges significantly ($\alpha \leq 0.05$) influenced the overall concordance statistic. Each species' annual density contributes to overall measures of concordance independently (Legendre, 2005). In some years, bobwhite or cotton rat density may have a greater influence than the other on the overall synchrony of population fluctuations. To acknowledge the effect of noise in the empirical data and understand how extremes in population abundances shaped patterns of synchrony, we measured the patterns the proportion of peaks (maxima) and troughs (minima) common to both bobwhite and cotton rat populations in time series. Specifically, we assessed the proportion of concurrent peaks and troughs using a Monte Carlo randomization to shuffle each species' time series, destroying both the autocorrelation structure and cross correlation between series. We assessed peaks and troughs with all sites pooled (regionally) and at each site individually (locally). We conducted our analysis using the synchrony package (Gouhier and Guichard, 2014) in Program R, which computed a p-value based on the number of randomizations conducted ($N = 999$).

Drivers of population density

To determine the relative influence of exogenous factors on bobwhite and cotton rat densities we generated generalized linear models (GLM) in the glmmTMB package (Magnusson et al., 2017) in R (R Core Team, 2021). We developed two additive models to evaluate the linkages between bobwhite and cotton rat densities and exogenous factors. We averaged our seasonal exogenous factors and measures of density across sites, providing a single seasonal estimate of each variable per year. We justified consolidating these data based on the similar relative synchrony observed across all study sites. We parameterized the model with a Gaussian distribution and seasonal estimates of EVI, precipitation, and temperature, and the annual densities of bobwhite and cotton rats (Models 1 and 2). Prior to modeling, we scaled each variable and analyzed the variance inflation factor (VIF) in package car (Fox et al., 2019) in R (R Core Team, 2021) to assess each temporal dataset for multicollinearity of explanatory variables. We removed variables with > 2.5 VIF (Allison, 1999) one-by-one to reduce correlation.

Model 1:

Bobwhite Density ~ Seasonal EVI + Seasonal Temperature (°C) + Seasonal Precipitation (cm)

Model 2:

Cotton Rat Density ~ Seasonal EVI + Seasonal Temperature (°C) + Seasonal Precipitation (cm)

We assessed model fit based on visual inspection of the normality of residuals and met the assumptions of normality. We computed a Wald-z-statistic from a Wald chi-square test (Wald and Wolfowitz, 1943) to calculate the *p*-values of the explanatory variables in each model with a significance level of $\alpha \leq 0.05$. We evaluated the relative strength of these predictors by comparing their scaled beta estimates and displaying them graphically.

Drivers of synchrony

To determine the relative influence of trophic interactions and exogenous factors on synchrony we generated a generalized linear model (GLM) in the glmmTMB package (Magnusson et al., 2017) in R (R Core Team, 2021). We developed an additive model to evaluate the linkages between our measure of regional relative synchrony (Kendall's *W* averaged from cotton rat and bobwhite Kendall's *W*s), exogenous factors, and trophic interactions (e.g., bobwhite and cotton rat densities). We averaged our seasonal exogenous factors and measures of density across sites, providing a single seasonal estimate of each variable per year. We justified consolidating these data based on the similar relative synchrony observed across all study sites. We parameterized the model with a Gaussian distribution and seasonal estimates of EVI, precipitation, and temperature, and the annual densities of bobwhite and cotton rats (Model 3). Prior to modeling, we scaled each exogenous factor variable and analyzed the variance inflation factor (VIF) in package car (Fox et al., 2019) in R (R Core Team, 2021) to assess each temporal dataset for multicollinearity of explanatory variables. We removed variables with > 2.5 VIF (Allison, 1999).

Model 3:

Relative Synchrony ~ Seasonal EVI + Seasonal Temperature (°C) + Seasonal Precipitation (cm) + Cotton Rat Density + Bobwhite Density

For each parameter, we computed a Wald-z-statistic from a Wald chi-square test (Wald and Wolfowitz, 1943) to calculate the *p*-values of the explanatory variables. We considered the explanatory relevance of each parameter, using a significance level of $\alpha \leq 0.05$. We evaluated the relative strength of these predictors by comparing their scaled beta estimates and displaying them graphically.

Trophic interactions and synchrony

To determine if trophic interactions were influenced by the amount of synchrony between the populations, we regressed the density of each species against an interaction between the other species density and our measure of relative synchrony (Kendall's *W*; Models 4 and 5). We also included exogenous factors (significant variables from Model 3) to account for their known influence on densities and synchrony. We parameterized the models as a GLM in the glmmTMB package (Magnusson et al., 2017) in R (R Core Team, 2021) with the bobwhite and cotton rat densities modeled to fit with a Gaussian distribution and evaluated the residuals to determine if any assumptions of normality were violated.

Models 4 and 5:

Bobwhite Density ~ Significant Exogenous Factors from Model 3 + Cotton Rat Density + Relative Synchrony + Cotton Rat Density*Relative Synchrony

Cotton Rat Density ~ Significant Exogenous Factors from Model 3 + Bobwhite Density + Relative Synchrony + Bobwhite Density*Relative Synchrony

For each parameter, we computed a Wald-z-statistic from a Wald chi-square test (Wald and Wolfowitz, 1943) to calculate the *p*-values of the explanatory variables. We considered the explanatory relevance of the interaction parameter as well as other variables, using a significance level of $\alpha \leq 0.05$. We evaluated the relative strength of these predictors by comparing their scaled beta estimates and displaying them graphically.

Results

Estimates of animal density

Cotton rats

The most parsimonious model of cotton rat density across sites was the behavioral response model *p*(.),*c*(.): TT: AIC_c = 19099.67, model weight: 1.0; JC: AIC_c = 10175.56, model weight: 1.0; Private property: AIC_c = 2753.53, model weight: 0.99 (SI 2). Cotton rat density averaged 25.40 ± SE 1.46 cotton rats/ha from 2002 to 2017 at TT, 10.90 ± SE 1.18 cotton rats/ha from 2003 to 2017 at JC, and 15.8 ± SE 3.74 cotton rats/ha from 2008 to 2017 at the private property (SI 3).

Bobwhite

We estimated the density of bobwhite at TT and the private property based on the most competitive detection model, with a uniform detectability with simple polynomial adjustments, AIC = 146.5 (Wellendorf and Palmer, 2005). Bobwhite density averaged 3.48 ± SE 0.19 birds/ha at TT, 4.82 ± SE 0.34 birds/ha at the private property, and varied little at JC, averaging 1.69 ± SE 0.05 birds/ha (SI 4).

Environmental variation

Enhanced vegetation index varied by site and year and was, on average, highest in summer (0.48 ± SE 0.007) and lowest in winter (0.27 ± SE 0.003) across all sites. Precipitation varied across years and sites. Precipitation peaked in summer (30.2 ± SE 3.22 cm) and was lowest in autumn (14.7 ± SE 2.25 cm). Air temperature varied across seasons and years, with the highest average temperatures in summer (27.20 ± SE 0.15° C) and lowest in winter (11.70 ± SE 0.36° C) across all sites (SI 5).

Drivers of population density

After removing highly correlated environmental variables (winter, spring, and autumn EVI and winter, autumn, and summer precipitation) using VIF, our model of bobwhite density included winter temperature, spring precipitation and temperature, summer EVI and temperature, and autumn temperature as explanatory variables. Bobwhite density was significantly associated with previous spring precipitation (β = 0.22 ± SE 0.11, z = 1.98, p = 0.05) and concurrent autumn temperature (β = 0.26 ± SE 0.13, z = 2.03, p = 0.04; Table 1).

Our model predicted that as prior spring precipitation increases from 5.5 to 32.51 cm, bobwhite density would increase from 2.82 ± SE 0.19 to 3.49 ± SE 0.20 individuals per hectare. Similarly, as autumn temperature increases from 18.74 to 23.28°C, bobwhite density is predicted to increase from 2.58 ± SE 0.29 to 3.63 ± SE 0.26 bobwhite per hectare (Figure 2).

Our model of cotton rat density included the same environmental variables as our model of bobwhite density except autumn temperature because those data were collected after cotton rat density each year. Cotton rat density was significantly associated

TABLE 1 Generalized linear mixed model results of the exogenous factors influence on bobwhite and cotton rat densities at the Jones left at Ichauway, a private property in Baker Co., GA, and Tall Timbers Research Station from 2002 to 2017.

Response Variable	Explanatory Variable	β Estimate	SE	*z*	*p*
Bobwhite Density	Winter Temperature	0.25	0.14	1.81	0.07
	Spring Precipitation	0.22	0.11	1.98	0.05*
	Spring Temperature	−0.02	0.11	−0.22	0.83
	Summer EVI	−0.08	0.10	−0.76	0.45
	Summer Temperature	−0.08	0.13	−0.63	0.53
	Autumn Temperature	0.26	0.13	2.03	0.04*
Cotton Rat Density	Winter Temperature	4.78	1.49	3.21	0.001*
	Spring Precipitation	4.30	1.39	3.10	0.002*
	Spring Temperature	−0.58	1.31	−0.44	0.66
	Summer EVI	4.19	1.31	3.21	0.001*
	Summer Temperature	3.12	1.52	2.05	0.04*

An autumn temperature was not included in the cotton rat density model because it was collected after cotton rat density each year. Variables with p ≤ 0.05 were considered statistically significant (*).

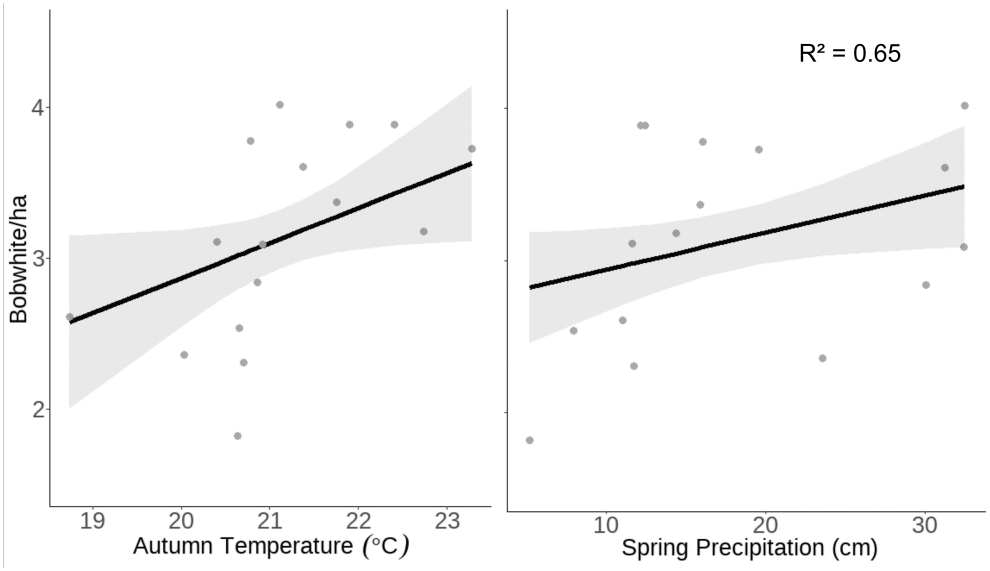

FIGURE 2
Raw data (gray dots) and model-predicted bobwhite density (black line) ± 95% confidence intervals (gray band) as prior spring precipitation and concurrent autumnal temperature increases at the Jones Center at Ichauway, a private property in Baker Co., GA, and Tall Timbers Research Station from 2002 to 2017.

with a number of variables, including positive significant relationships with winter (β = 5.83 ± SE 1.40, z = 4.17, p < 0.001) and summer temperature (β = 2.95 ± SE 1.40, z = 2.11, p = 0.04), spring precipitation (β = 4.21 ± SE 1.29, z = 3.26, p = 0.001), and summer EVI (β = 4.81 ± SE 1.25, z = 3.84, p < 0.001; Table 1).

Our model of cotton rat density predicted that as winter temperature increases from 8.81 to 14.46° C, cotton rat density would increase from 9.76 ± SE 3.03 to 27.84 ± SE 3.13 cotton rats/ha. Similarly, as summer temperature increases from 26.38 to 28.24° C, cotton rat density is predicted to increase from 13.93 ± SE 2.60 to 23.67 ± SE 2.75 cotton rats/ha. Our model predicted that as spring precipitation increases from 5.15 to 32.51 cm, cotton rat density will double, increasing from 12.59 ± SE 2.31 to 25.45 ± SE 2.53 individuals/ha. Our model predicted that as summer EVI increases from 0.43 to 0.55, cotton rat density will nearly triple, increasing from 12.49 ± SE 2.83 to 29.32 ± SE 3.56 cotton rats/ha (Figure 3).

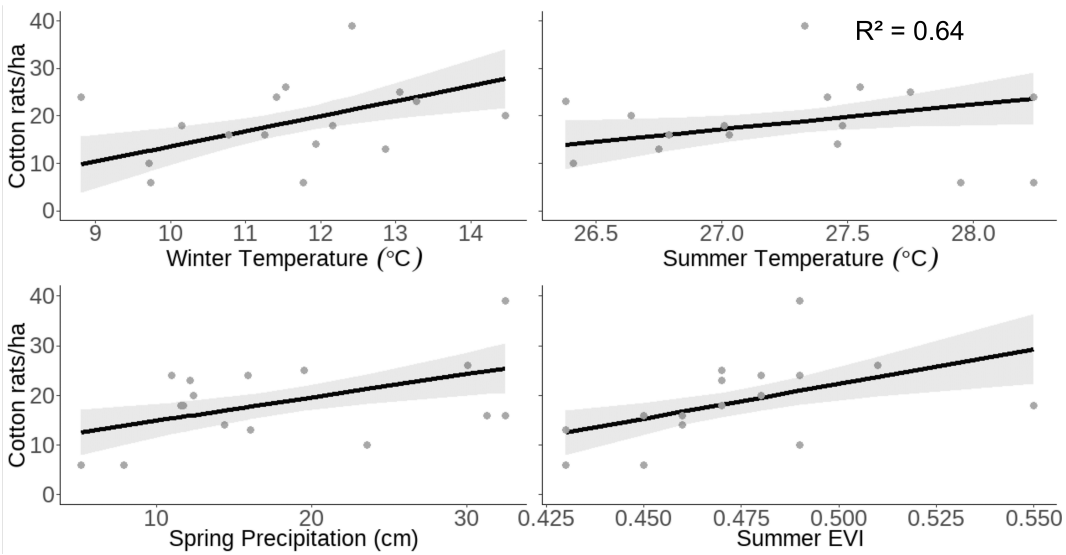

FIGURE 3
Raw data (gray dots) and model-predicted cotton rat density (black line) ± 95% confidence intervals (gray band) as prior winter temperature, prior spring precipitation, and concurrent summer EVI and temperature increase at the Jones Center at Ichauway, a private property in Baker Co., GA, and Tall Timbers Research Station from 2002 to 2017.

Synchrony of cotton rats and bobwhite

Regionally, when we pooled cotton rat and bobwhite density across sites as judges (N = 2), we found significant concordance (W = 0.76, F_3 = 3.09, p < 0.001, χ^2 = 58.93, corrected p < 0.001) indicating substantial levels of regional relative synchrony. At the site level, relative synchrony ranged from substantial at the Jones Center (W = 0.73; p = 0.05) and private property (W = 0.79; p = 0.04) to almost perfect at Tall Timbers (W = 0.90; p <0.001; Table 2). Overall, we found significant but fair levels of regional synchrony across years (W = 0.40, F_{32} = 20.87, p < 0.001, χ^2 = 25.75, corrected p = 0.001). *Post-hoc* testing revealed that the strongest indication of synchrony were bobwhite and cotton rat densities in 2003, 2005, 2006, 2007, 2016, and 2017 (all W = 0.63), and bobwhite from 2011 to 2016 (all W = 0.63; SI 6). The regional proportion of concurrent peaks of bobwhite and cotton rat population maxima and minima was 56% (p = 0.01) suggesting synchrony occurred when abundances were relatively high and low.

Drivers of synchrony

After removing highly correlated environmental variables (winter, spring, and autumn EVI and winter, autumn, and summer precipitation), our model of relative synchrony included winter temperature, spring precipitation and temperature, summer EVI and temperature, autumn temperature, and bobwhite and cotton rat densities as explanatory variables. Relative synchrony was negatively associated with bobwhite density (β = −0.26 ± SE 0.10, z = −2.68, p = 0.007; Table 3). Our model predicted that as bobwhite density increases from 1.82 to 4.49 individuals per hectare, relative synchrony will decrease from 0.95 ± SE 0.19 to 0.10 ± SE 0.13 (Figure 4).

Trophic interactions and synchrony

We found evidence that both bobwhite and cotton rats were positively associated with the density of the other species. We modeled bobwhite density with the significant environmental factors from Model 1 (spring precipitation and autumn temperature), relative synchrony, and the interaction of relative synchrony and cotton rat density. Bobwhite density was positively associated with cotton rat density (β = 0.30 ± SE 0.11, z = 2.58, p = 0.01; Table 4) but not the interaction of cotton rat density and synchrony. Our model predicted that as cotton rat density increases from 6 to 39 individuals/ha, bobwhite density will increase from 2.71 ± SE 0.20 to 3.87 ± SE 0.30 bobwhite/ha (Figure 5).

We modeled cotton rat density from the significant environmental variables from Model 2 (winter and summer temperature, spring precipitation, and summer EVI), relative synchrony, bobwhite density, and the interaction of relative synchrony and bobwhite density. Cotton rat density was positively associated with bobwhite density (β = 6.83 ± SE 1.45, z = 4.70, p < 0.001) and negatively associated with the interaction of relative synchrony and bobwhite density (β = −2.71 ± SE 1.03, z = −2.63, p = 0.009; Table 4). Our model of cotton rat

TABLE 2 Results of *post-hoc* testing of Kendall's *W* showing the synchrony of cotton rats and bobwhite at each site relative to overall concordance (*W*).

Site	Kendall's *W*	*F*	*p*	Corrected *p*
Jones Center	0.73	2.73	0.05*	0.05*
Private	0.79	3.87	0.04*	0.04*
Tall Timbers	0.90	9.46	<0.001*	<0.001*

Kendall.post provides the contribution to overall concordance (*W*), F statistic, probability of the F statistic, and the probability of the Holm correction (significance of α ≤ 0.05, denoted by *).

TABLE 3 Generalized linear mixed model results of the exogenous and trophic interaction factors on relative synchrony at the Jones Center at Ichauway, a private property in Baker Co., GA, and Tall Timbers Research Station from 2002 to 2017.

Response Variable	Explanatory Variable	β Estimate	SE	*z*	*p*
Relative Synchrony	Winter Temperature	0.09	0.06	1.59	0.11
	Spring Precipitation	−0.03	0.05	−0.63	0.53
	Spring Temperature	−0.008	0.04	−0.23	0.15
	Summer EVI	−0.09	0.07	−1.33	0.30
	Summer Temperature	−0.07	0.06	−1.04	0.82
	Autumn Temperature	0.09	0.06	1.44	0.18
	Cotton Rat Density	0.12	0.10	1.26	0.21
	Bobwhite Density	−0.26	0.10	−2.68	0.007*

Variables with p ≤ 0.05 were considered statistically significant (*).

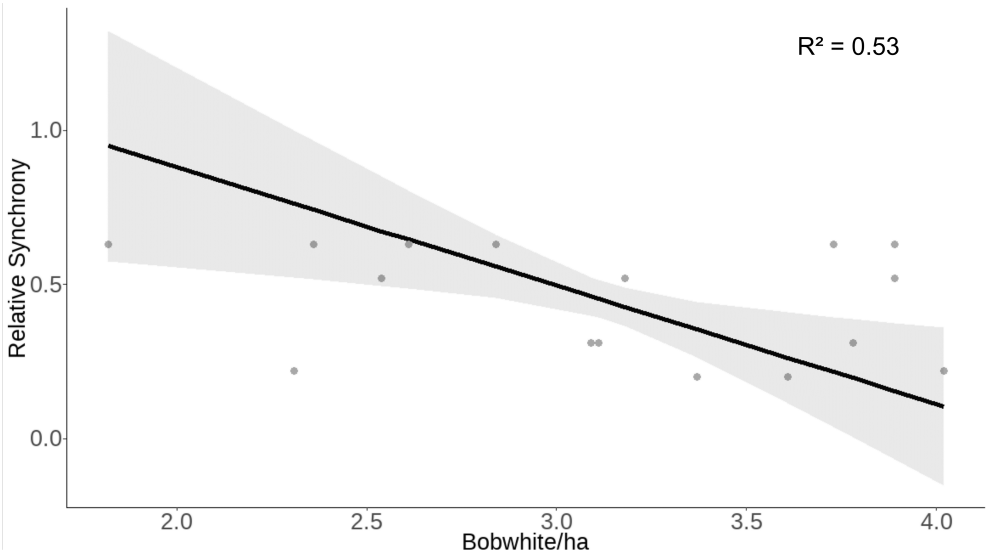

FIGURE 4
Raw data (gray dots) and model-predicted relative synchrony (black line) ± 95% confidence intervals (gray band) as bobwhite density increases at the Jones Center at Ichauway, a private property in Baker Co., GA, and Tall Timbers Research Station from 2002 to 2017.

density predicted that as bobwhite density increases from 1.82 to 4.02 bobwhite/ha, cotton rat density will increase from 4.45 ± SE 3.07 to 26.93 ± SE 1.99 cotton rats/ha (Figure 5). Our model indicated that as synchrony between species increases, the association between bobwhite density on cotton rat density decreases. At low levels of concordance (W = 0.20), our model predicted a positive association between bobwhite density and cotton rat density, predicting that as bobwhite density increases from 1.82 to 4.02 bobwhite/ha, cotton rat density would increase from 0.0 ± SE 5.58 to 30.88 ± SE 2.79 cotton rats/ha. Similarly, at fair levels of synchrony (W = 0.31), as bobwhite density increases from 1.82 to 4.02 individuals/ha, cotton rat density is predicted to increase from 0.06 ± SE 4.35 to 29.10 ± SE 2.19 cotton rats/ha. At the highest levels of synchrony observed between species (W = 0.63), as bobwhite density increases from 1.82 to 4.02 individuals/ha, cotton rat density is predicted to increase from 10.51 ± SE 2.49 to 23.93 ± SE 2.77 cotton rats/ha (Figure 6).

Discussion

In our examination of a complex predator–prey system, we found evidence of regional and site-specific synchrony between two taxonomically divergent primary consumers demonstrated by both substantial levels of concordance and high proportions of

TABLE 4 Generalized linear mixed model results of the global model of exogenous factors and synchrony at the Jones Center at Ichauway, two sites at a private property in Baker Co., GA, and Tall Timbers Research Station from 2002 to 2017.

Response Variable	Explanatory Variable	β Estimate	SE	*z*	*p*
Bobwhite Density	Spring Precipitation	0.04	0.12	0.37	0.71
	Autumn Temperature	0.33	0.10	3.21	0.001*
	Relative Synchrony	−0.15	0.11	−1.35	0.18
	Cotton Rat Density	0.30	0.11	2.58	0.01*
	Relative Synchrony*Cotton Rat Density	0.10	0.10	1.01	0.31
Cotton Rat Density	Winter Temperature	1.09	1.35	0.81	0.42
	Spring Precipitation	0.99	1.08	0.92	0.36
	Summer EVI	6.22	0.95	6.53	<0.001*
	Summer Temperature	2.69	0.94	2.87	0.004*
	Relative Synchrony	0.64	1.04	0.62	0.54
	Bobwhite Density	6.83	1.45	4.70	<0.001*
	Relative Synchrony*Bobwhite Density	−2.71	1.03	−2.63	0.009*

Cotton rat and bobwhite density models include only the statistically significant exogenous variables from Table 1. Variables with p ≤ 0.05 were considered statistically significant (*).

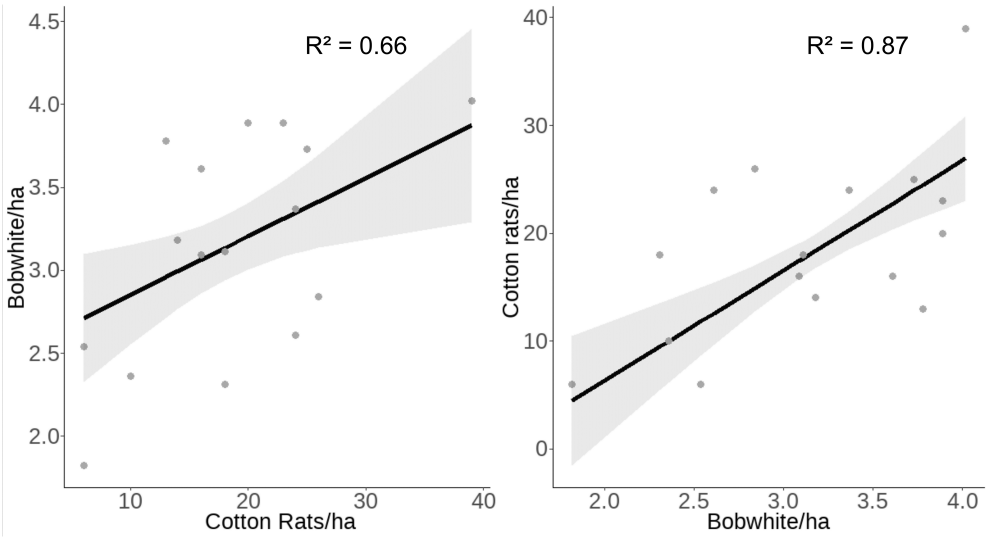

FIGURE 5
Raw data (gray dots) and model-predicted cotton rat and bobwhite density (black line) ± 95% confidence intervals (gray band) as the other species' density increases at the Jones Center at Ichauway, a private property in Baker Co., GA, and Tall Timbers Research Station from 2002 to 2017.

concurrent maxima and minima. Unlike many synchronous populations, we found negligible evidence that variation in the relative amounts of synchrony were tied to exogenous factors (Post and Forchhammer, 2002; Stien et al., 2012). We did find that trophic interactions between cotton rats and bobwhite were associated with relative synchrony between these populations, but these interactions appeared to weaken in years of greater synchrony (Lee et al., 2020). If populations were synchronized by mechanisms like predation and competition, we would have expected a positive association between synchrony and trophic interactions (Ims and Steen, 1990; De Roos et al., 1991). Accordingly, our research suggests that the patterns of fluctuation among taxonomically divergent primary consumers in our system cannot be easily explained by our current suite of theoretical constructs that focus solely on exogenous factors (Moran, 1953) or trophic predator–prey interactions (Hagen, 1952; Lack, 1954; Angelstam et al., 1984) and may be influenced by the interaction of these factors (Coulson et al., 2004; Stenseth et al., 2004).

The pattern of synchrony between bobwhite and cotton rats varied considerably across years, fluctuating from no relationship to moderate synchrony. Declines in relative synchrony were associated with increasing bobwhite density. When regional synchrony between the populations was highest (2003, 2005, 2006, 2007), environmental conditions were characterized by above average greenness across multiple seasons and summer precipitation. During those same years,

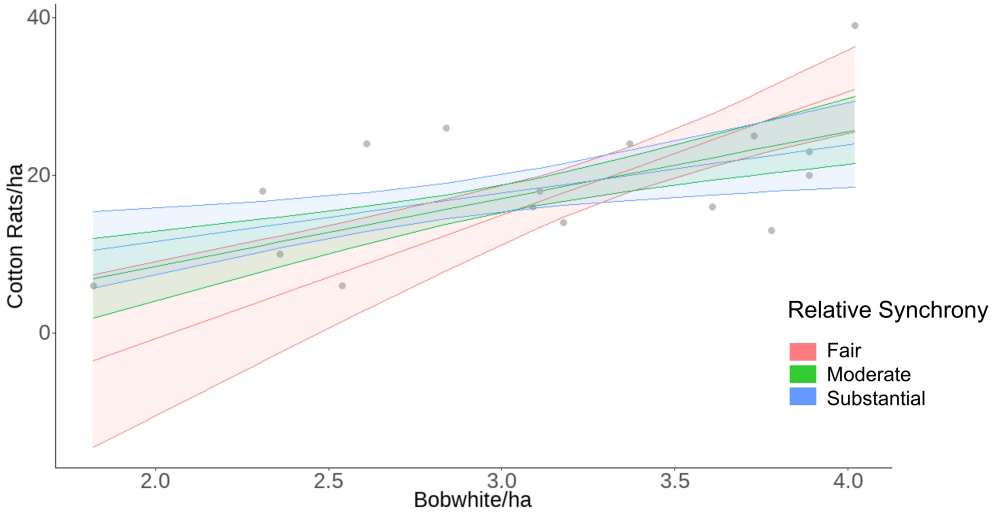

FIGURE 6
Raw data (gray dots) and model predicted relationship of the interaction of bobwhite density and relative synchrony on cotton rat density at the Jones Center at Ichauway, a private property in Baker Co., GA, and Tall Timbers Research Station from 2002 to 2017.

bobwhite density which are known to be sensitive to temperature and precipitation (Table 1; Lusk et al., 2001), was low; and cotton rat density, sensitive to seasonal greenness, precipitation, and temperature (Table 1; Reed and Slade, 2006), was variable. Alternatively, during years of reduced synchrony (2002, 2004, 2010), environmental conditions were characterized by above average spring precipitation and below average winter and summer precipitation as well as reduced cotton rat densities and average bobwhite densities. These patterns suggest that differences in synchrony can potentially be partially explained by the subtly different ways climatic conditions influence the population densities of these taxonomically divergent species. Yet they do not conform well with Moran (1953), commonly used to explain patterns between populations, suggests synchrony occurs during extreme weather events that reduce population densities. Following this concept, we would have expected increases in synchrony when bobwhite and cotton rat densities were both at their lowest. Based on maxima and minima across sites, bobwhite and cotton rat populations fluctuated concurrently in more than 50% of the study years (SI 7); however, these fluctuations were not clearly linked to exogenous factors as indicators of population change. Across sites, cotton rats appear to deviate from synchronous fluctuations more frequently than bobwhite (SI 7), possibly due to their reproductive plasticity relative to bobwhite's defined breeding season. Cotton rats' natural history facilitates opportunistic breeding when environmental conditions are favorable (Linzey, 1998), while bobwhite are restricted to a defined breeding season (Stoddard, 1931). Accordingly, although exogenous factors appeared to influence the population dynamics of each species individually and the proportions of concurrent maxima and minima were substantial across sites, there was not a strong relationship between synchrony and exogenous factors. However, it is important to note that we did not observe the extreme weather events that commonly support Moran (1953).

While both populations were positively associated with one another, only cotton rats were influenced by the interaction of relative synchrony and bobwhite density (Table 4). Numerous observational studies have suggested that cotton rats positively influence bobwhite density through generalist predators switching their prey selection (Staller et al., 2005; Ellis-Felege et al., 2017; Palmer et al., 2019). Predation by birds of prey and mammals is the leading cause of bobwhite mortality at all life stages (Burger et al., 1995; Rollins and Carroll, 2001; Cox et al., 2004). Similarly, avian and mammalian predators account for the majority of mortalities of adult cotton rats (Morris et al., 2011; McCampbell et al., 2023). Moreover, seasonal predation pressure has been shown to considerably alter both cotton rat (Wiegert, 1972) and bobwhite populations (Carroll et al., 2007). We found that as synchrony between bobwhite and cotton rats increases, the positive association of bobwhite density on cotton rat density declines, possibly due to prey switching by predators when both species populations are at relatively high densities. This differs from the trophic interactions commonly attributed to synchrony in taxonomically divergent primary consumer species. The alternative prey hypothesis (APH) suggests that predators are selective and synchronize prey population densities by depredating their primary prey (i.e., numerically dominant) until its population declines before switching to an alternative prey and instigating its decline (Hagen, 1952; Lack, 1954; Angelstam et al., 1984). We have no evidence that the generalist predators in our system are selective (Godbois et al., 2003; Cherry et al., 2016; Rectenwald et al., 2021), and if the APH was occurring, we would expect an inverse relationship between prey densities. As cotton rat densities are reduced by predation, bobwhite density would increase to synchronize with cotton rat densities (Angelstam et al., 1984). However, we observed periods of elevated synchrony after years of both increasing and decreasing cotton rats.

Another explanation of trophic interactions is the shared predator hypothesis which posits that predators can synchronize prey species populations through indiscriminate predation of primary and alternate prey to cause simultaneous increases and declines (Norrdahl and Korpimäki, 2000). Synchrony seemed to occur after years of both increasing and decreasing cotton rats; however, these associations were inconsistent. Under the shared predator hypothesis, we would also expect that alternative prey (e.g., bobwhite) and primary prey (e.g., cotton rat) would consistently decline after spikes in the population of the numerically dominant prey, which should facilitate increased predator activity and encounter rates (Bety et al., 2002; Ježková et al., 2014); however, we did not see evidence of this pattern either (Ydenberg, 1987; Ims and Steen, 1990).

Without a clear mechanistic explanation of the patterns in our data, we propose an alternative climate- mediated predation framework for understanding the linkages of prey in complex predator–prey systems with numerous non-selective predators. First, in keeping with classic bottom-up theories of regulation (White, 1978; Hunter and Price, 1992), exogenous conditions influence the populations of each prey species *via* availability of resources (Meserve et al., 2001; Meserve et al., 2009). Next, population fluctuations of the numerically dominant prey changes predator communities. Finally, changes in the predator community alter the predation risk and populations of species with the same predators in a manner consistent with the shared predator hypothesis. While this hypothesis needs to be tested, there is substantial support for its components, 1) fluctuations of numerically dominant prey are closely linked to climate-induced changes in resources (Lima et al., 1999; Ernest et al., 2000), 2) fluctuations of numerically dominate prey are tied to changes in populations and communities of their predators (Post and Forchhammer, 2002; Beaugrand et al., 2009; Turkia et al., 2020), and 3) changes in predator communities alter the population demographics of species with the same predators (Rooney et al., 2006; Stoessel et al., 2019; Quéroué et al., 2021). This framework (Figure 7) is more consistent with many patterns of our data than existing constructs.

Although we used data from three sites across 15 years, our study had several limitations which should be noted. Most importantly, because of the coarse spatial and temporal

10.3389/fevo.2023.1159464

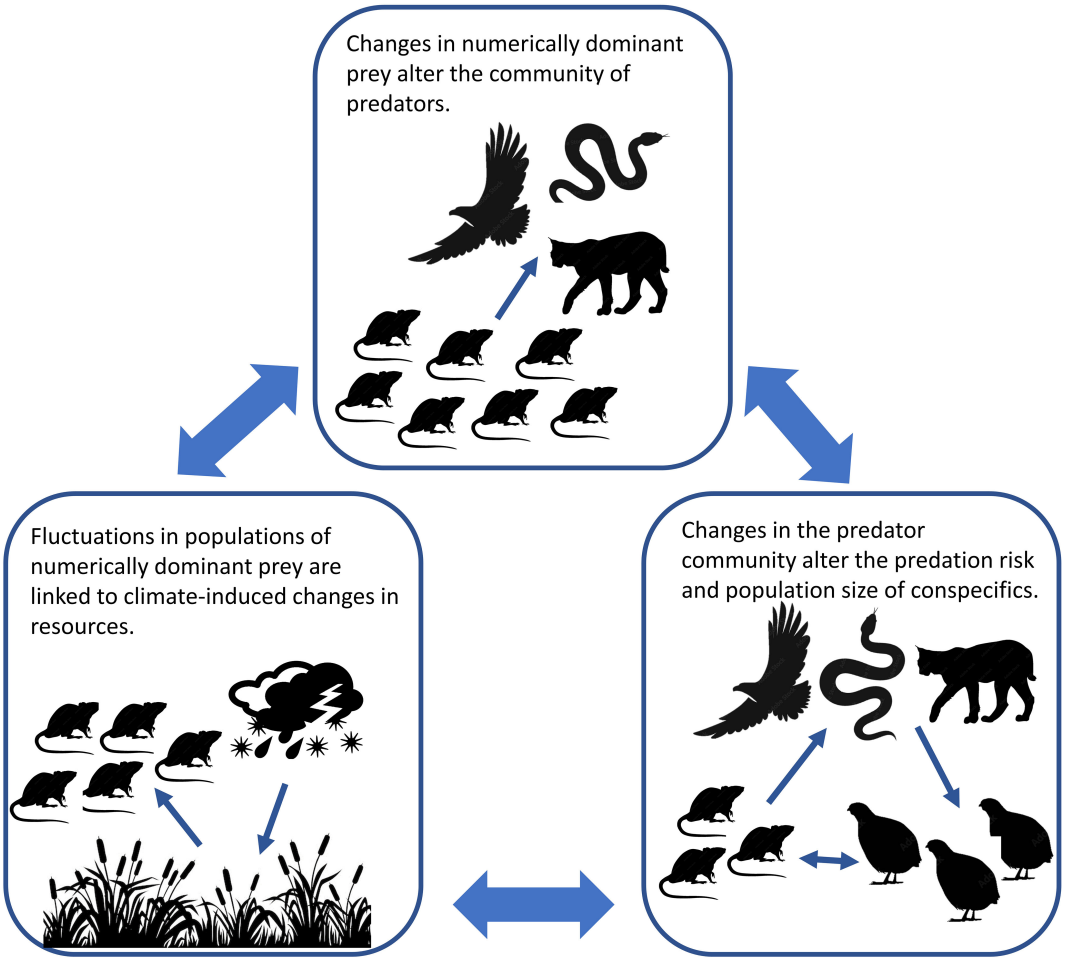

FIGURE 7
Climate-mediated predation framework proposed to explain the simultaneous interactions of the environment, predators, and prey species in ecosystems with numerous non-selective predators.

resolution (i.e., annual) of our population and remote sensing data, the patterns in our data might change at more biologically relevant temporal and spatial scales that more closely track species' interactions. Another important caveat was that cotton rat and bobwhite population data were collected in different areas of each study site, which may have inadvertently influenced our findings as the species were not experiencing the same microclimatic conditions. Moreover, while annual population density data were collected at times of peak density, our sampling occurred at slightly different seasons for each species, potentially limiting our ability to detected linkages between them. Both species have an average lifespan of approximately 6 months (Brennan, 1999; Curlee and Cooper, 2012; McCampbell et al., 2023), suggesting limited annual carryover of population densities; however, we did not investigate this assumption with the inclusion of time lags. Additionally, without data on predator density we were unable to fully investigate the drivers of bobwhite and cotton rat population fluctuations. Although cotton rats are the most commonly trapped small mammal at these sites, they are not the only small mammals in these systems. Fluctuations in other small mammal populations, most notably *Peromyscus gossypinus* (cotton mouse) and *Mus musculus* (house mouse) may have influenced our results and therefore these populations should be acknowledged and accounted for in future studies. Another concern was the variation in population data collection, especially bobwhite density, across sites. While two sites used the same methodology, the assumptions made regarding covey size at the Jones Center may have skewed the data and influenced the results. Lastly, our lack of strong effects may have been influenced by the removal or mesomammalian predators and supplemental feeding that occurred across all sites and throughout the study. Although we have identified factors associated with synchrony within our dataset, further investigation should aim to collect population and predator data on finer spatial and temporal scales to capture the within-year variation in population fluctuations.

While a climate-mediated predation framework may provide a better explanation of the fluctuation patterns in populations of taxonomically divergent primary consumers in complex food webs, there is considerable work that needs to be done before attributing mechanisms to these patterns. Specifically, we suggest two important steps to determine the applicability of this construct. First, there is a need to link survival, cause-specific mortality, predator populations, and specific resources (i.e., vegetation characteristics, food availability) to the annual fluctuations of primary and alternative prey species. To do this, contrary to the coarse resolution of this study, research will need to investigate these populations on finer spatiotemporal scales that allow for the inference of mechanism. Second, we advocate for manipulations of resources for the numerically dominant prey to determine if they lead to population increases, alter predator communities, and change the predation rate of other prey populations in the system. We present this paper as a foundation to generate a greater understanding of the integral drivers of synchrony within complex systems.

Data availability statement

The raw data supporting the conclusions of this article will be made available by the authors, without undue reservation.

Ethics statement

The animal study was reviewed and approved by Tall Timbers Research Station and Land Conservancy: IACUC permit GB-2001-01-15; the Jones Center at Ichauway: Georgia Department of Natural Resources Scientific collecting permit 1000528068; the private property in Baker County, Georgia: Georgia Department of Natural Resources Scientific collecting permit 1000650622.

Author contributions

KRH: data analysis, study design, manuscript writing. LC: study design, data collection, manuscript editing. SJ: study design, data collection. GM: data collection, manuscript editing. WP: study design, data collection, manuscript editing. BR: study design, data collection. DS: study design, data collection, manuscript editing. TT: data analysis, study design, manuscript editing. SW: study design, data collection, manuscript editing. RM: study design, data analysis, manuscript writing. All authors contributed to the article and approved the submitted version.

Funding

Funding provided by Tall Timbers Research Station and Land Conservancy.

Acknowledgments

The authors thank the numerous interns, staff, and administrative personnel of Tall Timbers Research Station and Land Conservancy, the Jones Center at Ichauway, and the private property in Baker County, Georgia for their assistance in data collection, logistics, and support. Additionally, we would like to thank Drs. Dale Rollins and Brad Kubečka, as well as Rebekah Ruzicka for feedback and review of previous versions of this manuscript.

Conflict of interest

The authors declare that the research was conducted in the absence of any commercial or financial relationships that could be construed as a potential conflict of interest.

Publisher's note

Supplementary material

The Supplementary Material for this article can be found online at: https://www.frontiersin.org/articles/10.3389/fevo.2023.1159464/full#supplementary-material

References

Akaike, H. (1973). *Information theory as an extension of the maximum likelihood principle–in: second international symposium on information theory*. Eds. B. N. Petrov and F. Csaki (BNPBF Csaki Budapest: Academiai Kiado).

Allison, P. D. (1999). *Multiple regression: a primer* (Newbury Park, CA: Pine Forge Press).

Allstadt, A. J., Liebhold, A. M., Johnson, D. M., Davis, R. E., and Haynes, K. J. (2015). Temporal variation in the synchrony of weather and its consequences for spatiotemporal population dynamics. *Ecology* 96, 2935–2946. doi: 10.1890/14-1497.1

Andrewartha, H. G., and Birch, L. C. (1954). *The distribution and abundance of animals* (Chicago, IL: University of Chicago Press).

Angelstam, P., Lindström, E., and Widén, P. (1984). Role of predation in short-term population fluctuations of some birds and mammals in fennoscandia. *Oecologia* 62, 199–208. doi: 10.1007/BF00379014

Barrett, G. W., Peles, J. D., and Bowne, D. R. (2001). Predation on the hispid cotton rat (Sigmodon hispidus) by snakes and owls. *Georgia J. Sci.* 59, 94–100.

Beaugrand, G., Luczak, C., and Edwards, M. (2009). Rapid biogeographical plankton shifts in the north Atlantic ocean. *Global Change Biol.* 15, 1790–1803. doi: 10.1111/j.1365-2486.2009.01848.x

Bellamy, P. E., Rothery, P., and Hinsley, S. A. (2003). Synchrony of woodland bird populations: the effect of landscape structure. *Ecography* 26, 338–348. doi: 10.1034/j.1600-0587.2003.03457.x

Bety, J., Gauthier, G., Korpimaki, E., and Giroux, J. F. (2002). Shared predators and indirect trophic interactions: lemming cycles and arctic-nesting geese. *J. Anim. Ecol.*, 88–98. doi: 10.1046/j.0021-8790.2001.00581.x

Bjørnstad, O. N., Ims, R. A., and Lambin, X. (1999). Spatial population dynamics: analyzing patterns and processes of population synchrony. *Trends Ecol. Evol.* 14, 427–432. doi: 10.1016/S0169-5347(99)01677-8

Borgmann-Winter, B. W., Oggenfuss, K. M., and Ostfeld, R. S. (2021). Blacklegged tick population synchrony between oak forest and non-oak forest. *Ecol. Entomol.* 46, 827–833. doi: 10.1111/een.13019

Brennan, L. (1999). Northern bobwhite. *Birds North America* 397, 1–28.

Brennan, L. A., Hernández, F., and Williford, D. (2014). *Northern bobwhite (Colinus virginianus). version 2.0. the birds of north America*. Ed. A. F. Poole (Ithaca, New York: Cornell Lab of Ornithology).

Brewer, R. (1988). *The science of ecology* (Fort Worth: Saunders College).

Burger, L. W.Jr., Dailey, T. V., Kurzejeski, E. W., and Ryan, M. R. (1995). Survival and cause-specific mortality of northern bobwhite in Missouri. *J. Wildlife Manage.* 59, 401–410. doi: 10.2307/3808954

Burnham, K. P., and Anderson, D. R. (1998). "Practical use of the information-theoretic approach," in *Model selection and inference* (New York, NY: Springer), 75–117.

Burnham, K. P., and Anderson, D. R. (2002). *Model selection and multimodel inference: a practical information-theoretical approach* (New York, NY: Springer-Verlag).

Burnham, K. P., and Anderson, D. R. (2004). Multimodel inference: understanding AIC and BIC in model selection. *Sociol Methods Res.* 33, 261–304. doi: 10.1177/0049124104268644

Burrows, M. T., Moore, J. J., and James, B. (2002). Spatial synchrony of population changes in rocky shore communities in Shetland. *Mar. Ecol. Prog. Series* 240, 39–48. doi: 10.3354/meps240039

Cameron, G. N. (1999). "Sigmodon hispidus," in *North American I mammals*. Eds. D. Wilson and S. Ruff. (Washington, DC: Smithsonian Institute).

Campbell-Kissock, L., Blankenship, L. H., and Stewart, J. (1985). Plant and animal foods of bobwhite and scaled quail in southwest Texas. *Southwestern Nat.* 30, 543–553. doi: 10.2307/3671048

Carroll, J. P., Ellis-Felege, S. N., and Palmer, W. E. (2007). Impacts of predators on northern bobwhites in the southeast. *Trans. North Am. Wildlife Natural Resour. Conf.* 72, 246–257.

Cavanaugh, D. C., and Marshall, J. D. Jr. (1972). The influence of climate on the seasonal prevalence of plague in the republic of Vietnam. *J. Wildlife Dis.* 8, 85–94. doi: 10.7589/0090-3558-8.1.85

Chapman, R. N. (1928). The quantitative analysis of environmental factors. *Ecology* 9, 111–122. doi: 10.2307/1929348

Cherry, M. J., Turner, K. L., Howze, M. B., Cohen, B. S., Conner, L. M., and Warren, R. J. (2016). Coyote diets in a longleaf pine ecosystem. *Wildlife Biol.* 22, 64–70. doi: 10.2981/wlb.00144

Cooch, E., and White, G. (2012). *A gentle introduction to program mark* (Fort Collins: Colorado State University).

Coulson, T., Rohani, P., and Pascual, M. (2004). Skeletons, noise and population growth: the end of an old debate? *Trends Ecol. Evol.* 19, 359–364. doi: 10.1016/j.tree.2004.05.008

Cox, S. A., Peoples, A. D., DeMaso, S. J., Lusk, J. J., and Guthery, F. S. (2004). Survival and cause-specific mortality of northern bobwhites in western Oklahoma. *J. Wildlife Manage.* 68, 663–671. doi: 10.2193/0022-541X(2004)068[0663:SACMON]2.0.CO;2

Curlee, J. F., and Cooper, D. M. (2012). *Cotton rat. the laboratory rabbit, Guinea pig, hamster, and other rodents* (London: Academic Press), 1105–1113.

Davenport, J. M., and Chalcraft, D. R. (2012). Evaluating the effects of trophic complexity on a keystone predator by disassembling a partial intraguild predation food web. *J. Anim. Ecol.* 81, 242–250. doi: 10.1111/j.1365-2656.2011.01906.x

De Roos, A. M., McCauley, E., and Wilson, W. G. (1991). Mobility versus density-limited predator-prey dynamics on different spatial scales. proceedings of the royal society of London. *Ser. B.: Biol. Sci.* 246, 117–122. doi: 10.1098/rspb.1991.0132

DeVos, T., and Mueller, B. S. (1993). "Reproductive ecology of northern bobwhite in north Florida," in *Quail III: national quail symposium*. Eds. K. E. Church and T. V. Dailey (Kansas Department of Wildlife and Parks, Pratt), 83–90.

Didan, K. (2015). *MOD13Q1 MODIS/Terra vegetation indices 16-day L3 global 250m SIN grid V006* (NASA EOSDIS Land Processes DAAC), 10. doi: 10.5067/MODIS/MOD13Q1.006

Eifler, M. A., and Slade, N. A. (1999). Effect of weather on individual growth rates in cotton rats, sigmodon hispidus. *J. Mammal* 80, 1277–1287. doi: 10.2307/1383178

Elton, C. S. (1949). Population interspersion: an essay on animal community patterns. *J. Ecol.* 37, 1–23. doi: 10.2307/2256726

Ellis-Felege, S., Albeke, S. E., Nibbelink, N. P., Conroy, M. J., Sisson, D. C., Palmer, W. E., et al. (2017). Landscape features affecting northern bobwhite predator-specific nest failures in southeastern USA. *Natl. Quail Symposium Proc.* 8, 89.

Ernest, S. M., Brown, J. H., and Parmenter, R. R. (2000). Rodents, plants, and precipitation: spatial and temporal dynamics of consumers and resources. *Oikos* 88, 470–482. doi: 10.1034/j.1600-0706.2000.880302.x

Errington, P. L., and Stoddard, H. L. (1938). Modifications in predation theory suggested by ecological studies of the bobwhite quail. *Transactions of the north American wildlife and natural resources conference* 3, 736–740.

Fleharty, E. D., and Olson, L. E. (1969). Summer food habits of microtus ochrogaster and sigmodon hispidus. *J. Mammal* 50, 475–486. doi: 10.2307/1378774

Fox, J., Weisberg, S., Price, B., Adler, D., Bates, D., Baud-Bovy, G., et al. (2019) *Car: companion to applied regression. r package version 3.0-2*. Available at: https://CRAN.R-project.org/package=car (Accessed 17 March 2020).

Godbois, I. A., Conner, L. M., and Warren, R. J. (2003). "Bobcat diet on an area managed for northern bobwhite," in *Proceedings of the southeastern association of fish and wildlife agencies*, 57, 228–234.

Goertz, J. W. (1964). The influence of habitat quality upon density of cotton rat populations. *Ecol. Monogr.* 34, 359–381. doi: 10.2307/2937068

Goertz, J. W. (1965). Reproductive variation in cotton rats. *Am. Midland Nat.* 74, 329–340. doi: 10.2307/2423263

Gouhier, T. C., and Guichard, F. (2014). Synchrony: quantifying variability in space and time. *Methods Ecol. Evol.* 5, 524–533. doi: 10.1111/2041-210X.12188

Gurney, W. S. C., Veitch, A. R., Cruickshank, I., and McGeachin, G. (1998). Circles and spirals: population persistence in a spatially explicit predator–prey model. *Ecology* 79, 2516–2530. doi: 10.1890/0012-9658(1998)079[2516:CASPPI]2.0.CO;2

Hagen, Y. (1952). *Rovfuglene Og Viltpleien. 1st Edition* (Gyldendal, Oslo, Norway In Norwegian).

Hannon, C. L. (2006). *Hispid cotton rat (Sigmodon hispidus) ecology in north florida. thesis* (Athens, GA: University of Georgia).

Hernández, F., Hernández, F., Arredondo, J. A., Bryant, F. C., Brennan, L. A., and Bingham, R. L. (2005). Influence of precipitation on demographics of northern bobwhites in southern Texas. *Wildlife Soc. Bull.* 33, 1071–1079. doi: 10.2193/0091-7648(2005)33[1071:IOPODO]2.0.CO;2

Huete, A. R., Didan, K., Shimabukuro, Y. E., Ratana, P., Saleska, S. R., Hutyra, L. R., et al. (2006). Amazon Rainforests green-up with sunlight in dry season. *Geophysical Res. Lett.* 33, 1–4. doi: 10.1029/2005GL025583

Huggins, R. M. (1989). On the statistical analysis of capture experiments. *Biometrika* 76, 133–140. doi: 10.1093/biomet/76.1.133

Hunter, M. D., and Price, P. W. (1992). Playing chutes and ladders: heterogeneity and the relative roles of bottom-up and top-down forces in natural communities. *Ecology* 73, 724–732. doi: 10.2307/1940152

Hurrell, J. W. (1995). Decadal trends in the north Atlantic oscillation: regional temperatures and precipitation. *Science* 269, 676–679. doi: 10.1126/science.269.5224.676

Ims, R. A., and Steen, H. (1990). Geographical synchrony in microtine population cycles: a theoretical evaluation of the role of nomadic avian predators. *Oikos* 57, 381–387. doi: 10.2307/3565968

Jackson, A. (1962). A pattern to population oscillations of the bobwhite quail in the lower plains grazing ranges of northwest Texas. *Proc. Southeastern Assoc. Game Fish. Commissioners* 16, 120–126.

Janke, A. K., Gates, R. J., and Wiley, M. J. (2013). Covey membership and size dynamics in a low-density population of northern bobwhites. *Wilson J. Ornithol.* 125, 833–840. doi: 10.1676/13-062.1

Ježková, M., Svobodová, J., and Kreisinger, J. (2014). Dynamics of rodent abundance and ground-nest predation risks in forest habitats of central Europe: no evidence for the alternative prey hypothesis. *Folia Zool.* 63, 269–280. doi: 10.25225/fozo.v63.i4.a6.2014

Jones, J., Doran, P. J., and Holmes, R. T. (2003). Climate and food synchronize regional forest bird abundances. *Ecology* 84, 3024–3032. doi: 10.1890/02-0639

Kendall, B. E., Bjørnstad, O. N., Bascompte, J., Keitt, T. H., and Fagan, W. F. (2000). Dispersal, environmental correlation, and spatial synchrony in population dynamics. *Am. Nat.* 155, 628–636. doi: 10.1086/303350

Koenig, W. D. (2001). Synchrony and periodicity of eruptions by boreal birds. *Condor* 103, 725–735. doi: 10.1093/condor/103.4.725

Koenig, W. D., and Liebhold, A. M. (2016). Temporally increasing spatial synchrony of north American temperature and bird populations. *Nat. Climate Change* 6, 614–617. doi: 10.1038/nclimate2933

Krebs, C. J. (1985). *Do changes in spacing behaviour drive population cycles in small mammals? in behavioural ecology*. Eds. R. M. Sibly and R. H. Smith (Oxford: Blackwell Scientific Publications).

Krebs, C. J., Kielland, K., Bryant, J., O'Donoghue, M., Doyle, F., McIntyre, C., et al. (2013). Synchrony in the snowshoe hare (Lepus americanus) cycle in northwestern north america 1970–2012. *Can. J. Zool.* 91, 562–572. doi: 10.1139/cjz-2013-0012

Laake, J. L. (2013). RMark: an r interface for analysis of capture-recapture data with MARK. *Alaska Fish. Sci. Cent., NOAA, Natl. Mar. Fish. Serv.* (Seattle, WA).

Lack, D. (1954). *The natural regulation of animal numbers. the natural regulation of animal numbers* (Oxford: Clarendon Press).

Landis, J. R., and Koch, G. G. (1977). The measurement of observer agreement for categorical data. *Biometrics* 33, 159. doi: 10.2307/2529310

Lee, A. M., Sæther, B. E., and Engen, S. (2020). Spatial covariation of competing species in a fluctuating environment. *Ecology* 101, e02901. doi: 10.1002/ecy.2901

Legendre, P. (2005). Species associations: the Kendall coefficient of concordance revisited. *J. Agricult. Biol. Environ. Stat* 10, 226–245. doi: 10.1198/108571105X46642

Liebhold, A., Koenig, W. D., and Bjørnstad, O. N. (2004). Spatial synchrony in population dynamics. *Annu. Rev. Ecol. Evolutionary Systems* 35, 467–490. doi: 10.1146/annurev.ecolsys.34.011802.132516

Lima, M., Marquet, P. A., and Jaksic, F. M. (1999). El Niño events, precipitation patterns, and rodent outbreaks are statistically associated in semiarid Chile. *Ecography* 22, 213–218. doi: 10.1111/j.1600-0587.1999.tb00470.x

Linzey, D. (1998). *The mammals of Virgina* (Blacksburg, VA: The McDonald and Woodward Publishing Company).

Lusk, J. J., Guthery, F. S., and DeMaso, S. J. (2001). Northern bobwhite (Colinus virginianus) abundance in relation to yearly weather and long-term climate patterns. *Ecol. Model.* 146, 3–15. doi: 10.1016/S0304-3800(01)00292-7

Lynch, J., Gholson, A., and Baker, W. (1986). *Natural features inventory of ichauway plantation, georgia. volume I* (Chapel Hill, NC: The Nature Conservancy Southeast Regional Office).

Brooks, M.E., Kristensen, K., van Benthem, K.J., Magnusson, A., Berg, C.W., Nielsen, A., et al. (2017). glmmTMB Balances Speed and Flexibility Among Packages for Zero-inflated Generalized Linear Mixed Modeling. *The R Journal* 9 (2), 378. doi: 10.32614/RJ-2017-066

McCampbell, M. E., Hunter, M. E., Stechly, J. V., Leist, K. N., Hart, K., and McCleery, R. A. (2023). Compensatory mortality explains rodent resilience to an invasive predator. *J. Mammal*, gyad043. doi: 10.1093/jmammal/gyad043

Meserve, P. L., Gutiérrez, J. R., Kelt, D. A., Previtali, M. A., and Milstead, W. B. (2009). *Global climate change and biotic-abiotic interactions in the northern Chilean semiarid zone: potential long-term consequences of increased El ninos. ocean circulation and El nino* (New York: Nova Science Publishers), 139–162.

Meserve, P. L., Milstead, W. B., and Gutiérrez, J. R. (2001). Results of a food addition experiment in a north-central Chile small mammal assemblage: evidence for the role of "bottom-up" factors. *Oikos* 94, 548–556. doi: 10.1034/j.1600-0706.2001.940316.x

Michel, N. L., Smith, A. C., Clark, R. G., Morrissey, C. A., and Hobson, K. A. (2016). Differences in spatial synchrony and interspecific concordance inform guild-level population trends for aerial insectivorous birds. *Ecography* 39, 774–786. doi: 10.1111/ecog.01798

Miller, W. E., and Epstein, M. E. (1986). Synchronous population fluctuations among moth species (Lepidoptera). *Environ. Entomol.* 15, 443–447. doi: 10.1093/ee/15.3.443

Moran, P. A. (1953). The statistical analysis of the Canadian lynx cycle. *Aust. J. Zool.* 1, 291–298. doi: 10.1071/ZO9530291

Morris, G., Hostetler, J. A., Conner, L. M., and Oli, M. K. (2011). Effects of prescribed fire, supplemental feeding, and mammalian predator exclusion on hispid cotton rat populations. *Oecologia* 167, 1005–1016. doi: 10.1007/s00442-011-2053-6

Myers, R. A., Mertz, G., and Bridson, J. (1997). Spatial scales of interannual recruitment variations of marine, anadromous, and freshwater fish. *Can. J. Fish. Aquat. Sci.* 54, 1400–1407. doi: 10.1139/f97-045

NCEI (2020). *Global monthly summaries of temperature and precipitation* (15 January 2020). https://ncei.noaa.gov/access

Nordberg, E. J., and Schwarzkopf, L. (2019). Predation risk is a function of alternative prey availability rather than predator abundance in a tropical savanna woodland ecosystem. *Sci. Rep.* 9, 1–11. doi: 10.1038/s41598-019-44159-6

Norrdahl, K., and Korpimäki, E. (2000). Do predators limit the abundance of alternative prey? experiments with vole-eating avian and mammalian predators. *Oikos* 91, 528–540. doi: 10.1034/j.1600-0706.2000.910315.x

Oksanen, J., Blanchet, F. G., Kindt, R., Legendre, P., Minchin, P. R., O'hara, R. B., et al. (2022). vegan: Community Ecology Package_. *R package version 2.6-2*. https://CRAN.R-project.org/package=vegan.

Otis, D. L., Burnham, K. P., White, G. C., and Anderson, D. R. (1978). Statistical inference from capture data on closed animal populations. *Wildlife Monogr.* 62, 3–135.

Palmer, W. E., Sisson, D. C., Wellendorf, S. D., Bostick, A. M., Terhune, T. M., and Crouch, T. L. (2012). Habitat selection by northern bobwhite broods in pine savanna ecosystems. *National Quail Symposium Proceedings* 7 (1), 70.

Palmer, W. E., Carroll, J. P., Sisson, D. C., Wellendorf, S. D., Terhune, T. M., Ellis-Felege, S. N., et al. (2019). Reduction in meso-mammal nest predators improves northern bobwhite demographics. *J. Wildlife Manage.* 83 (3), 646–656.

Perez, R. M., Gallagher, J. F., and Frisbie, M. C. (2002). "Fine scale influence of weather on northern bobwhite abundance, breeding success, and harvest in south Texas," in *Quail V: proceedings of the fifth national quail symposium*. Eds. S. J. DeMaso, W. P. Kuvlesky Jr, F. Hernandez and M. E. Berger (Austin, TX: Texas Parks and Wildlife Department), 106–110.

Post, E., and Forchhammer, M. C. (2002). Synchronization of animal population dynamics by largescale climate. *Nature* 420, 168–171. doi: 10.1038/nature01064

Quéroué, M., Barbraud, C., Barraquand, F., Turek, D., Delord, K., Pacoureau, N., et al. (2021). Multispecies integrated population model reveals bottom-up dynamics in a seabird predator–prey system. *Ecol. Monogr.* 91, 01459. doi: 10.1002/ecm.1459

Raimondo, S., Liebhold, A. M., Strazanac, J. S., and Butler, L. (2004a). Population synchrony within and among Lepidoptera species in relation to weather, phylogeny, and larval phenology. *Environ. Entomol.* 29, 96–105. doi: 10.1111/j.0307-6946.2004.00579.x

Raimondo, S., Turcáni, M., Patoèka, J., and Liebhold, A. M. (2004b). Interspecific synchrony among foliage-feeding forest Lepidoptera species and the potential role of generalist predators as synchronizing agents. *Oikos* 107, 462–470. doi: 10.1111/j.0030-1299.2004.13449.x

Ranta, E., Kaitala, V., Lindström, J., and Helle, E. (1997). The Moran effect and synchrony in population dynamics. *Oikos* 78, 136–142. doi: 10.2307/3545809

Ranta, E., Kaitala, V., and Lundberg, P. (1998). Population variability in space and time: the dynamics of synchronous population fluctuations. *Oikos* 83, 376–382. doi: 10.2307/3546852

R Core Team (2021) *R: a language and environment for statistical computing. r foundation for statistical computing, Vienna, Austria*. Available at: https://www.R-project.org/.

Rectenwald, J. A., Bellier, E., Sisson, D. C., Terhune, T. M., and Martin, J. A. (2021). Top–down effects of raptor predation on northern bobwhite. *Oecologia* 197, 143–155. doi: 10.1007/s00442-021-04995-8

Reed, A. W., and Slade, N. A. (2006). Demography and environmental stochasticity: empirical estimates of cotton rat survival. *J. Mammal* 87, 433–439. doi: 10.1644/05-MAMM-A-131R2.1

Rehmeier, R. L., Kaufman, G. A., Kaufman, D. W., and McMillan, B. R. (2005). Long-term study of abundance of the hispid cotton rat in native tallgrass prairie. *J. Mammal* 86, 670–676. doi: 10.1644/1545-1542(2005)086[0670:LSOAOT]2.0.CO;2

Robertson, G. S., Bolton, M., Morrison, P., and Monaghan, P. (2015). Variation in population synchrony in a multi-species seabird community: response to changes in predator abundance. *PloS One* 10, e0131543. doi: 10.1371/journal.pone.0131543

Rollins, D., and Carroll, J. P. (2001). Impacts of predation on northern bobwhite and scaled quail. *Wildlife Soc. Bull.* 29, 39–51.

Rooney, N., McCann, K., Gellner, G., and Moore, J. C. (2006). Structural asymmetry and the stability of diverse food webs. *Nature* 442, 265–269. doi: 10.1038/nature04887

Royama, T. (1992). *Analytical population dynamics. vol. 10. population and community biology series* (London: Chapman & Hall).

Schnell, J. H. (1968). The limiting effects of natural predation on experimental cotton rat populations. *J. Wildlife Manage.* 32, 698–711. doi: 10.2307/3799543

Sikes, R. S.Animal Care and Use Committee of the American Society of Mammalogists (2016). 2016 guidelines of the American society of mammalogists for the use of wild mammals in research and education. *J. Mammal* 97, 663–688. doi: 10.1093/jmammal/gyw078

Speake, D. W., and Haugen, A. (1960). Quail reproduction and weather in Alabama. *Proc. Southeastern Assoc. Game Fish. Commissioners* 14, 85–97.

Spiller, D. A., Schoener, T. W., and Piovia-Scott, J. (2016). Predators suppress herbivore outbreaks and enhance plant recovery following hurricanes. *Ecology* 97, 2540–2546. doi: 10.1002/ecy.1523

Staller, E. L., Palmer, W. E., Carroll, J. P., Thornton, R. P., and Sisson, D. C. (2005). Identifying predators at northern bobwhite nests. *J. Wildlife Manage.* 69, 124–132. doi: 10.2193/0022-541X(2005)069<0124:IPANBN>2.0.CO;2

Stenseth, N. C., Chan, K. S., Tavecchia, G., Coulson, T., Mysterud, A., Clutton-Brock, T., et al. (2004). Modelling non–additive and nonlinear signals from climatic noise in ecological time series: Soay sheep as an example. *Proc. R. Soc. London. Ser. B: Biol. Sci.* 271 (1552), 1985–1993.

Stien, A., Ims, R. A., Albon, S. D., Fuglei, E., Irvine, R. J., Ropstad, E., et al. (2012). Congruent responses to weather variability in high arctic herbivores. *Biol. Lett.* 8, 1002–1005. doi: 10.1098/rsbl.2012.0764

Stoddard, H. L. (1931). *The bobwhite quail; its habitats preservation and increase* (New York: Charles Scribner's Sons).

Stoessel, M., Elmhagen, B., Vinka, M., Hellström, P., and Angerbjörn, A. (2019). The fluctuating world of a tundra predator guild: bottom-up constraints overrule top-down species interactions in winter. *Ecography* 42 (3), 488–499. doi: 10.1111/ecog.03984

Sutcliffe, O. L., Thomas, C. D., and Moss, D. (1996). Spatial synchrony and asynchrony in butterfly population dynamics. *J. Anim. Ecol.* 65, 85–95. doi: 10.2307/5702

Terhune, T. M., Palmer, W. E., and Wellendorf, S. D. (2019). Northern bobwhite chick survival and effects of weather. *J. Wildlife Manage.* 83 (4), 963–974.

Thomas, L., Buckland, S. T., Rexstad, E. A., Laake, J. L., Strindberg, S., Hedley, S. L., et al. (2010). Distance software: design and analysis of distance sampling surveys for estimating population size. *J. Appl. Ecol.* 47, 5–14. doi: 10.1111/j.1365-2664.2009.01737.x

Tri, A. N., Hernandez, F., Hewitt, D. G., Kuvlesky, W. P.Jr., and Brennan, L. A. (2012). Effects of carbohydrate-based and protein-carbohydrate rations on wild bobwhite nesting and harvest demographics. *Natl. Quail Symposium Proc.* 7 (1), 68. doi: 10.7290/nqsp0781b2

Turkia, T., Jousimo, J., Tiainen, J., Helle, P., Rintala, J., Hokkanen, T., et al. (2020). Large-Scale spatial synchrony in red squirrel populations driven by a bottom-up effect. *Oecologia* 192, 425–437. doi: 10.1007/s00442-019-04589-5

Wald, A., and Wolfowitz, J. (1943). An exact test for randomness in the non-parametric case based on serial correlation. *Ann. Math. Stat* 14, 378–388. doi: 10.1214/aoms/1177731358

Wellendorf, S. D., and Palmer, W. E. (2005). Investigating the use of covey call point counts to estimate autumn density of northern bobwhites. *Wildlife Biol. Pract.* 1, 140–145. doi: 10.2461/wbp.2005.1.16

Wells, R. (2008). Quail habitat management. *Habitat management for bobwhites: a basic guide for the land manager* (Americus, KS: Quail Unlimited).

White, T. C. (1978). The importance of a relative shortage of food in animal ecology. *Oecologia* 33, 71–86. doi: 10.1007/BF00376997

Wiegert, R. G. (1972). Avian versus mammalian predation on a population of cotton rats. *J. Wildlife Manage.* 36, 1322–1327.

Yates, S. W., Sisson, D. C., Stribling, H. L., and Speake, D. W. (1995). Northern bobwhite brood habitat use in south georgia. *Proceedings of the annual conference of the southeastern association of fish and wildlife agencies* 49. 498–504.

Ydenberg, R. (1987). Nomadic predators and geographic synchrony in microtine population cycles. *Oikos* 50, 270–272. doi: 10.2307/3566014

frontiers | Frontiers in Ecology and Evolution

TYPE Original Research
PUBLISHED 26 July 2023
DOI 10.3389/fevo.2023.1108914

OPEN ACCESS

EDITED BY
Jurek Kolasa,
McMaster University, Canada

REVIEWED BY
Ricardo Martinez-Garcia,
Helmholtz Association of German Research Centers (HZ), Germany
Ning Chen,
Lanzhou University, China

*CORRESPONDENCE
Christelle Hély
christelle.hely@ephe.psl.eu

RECEIVED 26 November 2022
ACCEPTED 05 July 2023
PUBLISHED 26 July 2023

CITATION
Hély C, Shugart HH, Swap RJ and Gaucherel C (2023) The Drape: a new way to characterize ecosystem states, dynamics, and tipping points from process-based models. *Front. Ecol. Evol.* 11:1108914. doi: 10.3389/fevo.2023.1108914

The Drape: a new way to characterize ecosystem states, dynamics, and tipping points from process-based models

Christelle Hély[1,2]*, Herman H. Shugart[3], Robert J. Swap[4] and Cédric Gaucherel[5]

[1]Institut des Sciences de l'Evolution de Montpellier (ISEM), Montpellier University, CNRS, EPHE, IRD, Montpellier, France, [2]EPHE, PSL University, Paris, France, [3]Department of Environmental Sciences, University of Virginia, Charlottesville, VA, United States, [4]Sciences and Exploration Directorate, Goddard Space Flight Center, NASA, Greenbelt, MD, United States, [5]AMAP – INRA, CIRAD, CNRS, IRD, Montpellier University, Montpellier, France

There are many ways to study ecosystem dynamics, all having several issues. Main limitations of differential equation systems are the necessarily small number of interactions between few variables used, and parameter values to be set before the system dynamics can be studied. Main drawbacks of large-scale snapshot observation datasets to build a stability landscape are assuming that the most represented conditions are the most stable states, and using the computed landscape to directly study the system's dynamics. To remedy these aforementioned shortcomings and study complex systems based on the processes that characterize them without having to limit the number of variables, neither set parameter values, nor to use observations serving both model buildup and system's dynamics analysis, we propose a geometric model as an additional and novel aid to study ecosystem dynamics. The Drape is a generic multi-dimensional analysis, derived from process-based model datasets that include disturbances. We illustrate the methodology to apply our concept on a continental-scale system and by using a mechanistic vegetation model to obtain values of state variables. The model integrates long-term dynamics in ecosystem components beyond the theoretical stability and potential landscape representations currently published. Our approach also differs from others that use resolution of differential equation systems. We used Africa as example, representing it as a grid of 9395 pixels. We simulated each pixel to build the ecosystem domain and then to transform it into the Drape – the mean response surface. Then, we applied a textural analysis to this surface to discriminate stable states (flat regions) from unstable states (gradient or crest regions), which likely represent tipping points. Projecting observed data onto the Drape surface allows testing ecological hypotheses, such as illustrated here with the savanna-forest alternative stable states, that are still today debated topics, mainly due to methods and data used. The Drape provides new insights on all ecosystem

types and states, identifying likely tipping points (represented as narrow ridges *versus* stable states across flat regions), and allowing projection and analysis of multiple ecosystem types whose state variables are based on the same three variables.

KEYWORDS

disturbance, multi-dimensional ecological space, response surface, textural analyses, stability, transient states, savannas, tropical forests

1 Introduction

Prediction of ecosystem change under novel conditions is a central issue for ecologists, especially with the apprehension that environmental changes are on multiple scales. A growing number of studies have investigated ecosystem dynamics and their role in planetary function as bases for projecting the Earth's future (e.g. Brook et al., 2013; Hughes et al., 2013a). From theoretical considerations of system dynamics, one may expect sharp changes can be a part of the dynamic ecosystem repertoire (Scheffer et al., 2001; Briske et al., 2010). Such changes have been analyzed for a diverse array of systems ranging from the Earth climate system (e.g. Lenton et al., 2008; Kriegler et al., 2009; Gaucherel and Moron, 2015), to the international financial system, and to terrestrial and aquatic ecosystems (e.g. Davis and Shaw, 2001; Chapin et al., 2004; Folke et al., 2004; Van Nes and Scheffer, 2007; Favier et al., 2012; Hughes et al., 2013a; Conversi et al., 2015; Martin et al., 2020). Such non-linear responses can profoundly affect the dynamics and management of natural systems (Scheffer et al., 2001).

For almost a century (Lotka, 1925; Volterra, 1926) with increased intensity since the 1970s (Holling, 1973; Noy-Meir, 1975; May, 1977; Walker et al., 1981), ecologists have developed models of ecosystem dynamics. Initially, these were for simplified systems such as predator–prey or competition interactions with the numbers of different populations defined as state variables. If needed, other components representing the environment are also defined as equation parameters.

Such models are often based on systems of ordinary differential equations (ODE). Qualitative or more complex models were first more conceptual, such as state-and-transition models (e.g. Ellis and Swift, 1988; Archer, 1989; Westoby et al., 1989). The use of ODE systems makes more tractable (analytically or numerically) the search for stationary points of the system (i.e. equilibria or periodic orbits) in the so-called phase portrait of the state variables, at least for ecosystem representations of small dimensions. One can characterize the equilibrium stability, which depends on the real part of the eigenvalues of the Jacobian matrix (for hyperbolic equilibria). By analyzing the nullclines, manifolds that go through the fixed points on the phase portrait, the behavior of system-dynamic solutions on the state space can be discerned. Ideally, the local stability of the dynamics is guaranteed by a potential function (in blue on Figure 1A), whose time derivative along the solutions of the system is negative, at least locally. If it is not strictly decreasing everywhere, then multiple steady states or periodic orbits occur, as do bifurcation points (i.e. tipping points) and hysteresis (e.g. May, 1977; Sternberg, 2001).

Subsequent studies have advanced in several different directions including: i) determination of leading indicators (also called early warning signal, e.g. Van Nes and Scheffer, 2007; Dakos et al., 2008, 2010; Livina et al., 2010), used to assess the proximity of a system to a tipping point; ii) the role of noise or variability in the system dynamics and intermediate stability creation (e.g. D'Odorico et al., 2005; Dakos et al., 2012); iii) linkage to spatial dynamics and patterns (e.g. van de Koppel et al., 2002; van de Koppel and Rietkerk, 2004; Bel et al., 2012; Kéfi et al., 2014; Ratajczak et al., 2017b); iv) analysis of the response to perturbations of finite magnitude and duration – instead of theoretical developments based on linear stability to infinitesimal perturbations (Ratajczak et al., 2017a) or even the response to continuous stochastic perturbations (Nolting and Abbott, 2016); v) use of space-for-time substitutions and related probability density functions built exclusively from observations in order to infer the potential shape as well as the presence of multiple stable states and tipping points (e.g. Hirota et al., 2011; Staver et al., 2011a; Favier et al., 2012; Scheffer et al., 2012).

Tipping points usually occur in response to a gradual change in a system process (internal and acting on parameter values) or in a system driver (external factor acting on state variables). Under an abrupt change in system state after crossing a tipping point, the system behavior is radically different from that previously observed. Despite intrinsic differences, many dynamic systems display similar early warnings signals prior to the occurrence of a tipping point. These include slowing rates (e.g. Wissel, 1984; Van Nes and Scheffer, 2007), temporal and spatial autocorrelations among system variables (Dakos et al., 2010; Boulton et al., 2013; Kéfi et al., 2014), and fluctuations of the variance increasing up to "flickering" (Wang et al., 2012; Dakos et al., 2013). Active debates regarding tipping points, their nature (Gaucherel et al., 2020), and detection mostly have origins from the catastrophe theory (Thom, 1972).

For global change, terrestrial ecosystem responses are conditioned by many interdependent processes (e.g. Brook et al., 2013; Hughes et al., 2013a). Catastrophic dynamics such as tipping point-events seem relatively rare among ecosystem behaviors. Concepts intending to capture ecosystem dynamics as a whole

10.3389/fevo.2023.1108914

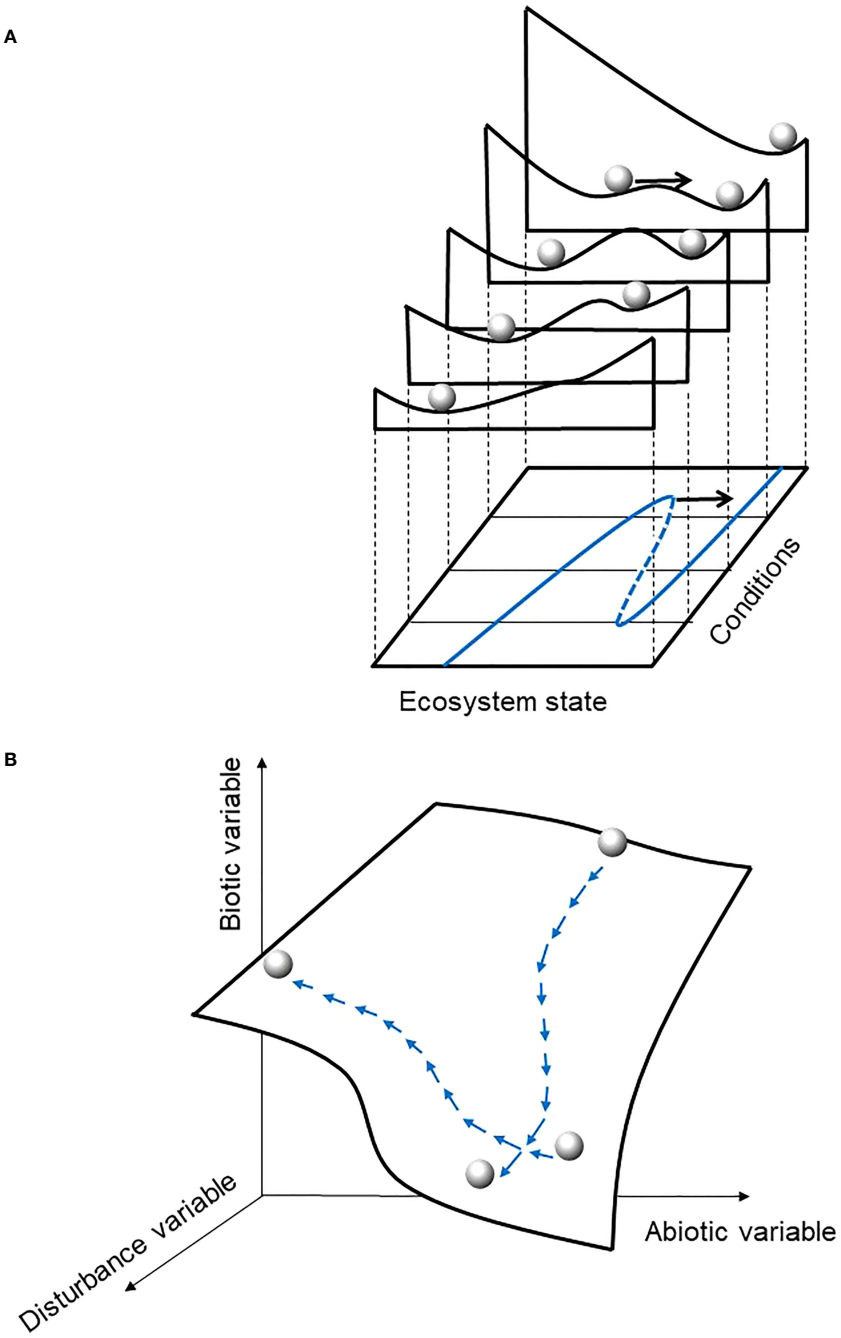

FIGURE 1
Conceptual representations of ecosystem dynamics **(A)** from ordinary differential equation system (adapted from Scheffer et al., 2001) or statistical method based on derivative of probability density function (Hirota et al., 2011; Scheffer et al., 2012) and **(B)** from the present study Drape concept. In both panels, the ball represents the system state at a given time. In **(A)** the black arrow represents a perturbation (disturbance, stochasticity, noise), considered as an external factor, that pushes the system to another place on the stability landscape (a narrow environmental range slice), on the potential landscape (all slices so the full environmental range), and likely to another equilibrium state (valley) if the ball crosses a ridge; the blue line represents the equilibria curve for this system. In panel **(B)**, the perturbation is stochastic and intrinsic to the vegetation model that created the data, and natural disturbance is embedded in the vegetation model and the system definition. The system may move on the Drape when state variable values change (i.e. at least in terms of climate known as an ongoing changing compartment of the system), which is ineluctable through time, even in terms of small changes. Conversely to the potential landscape in **(A)** the Drape topography in **(B)** is not related to the value distribution of each state variable dataset. See Figure 2 for further explanation.

should also account for the wide range of smooth (gradual) and/or relatively stable behaviors often observed in nature (Dutta et al., 2018). Inclusion of the internal processes responsible for the system dynamics, even in a synthetic and simplified way, provides a better understanding of past and current dynamics by making explicit explanations of the processes. Such inclusion can also improve representation and visualization of concepts such as stable, transient, or alternative states, and system trajectories and system

tipping points, if they exist (e.g. Boettiger et al., 2013; Dutta et al., 2018). Nolting and Abbott (2016) showed that to properly detect and study alternative stable states, linear stability analysis, as in traditional deterministic ODE models, is not appropriate to study the potential, thereby necessitating the inclusion of stochasticity.

While using snapshot measurements from extensive datasets is relevant to describe current patterns (e.g. Hirota et al., 2011; Staver et al., 2011a; Scheffer et al., 2012), a number of studies of different ecosystem types and different time scales showed significant discrepancies when testing the space-for-time substitution approach (e.g. Adler and Levine, 2007; Blois et al., 2013). Different observed localities may not have undergone the same historical changes (e.g. disturbance types and regimes), and so, their use in space-for-time analyses may be inappropriate. Interpretations of the underlying ecosystem dynamics (including definitions of equilibria and alternative stable states) should be performed with caution when using the space-for-time substitution approach. This justification is particularly true if these interpretations are not linked to nor validated by a deterministic model, a point wisely suggested by several authors (e.g. Boettiger et al., 2013; Dutta et al., 2018). Fortunately, an increasing number of studies both rely on ecosystem models built with deterministic or stochastic skeletons and then use statistical approaches to compute and test early warning signals, existence of tipping points, and multiple stable states (e.g. Staver et al., 2011b). To analyze the dynamics of a large-scale system, where multiple system states can appear in the studied region as a result of different underlying processes at play, it may be difficult or intractable to rely on a complicated differential equation system. This likely explains why several studies have chosen to statistically analyze observations to differently apprehend the potential and its associated stabilities on the so-called landscape stability (Hirota et al., 2011; Scheffer et al., 2012). This type of applications exhibits several limitations. For instance, the attribution of stable states to the most frequently represented states (and reversely for unstable states) has been criticized (Ratajczak and Nippert, 2012).

From Tansley's (1935) original ecosystem definition, ecosystems are composed of biotic and abiotic components. It would then be logical to expect an ecosystem to include complexities and interactions beyond merely the populations of organisms it contains (e.g. Gignoux et al., 2011; Gaucherel, 2014). While there are a number of current models that account for abiotic processes, most if not all of them significantly simplify these processes: i) abiotic considerations are reduced to a single limiting-nutrient variable or a synthetic single parameter "resource"; ii) natural disturbances are rarely included in the system definition or considered as parameters only (e.g. D'Odorico et al., 2005; Van Nes et al., 2014; Touboul et al., 2018); iii) dynamics depends on the systems perturbation, considered as either a change in the abiotic resource or in the biotic variable resulting from exogenous factor or from intrinsic stochasticity (e.g. Beisner et al., 2003; Bel et al., 2012).

Many authors have used the so-called ball-in-cup analogy (Figure 1A) to illustrate the system (i.e. the ball) and its dynamics, represented as the movement of the ball along the cup-shaped landscape (e.g. Scheffer et al., 2001; Beisner et al., 2003; Nolting and Abbott, 2016). Regarding ecological systems, Beisner et al. (2003) showed that the concept of alternative stable states was initially apprehended by two different schools (the "community perspective" and the "ecosystem perspective", respectively), which can be integrated into a common conceptual framework. From the community perspective, the environment, defined by the state variables and the associated potential and landscape stability, is fixed. Conversely, from the ecosystem perspective, the topology of the environment is not fixed because it depends on the parameter values that may change and, in turn, impact state variables. There is therefore an interest in developing tools that allow integrative understanding and visualization of system dynamics. Moreover, for an applied perspective of managing ecosystems, Beisner et al. (2003) also suggest that we should seek to define the boundaries of desirable stable states, and understand the processes that bring resilience nearby these desirable states.

The present work aims to propose a new concept of understanding ecosystem dynamics, the Drape, designed to circumvent some of the aforementioned limitations. It is designed to explore new and likely more informative avenues to understanding ecosystem dynamics. We propose a novel approach, one that is not based on differential equations, to elucidate ecosystem dynamics, across vast spatial scales able to encompass several ecosystems and biomes. Rather than employing more traditional approaches that rely heavily upon differential equations, we use a mechanistic model (mainly deterministic but with some stochasticity) to extract the main state variables (abiotic, biotic, and disturbance, respectively), from which we build two multidimensional representations of the system (the 3D-domain and the 2D-Drape, respectively). We then perform a textural analysis of the Drape, which characterizes its "topography" (variations) in terms of number of stable, unstable and transient states, and their locations on the Drape. Below, we present the Drape theoretical framework, and then illustrate it with African ecosystems and biomes to test several ecological hypotheses before discussing its benefits and limitations.

2 Materials and methods

2.1 Theoretical framework

2.1.1 General characteristics

Following Tansley's (1935) original definition of the ecosystem as a systems of biotic and abiotic parts and explicitly including disturbances (see Drukenbrod et al. (2019) for a recent review), a minimal ecosystem representation must be multi-dimensional (Figure 1B), with at least three dimensions based on the three most important abiotic, biotic components and disturbance factors (variables), respectively (Gignoux et al., 2011; Gaucherel, 2014). These are the properties of the "conceptual space" used here to capture ecosystem dynamics.

For terrestrial ecosystems, climate conditions are often considered as the main abiotic factor at the continental scale and the vegetation as the main biotic factor. Fire, grazing, or pest outbreak are example of a dominant disturbance (e.g. Pickett and

White, 1985; Johnson, 1992; Scholes and Walker, 1993; Sankaran et al., 2005; Staver et al., 2011b). These three minimal factors may provide the synthetic state variables of the system (Figure 1B). For example: 1) annual rainfall, rainfall seasonality or growth season temperature could serve as proxies for the abiotic factor of climate; 2) biomass, leaf area index or tree cover could serve as proxies for the biotic factor; 3) and frequency or return time interval for the main disturbance factor. This representation considers disturbance to be an endogenous variable, unlike the consideration of disturbance as an exogenous factor if considered as the system perturbation, or simply as a limiting parameter in many studies (e.g. Carpenter et al., 2001; Scheffer et al., 2001; Touboul et al., 2018).

All three variables define the ecosystem. This second property is compulsory in this conceptual space: state variables are fully "symmetric" (i.e. interchangeable). The ecosystem is not (purely) biotic, neither is it abiotic. Consequently, an (eco)system could be represented by any of the six permutations of a 3D-space, considering how each state variable may act on the other two through various feedbacks (Scheffer et al., 2005, 2012; Hirota et al., 2011). While vegetation response is usually analyzed as a function of the climate and of the main disturbance, it may be relevant for example to analyze the ecosystem disturbance as a function of the two other factors, as performed in several paleoecological studies (e.g. Hély et al., 2010, Hély et al., 2020; Ali et al., 2012; Aleman et al., 2013).

To illustrate this new approach, we selected Africa as example because this continent encompasses a wide range of environmental conditions and ecosystem types that are all driven by rainfall as the main abiotic variable and most of them as well by fire as the main natural disturbance. We first focused on testing ecological hypotheses related to the forest and savanna states and transitions (see section 2.1) as this is still an ongoing debated topic due to methods used (e.g., Hirota et al., 2011; Ratajczak and Nippert, 2012; Hanan et al., 2014, Hanan et al., 2015; Staver and Hansen, 2015; Aleman et al., 2020). Therefore, the 3D-space for the African terrestrial tropics has been defined using annual rainfall as the climate axis, aboveground biomass as the vegetation axis, and fire frequency (number of fires per year over a fixed interval, e.g. 500 years) as the disturbance axis (Figure 2A). Fire is indeed a major disturbance in these ecosystems (e.g. Scholes and Walker, 1993; Bond et al., 2005; Staver et al., 2011a). Tropical fires currently shifting from natural to human-induced fires could be included to produce a four-dimensional space with a fourth, human-related state variable (Cincotta et al., 2000), if so desired. Numerous studies indicate for instance that tropical forests and savannas are two dominant states that can coexist under the same environmental conditions (e.g. Sankaran et al., 2005; Staver et al., 2011b; Favier et al., 2012). Alternations from one state to the other presumably reflect changes within the environment. Therefore, a third rule in building our example conceptual space is to consider a spatial extent large enough to encompass broad changes within biomes (different savanna ecosystems based on tree cover changes or grass composition changes (e.g. Ringrose et al., 1998; Scholes et al., 2002)), and between biomes (i.e. regime shifts and/or alternation between savannas and forests). Therefore, thanks to this new approach, we were also able to characterize all other ecosystems (from desert to tropical rainforests) and their states on the Drape based on their location and their neighborhood heterogeneity.

Instead of a purely statistical analyses based on observations (e.g. Hirota et al., 2011; Staver et al., 2011a; Scheffer et al., 2012), the fourth rule is to impose the use of state variables that result from process-explicit models. As in many other ecological studies (e.g. Prentice and Webb III, 1998; Sitch et al., 2008; McMahon et al., 2011), we chose to work with the Lund-Potsdam-Jena General Ecosystem Simulator model (hereafter LPJ-GUESS model, Smith et al., 2001; Hély et al., 2006; Hickler et al., 2012; Chaste et al., 2018), a Dynamic Global Vegetation Model (DGVM, see Supplementary information S1.1) to build the conceptual space of African terrestrial ecosystems.

2.1.2 Building the domain

Once the state variables of the studied domain are identified, their values can be extracted from specific variables that may have been serving as input in the DGVM or have been simulated by it (Hély et al., 2006; Gaucherel et al., 2008) to build the axes of the 3D conceptual space (Figure 2). In this 3D-space, projection of all geographical continental locations (i.e. pixels) through their simulated values at the end of a DGVM run generates the equilibria state hereafter called the domain (Figure 2). See Supplementary information S1.1 and Supplementary Figure S1 for details about how equilibrium state is reached for each geographical location. In general, many DGVM-based studies produce satisfactory assessments of present and past ecosystem component dynamics when compared with independent reconstructions (e.g. Hély et al., 2009; Prentice et al., 2011; Chaste et al., 2018). One can therefore use a DGVM with modern, past, or even future environmental conditions experienced for a given geographic region, such as Africa here, with 20th century climate condition in the current example. The built 3D domain represents a prospective domain that contains all geographic locations for which simulated data can be compared with observed data from present or with reconstructed data from past for exploration and/or validation purposes.

Within the prospective domain, the realized domain is the set of points or cloud that represents the system states (Figures 2A, B) for a given past, present or future set of conditions. The system state is represented at any time by the values of the three state variables. In our example, the cloud is more or less extended on the X–Y plan (e.g. climate-fire), and varies in thickness on the Z-axis (vegetation) mainly according to the Z-values reported by the points (geographic locations) that fit within such domain region.

2.1.3 From the domain to the Drape

For the sake of clarity, and assuming that system states exhibit a reduced range in Z, we replace this point-cloud by a response surface called the Drape. To develop the Drape, a statistical moment (e.g. mean or median) of the Z variable is first computed for each narrow X×Y bin (Figure 2C). Several bin sizes were tested to identify the best trade-off between accuracy and smoothness of the Drape, in particular considering areas with only few cloud points (Wiens, 1989). We checked that any bin size led to the same

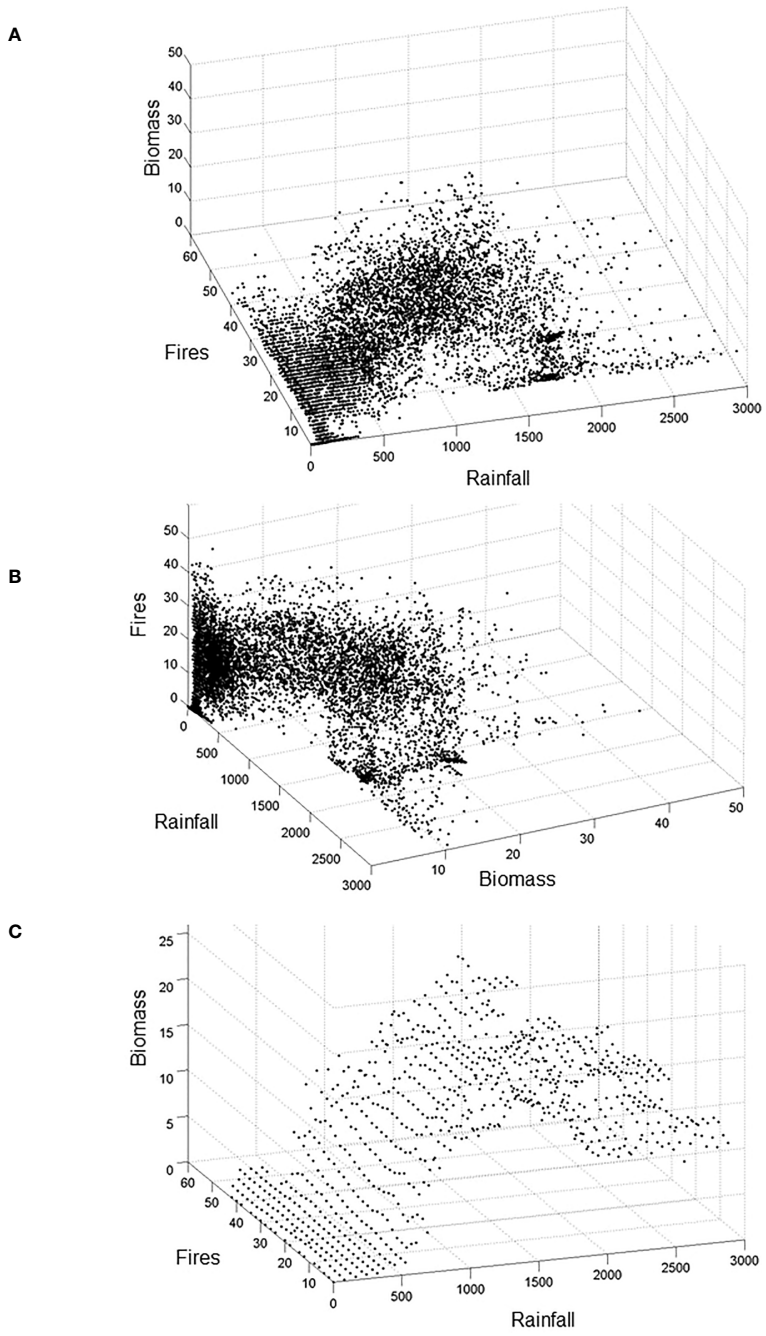

FIGURE 2
Representations of the tropical domain (cloud of points) within the ecosystem 3D-space. This space is defined by annual Rainfall (in mm.year^{-1}), vegetation carbon Biomass (in kg C.m^{-2}), and Fire (i.e. number of significant fires over 500 years, see Supplementary Figure 1B for computation details), each one representing the most important abiotic, biotic, and disturbance state variables of the system, respectively. In this example, each cloud point represents a continental geographical location in Africa for which the LPJ-GUESS Model (Smith et al., 2001; Sitch et al., 2008) has been previously run (Hély et al., 2006; Gaucherel et al., 2008) using modern climate from the CRU time-series datasets (New et al., 2002). Each point represents the equilibrium state reached by the DGVM at that location, such equilibrium being defined by values of the state variables (see Supplementary Figure S1). **(A, B)** illustrate the property of axis symmetry, while **(C)** reports the domain view as in **(A)** but based on averaged Biomass values in bins along Rainfall and Fire axes, which is an intermediate stage between the domain (point cloud) and the Drape.

qualitative features (ridges, valleys…) on the Drape. The smoothed (hyper-)surface (Figure 3A) of the Drape results from the data autocorrelation only. Beyond the Drape construction procedure explained here, one could use the full range of values within bins to test the three proposed hypotheses described in the section below.

The Drape is not a potential function, but it is associated with all possible types rather than with any specific catastrophe type. The computation of the Z-variable variance allows the capture of the inherent variability of the third ecosystem state-variable (the vegetation in Figure 3B) relative to the other two. Compared to

10.3389/fevo.2023.1108914

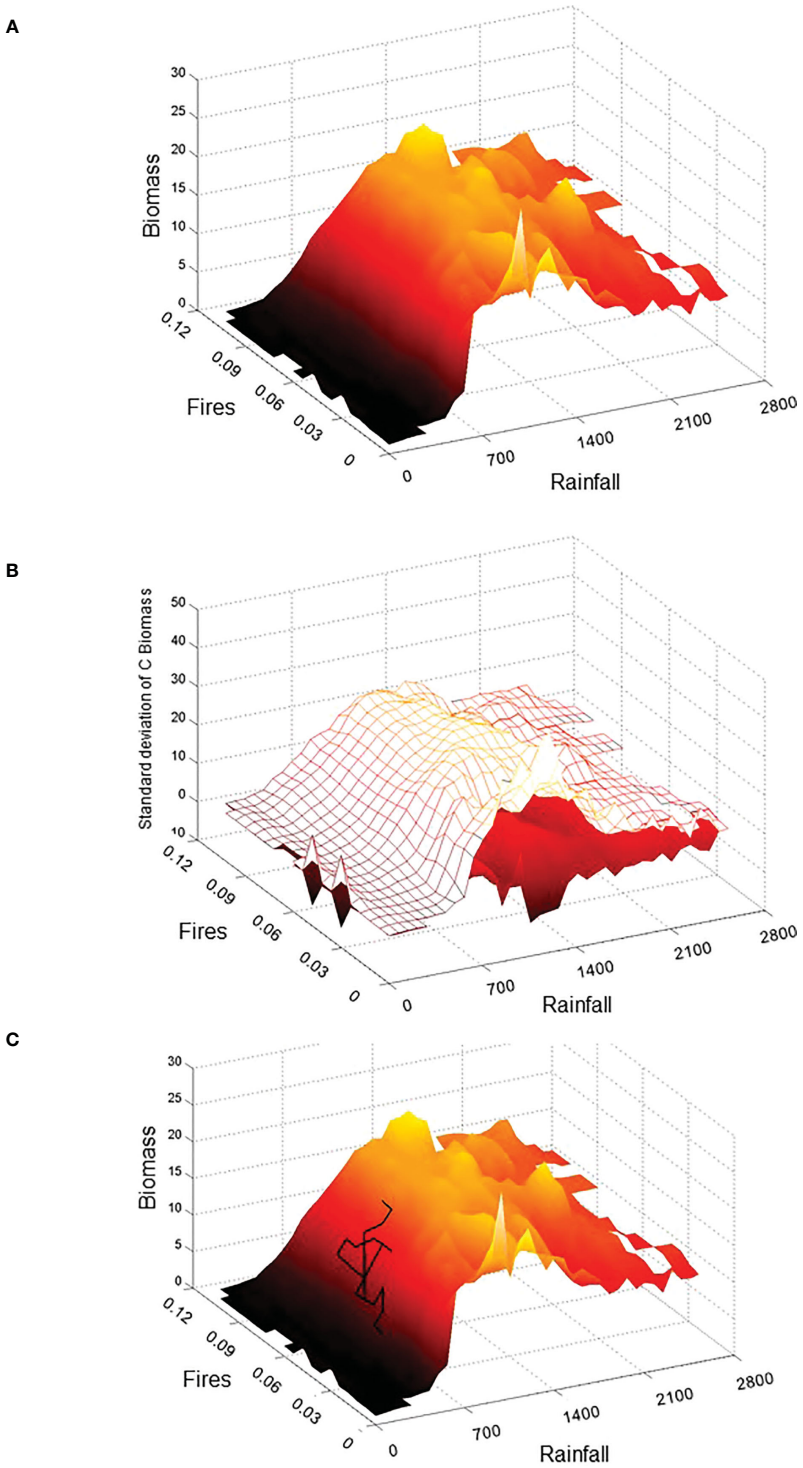

FIGURE 3
3D-representation of the tropical domain through the system Drape based on rasterized bin average biomass values **(A)** and its thickness (i.e. mean $\pm$ 1σ) **(B)**. Axes units relate to annual Rainfall (in mm.year^{-1}), vegetation carbon Biomass (in kg C.m^{-2}), and Fire frequency (i.e. number of fires year^{-1}). A hypothetical trajectory has been superimposed on the Drape for illustrative purpose **(C)**. This trajectory could represent a geographical site and its lacustrine paleoecological reconstruction over the last 9000 years for climate (e.g., based on diatoms, chironomids, speleothems...), fires (e.g. micro-carbons), and vegetation (e.g., pollen, phytoliths, biomarkers...). We could project the chronological states obtained on the Drape, which would constitute the trajectory of this site and we could therefore follow this trajectory to highlight periods when the site has been in a stable state (homogeneous region see Figure 4) or inversely when its dynamics has experienced a major modification symbolized by the passage of the trajectory in a gradient or ridge zone (see Figure 4 for stable and unstable state detection).

the potential landscape from previous studies (Hirota et al., 2011; Scheffer et al., 2012), the neighborhood of each geographical location is lost in our proposed domain and Drape, other than that a location's neighborhood is partially preserved in the spatial autocorrelation of the soil type (Supplementary Figure S2) and climate input data in the DGVM.

2.2 Analysis of the Drape: towards system states, resilience and trajectory understanding

Through the analysis of its heterogeneity, the Drape concept provides rich insights about a particular ecosystem or a biome shift. Using multiscale textural analysis (e.g. Gaucherel, 2007) on a 2D projection of the Drape (Figure 4A, similar to Figure 3A) produces a Drape heterogeneity map (Figure 4B) that can help detect different behaviors of the system. The heterogeneity index used is the evenness diversity index (see Supplementary information S1.2 for details of the computation). The higher the evenness diversity, the more heterogeneous the neighbor pixels on the map. Heterogeneous areas are therefore defined as having a high degree of evenness diversity amongst neighboring pixels (Figure 4B) highlighting statistically significant differences in the averaged biomass between neighboring pixels on the Drape (Figure 4A). Homogeneous areas (plateaus and valleys where neighboring pixels have low relative evenness diversity values) imply stable states and potential basins of attraction to explore through additional tests.

This heterogeneity analysis may seem to be in the same spirit as methods applied for the case of potential landscapes. An increased variance in Z associated with a small change in X or Y, measured as Drape heterogeneity, has utility to distinguish among stable (homogeneous zones), transient (gradients) and unstable (narrow ridges or peaks) behaviors (Briske et al., 2010). Such state characteristics result from the Drape's topography, and not from the dataset value distribution as in the potential landscape concept (Hirota et al., 2011; Scheffer et al., 2012).

2.3 Use of the Drape to test ecological hypotheses

Beyond the presentation of the Drape, the objectives of this study were threefold. The first objective was to test whether the 600–1000 $mm.yr^{-1}$ rainfall range, first proposed to discriminate closed-canopy forests from savannas (Sankaran et al., 2005), could be characterized on the Drape as a specific area such as a ridge or gradient). The second objective was to see whether several savanna types could be highlighted on the Drape due to climate–fire interactions (Hirota et al., 2011; Staver et al., 2011a; Favier et al., 2012) and whether these different types of savanna qualified as different stable states. Finally, the third objective was to test whether savanna and forest stable states would be found close enough to each other on the Drape to be considered as likely, adjacent alternative system states.

We used the dataset from Ruesh and Gibbs (2008) and their reporting of observed ranges of biomass based on climatic zones (IPCC, 2006), Global Ecofloristic Zones (FAO, 2001), and the Global Land Cover 2000 ecosystem classification (Bartholomé and Belward, 2005) to compare with the Drape value ranges.

3 Results and discussion

3.1 From the study-case: African ecosystems and states, and insights from the Drape for ecological hypotheses

The African Drape analysis using the Multiscale Heterogeneity Map method and the computation of the evenness diversity index revealed three homogeneous areas (namely S1, S2, S3 in Figure 4B) that we interpret as stable states, and two heterogeneous areas (the G1 gradient area interpreted as a transient state and the R1 ridge area interpreted as an unstable state in Figure 4B). Based on their African geographic locations (Supplementary Figure S3), we compared the characteristics of each revealed Drape area with those from the compiled observations (Ruesh and Gibbs, 2008) for precipitation, biomass, and ecosystem types (Table 1).

The S1 stable state (Figure 4B) represents the most arid regions with the lowest biomass range (Figure 4A; Table 1). Such characteristics and their associated geographic locations extracted from the LPJ-GUESS simulation (Supplementary Figure S3A), are in agreement with ecosystems from sparse grasslands to shrub-dominated savannas. The S1 biomass range likely matches the lower third of the observed range, because the S1 woody components represent less than 30% (not shown) of the potential C biomass simulated. S1 represents a stable state (a valley) on the Drape constituted by arid and semi-arid grassy biomes. They range from desert to tropical steppes to savannas with low woody cover.

The S2 stable state (Figure 4B) represents a plateau composed of regions with 1300–1800 mm annual rainfall, intermediate fire frequencies, and C biomass that is at least ten times heavier than that found in S1. These characteristics and their geographic locations (Supplementary Figure S3B) match perfectly with the tropical moist deciduous forest and rainforest (Table 1).

The S3 stable state (Figure 4B) having biomass range similar to that of S2 and with more than 2300 mm annual rainfall, is a plateau typified by rainforests (Supplementary Figure S3C). Simulated and observed characteristics of these locations conform with the African tropical wet climate regions (Table 1). While simulated biomasses are slightly lower than the mean observed, their range (Table 1) is in agreement with the full range (8.5–33 $kgC.m^{-2}$) of observed rainforest biomasses. Note that vegetation models predict potential vegetation, so that slightly higher biomass than observed biomass is expected – even from reserves such as national parks in which low intensity management activities still exist.

Among the heterogeneous areas revealed by the multiscale map, R1 represents the most heterogeneous area even after discarding outlier pixels (Figure 4B). We describe the R1 area as a ridge because over such small extent area on the multiscale map of the Drape,

10.3389/fevo.2023.1108914

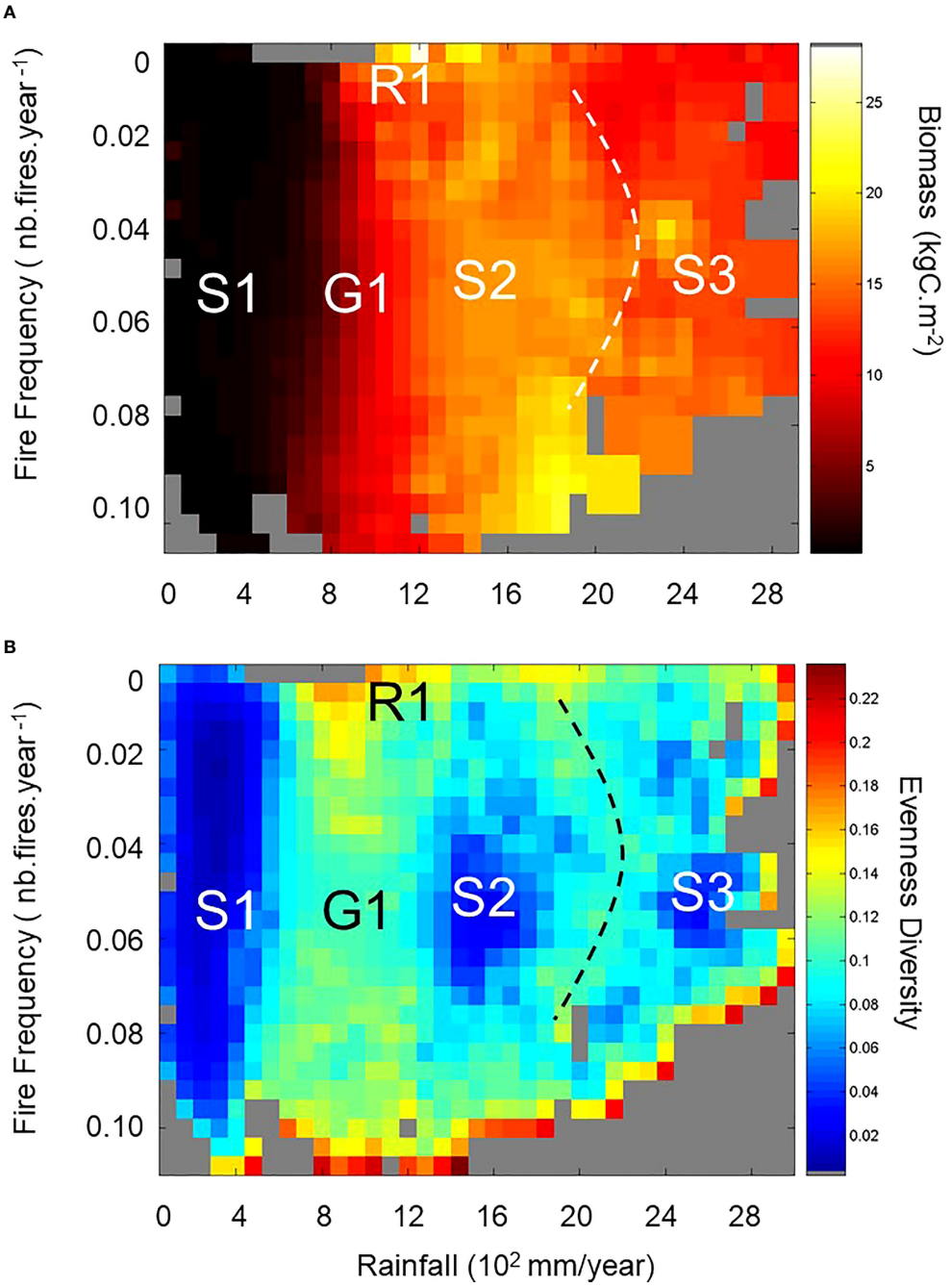

FIGURE 4
Analysis of the African Drape. **(A)** presents the Drape projection in the Rainfall–Fire plane. Note the position of the first bin (no fire, no rainfall) in the upper left corner compared to its position in the lower forward corner on Figure 3A, 3C. Here panel **(A)** also reports the projected stable and unstable states found with the textural analysis and highlighted in **(B)**. Grey pixel areas could correspond with other tropical continental conditions (Southern America, Indonesia, Australia) not found currently in Africa, or with past conditions from which there is no present-day analogue condition. **(B)** shows the spatially explicit heterogeneity index (i.e., evenness diversity) resulting from the textural analysis based on the MHM method (see Supplementary information S1.2 and Gaucherel (2007)). The higher the index, the more heterogeneous the neighboring pixels on the multiscale map. Three stable (homogeneous – low evenness diversity with dark blue colors) and two unstable (heterogeneous – from light blue-yellow to red colors) state regions are highlighted. Grey areas on both panels represent non-existing system states based on the modern condition simulation. Note that red pixels, located on the lower and right edges of the plan in **(B)** result from edge effect computations due to poorly filled pixels and empty neighbouring pixels. We do not consider them as real heterogeneous pixels.

characterized by a narrow range of quasi inexistent fires and a 700–1200 mm.yr^{-1} rainfall range, the simulated biomass range is the widest recorded (Figure 4A; Table 1, and Supplementary Figure S3D). This may be partly explained by the rainfall range that crosses the 1000 mm.yr^{-1} threshold discriminating tropical dry from tropical moist climates (Table 1). Consequently, these geographic areas include several ecosystems from sparse grasslands to tropical moist deciduous forests and rainforests whose observed biomasses,

TABLE 1 Characteristics of stable and unstable African state regions revealed from the Drape textural analysis (Figure 4).

Drape state and ratio	Drape annual rainfall (mm)	Drape annual fire frequency (#fires)	Drape biomass (kg C.m^{-2})	Observed biomass (kgC.m^{-2})	Climate zones and annual rainfall (mm)	*GEZ*	GLC2000 ecosystems (class numbers)
S1 162/4658	<500	0–0.10	0.12–1.12	0.1–4.6	Trop. Dry Warm Temp. Dry <1000	TBWh TBSh TAWb	Bare areas (19), Sparse grassland and grassland mosaics (14 & 18), Grasslands (13), and Shrub covers (11, 12 & 15)
S2 63/441	1300–1800	0.04–0.07	14.8–17.8	15.2	Trop. Moist 1000–2000	TAWa Tar	Tropical broadleaf (1–3) and mixed forests (6–8)
S3 36/19	>2300	0.04–0.06	12.8–16.6	20.0	Trop. Wet >2000	Tar	Tropical broadleaf forests (1–3) and mixed forests (6–8)
R1 32/77	700–1200	0–0.02	2.1–22.9	0.2–15.2	Trop. Dry Trop. Moist Warm Temp. Moist <2000	TBSh TAWb TAWa Tar	Sparse grassland and grassland mosaics (14 & 18), Grasslands (13), and Shrub covers (11, 12 & 15), Tropical broadleaf forests (1–3) and mixed forests (6–8)
G1 180/3008	500–1300	0.02–0.10	0.8–14.5	0.2–15.2	Trop. Dry Warm Temp. Dry Warm Temp. Moist Trop. Montane Trop. Moist <2000	TAWb TAWa Tar TM	Sparse grassland and grassland mosaics (14 & 18), Grasslands (13), Shrub covers (11, 12 & 15), Tropical broadleaf forests (1–3) and mixed forests (6–8)

The Global Ecofloristic Zones are: Tropical desert (TBWh), Tropical Shrublands (TBSh), Tropical Moist deciduous forest (TAWa), Tropical dry forest (TAWb), Tropical rainforest (Tar), Tropical mountain systems (TM).
For each given each stable (S1–S3) and unstable (R1 and G1) state, based on geographical African locations composing it (see SI-3) simulated values from the LPJ-GUESS model are compared to continental compiled observations from Ruesh and Gibbs (2008). We report the Climatic zones (IPCC, 2006), Global Ecofloristic Zones (FAO, 2001), and Global Land Cover 2000 ecosystem classification from Bartholomé and Belward (2005). The ratio in the first column is the number of pixels defining such state on the Drape over the number of pixels over Africa representing it. The overall number of pixels on the Drape and in Africa are 843 and 9395, respectively.

ranging from 0.2 to 15.2 kgC.m^{-2}, agree well with the wide range extracted from the Drape (Table 1). The last large heterogeneous area is the G1 area, squeezed between S1 and S2 areas on the multiscale map (Figure 4B). G1 is a gradient representative of regions with a slightly wider rainfall range (500–1300 mm.yr^{-1}) than that of R1, a wide range of fire occurrences, and as a consequence with a quite wide range of biomasses (Figure 4A; Table 1) but narrower than that of R1. Simulated characteristics and locations of G1 conditions (Table 1; Supplementary Figure S3E) include regions that are similar to those of R1 and mountain regions. Actually, the R1 ridge could also be considered as the most extreme conditions of the G1 gradient (see Supplementary Figure S3D), where heterogeneity is so high that the system switches from transient states along G1 to unstable states in the R1 area. It is worth noting that African regions composing the G1 transient states (alone or even associated with the R1 regions) are very similar to the regions classified as the projected worst-case biome changes expected in Africa over the 2071–2100 period as compared to the 1961–1990 reference (Niang et al., 2014). Finally, one could also see on the multiscale map a second gradient (dashed line on Figure 4), squeezed between S2 and S3 areas, but narrower and weaker than G1.

Based on these results, we confirm the first hypothesis since the 600–1000 mm.yr^{-1} rainfall range actually belongs to the G1 gradient that we consider as a transient state area, and to the R1 ridge that we consider as an unstable state occurring in the quasi absence of fires. However, we must reject the second and the third hypotheses because there is no stable state (homogeneous area) within this 600–1000 mm.yr^{-1} gradient that could be representative of any savanna stable state (second hypothesis), and in turns, the savanna-forest dynamics cannot be considered as alternative stable states. Conversely, we showed that S2 and S3 stable state areas represent different forest stable states and that part of the S1 stable state pixels may represent savannas with low woody cover (less than 30% of the very light biomass (<1.5 kgC.m^{-2})). However, these stable savannas grow with less than 500 mm.yr^{-1} in rainfall, which is at least 2.6 and 4.6 times drier than annual rainfall for S2 and S3, respectively.

Several paleoecological studies have shown that during the Holocene African Humid Period (de Menocal et al., 2000) and the so-called "Green Sahara" (Chikira et al., 2006; Watrin et al., 2009), several paleolakes were present in the current Saharan and Sahelian regions (Lézine et al., 2011). This was a response to intensified monsoonal rainfall that penetrated inland more than 10° northwards. The rainbelt core migrated up to 5° northwards during the humidity optimum (Texier et al., 2000). Such moister conditions over the 15–20°N latitudinal region, as compared to its present-day aridity, created good environmental conditions for the Guinean-Congolian pollen taxa (Hély et al., 2014) that are exclusively representative of modern tropical rainforest. This suggests that some geographic locations have therefore experienced ecosystem or even biome shifts over the last millennia that may have been similar to those from the S1 to S2 and/or to S3 stable states. Further research is needed to assess the speed of these past changes, to plot geographic-site trajectory on the Drape (as conceptually illustrated on Figure 3C), and to apprehend paths and likely direction shifts.

The multiscale map analysis suggests that most savannas (i.e. GLC2000 forest mosaic and shrub cover classes with 5.0–10.0 kgC.m^{-2} biomass range (Ruesh and Gibbs, 2008)) lie on the G1 gradient area and are therefore transient states but without delimited stable states. These savannas could shift to R1 unstable states if only fire (or a similar disturbance such as grazing (Bond et al., 2005) would almost disappear, while they could shift to S2 (S1) stable states if only rainfall would increase (decrease), and only to S1 if both rainfall would decrease and fire would change. Past savanna dynamics applied on the Drape could provide insights on past realized-trajectories and speed. The overall Drape information could be useful for savanna-ecosystem sustainable management, for instance to avoid bush-encroachment (Ringrose et al., 1998) that one could consider as a shift to R1 conditions.

Once valleys (S1) and plateaus (S2 and S3) are identified on the Drape, their location, width and depth could quantify the importance of these basins of attraction, such characterization corresponding well with the system resilience as defined by Walker et al. (2004) and discussed by Beisner et al. (2003) for ecosystem management perspectives. Similarly, ridges could represent the boundaries of contiguous basins of attraction. As previously noted, ridges could be interpreted as bifurcation states (i.e. tipping points) from which small changes in the state variables would induce an ecosystem shift or even a biome shift. From the location (state) of the system on these Drape areas, one could also estimate objectively the latitude (i.e. width) and the resistance (i.e. depth) of the basin of current ecosystems, as well as its precariousness (i.e. its distance to the ridge, which is the boundary of the basin of attraction) and its likely resilience as suggested by Beisner et al. (2003) and Walker et al. (2004).

Observations from current conditions, from past reconstructions or from future projections based on different socio-economic and climatic scenarios can provide the realized states found in different areas of the Drape. Analysis of an ecosystem at a given geographical location and its trajectory on the Drape could provide expected temporal changes of the state variables. One could therefore analyze and validate the Drape variations (i.e. its topography) from embedded system trajectories reconstructed from observations and/or paleoecological studies as conceptually illustrated in Figure 3C.

3.2 Benefits of the Drape concept

Understanding ecosystem dynamics as a scientific objective and predicting future responses as a more practical objective are difficult tasks. We propose departing from the current methods based on differential equation systems and/or statistical approaches, as well as from simplifications of the abiotic and disturbance components of ecosystems. Because our method only relies on observed data for validation, one avoids misinterpretation. Debates concerning possible extrapolation in cases of slow dynamics (as suggested above) should move toward synthesis (e.g. Hirota et al., 2011; Ratajczak and Nippert, 2012). The proposed Drape concept is an improvement in ecosystem understanding for the following seven reasons:

i) The Drape presents in a single multidimensional space all ecosystems governed by the same first-order state variables and allows to position and characterize the different states of these ecosystems in order to later study past, present, or future trajectories. (Figure 2 and Supplementary information S1.1). This process-based approach will allow including ecosystem responses over long periods of time and through several spatial (from local to continental) scales. This satisfies the need to retrieve slow but integrative changes during regime shifts that may appear incremental at human time scales (Ratajczak and Nippert, 2012; Hughes et al., 2013b). For example, the response to global warming by terrestrial ecosystems at the end of the last ice age (Minckley et al., 2012) or at the end of the African Humid Period (Lézine et al., 2011; Hély et al., 2014) took millennia, long after the ice sheets had melted or after the African monsoon intensification had terminated.

ii) The Drape, built from the outputs of the process-based model, includes disturbances as a state variable as important as vegetation or precipitation and thus allows to better characterize each ecosystem, its states, and its functional neighbors. Indeed, disturbances were previously considered as parameters or external forces in the representation of system dynamics and manifested an effect on the ecosystem through the biotic component only (e.g. Staver et al., 2011b; Touboul et al., 2018). By definition, ecosystems are simultaneously biotic and abiotic, with several tightly interacting components (e.g. flora, fauna, soils, atmosphere and humans). There is no conceptual reason to focus on a specific component over the others (Gignoux et al., 2011; Schwartz and Jax, 2011; Gaucherel, 2014). This matches the observation that ecosystems are simultaneously conditioned by the laws of thermodynamics and the by natural selection.

iii) The state variables used to build the space and the Drape are symmetric in the system functioning. Each axis has the same weight and equal role in constructing the domain (Figure 2). With this property in mind, the 3D space is the smallest multidimensional space aiming at synthetizing any ecosystem state. More complicated domains can take into account additional extra state variables (e.g. human activities or fauna), if required (Cincotta et al., 2000). The symmetry between state variables also allows the study of the system and its states from different points of view (Figures 2A, B), while maintaining the mechanistic relationships among the state variables.

iv) The Drape itself provides an instantaneous and convenient visualization of the different states encountered, as well as their characterization in terms of associated state variable values. This is interpreted in the example case as an averaged and rasterized (grid-based) surface (Figures 3, 4) of the realized domain (Figure 2).

v) The textural analysis explores the Drape variations to identify basins of attraction, characteristic tipping points and their relationships in terms of distance (Figure 4; Appendix 2). Using a statistical moment such as the mean to build the Drape surface prevents from finding "folded backward" regions previously considered as tipping-points or induced catastrophic shifts (Scheffer et al., 2001). However, tipping-points on the Drape are materialized as ridges (i.e. most heterogeneous areas, Figure 3A). Once identified and delineated, the analysis informs the possible system behavior further away. Methods other than the multiscale

textural analysis shown here may be used to analyze the Drape, such as a spectral analysis (e.g. Keitt, 2000).

vi) The Drape concept is generic. It allows featuring all states and associated state variables values extracted from a process-based model. The Drape concept could therefore be used to study other terrestrial, marine, or fresh water ecosystems as long as the chosen state variables are the best representative ones and that values are extracted from (state-of-the-art) process-based model. The Drape can be used for different periods than nowadays, which may point to states being located in different areas of the Drape as compared to the present-day state.

vii) By reporting onto the Drape the trajectory a given geographical location would record through time (observed from time-series such as remote-sensing datasets, simulated from process-based models, or reconstructed from paleoecological datasets, see Figure 3C) we would visualize and analyze its dynamics and clearly characterize the states it went through. Despite its resemblance with real topography or a Waddington's landscape (Goldberg et al., 2007), it is worth emphasizing that the third axis (Z) of the domain does not carry the meaning of a vertical and oriented direction such as the one constrained by gravity (e.g. Scheffer et al., 2001; Beisner et al., 2003). On this Drape, a ball representing the ecosystem state at a specific location and time could easily move up to higher Z values due to any ecological process. As such, the Drape surface appears much more similar to a chaotic manifold (further discussed below) than the stability landscape of the potential mentioned in previous studies. The Drape surface also seems to combine the ecosystem and the community perspectives from Beisner et al. (2003). Indeed, no process directly acts on this ball (*i.e.* the ball is not pushed by an external force), but rather intrinsic and stochastic processes modify one or several state variable values which, in turn, "push" the system toward another area of the Drape (Abarbanel, 1996; Strogatz, 2001). Moreover, basins of attraction are not systematically the lowest Drape areas.

In practice, a different domain (and its associated Drape) should be recomputed whenever a state variable should be replaced by another more important or representative variable. This allows different neighboring ecosystems (or even biomes) to occur within the same domain, and approximated by a common Drape. It seems reasonable to find tropical forest and savanna biomes in the same domain, but boreal biomes (e.g. coniferous forests and tundra) would be in another distinct domain, as they would require different ecosystem state variables (e.g. temperature instead of precipitation). This should also allow identifying past ecosystem states for which there are no modern analogues (e.g. the "green Sahara" during the mid-Holocene) in specific areas of the Drape (e.g. Figure 4B, lower right region, which is currently empty). Every biome observed during a given period will likely not occupy all of its potential Drape area. So, the Drape concept does not fully solve the problem of defining the ecosystem or biome boundaries (Gignoux et al., 2011; Gaucherel, 2014). The limits, here defined by the extreme values of each state variable, are physically constrained, while *a priori* the Drape extent is not. Such boundaries would simultaneously depend on the maximum system variability and by the addressed question.

The Drape concept applied to ecosystems can play an important role in the tipping point debate (Ratajczak and Nippert, 2012; Brook et al., 2013; Gaucherel and Moron, 2015). With tipping points defined as sharp changes in ecosystem dynamics, such changes would fit with all sharp gradients (clines) and sharp peaks observed in the Drape variations. Indeed, to shift from a relatively smooth or flat (i.e. homogeneous) area of the Drape to another one by a sharp gradient is a clue of abrupt variations in states (Lenton et al., 2008; Kriegler et al., 2009). Such tipping points could easily be identified and quantified on the Drape based on their sharpness (relatively to other zones) and from their direction.

In our African example, the G1 gradient appeared approximately twice as heterogeneous as its neighboring stable states (S1 and S2) assimilated to steppes-grassy savannas and forest types, respectively, based on state variable values (Figure 4A). We stress that such transitions are not necessary "state transitions" such as those observed in chaotic systems (Abarbanel, 1996; Ghil et al., 2002), and they would definitely need a detailed and rigorous mathematical analysis to be demonstrated as attempted in some recent studies (Accatino et al., 2010; Zaliapin and Ghil, 2010).

3.3 Limitations of the domain and perspectives

The limitations of the Drape concept presented here are of two sorts. First, there are methodological limitations, which hopefully can be improved upon and progressively removed. For instance, the variability arising from similar geographic areas (i.e. close points in the domain) probably contributes to the volume or "thickness" of the realized domain (Figure 3B). This variability may be retrieved by the calculation and representation of another statistical moment (e.g. variance) of the domain, and be analyzed in a similar manner than the averaged Drape (Figure 4). Moreover, using different moments or statistics such as the mode would allow representation of bimodal distributions in each (X, Y) interval bin if they exist, and thus to the plotting of more complicated (e.g. folded) Drape variations. Such complicated responses have been studied in detail in the catastrophe theory (e.g. the cusp geometry (Thom, 1972)), and ecological studies would gain in applying such a rigorous analysis to ecosystems (Gaucherel et al., 2020).

For clarity, we did not explore the specific role of human beings as one of the ecosystem components. As with other unmentioned ecosystem components (e.g. soils), humans could partly be involved as part of one of the already included components (e.g. climate and/or fires), or as an additional component. The resultant four-dimensional space and the more complicated 3D-Drape (called a hypersurface) could be treated without technical difficulties. This is obviously useful for applied questions related to ecosystem management and environmental policies, and it would be relevant to explore this possibility in human-perturbed systems (Cincotta et al., 2000; Gaucherel et al., 2012).

The second category of limitations of the Drape concept involves the effort needed ultimately to represent a more functional concept such as ecosystem chaos. The Drape concept

carries on the ecosystem trajectory that follows the Drape response surface from the spatial and temporal autocorrelations of system components (Figure 3C). With the exception of ridge areas and other possible singularities, each ecosystem state globally shows a high correlation with the next (and nearby) state (Figure 4), due to the processes involved and function of model equations (e.g. Cramer et al., 1999; Smith et al., 2001; Sitch et al., 2008), as well as due to the spatial autocorrelation in the abiotic state variables.

It would be convenient and parsimonious to build the Drape with the system trajectories themselves, which is the approach that provides the dynamical system theory and chaotic system representations in previous studies (Lorenz, 1963; Takens, 1981). To write and solve the equations for a dynamical system would directly lead to a trajectory in the phase-space. This approach assumes that ecosystems are dynamical and possibly chaotic, i.e. fully deterministic, ergodic and sensitive to small variations in initial conditions (Lorenz, 1963; Strogatz, 2001). To our knowledge, this has never been demonstrated for an ecosystem as a whole, although it is documented for some components such as prey–predator subsystems (May, 1977), vegetation dynamics (Solé and Bascompte, 2006) or climate dynamics (e.g. Ghil et al., 2002). However, a focus on purely biotic (or abiotic) components omits the necessary symmetry between biotic, abiotic and disturbance components (e.g. Gaucherel et al., 2020). This is the spirit of the present study.

4 Conclusion

We propose and illustrate a new and potentially powerful concept to capture ecosystem dynamics and the related complexity. With a Drape structure embedded into a multidimensional space made up with biotic, abiotic and disturbance state variables, the representation provides a simplification of ecosystem dynamics into a smoothed, quantitative and intuitive representation. It is our hope that the Drape concept and its associated properties, which are borrowed from dynamic system theory and catastrophe theory, will facilitate understanding, visualization and prediction of ecosystem dynamics. The Drape concept is a next step in the direction of analytically demonstrating the complex and possibly chaotic behaviors commonly assumed for ecosystems. It needs to be tested and validated based on further observations and simulations. We fully expect that it will prove useful for further exploration of ecosystem functioning and tipping-point related issues.

Data availability statement

The raw data supporting the conclusions of this article will be made available by the authors, without undue reservation.

Author contributions

CH and CG designed the research, CH provided data and CG performed the textural analysis. CH, CG, RS and HS discussed the results, and CH wrote the first draft of the manuscript. All authors contributed to the article and approved the submitted version.

Acknowledgments

This work has been performed in the framework of the French Labex CeMEB. We warmly thank Samuel Alleaume for proposing the “Drape” term to pinpoint this milestone concept.

Conflict of interest

The authors declare that the research was conducted in the absence of any commercial or financial relationships that could be construed as a potential conflict of interest.

Publisher’s note

Supplementary material

The Supplementary Material for this article can be found online at: https://www.frontiersin.org/articles/10.3389/fevo.2023.1108914/full#supplementary-material

References

Abarbanel, H. D. I. (1996). *Analysis of observed chaotic data* (New York: Springer-Verlag).

Accatino, F., De Michele, C., Vezzoli, R., Donzelli, D., and Scholes, R. J. (2010). Tree–grass co-existence in savanna: interactions of rain and fire. *J. Theor. Biol.* 267, 235–242. doi: 10.1016/j.jtbi.2010.08.012

Adler, P. B., and Levine, J. M. (2007). Contrasting relationships between precipitation and species richness in space and time. *Oïkos* 116, 221–232. doi: 10.1111/j.0030-1299.2007.15327.x

Aleman, J., Blarquez, O., Bentaleb, I., Bonté, P., Brossier, B., Carcaillet, C., et al. (2013). Tracking land-cover changes with sedimentary charcoal in the afrotropics. *Holocene* 23, 1853–1862. doi: 10.1177/0959683613508159

Aleman, J. C., Fayolle, A., Favier, C., Staver, A. C., Dexter, K. G., Ryan, C. M., et al. (2020). Floristic evidence for alternative biome states in tropical Africa. *Proc. Natl. Acad. Sci. U.S.A.* 117, 28183–28190. doi: 10.1073/pnas.2011515117

Ali, A. A., Blarquez, O., Girardin, M. P., Hély, C., Tinquaut, F., El Guellab, A., et al. (2012). Control of the multimillennial wildfire size in boreal north America by spring climatic conditions. *Proc. Natl. Acad. Sci.* 109, 20966–20970. doi: 10.1073/pnas.1203467109

Archer, S. (1989). Have southern texas savannas been converted to woodlands in recent history? *Am. Nat.* 134, 545–561. doi: 10.1086/284996

Bartholomé, E., and Belward, A. S. (2005). GLC2000: a new approach to global land cover mapping from earth observation data. *Int. J. Remote Sens.* 26, 1959–1977. doi: 10.1080/01431160412331291297

Beisner, B. E., Haydon, D. T., and Cuddington, K. (2003). Alternative stable states in ecology. *Front. Ecol. Environ.* 1, 376–382. doi: 10.1890/1540-9295(2003)001[0376:ASSIE]2.0.CO;2

Bel, G., Hagberg, A., and Meron, E. (2012). Gradual regime shifts in spatially extended ecosystems. *Theor. Ecol.* 5, 591–604. doi: 10.1007/s12080-011-0149-6

Blois, J. L., Williams, J. W., Fitzpatrick, M. C., Jackson, S. T., and Ferrier, S. (2013). Space can substitute for time in predicting climate-change effects on biodiversity. *Proc. Natl. Acad. Sci.* 110, 9374–9379. doi: 10.1073/pnas.1220228110

Boettiger, C., Ross, N., and Hastings, A. (2013). Early warning signals: the charted and uncharted territories. *Theor. Ecol.* 6, 255–264. doi: 10.1007/s12080-013-0192-6

Bond, W. J., Woodward, F. I., and Midgley, G. F. (2005). The global distribution of ecosystems in a world without fire. *New Phytol.* 165, 525–537. doi: 10.1111/j.1469-8137.2004.01252.x

Boulton, C. A., Good, P., and Lenton, T. M. (2013). Early warning signals of simulated Amazon rainforest dieback. *Theor. Ecol.* 6, 373–384. doi: 10.1007/s12080-013-0191-7

Briske, D. D., Washington-Allen, R. A., Johson, C. R., Lockwood, J. A., Lockwood, D. R., Stringham, T. K., et al. (2010). Catastrophic thresholds: a synthesis of concepts, perspectives, and applications. *Ecol. Soc.* 15. doi: 10.5751/ES-03681-150337

Brook, B. W., Ellis, E. C., Perring, M. P., Mackay, A. W., and Blomqvist, L. (2013). Does the terrestrial biosphere have planetary tipping points? *Trends Ecol. Evol.* 28, 396–401. doi: 10.1016/j.tree.2013.01.016

Carpenter, S., Walker, B., Anderies, J. M., and Abel, N. (2001). From metaphor to measurement: resilience of what to what? *Ecosystems* 4, 765–781. doi: 10.1007/s10021-001-0045-9

Chapin, F. S. I., Callaghan, T. V., Bergeron, Y., Fukuda, M., Johnstone, J. F., Juday, G., et al. (2004). Global change and the Boreal forest: thresholds, shifting states or gradual change? *Ambio* 33, 361–365. doi: 10.1579/0044-7447-33.6.361

Chaste, E., Girardin, M. P., Kaplan, J. O., Portier, J., Bergeron, Y., and Hély, C. (2018). The pyrogeography of eastern boreal Canada from 1901 to 2012 simulated with the LPJ-LMfire model. *Biogeosciences* 15, 1273–1292. doi: 10.5194/bg-15-1273-2018

Chikira, M., Abe-Ouchi, A., and Sumi, A. (2006). General circulation model study on the green Sahara during the mid-Holocene: an impact of convection originating above boundary layer. *J. Geophysical Res.* 111. doi: 10.1029/2005JD006398

Cincotta, R. P., Wisnewski, J., and Engelman, R. (2000). Human population in the biodiversity hotspots. *Nature* 404, 990–992. doi: 10.1038/35010105

Conversi, A., Dakos, V., Gardmark, A., Ling, S., Folke, C., Mumby, P. J., et al. (2015). A holistic view of marine regime shifts. *Philos. Trans. R. Soc. B-Biological Sci.* 370. doi: 10.1098/rstb.2013.0279

Cramer, W., Kicklighter, D. W., Bondeau, A., Moore, B.III, Churkina, G., Nemry, B., et al. (1999). Comparing global models of terrestrial net primary productivity (NPP): overview and key results. *Global Change Biol.* 5, 1–15. doi: 10.1046/j.1365-2486.1999.00009.x

Dakos, V., Carpenter, S. R., Brock, W. A., Ellison, A. M., Guttal, V., Ives, A. R., et al. (2012). Methods for detecting early warnings of critical transitions in time series illustrated using simulated ecological data. *PloS One* 7. doi: 10.1371/journal.pone.0041010

Dakos, V., Scheffer, M., van Nes, E. H., Brovkin, V., Petoukhov, V., and Held, H. (2008). Slowing down as an early warning signal for abrupt climate change. *Proc. Natl. Acad. Sci. United States America* 105, 14308–14312. doi: 10.1073/pnas.0802430105

Dakos, V., van Nes, E. H., Donangelo, R., Fort, H., and Scheffer, M. (2010). Spatial correlation as leading indicator of catastrophic shifts. *Theor. Ecol.* 3, 163–174. doi: 10.1007/s12080-009-0060-6

Dakos, V., van Nes, E. H., and Scheffer, M. (2013). Flickering as an early warning signal. *Theor. Ecol.* 6, 309–317. doi: 10.1007/s12080-013-0186-4

Davis, M. B., and Shaw, R. G. (2001). Range shifts and adaptative responses to quaternary climate change. *Science* 292, 673–679. doi: 10.1126/science.292.5517.673

de Menocal, P., Ortiz, J., Guilderson, T., Adkins, J., Sarnthein, M., Baker, L., et al. (2000). Abrupt onset and termination of the African humid period: rapid climate responses to gradual insolation forcing. *Quaternary Sci. Rev.* 19, 347–361. doi: 10.1016/S0277-3791(99)00081-5

D'Odorico, P., Laio, F., and Ridolfi, L. (2005). Noise-induced stability in dryland plant ecosystems. *Proc. Natl. Acad. Sci.* 102, 10819–10822. doi: 10.1073/pnas.0502884102

Drukenbrod, D. L., Martin-Benito, D., Orwig, D. A., Pederson, N., Poulter, B., Renwick, K. M., et al. (2019). Redefining temperate forest responses to climate and disturbance in the eastern united states: new insights at the mesoscale. *Global Ecol. Biogeography* 28, 557–575. doi: 10.1111/geb.12876

Dutta, P. S., Sharma, Y., and Abbott, K. C. (2018). Robustness of early warning signals for catastrophic and non-catastrophic transitions. *Oïkos* 127, 1251–1263. doi: 10.1111/oik.05172

Ellis, J. E., and Swift, D. (1988). Stability of African pastoral ecosystems: alternate paradigms and implications for development. *J. Range Manage.* 41, 450–459. doi: 10.2307/3899515

FAO (2001). *Global forest resources assessment 2000* (Rome: Food and Agriculture Organization of the United Nations).

Favier, C., Aleman, J., Bremond, L., Dubois, M. A., Freycon, V., and Yangakola, J.-M. (2012). Abrupt shifts in African savanna tree cover along a climatic gradient. *Global Ecol. Biogeography* 21, 787–797. doi: 10.1111/j.1466-8238.2011.00725.x

Folke, C., Carpenter, S., Walker, B., Scheffer, M., Elmqvist, T., Gunderson, L., et al. (2004). Regime shifts, resilience, and biodiversity in ecosystem management. *Annu. Rev. Ecology Evolution Systematics* 35, 557–581. doi: 10.1146/annurev.ecolsys.35.021103.105711

Gaucherel, C. (2007). Multiscale heterogeneity map and associated scaling profile for landscape analysis. *Landscape Urban Plann.* 82, 95–102. doi: 10.1016/j.landurbplan.2007.01.022

Gaucherel, C. (2014). Ecosystem complexity through the lens of logical depth: capturing ecosystem individuality. *Biol. Theory* 9, 440–451. doi: 10.1007/s13752-014-0162-2

Gaucherel, C., Alleaume, S., and Hély, C. (2008). The comparison map profile method: a statistical tool for spatially explicite and multiscale comparison of quantitative and qualitative images. *IEEE Geosci. Remote Sens. Lett.* 46, 2708–2719. doi: 10.1109/TGRS.2008.919379

Gaucherel, C., Boudon, F., Houet, T., Castets, M., and Godin, C. (2012). Understanding patchy landscape dynamics: towards a landscape language. *PloS One* 7, e46064. doi: 10.1371/journal.pone.0046064

Gaucherel, C., and Moron, V. (2015). Potential stabilizing points to mitigate tipping point interactions in earth's climate. *Int. J. Climatology*. doi: 10.1002/joc.4712

Gaucherel, C., Pommereau, F., and Hély, C. (2020). Understanding ecosystem complexity via application of a process-based state space rather than a potential. *Complexity*. doi: 10.1155/2020/7163920

Ghil, M., Allen, M. R., Dettinger, M. D., Ide, K., Kondrashov, D., Mann, M. E., et al. (2002). Advanced spectral methods for climatic time series. *Rev. Geophysics* 40, 3-1-3–3-141. doi: 10.1029/2000RG000092

Gignoux, J., Davies, I. D., Flint, S. R., and Zucker, J.-D. (2011). The ecosystem in practice : interest and problems of an old definition for constructing ecological models. *Ecosystems* 14, 1039–1054. doi: 10.1007/s10021-011-9466-2

Goldberg, A. D., Allis, C. D., and Bernstein, E. (2007). Epigenetics: a landscape takes shape. *Cell* 128, 635–638. doi: 10.1016/j.cell.2007.02.006

Hanan, N. P., Tredennick, A. T., Prihodko, L., Bucini, G., and Dohn, J. (2014). Analysis of stable states in global savannas: is the CART pulling the horse? *Global Ecol. Biogeography* 23, 259–263. doi: 10.1111/geb.12122

Hanan, N. P., Tredennick, A. T., Prihodko, L., Bucini, G., and Dohn, J. (2015). Analysis of stable states in global savannas – a response to staver and Hansen. *Global Ecol. Biogeography* 24, 988–989. doi: 10.1111/geb.12321

Hély, C., Braconnot, P., Watrin, J., and Zheng, W. (2009). Climate and vegetation : simulating the African humid period. *Comptes Rendus Géoscience* 341, 671–688. doi: 10.1016/j.crte.2009.07.002

Hély, C., Bremond, L., Alleaume, S., Smith, B., Sykes, M. T., and Guiot, J. (2006). Sensitivity of African biomes to changes in the precipitation regime. *Global Ecol. Biogeography* 15, 258–270. doi: 10.1111/j.1466-8238.2006.00235.x

Hély, C., Chaste, E., Girardin, M. P., Remy, C., Blarquez, O., Bergeron, Y., et al. (2020). A Holocene perspective of vegetation controls on seasonal Boreal wildfire sizes using numerical paleo-ecology. *Front. In Forests Global Change* 3. doi: 10.3389/ffgc.2020.511901

Hély, C., Girardin, M. P., Ali, A. A., Carcaillet, C., Brewer, S., and Bergeron, Y. (2010). Eastern Boreal north American wildfire risk of the past 7000 years: a model-data comparison. *Geophysical Res. Lett.* 37. doi: 10.1029/2010GL043706

Hély, C., Lézine, A. M.APD Contributors (2014). Holocene Changes in African vegetation: tradeoff between climate and water availability. *Climate Past* 10, 681–686. doi: 10.5194/cpd-9-6397-2013

Hickler, T., Vohland, K., Feehan, J., Miller, P. A., Smith, B., Costa, L., et al. (2012). Projecting the future distribution of European potential natural vegetation zones with a generalized, tree species-based dynamic vegetation model. *Global Ecol. Biogeography* 21, 50–63. doi: 10.1111/j.1466-8238.2010.00613.x

Hirota, M., Holmgren, M., Van Nes, E. H., and Scheffer, M. (2011). Global resilience of tropical forest and savanna to critical transitions. *Science* 334, 232–235. doi: 10.1126/science.1210657

Holling, C. S. (1973). Resilience and stability of ecological systems. *Annu. Rev. Ecol. Systematics* 4, 1–23. doi: 10.1146/annurev.es.04.110173.000245

Hughes, T. P., Carpenter, S., Rockström, J., Scheffer, M., and Walker, B. (2013a). Multiscale regime shifts and planetary boundaries. *Trends Ecol. Evol.* 28, 389–395. doi: 10.1016/j.tree.2013.05.019

Hughes, T. P., Linares, C., Dakos, V., van de Leemput, I. A., and van Nes, E. H. (2013b). Living dangerously on borrowed time during slow, unrecognized regime shifts. *Trends Ecol. Evol.* 28, 149–155. doi: 10.1016/j.tree.2012.08.022

IPCC (2006). "2006 guidelines for national greenhouse gas inventories," in *Agriculture, forest, and other land use*, vol. 4. (Hayama, Japan: IGES).

Johnson, E. A. (1992). *Fire and vegetation dynamics: studies from the north American boreal forest* (Cambridge: Cambridge University Press).

Kéfi, S., Guttal, V., Brock, W. A., Carpenter, S. R., Ellison, A. M., Livina, V. N., et al. (2014). Early warning signals of ecological transitions: methods for spatial patterns. *PloS One* 9, e92097 1–13. doi: 10.1371/journal.pone.0092097

Keitt, T. H. (2000). Spectral representation of neutral landscapes. *Landscape Ecol.* 15, 479–493. doi: 10.1023/A:1008193015770

Kriegler, E., Hall, J. W., Held, H., Dawson, R., and Schellnhuber, H. J. (2009). Imprecise probability assessment of tipping points in the climate system. *Proc. Natl. Acad. Sci.* 106, 5041–5046. doi: 10.1073/pnas.0809117106

Lenton, T. M., Held, H., Kriegler, E., Hall, J. W., Lucht, W., Rahmstorf, S., et al. (2008). Tipping elements in the earth's climate system. *Proc. Natl. Acad. Sci.* 105, 1786–1793. doi: 10.1073/pnas.0705414105

Lézine, A.-M., Hély, C., Grenier, C., Braconnot, P., and Krinner, G. (2011). Sahara And sahel vulnerability to climate changes, lessons from Holocene hydrological data. *Quaternary Sci. Rev.* 30, 3001–3012. doi: 10.1016/j.quascirev.2011.07.006

Livina, V. N., Kwasniok, F., and Lenton, T. M. (2010). Potential analysis reveals changing number of climate states during the last 60 kyr. *Climate Past* 6, 77–82. doi: 10.5194/cp-6-77-2010

Lorenz, E. N. (1963). Deterministic nonperiodic flow. *J. Atmospheric Sci.* 20, 130–141. doi: 10.1175/1520-0469(1963)020<0130:DNF>2.0.CO;2

Lotka, A. J. (1925). *Elements of physical biology* (Baltimore).

Martin, R., Schlüter, M., and Blenckner, T. (2020). The importance of transient social dynamics for restoring ecosystems beyond ecological tipping points. *Proc. Natl. Acad. Sci.* 117, 2717–2722. doi: 10.1073/pnas.1817154117

May, R. M. (1977). Thresholds and breakpoints in ecosystems with a multiplicity of stable states. *Nature* 269, 471–477. doi: 10.1038/269471a0

McMahon, S. M., Harrison, S., Armbruster, W. S., Bartlein, P. J., Beale, C. M., Edwards, M. E., et al. (2011). Improving assessment and modelling of climate change impacts on global terrestrial biodiversity. *Trends Ecol. Evol.* 26, 249–259. doi: 10.1016/j.tree.2011.02.012

Minckley, T. A., Shriver, R. K., and Shuman, B. (2012). Resilience and regime change in a southern rocky mountain ecosystem during the past 17 000 years. *Ecol. Monogr.* 82, 49–68. doi: 10.1890/11-0283.1

New, M. G., Lister, D., Hulme, M., and Makin, I. (2002). A high-resolution data set of surface climate over global land areas. *Climate Res.* 21, 1–25. doi: 10.3354/cr021001

Niang, I., Ruppel, O. C., Abdrabo, M. A., Essel, A., Lennard, C., Padgham, J., et al. (2014). "Africa," in *Climate change 2014: impacts, adaptation, and vulnerability. part b: regional aspects. contribution of working group II to the fifth assessment report of the intergovernmental panel on climate change*. Eds. V. R. Barros, C. B. Field, D. J. Dokken, M. D. Mastrandrea, K. J. Mach, T. E. Bilir, et al (Cambridge, United Kingdom and New York, NY, USA: Cambridge University Press), 1199–1265.

Nolting, B. C., and Abbott, K. C. (2016). Balls, cups, and quasi-potentials: quantifying stability in stochastic systems. *Ecology* 94, 850–864. doi: 10.1890/15-1047.1

Noy-Meir, I. (1975). Stability of grazing systems: an application of predator-prey graphs. journal of ecology. *J. Ecol.* 63, 459–481. doi: 10.2307/2258730

Pickett, S. T. A., and White, P. S. (1985). *The ecology of natural disturbance and patch dynamics* (Academic Press Inc. New york: Academic press).

Prentice, I. C., Kelley, D. I., Foster, P. N., Friedlingstein, P., Harrison, S., and Bartlein, P. J. (2011). Modeling fire and the terrestrial carbon balance. *Global Biogeochemical Cycles* 25. doi: 10.1029/2010GB003906

Prentice, I. C., and Webb, T.III (1998). BIOME 6000: reconstructing global mid-Holocene vegetation patterns from palaeoecological records. *J. Biogeography* 25, 997–1005. doi: 10.1046/j.1365-2699.1998.00235.x

Ratajczak, Z., D'Odorico, P., Collins, S. L., Bestelmeyer, B. T., Isbell, F. I., and Nippert, J. B. (2017a). The interactive effects of press/pulse intensity and duration on regime shifts at multiple scales. *Ecol. Monogr.* 87, 198–218. doi: 10.1002/ecm.1249

Ratajczak, Z., D'Odorico, P., Nippert, J. B., and Collins, S. L. (2017b). Changes in spatial variance during a grassland to shrubland state transition. *J. Ecol.* 105, 750–760. doi: 10.1111/1365-2745.12696

Ratajczak, Z., and Nippert, J. B. (2012). Comment on "Global resilience of tropical forest and savanna to critical transitions." *Science* 336, 541. doi: 10.1126/science.1219346

Ringrose, S., Matheson, W., and Vanderpost, C. (1998). Analysis of soil organic carbon and vegetation cover trends along the Botswana Kalahari transect. *J. Arid Environments* 38, 379–396. doi: 10.1006/jare.1997.0344

Ruesh, A., and Gibbs, H. K. (2008). *New IPCC tier-1 global biomass carbon map for the year 2000* (Oak Ridge, Tennessee: Oak Ridge National Laboratory). Available online from the Carbon Dioxide Information Analysis Center. Available at: http://cdiac.ess-dive.lbl.gov.

Sankaran, M., Hanan, N. P., Scholes, R., Ratnam, J., Augustine, D. J., Cade, B. S., et al. (2005). Determinants of woody cover in African savannas. *Nature* 438, 846–849. doi: 10.1038/nature04070

Scheffer, M., Carpenter, S., Foley, J. A., Folke, C., and Walker, B. (2001). Catastrophic shifts in ecosystems. *Nature* 413, 591–596. doi: 10.1038/35098000

Scheffer, M., Hirota, M., Holmgren, M., Van Nes, E. H., and Chapin, F. S. I. (2012). Thresholds for boreal biome transitions. *Proc. Natl. Acad. Sci.* 109, 21384–21389. doi: 10.1073/pnas.1219844110

Scheffer, M., Holmgren, M., Brovkin, V., and Claussen, M. (2005). Synergy between small- and large-scale feedbacks of vegetation on the water cycle. *Global Change Biol.* 11, 1003–1012. doi: 10.1111/j.1365-2486.2005.00962.x

Scholes, R. J., Dowty, P. R., Caylor, K., Parsons, D. A. B., Frost, P. G. H., and Shugart, H. H. (2002). Trends in savanna structure and composition along an aridity gradient in the Kalahari. *J. Vegetation Sci.* 13, 419–428. doi: 10.1111/j.1654-1103.2002.tb02066.x

Scholes, R. J., and Walker, B. H. (1993). *An African savanna: synthesis of the nylsvley study* (New York: Cambridge Univ. Press).

Schwartz, A., and Jax, K. (2011). *Ecology revisited: Reflecting on Concepts, Advancing Science* (Dordrecht, Germany: Springer).

Sitch, S., Huntingford, C., Gedney, N., Levy, P. E., Lomas, M., Piao, S. L., et al. (2008). Evaluation of the terrestrial carbon cycle, future plant geography and climate-carbon cycle feedbacks using five dynamic global vegetation models (DGVMs). *Global Change Biol.* 14, 2015–2039. doi: 10.1111/j.1365-2486.2008.01626.x

Smith, B., Prentice, I. C., and Sykes, M. T. (2001). Representation of vegetation dynamics in the modelling of terrestrial ecosystems : comparing two contrasting approaches within European climate space. *Global Ecol. Biogeography* 10, 621–637. doi: 10.1046/j.1466-822X.2001.t01-1-00256.x

Solé, R. V., and Bascompte, J. (2006). *Self-organization in complex ecosystems* (Princeton, USA: Princeton University Press).

Staver, A. C., Archibald, S., and Levin, S. (2011a). The global extent and determinants of savanna and forest as alternative biome states. *Science* 334, 230–232. doi: 10.1126/science.1210465

Staver, A. C., Archibald, S., and Levin, S. (2011b). Tree cover in sub-Saharan Africa: rainfall and fire constrain forest and savanna as alternative stable states. *Ecology* 92, 1063–1072. doi: 10.1890/10-1684.1

Staver, A. C., and Hansen, M. C. (2015). Analysis of stable states in global savannas: is the CART pulling the horse? – a comment. *Global Ecol. Biogeography* 24, 985–987. doi: 10.1111/geb.12285

Sternberg, L. D. S. L. (2001). Savanna-forest hysteresis in the tropics. *Global Ecol. Biogeography* 10, 369–378. doi: 10.1046/j.1466-822X.2001.00243.x

Strogatz, S. H. (2001). *Nonlinear dynamics and chaos: with applications to physics, biology and chemistry. 2nd edition* (Boca Raton, USA: CRC Press, Taylor & Francis Group).

Takens, F. (1981). Detecting strange attractors in turbulence. *Lecture Notes Mathematics* 898, 366–381. doi: 10.1007/BFb0091924

Tansley, A. G. (1935). The use and abuse of vegetational concepts and terms. *Ecology* 16, 284–307. doi: 10.2307/1930070

Texier, D., de Noblet, N., and Braconnot, P. (2000). Sensitivity of the African and Asian monsoons to mid-Holocene insolation and data-inferred surface changes. *J. Climate* 13, 164–181. doi: 10.1175/1520-0442(2000)013<0164:SOTAAA>2.0.CO;2

Thom, R. (1972). *Structural stability and morphogenesis: an outline of a general theory of models* (Reading,Massachusetts, USA: Inc. Advanced Book Program).

Touboul, J. D., Staver, A. C., and Levin, S. A. (2018). On the complex dynamics of savanna landscapes. *Proc. Natl. Acad. Sci.* 115, E1336–E1345. doi: 10.1073/pnas.1712356115

van de Koppel, J., and Rietkerk, M. (2004). Spatial interactions and resilience in arid ecosystems. *Am. Nat.* 163, 113–121. doi: 10.1086/380571

van de Koppel, J., Rietkerk, M., van Langevelde, F., Kumar, L., Klausmeier, C. A., Fryxell, J. M., et al. (2002). Spatial heterogeneity and irreversible vegetation change in semiarid grazing systems. *Am. Nat.* 159, 209–218. doi: 10.1086/324791

Van Nes, E. H., Hirota, M., Holmgren, M., and Scheffer, M. (2014). Tipping points in tropical tree cover: linking theory to data. *Global Change Biol.* 20, 1016–1021. doi: 10.1111/gcb.12398

Van Nes, E. H., and Scheffer, M. (2007). Slow recovery from perturbations as a generic indicator of a nearby catastrophic shift. *Am. Nat.* 169, 738–747. doi: 10.1086/516845

Volterra, V. (1926). Fluctuations in the abundance of a species considered mathematically. *Nature* 188, 558–560. doi: 10.1038/118558a0

Walker, B., Holling, C. S., Carpenter, S., and Kinzig, A. (2004). Resilience, adaptability and transformability in social–ecological systems. *Ecol. Soc.* 9, 5. doi: 10.5751/ES-00650-090205

Walker, B. H., Ludwig, D., Holling, C. S., and Peterman, R. M. (1981). Stability of semi-arid grazing systems. *J. Ecol.* 69, 473–498. doi: 10.2307/2259679

Wang, R., Dearing, J. A., Langdon, P. G., Zhang, E. L., Yang, X. D., Dakos, V., et al. (2012). Flickering gives early warning signals of a critical transition to a eutrophic lake state. *Nature* 492, 419–422. doi: 10.1038/nature11655

Watrin, J., Lézine, A. M., Hély, C.contributors (2009). Plant migration and ecosystems at the time of the "green sahara." *Comptes Rendus l'Académie Des. Sci. Géosciences* 341, 656–670. doi: 10.1016/j.crte.2009.06.007

Westoby, M., Walker, B., and Noy-Meir, I. (1989). Opportunistic management for rangelands not at equilibrium. *J. Range Manage.* 42, 266–274. doi: 10.2307/3899492

Wiens, J. A. (1989). Spatial scaling in ecology. *Funct. Ecol.* 3, 385–397. doi: 10.2307/2389612

Wissel, C. (1984). A universal law of the characteristic return time near thresholds. *Oecologia* 65, 101–107. doi: 10.1007/BF00384470

Zaliapin, I., and Ghil, M. (2010). Another look at climate sensitivity. *Nonlinear Processes Geophysics* 17, 113–122. doi: 10.5194/npg-17-113-2010

frontiers | Frontiers in Ecology and Evolution

TYPE Perspective
PUBLISHED 30 October 2023
DOI 10.3389/fevo.2023.1253084

OPEN ACCESS

EDITED BY
Jurek Kolasa,
McMaster University, Canada

REVIEWED BY
Blai Vidiella,
Spanish National Research Council (CSIC), Spain

*CORRESPONDENCE
Andy Dobson
dobson@princeton.edu
Matthew C. Hutchinson
mhutchinson6@ucmerced.edu
Sarah Batterman
sabatterman@googlemail.com

RECEIVED 04 July 2023
ACCEPTED 28 September 2023
PUBLISHED 30 October 2023

CITATION
Dobson A, Hutchinson MC and Batterman S (2023) Plant communities and food webs. *Front. Ecol. Evol.* 11:1253084. doi: 10.3389/fevo.2023.1253084

Plant communities and food webs

Andy Dobson[1,2,3]*, Matthew C. Hutchinson[1,4]* and Sarah Batterman[3,5,6]*

[1]Department of Ecology and Evolutionary Biology, Princeton University, Princeton, NJ, United States, [2]Santa Fe Institute, Santa Fe, NM, United States, [3]Smithsonian Tropical Research Institute, Panama City, Panama, [4]Department of Life and Environmental Sciences, University of California, Merced, Merced, CA, United States, [5]Biology Department, Leeds University, Leeds, United Kingdom, [6]Cary Institute of Ecosystem Studies, Millbrook, NY, United States

Recent theoretical work has provided major new insights into the ways that species interactions in food webs are organized in ways that permit the coexistence of significant numbers of species. But, we seem to have forgotten about trees! Not the phylogenetic ones that are increasingly important for dissecting the evolutionary structure of food webs, but the trees, shrubs and grasses that are the basal species in all terrestrial ecosystems. Many of the food webs available for analysis over the last 30 years were based on freshwater or marine systems where algae were the main plants. Trees are very different from algae; they can live for centuries, while annually producing leaves, fruits and seeds that provide nutrients for a diversity of species on higher trophic levels. In sharp contrast to algae, they are only partly consumed by herbivores and usually compensate or recover from herbivory. Most of the biomass in terrestrial systems is in the plants, this again contrasts with aquatic systems, where most of the biomass is in primary and secondary consumers. Moreover, each individual tree supports its own food web of species that are only partially coupled to those of surrounding trees. If we are going to apply our theoretical understanding of food-web structure to species-rich terrestrial ecosystems in ways that are insightful for conservation, then we need a deeper examination of the role that higher plants play in food webs. While community ecology has developed an increasingly detailed understanding of the ways plant communities are organized, this seems to have evolved almost independently of the food-web literature. In this article, we make a plea to more sharply consider higher plants in food webs and to do this by combining recent theoretical work on food webs, with recent empirical and theoretical work on plant communities. Ultimately, we argue for a deeper integration of plant community ecology into studies of food webs.

KEYWORDS

food webs, trees, stability, plant communities, pollination, mutualism

Neutral, omniscient and basal

If you walk around Windsor Great Park in the south of England, you are surrounded by some of Britain's oldest inhabitants. Not the British Royal Family, who live on the Estate, but the oak trees that have lived in the park since Henry VIII wooed his multiple wives here, trees that were already established when William the Conqueror and the Normans arrived in England in 1066 (Figure 1 - Green, pers comm). Trees are some of the oldest organisms on the planet, if we go to the western United States, we can find Bristlecone pines that are almost 5,000 years old (Brown, 1996); not far away in Sierra are Giant Sequoia's that are several thousand years old and the largest organisms on the planet. In the Namibian desert, *Welwitschia* plants can be thousands of years old with same two leaves they first sprouted (Herre, 1961); Figure 1); in Sri Lanka, Jaya Sri Maha Bodhi—a sacred fig (*Ficus religiosa*) and the oldest planted tree—has stood since 288 BC (Ram, 2016). Simply seeing trees as perches, dens, or nest sites for the mammals and birds that live on, and in the tree, massively underestimates the foundational role that individual trees play for the multiple generations of species that they support. All ancient trees, and indeed, all higher plants are host to a community of fungi, bacteria, insects and nematodes that form a network of organisms that feeds on, or exchanges nutrients with the tree (Hardoim et al., 2015) (Parihar et al., 2020; Hawkins et al., 2023). Most trees sustain their own food web of diverse organisms that feed on, or in, them (Price, 2002). Ultimately, the food webs of forests are meta-webs, where each individual tree is a node that hosts its own sub-web of multi-species interactions. The long life of trees and the relatively short life of species that use them as resources, and the even shorter lives of the fungi and bacteria that form their microbiome, makes it unlikely that two trees in the same forest support identical food webs. Furthermore, the mature stages of most individual trees live longer than the careers of the researchers who study them! Indeed, some of the trees mentioned above are older than most religions and the evolutionary origin of conifers predates most terrestrial vertebrates! (Farjon, 2008). Does this longevity provide an underappreciated level of stability to terrestrial ecosystems? And does this ineluctably constrain the persistence of terrestrial animal and microbial communities to the survival of the trees and grasses that contain most of the biomass in terrestrial ecosystems?

Trees are some of the most ubiquitous organisms on Earth; a recent study estimates there are around 3.04 trillion trees on the planet (Crowther et al., 2015), just under half of these (1.39 Trillion) are in tropical and subtropical forests, the rest are split almost equally between boreal (0.74T) and temperate regions (0.61T); each

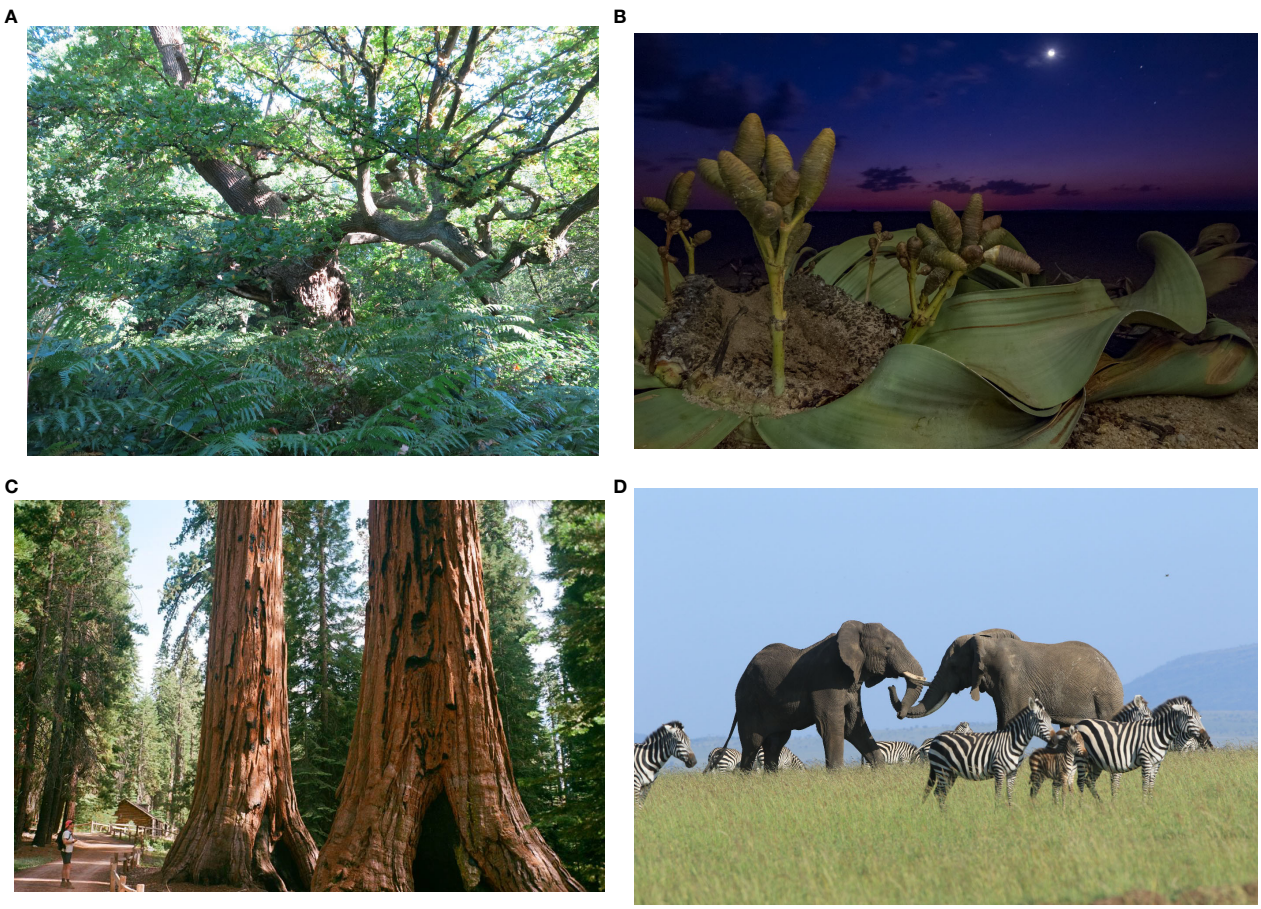

FIGURE 1
Three long-lived trees. **(A)** Oak tree in Windsor Great Park (Photo by Andy Dobson). **(B)** Welwitschia in the Namibian desert (Photo by Jennifer Guyton). **(C)** Giant Sequoia in the Mariposa Grove of Giant Sequoias, California (Photo Allegra Dobson). **(D)** Elephants and Zebra in Serengeti National Park surrounded by grasses that annually regrow from deep roots to support a large diversity and biomass of ungulates (Photo Andy Dobson).

tree contains a food web of interacting fungal, bacterial, insect and nematode species, and acts as a discrete patch in the habitats and territories of many bird and mammal species. Most individual plants have a web of mycorrhizal fungi associated with them and this may contain a significant proportion of the carbon dioxide scrubbed from the atmosphere by the tree A recent review estimates that as much as 30% of the carbon captured by trees from the atmosphere is stored in these fungal mutualists (Hawkins et al., 2023). Although individual trees can be incredibly long-lived, recent studies of data from long-term tropical forest plots show significant turnover in the populations of individual trees on multi-decadal timescales (Chisholm et al., 2014). A beguiling pattern underlies these data: variation in the population size of abundant trees tends to be driven by environmental variation (most likely climate and natural enemies), while variation in the abundance of rarer trees is dominated by demographic stochasticity. Presumably the food web associated with more abundant trees can persist as meta-communities whose species continuously recruit into the adult populations from the population of younger trees waiting to develop in the understory, or as seeds in the soil seed bank. These age-structured effects could also operate in rarer trees where higher levels of variability in abundance may compensate for the reduced probability of specific fungal, insect, and nematode species locating their host.

At a macro-ecological scale, it is also intriguing to ask how these patterns change from species-rich rainforests to species-poor boreal forests where the biomes associated with each tree are likely less dissimilar, than those associated with individual tropical trees. Likewise, the food webs associated with individuals trees in closed canopy forests may be more similar than the food webs associated to widely spaced savanna trees. What are the dynamic and structural consequences for food webs of switching our botanical perspective from algae in ponds, to oaks, yews, figs, Bristlecone pines in forests, and grasses in savannas? Recent work on forces that determine the stability of food webs has emphasized the role of long-lived species that create slow dynamics where changes in abundance occur on timescales that are orders of magnitude slower than for consumer species in the web (McCann et al., 2005; Rooney et al., 2006; McCann, 2011). Trees canonically fill this role in the food web dynamics of tropical, temperate and boreal forests; perennial grasses play an analogous role in savannas. While there is a rapid turnover and variance in the abundance of early life stages—fruits, seeds and seedlings are produced on a regular annual basis, or occasionally at longer time intervals in masting species.—The longevity of adult mature trees consistently and predictably generates, on a time scale of decades to centuries, spatially local resources for species on higher tropic levels that feed on fruits, seeds, and leaves, as well as for the decomposer community that feeds on fallen leaves and branches (Table 1). Variation in annual levels of productivity is partially offset by interactions between plants competing for space, nutrients, water, and sunlight (Tilman, 1982; Tilman, 1988). While this initially creates problems for stability from a theoretical food web perspective, as explicit competition is destabilizing (Loreau and De Mazancourt, 2013), these problems could be surmounted if light, water and nutrients were included as additional 'limiting factors' in the web, competition between plants would then be explicitly resource based (Allesina and Tang, 2012; Tang et al., 2014; Allesina and Tang, 2015).

Food web models

Are there more explicit ways of dealing with the longevity of mature plants in food web models? Could this be captured by age- or stage-structured models that allow long-lived mature trees to compete slowly for light, water and nutrients, while supplying a variable annual supply of leaves, sap, fruits, pollen and seed stages to the consumers that form the rest of the web? Ultimately, this suggests we should use models of plant communities to provide a basal layer to models of terrestrial food webs. We could then add on top of these the faster and more ephemeral interactions between plant reproduction and animal, bacterial and fungal consumer species? Although some site-specific computer food-web models take this approach, it is missing from the more analytical models based on random networks (Box 1). Ultimately what happens at the base of the web determines the dynamics of what happens in higher trophic levels; so one major route that food web studies need to develop is to integrate the consumer-resource parts of food-web models with models for dynamics of plant communities (Tilman, 1982; Tilman, 1988; Hubbell, 2001).

The species composition and spatial distribution of the underlying plant community is the primary determinant of the foraging/grouping structure of the herbivore community, whose feeding activities interact with local soil and climate conditions to shape the local plant community. Most insects, birds and mammals display strong preferences for the plants that they feed upon (Fine et al., 2004; Hutchinson et al., 2022). In savanna ecosystems,

TABLE 1 Table comparing the biomass of plants in different ecosystems and relative timescales at which plant demography and ecosystem succession operate.

Ecosystem type	Biomass of primary consumers	Lifespan of primary consumers	Biomass of primary producers (kg)	Lifespan of primary producers (years)	Turnover time of ecosystem (years)
Lake/Aquatic	Small to intermediate	Days to years	~1 x 10^{-10}	0.1 - 1	0.1 - 1
Grassland	Intermediate to large	Days to years	0.1 - 1 kg	0.1 - 10	1 - 10
Tropical forest	Small to large	Days to years	100 - 100,000 kg	10 - 1,000	1,000's

BOX 1 field guide to random matrix food web models.

The original 'random-graph' food web models developed from "spin-glass theory" by Gardner and Ashby (1970) were refined by Robert May (1973) to produce a result that has had ecologists scratching their heads for forty years. The result showed that if a food web was characterized by a matrix of random positive and negative interactions between species (of magnitude 0<->1) then stability would always decrease with increasing species diversity. So how could complex ecological communities persist? May's result showed that stability requires all the eigenvalues of the community interaction matrix to be negative, this requires $i^2\sqrt{s \cdot c} < 1$, where s is number of species, c is connectance, or number of links in the web and i is average interaction strength. May suggested that 'modularity', organizing species into sub-webs of species that interacted more with each other than with other species might help enhance stability, although stability would still always decline with increased species diversity.

Allesina et al. (2008) helped formalize this conjecture when they showed that that subdividing webs into groups of highly interactive species could enhance stability. They then made a major breakthrough (Allesina and Pascual, 2009) when they realized May's original formulation allocated each interaction strength a random number between -1 and 1. This meant that 1/4 of web interactions would be mutualisms (+/+), 1/4 would be competition (-/-) and half would be consumer-resource or predator-prey (+/-) relationships. This makes it very hard to have negative eigenvalues as the product of all the negative interactions will be balanced by the product of all the positive interactions (remembering -/- is always positive)!. They showed that if competitive and mutualistic interactions are more accurately characterized by the consumer-resource relationships that underlie them then it was much more likely that the community matrix would have negative eigenvalues and the community would be stable. Allesina and Tang (2012) extended this result to show that stability was possible with much larger community matrices when the vast majority of links were consumer resource (+/-) links, although May's central conjecture still held, stability will still decline with increased species diversity, but the intercept of the relationship will be much higher. Some of these results were partly discovered by a paper written in direct response to May's (1973) paper by (Roberts, 1974). He suggested that if the subset of random webs with feasible properties are considered (where feasible implies interaction strengths that permit all species to persist), then webs with more species are more stable. However, Roberts set up his arrays in a way that generates very strong within species regulation, which would inherently increase the stability of the web as more species are added.

Allesina and Levine (2011) then expanded the work to examine interactions between species coexisting on the same trophic level, essentially plant communities. This work showed that framing this debate within the traditional and algebraically tractable framework of interactions between two species is misleading, particularly when the traditional framework is expanded to include multiple species all of which are assumed to have similar demographic properties and interact by competing for the gaps that appear when an individual of one species dies and is replaced by any other species ("neutral" models that make a large bow to Peter Grubb's "regeneration niche" Grubb, 1977). They showed that if species have higher-order interactions with each other such that A outcompetes B, but the presence of C allows B to outcompete A, then it is possible for many species to coexist on the same trophic level in ways that produce patterns that are closer to those observed empirically than occur in "neutral' communities.

Grilli et al. (2017), expanded this framework to consider indirect interactions in whole food webs; this work showed that indirect interactions can considerably enhance the stability of multi trophic webs. Several ecologists have long argued for the importance of indirect interactions and this work confirms these interactions are important for web stability (Gibbs et al., 2022).

Allesina et al. (2015) also developed elegant methods for adding structure to webs that built upon Williams and Martinez 'niche model' which assumes that species can be arranged by body size such that larger species tend to feed on species within a range of smaller body sizes. This means that empirical webs tend to be 'interval' and can be arranged as sequence of species along an axis where species to the right can only feed on species to the left (an idea originally suggested by Joel Cohen in 1978). Webs of this type are more similar to empirical webs than 'random graph' webs which are not interval. This work further suggested that incorporating modularity considerably reduces the importance of interaction strength in determining stability. Modularity is the presence of substructure within the web such that species tend to form groups that interact much more frequently with each other than with other species. This again significantly increased the stability of the model webs. However, results from these analyses suggest modularity is only important under restrictive conditions and observed patterns of nestedness may simply be an epiphenomenon of intervality and is more likely to observed when food webs are assembled using binary (presence-absence) diet data, than when using quantitative diets (Staniczenko et al., 2013).

vertebrate herbivores can quickly be divided into browsers and grazers, these will in turn divide the habitat into open areas of grassland and bush with tree density increasing in the occasional riparian areas. For example, the Serengeti grasslands are divided into different plant communities of short and long grasslands, woodlands and kopjes that have their own fairly well-delineated groups of herbivores that feed on them (Baskerville et al., 2011). These compete seasonally with the larger migratory herbivores (wildebeest, zebra, and elephants) that only use each of these communities for a few months each year (Figure 2). In turn, the herbivore communities in any location have both specialized local and generalized more widely spread carnivores that feed on them. Spatial patterns in tropical forests will be more complex, individual trees will have sharply defined insect webs closely associated with them that are coupled to the webs of other trees by the generalist birds, insects, and mammals that feed on fruit and leaves of different tree species and by the predators that then feed upon these primary consumers. This contrasts with aquatic systems where algae that are the dominant plant species, in general, these are more homogeneously distributed and do not generate the distinct patterns in the distribution of vegetation that characterize forests and savannas. Although vertical and horizontal stratification in the abundance of different algae do create subtle groupings in the web that only emerges when the full details of the feeding relationships are delineated (Hutchinson, 1961; D'Alelio et al., 2016). Nevertheless, algal-plankton driven, aquatic food webs will tend to be relatively spatially homogenous and generate an inverse biomass pyramid: most of the rapidly generated primary productivity in algal communities is consumed and turned into relatively short-lived fish and invertebrate species at higher trophic levels. This may make them intrinsically more unstable than spatially complex terrestrial systems where most of the biomass is in the long-lived plants at the base of the food web (Allesina et al., 2015).

An overenthusiastic emphasis on algae as 'canonical plants' is not restricted to studies of food webs, in a survey and meta-analysis of experimental consumer and fertilization manipulation experiments researchers found that only 7% and 14% of the studies were of terrestrial systems (Hillebrand et al., 2007; Gruner et al., 2008). The international NutNet system has begun to address this balance, a review of the first decade of data from grassland communities at the core of NutNet (Borer et al., 2017) suggests that the stability of these grassland webs reflects a balance between competition among plants for nutrients and light, that is constantly redressed by the grazing of herbivores. Artificial fertilization or reduction in herbivores always leads to reductions in plant diversity

due to intensification of competition between plants, disconcertingly echoing the mass uncontrolled experiments that humans are undertaking in many natural ecosystems. If we are ever going to use food-web models to understand these trophic-cascade effects, we will need to develop models that realistically capture the dynamics of the plant community.

The last ten years have seen considerable advances in our understanding of the forces that structure theoretical food webs; the advances developed by Allesina and colleagues almost match the increases of understanding gained in the previous four decades and take us a long way towards resolving the initial 'complexity versus stability' conundrum first described by May (see Box 1). The 'devious strategies which make for stability in enduring natural systems' that allow coexistence have now been considerably untangled. A major next step will be to develop new hybrid methods that combine insights from plant community ecology into food web theory. This will then provide a new framework for examining the structure of the temperate woodlands, tropical forests and savannas that contain most of the terrestrial biodiversity on the planet.

A key result to emerge from recent work on food webs described in Box 1 emphasizes the powerful stabilizing influence of indirect interactions between species that are mediated by a third or fourth species (Allesina et al., 2015; Grilli et al., 2017; Mayfield and Stouffer, 2017). Such interactions are central to the recruitment and survival of many tropical and temperate plant species; particularly the presence of fungal pathogens and mutualists. Ecologists have increasingly realized that Janzen-Connell effects that minimize recruitment of seedlings in sites adjacent to their parent tree are driven by fungal pathogens (Augspurger, 1983; Gilbert and Hubbell, 1996; Packer and Clay, 2000; Bagchi et al., 2010; Mangan et al., 2010). This in turn ensures that competition for light and soil resources between plants in tropical forests is mediated at the recruitment stage by indirect inter-specific interactions largely driven by fungal pathogens. The impact of fungal, nematode, insect, and bacterial pathogens that attack seedlings and older plants is considerably modified and ameliorated by the presence of a diversity of symbiotic fungi that organize themselves into a "symbiotic immune system" that helps protect older plants against further attacks (Jones and Dang, 2006; Lo Presti et al., 2015). The key thing about these fungal associations from a food-web perspective is that they generate a diversity of indirect effects that modulate more direct impacts on the plant's fitness. They also create blocks of interactions that are specific to each tree species, and often to individual trees, thus creating patchy block motifs within the overall matrix of food web interactions (Grilli et al., 2016). These effects, and the modular compartmentalized structure they promote, could have a stabilizing influence on the overall structure of the web, a result that would not have been apparent using the earlier models for food web structure. Fungal interactions are considerably less diverse in marine and freshwater systems, perhaps because algae produce classes of toxins that are particularly detrimental to fungi and bacteria (Kini et al., 2020).

The community of host-specific fungal pathogens and insects combines with those generated by less specific seed-dispersers and

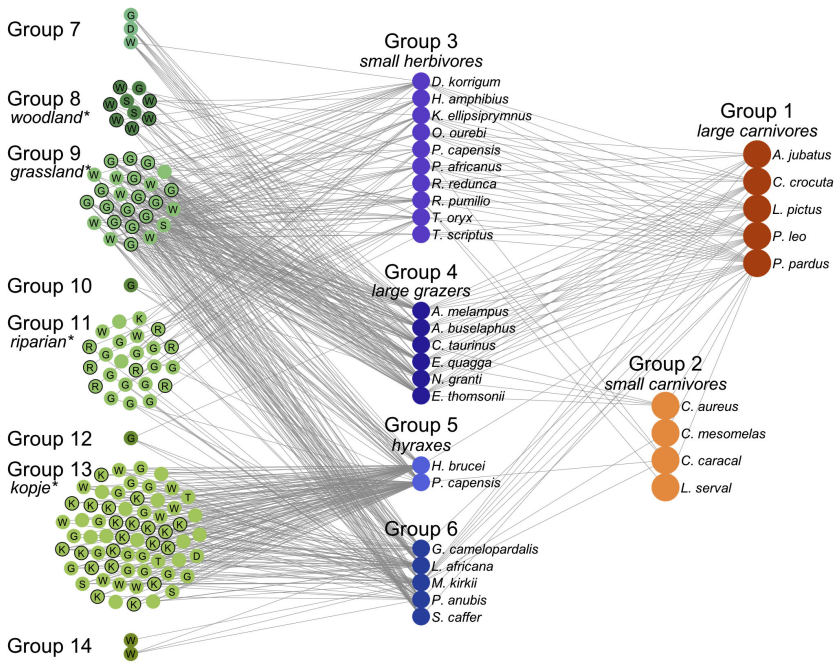

FIGURE 2
The Serengeti food web. The network is shown organized and colored by group according to the consensus partition method and arranged by trophic level from left (plants) to right (carnivores). Plants are identified by the first letter of identified habitat type, if available: (G)rassland, (W)oodland, (R)iparian, (K)opje, (S)hrubland, (T)hicket, and (D)isturbed. Plant groups are labeled by significantly overrepresented habitat types, and species assigned to the overrepresented type are labeled with black borders. An interactive version of this figure is available at http://edbaskerville.com/research/serengeti-food-web/. (Baskerville et al., 2011).

pollinators to create considerable modularity the overall matrix of interactions between species in the food web for the ecosystem. Each modular group reflects the large number of interactions that occur between fungi, bacteria, nematodes and insects that are specialists on each plant species, or perhaps even each individual trees. In contrast, the overall matrix of species interactions will be shadowed by the more diffuse connections of generalist pollinators, seed-dispersers and herbivores species that utilize multiple species of trees. Theoretical studies show that the heterogeneities generated by specialists are likely to be more stabilizing than when generalists dominate these components of food web structure (Grilli et al., 2016). Similar patterns occur in the communities of parasites and pathogens that feed in and upon all the species that feed in the herbivorous and carnivorous trophic levels of the web (Lafferty et al., 2008).

Seasonal fluctuations and microbiomes

Deciduous forests are characterized by a huge annual fluctuation in basal resources when the leaves and fruit produced in the spring and consumed throughout the summer; concomitantly their leaves convert atmospheric CO_2 into carbohydrates and add new structure to the canopy and roots as well as nutrients for consumers. Recent studies illustrate that in many temperate, tropical and boreal forests, a high proportion of carbon uptake is stored in fungi associated with the roots systems (Hawkins et al., 2023). In the autumn, leaf fall moves a huge volume of nutrients back to the ground and into the soil, sequentially (but asymmetrically) connecting the canopy food webs with those of the understory and the soil. These nutrients are consumed by a large community of fungi, worms and bacteria, many of which have symbiotic relationships with the roots of the parent tree (Cornwell et al., 2009; Hardoim et al., 2015). Other fungi are less altruistic and drive the 'Janzen-Connell' effect described above that provide an important driver of tropical forest diversity by preventing offspring of the parent tree establishing in their near vicinity (Bagchi et al., 2010; Mangan et al., 2010). These mechanisms most likely underlie the strong conspecific negative density-dependence, recently quantified in the 50 hectare forest plot on Barro Colorado Island in Panama (Kalyuzhny et al., 2023).

Similar plant-microbial couplings also operate in savannas and grassland (Petermann et al., 2008): the rainy season converts an almost barren and inedible landscape into high quality pasture that can feed a huge abundance of herbivores. In the Serengeti, when the rains end, and the long dry season begins, larger herbivores such as wildebeest and zebra migrate away from nutrient rich soils where they've fed during lactation. Their dung, urine, and the death of young calves and adults slowly disperse these nutrients to the soil in nutrient poor regions of the ecosystem. Recent studies of the Serengeti food web illustrate how the long-lived perennial grasses create an annual pulse of nutrients that drives the fast dynamics of the wildebeest and their predators, while the woodlands and the kopjes (rocky outcrops or inselbergs) support sub-communities of less abundant vertebrates that operate on a much slower timescale (Dobson, 2009). We are only just beginning to glimpse how the above ground heterogeneity created by different plant communities is matched by the mycorrhizal and invertebrate communities feeding on the roots beneath the soil surface (Wardle et al., 2004; Crowther et al., 2013). We suspect that it is similar, but soil organisms and other microbes are all too rarely considered in savanna food web studies.

Our hopes that food web studies will help us understand how ecosystems will respond to climate change and other anthropogenic insults founder on the paucity of food web-studies that include trees and their mycorrhizal associations. Acid rain is devastating for fungi, so many temperate plant communities have only been observed in the absence of the mycorrhizae they co-evolved with; similarly fires destroy mycorrhizae. If you visit Yellowstone National Park there are still bare areas of ground with essentially no tree recruitment since the fires of 1988 (Turner et al., 1997; Turner et al., 2003). These are areas where the hottest fires destroyed the mycorrhizal community and pine seedlings are denied the symbiotic mechanism that allows them access to vital soil nutrients (Franke, 2000). The really bad news here is that the last two years have seen extensive fires across the boreal forests and tundra of northern Canada; this has destroyed huge areas of habitat, if the mycorrhizae are lost, these areas may take even longer to recover.

Fire is an important component of many savanna and forest ecosystems; plants are the species that supply fuel for fires and fires return nutrients to the soil; but few food-web models consider fire as a component of the web (although see (Bowman et al., 2016). Some authors have suggested fire appears as a super-herbivore that profoundly effects the dynamics of tree-grass interaction in savannas (McNaughton, 1985; Bond and van Wilgren, 1996; Bond and Keeley, 2005). We tend to see it as more closely resembling an "uber-virus"; it has essentially zero mass and requires a threshold level of host abundance to establish. Like true viruses, the impact of fire on ecosystem structure can be subtle and profound (Holdo et al., 2009; Staver et al., 2011; Beale et al., 2018), to date no food-web models include fire in any form, yet it is essential to the structure and diversity of vegetation in savannas, fynbos, and drier forests (Bond and van Wilgren, 1996; Higgins et al., 2000). Our major concern here is that when fire removes trees and burns at sufficient heat to destroy the soil mycorrhizal community, then the most important stabilizing component of the food web may have been lost and may take the time of many generations of shorter-lived, tree-dependent taxa to recover.

Reproduction and the other webs

While mycorrhizal associations are the most well-known examples of plant-microbe interactions, there are a suite of additional ways in which plants are foundational to microbial ecosystems. Among these, floral nectaries play host to suites of microbial organisms that disperse and establish through flower-visiting animal vectors (Herrera et al., 2009; Belisle et al., 2012). Similarly, carnivorous pitcher plants support a diverse microbial

10.3389/fevo.2023.1253084

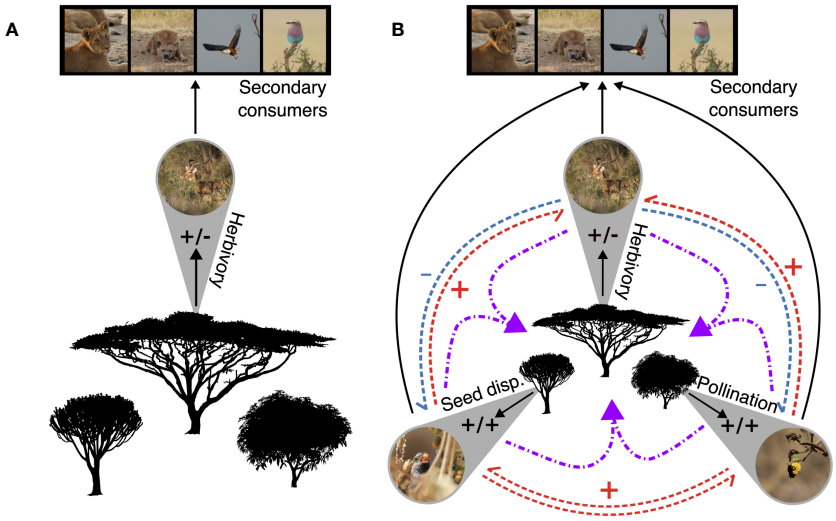

FIGURE 3
A comparison of two food webs. The first, **(A)**, is a three-trophic-level food web of East African primary producers and consumers. Herbivory, as represented by the browsing impala, is the only form of primary consumption. This linear food web represents the classic mental model of feeding relationships and energetic pathways in an ecosystem. **(B)** Increasing the resolution of primary consumer guilds in the this food-web changes its complexity, the potential for indirect (blue and red) and higher-order (purple) interactions among primary consumer guilds, and illustrates how including a wider range of interactions and taxa into food webs can lead to a new mental model of feeding relationships, where plant population and community dynamics are central, primary consumer guilds are arrayed around them, and secondary consumers attach at the outer edges. All photos courtesy of MCH.

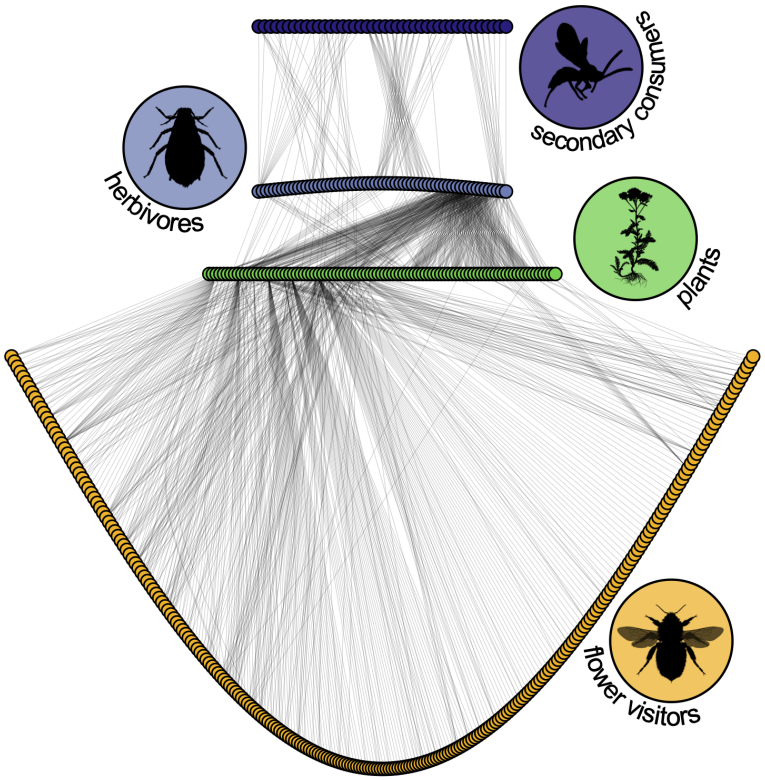

FIGURE 4
The food-web of Norwood Farm (Somerset, UK) collected by and recreated from the data of Pocock, Evans and Memmott (Pocock et al., 2012). Green circles represent plant species, gray-blue circles are antagonistic primary consumers (aphids and seed-feeders), dark purple circles are parasites and parasitoids, and yellow circles potential pollinators (flower visitors and butterflies). Out of the more than 1200 interactions, 45% are between plants and flower visitors. Likewise, 56% of taxa (252/451) are flower visitors. Their inclusion dramatically alters this food-web. Plant interactions with leaf-miner parasitoids were excluded from the original dataset. All silhouettes are from phylopic.org and the bee image was contributed by Melissa Broussard.

ecosystem within the aqueous solution that decomposes their prey (Baiser et al., 2012). Among plants that do not 'eat' animals, diverse microbial communities are found on the surface (Vorholt, 2012) and inside of their leaves (Arnold, 2007). What is becoming clear is that the trophic relationships within the microbial communities of many individual plants may be as complex as even the most diverse of currently resolved macroscopic food webs!

Integrating higher plants into food web theory requires a shift from these species being the basal fodder of grazers and browsers to the central assemblage in terrestrial ecosystems upon which the vast majority of animal and microbial communities and their direct, indirect, and higher-order interactions are assembled (Figure 3). The historical dominance of aquatic ecosystems in food-web ecology has meant that the non-folivorous webs that higher plants host are often not explicitly accounted for in food-web theory. An increasingly large literature on the associations between plants and their pollinators and seed-dispersers, who are both mutualists and consumers of higher plants, coupled with their importance for plant reproduction primes these interactions for inclusion in broader food-web models. In short, to adequately incorporate higher plants into food-web theory we must not forget the birds and the bees!

Animal pollinators facilitate reproduction for around 88% of all flowering plants (Ollerton et al., 2011), a proportion that can reach 98-99% in tropical forests (Bawa, 1990). Similarly, up to 90% of woody plants rely on vertebrates for seed-dispersal (Jordano, 2000), while a substantial proportion of herbaceous seeds are dispersed by ants (Howe and Smallwood, 1982). More specifically, endozoochorous seed-dispersal (i.e., where the disperser receives a meal and the association is often mutually beneficial) ranges from 30–40% of woody species in temperate forests, to 70–94% in neotropical rainforests (Jordano, 2000). Given the nature and ubiquity of these associations, this means that many of the primary consumers in any real food web rely on something other than a plant's leaves (Figure 4).

While 'consumers of fruits and nectar' are occasionally included in empirical food webs (Polis, 1991; de Visser et al., 2011), pollinators and seed-dispersers are generally beneficial to plants, in contrast to folivores that suppress plants (Pringle et al., 2023). When pollinators and seed-dispersers are lost, plant recruitment can be significantly reduced (Robertson et al., 1999; Cordeiro and Howe, 2001; Clark et al., 2007). Similarly, the importance of these species is highlighted by the fact that their loss can drive rapid directional evolutionary change in plant reproductive morphology (Galetti et al., 2013; Gervasi and Schiestl, 2017), and the long-term dynamics of plant communities are intimately bound to these mutualistic primary consumers (Jordano, 2000). The reproduction of higher plants also represents an under-appreciated avenue through which plants drive food web dynamics. While the annual loss and growth of foliage by deciduous trees is a temporally consistent resource pulse in food webs, the phenology of plant reproduction can be more variable and suggests how animal populations may be stabilized by a trickle of resources as opposed to a pulse. For example, the reproduction of *Ficus* species in the tropics is often aseasonal both at the scale of individual trees (Bronstein and Patel, 1992) and among species (Lambert and Marshall, 1991). The result of this asynchrony is a steady supply of fruit and floral resources for mutualistic primary consumers. Crucially, figs are the major source of calcium for many frugivorous birds and mammals (O'Brien et al., 1998). Even in climatically harsh boreal and tundra biomes, some plants retain fruits into the autumn and winter (Mulder et al., 2021), representing a crucial resource of frugivores outside of the growing season. Shifting availability of floral and fruit resources can also have strong effects on the spatial and temporal distribution of pollinators and frugivorous seed-disperser populations (Levey, 1988a; Levey, 1988b; Kinnaird et al., 1996; Olesen et al., 2011). Over the past 30 years, a rapidly growing literature on the structure and function of bipartite plant-mutualist networks has developed (Jordano, 1987; Bascompte and Jordano, 2013; Valdovinos, 2019; Valdovinos and III, 2021), yet it has remained largely distinct from classic food web studies. The incorporation of reproductive mutualisms into food web theory would represent the conceptual coupling of two dominant fields in community ecology. Food-web models that consider higher-plant population dynamics and the mutualists that drive those dynamics will also benefit from the conceptual advances in mutualistic-network ecology on the phenology of species interactions (CaraDonna et al., 2014; Ponisio et al., 2017), species-species interactions that do not occur (Olesen et al., 2011), and structure-stability relationships in different ecological networks (Thébault and Fontaine, 2010; Sauve et al., 2014).

The integration of pollination and seed-dispersal associations into food web theory has the potential to alter the image of complexity and stability of currently resolved food webs while also improving the biological realism of plant-population models (Figure 4). May's stability criterion (Box 1) relies on species richness, interaction strength, and connectance (i.e. the proportion of trophic links observed out of the total possible links) (May, 1973; van Altena et al., 2016). Pollinators are a mega-diverse guild; the addition of these species to food webs will increase species richness and almost certainly alter connectance and network macrostructures (Figure 4). Furthermore, the links between pollinators, seed-dispersers, and their respective predators may produce more accurate food web representations by filling in some of the 'missing links' (Dobson et al., 2008; Lafferty et al., 2008). For precedence, the incorporation of parasites into food webs this has had startling implications for studies of food web complexity (Lafferty et al., 2006). Incorporating the population and community dynamics of higher plants to food web theory will not only improve the resolution of the basal resource level but also necessitate the inclusion of entire guilds of animal species not typically represented in classic predator-prey food webs, such as pollinators and frugivorous seed-dispersers.

Incorporating reproductive mutualisms into food-web theory involves more than tacking on a plant-pollinator or plant-frugivore module to existing food-webs and assuming that all interactions in these mutualistic modules are always mutually beneficial. Mutualisms are prone to cheating behaviors, which can shift these interactions, at least temporarily, towards parasitism (Jones et al., 2015). For example, endozoochorus dispersal—by virtue of fruits and seeds being ingested—tends to involve some kind of nutritional reward to the consumer, but the effect on the plant can

range from seeds requiring gut passage for germination to seed predation. Epizoochorus dispersal, where seeds are dispersed without ingestion, such as by hooking onto fur, offer no cost to the disperser, but also no benefit. Furthermore, obligate frugivores are few and far between (Jordano, 2000), seed-predators, such as ants and small mammals, can still be important seed dispersers) (Janzen, 1971), and seed-dispersal by large folivores may be negated by their leaf and stem consumption. Browsing ungulates can be important seed-dispersers (Rodríguez-Pérez et al., 2011; Pringle et al., 2014) despite their largely folivorous diets and negative effect on plants (Pringle et al., 2023). Therefore, the devil of integrating plant reproduction into food webs almost certainly lies in the details of how reproductive mutualisms function and are quantified.

Seeing the web with the trees

In conclusion, we argue that a deeper consideration of the role of higher plants in food webs is needed to create the "next generation" of food web models. The simplest way to do this would be to include trees and plants as basal species in food webs where spatial competition for light, water, and nutrients creates a community of species that live for a very long time and thus generate significant underlying stability that trickles up to the species that feed in and upon them. These primary consumers can be divided into two broad classes of species: (1) those that feed on the regular production of fruits, leaves, sap and bark of the plant; and (2) the large community of fungi, bacteria and parasitic plants that drive interactions with the plant and its surrounding environment and through time modify the structure of the individual tree, in ways that usually enhance the persistence of both the tree and its 'symbiotic' community. The inclusion of this huge diversity of parasitic and mutualistic species echoes recent pleas to include parasites and pathogens into models for food webs (Lafferty et al., 2006; Dobson et al., 2008; Lafferty et al., 2008). Each of these groups of species generate fuzzy but modular blocks within the matrix of interactions between species that form the overall structure of any food web matrix.

The theoretical and technical advances required to bring higher plants into food web studies is beginning to emerge. Multilayer and multiplex ecological networks are an exciting development that allow several webs (be they the webs associated to individual trees in a forest or webs describing different types of ecological interactions) to be described as single mathematical object (Pilosof et al., 2015; García-Callejas et al., 2018; Guimaraes, 2020). An important recent study has plotted a potential course for the integration of niche theory with food web theory (Godoy et al., 2018). Yet others have described how bioenergetic food-web models may be extended to include terrestrial plant-herbivore interactions. (Valdovinos et al., 2022). These approaches will generate the food-web descriptions that will be used to explore the organization of terrestrial species interactions at the broadest community level and can quickly become the grist for the next generation of food-web models that needed to help understand the consequences resource exploitation and deforestation in all the world's forests. Hopefully, they can also provide important guides for pathways to forest restoration.

We conclude on a final note of urgency. We are losing trees, forest and grasslands at a rapid rate. If the stability and persistence of terrestrial ecosystems is dependent upon long-lived plant species we need to considerably upgrade attempts to protect them. There are roughly 400 trees for every human on the planet, this number is decreasing for two reasons: increasing human population and the loss of 15 billion trees each year (Crowther et al., 2015); land-use conversion since the dawn of agriculture has led to the loss of around 46% of global tree abundance. Slowing this loss of trees, forests, and perennial grasslands is arguably the most efficient way to reduce the net rate of species extinction (Schleuning et al., 2016). Restoring degraded forests, savannas, and grasslands is arguably the most cost-effective and efficient way to reverse global climate heating. As most of the freshwater used by humans is supplied by rivers and streams that have their origins in forests and water sheds, then human dependence on freshwater should form the basis of any cogent argument about the importance of protecting forests (Garrick et al., 2017). This should protect both the forests and the trees that are arguably the key components of most terrestrial food webs.

Data availability statement

The original contributions presented in the study are included in the article/supplementary material. Further inquiries can be directed to the corresponding authors.

Author contributions

All authors listed have made a substantial, direct, and intellectual contribution to the work and approved it for publication.

Acknowledgments

The original genesis for this article came from a day wandering around Windsor Great Park with Ted Greene and Mick Crawley, we thank them for many inspiring conversations about plants. This paper is dedicated to them as lifetime sources of inspiration. Many thanks to Jen Guyton for the photograph of Welwitschia in Figure 1. We have also benefited hugely from conversations with Bob May, Mercedes Pascual, Jennifer Dunne, Jonathan Levine and Stefano Allesina about food webs and annual conversations at STRI in Panama with Allan Herre, Stefan Schnitzer, Scott Mangon, John Schroeder, Dan Petticord, and Luis Mejía about tropical plants and their pathogens.

Conflict of interest

The authors declare that the research was conducted in the absence of any commercial or financial relationships that could be construed as a potential conflict of interest.

Publisher's note

References

Allesina, S., Grilli, J., Barabás, G., Tang, S., Aljadeff, J., and Maritan, A. (2015). Predicting the stability of large structured food webs. *Nat. Commun.* 6, 7842. doi: 10.1038/ncomms8842

Allesina, S., and Pascual, M. (2009). Food web models: a plea for groups. *Ecology letters* 12 (7), 652-662.

Allesina, S., and Levine, J. M. (2011). A competitive network theory of species diversity. *Proc. Natl. Acad. Sci.* 108 (14), 5638–5642.

Allesina, S., and Tang, S. (2012). Stability criteria for complex ecosystems. *Nature* 483, 205–208. doi: 10.1038/nature10832

Allesina, S., and Tang, S. (2015). The stability–complexity relationship at age 40: a random matrix perspective. *Population Ecol.* 57, 63–75. doi: 10.1007/s10144-014-0471-0

Allesina, S., Alonso, D., and Pascual, M. (2008). A general model for food web structure. *Science* 320 (5876), 658-661.

Arnold, A. E. (2007). Understanding the diversity of foliar endophytic fungi: progress, challenges, and frontiers. *Fungal biology reviews* 21 (2-3), 51-66.

Augspurger, C. K. (1983). Seed dispersal by the tropical tree, Platypodium elegans, and the escape of its seedlings from fungal pathogens. *J. Of Ecol.* 71, 759–771. doi: 10.2307/2259591

Bagchi, R., Swinfield, T., Gallery, R. E., Lewis, O. T., Gripenberg, S., Narayan, L., et al. (2010). Testing the Janzen-Connell mechanism: pathogens cause overcompensating density dependence in a tropical tree. *Ecol. Lett.* 13, 1262–1269. doi: 10.1111/j.1461-0248.2010.01520.x

Bascompte, J., and Jordano, P. (2013). *Mutualistic networks* (Princeton University Press).

Baiser, B., Gotelli, N. J., Buckley, H. L., Miller, T. E., and Ellison, A. M. (2012). Geographic variation in network structure of a nearctic aquatic food web. *Global Ecology and Biogeography* 21 (5), 579-591.

Baskerville, E. B., Dobson, A. P., Bedford, T., Allesina, S., Anderson, T. M., and Pascual, M. (2011). Spatial guilds in the serengeti food web revealed by a Bayesian group model. *PLoS Comput. Biol.* 7, e1002321. doi: 10.1371/journal.pcbi.1002321

Bawa, K. (1990). Plant-pollinator interactions in tropical rain forests. *Annu. Rev. Of Ecol. And Systematics* 21, 399–422. doi: 10.1146/annurev.es.21.110190.002151

Beale, C. M., Courtney Mustaphi, C. J., Morrison, T. A., Archibald, S., Anderson, T. M., Dobson, A. P., et al. (2018). Pyrodiversity interacts with rainfall to increase bird and mammal richness in African savannas. *Ecol. Lett.* 21, 557–567. doi: 10.1111/ele.12921

Belisle, M., Peay, K. G., and Fukami, T. (2012). Flowers as islands: spatial distribution of nectar-inhabiting microfungi among plants of Mimulus aurantiacus, a hummingbird-pollinated shrub. *Microbial ecology* 63 (7), 711-718.

Bond, W. J., and Keeley, J. E. (2005). Fire as a global "herbivore": the ecology and evolution of flammable ecosystems. *Trends In Ecol. Evol.* 20, 387–394. doi: 10.1016/j.tree.2005.04.025

Bond, W. J., and van Wilgren, B. W. (1996). *Fire and Plants* (London: Chapman and Hall).

Borer, E. T., Grace, J. B., Harpole, W. S., MacDougall, A. S., and Seabloom, E. W. (2017). A decade of insights into grassland ecosystem responses to global environmental change. *Nat. Ecol. Evol.* 1, 0118. doi: 10.1038/s41559-017-0118

Bowman, D. M., Perry, G. L., Higgins, S. I., Johnson, C. N., Fuhlendorf, S. D., and Murphy, B. P. (2016). Pyrodiversity is the coupling of biodiversity and fire regimes in food webs. *Philos. Trans. R. Soc. B: Biol. Sci.* 371, 20150169.

Bronstein, J. L., and Patel, A. (1992). Causes and consequences of within-tree phenological patterns in the Florida strangling fig, Ficus aurea (Moraceae). *Am. J. Of Bot.* 79, 41–48. doi: 10.1002/j.1537-2197.1992.tb12621.x

Brown, P. M. (1996). "OldList: A Database of Maximum Tree Ages" Radiocarbon. In "*Tree Rings, Environment and Humanity*" eds. J. S. Dean, D. M. Meko, T. W. Swetnam. pp. 727-731.

CaraDonna, P. J., Iler, A. M., and Inouye, D. W. (2014). Shifts in flowering phenology reshape a subalpine plant community. *Proc. Natl. Acad. Sci.* 111, 4916–4921. doi: 10.1073/pnas.1323073111

Chisholm, R. A., Condit, R., Rahman, K. A., Baker, P. J., Bunyavejchewin, S., Chen, Y. Y., et al. (2014). Temporal variability of forest communities: empirical estimates of population change in 4000 tree species. *Ecol. Lett.* 17, 855–865. doi: 10.1111/ele.12296

Clark, C., Poulsen, J., Levey, D., and Osenberg, C. (2007). Are plant populations seed limited? A critique and meta-analysis of seed addition experiments. *Am. Nat.* 170, 128–142. doi: 10.1086/518565

Cordeiro, N. J., and Howe, H. F. (2001). Low recruitment of trees dispersed by animals in African forest fragments. *Conserv. Biol.* 15, 1733–1741. doi: 10.1046/j.1523-1739.2001.99579.x

Cornwell, W. K., Cornelissen, J. H., Allison, S. D., Bauhus, J., Eggleton, P., Preston, C. M., et al. (2009). Plant traits and wood fates across the globe: rotted, burned, or consumed? *Global Change Biol.* 15, 2431–2449.

Crowther, T. W., Glick, H. B., Covey, K. R., Bettigole, C., Maynard, D. S., Thomas, S. M., et al. (2015). Mapping tree density at a global scale. *Nature* 525, 201–205. doi: 10.1038/nature14967

Crowther, T. W., Stanton, D. W., Thomas, S. M., A'Bear, A. D., Hiscox, J., Jones, T. H., et al. (2013). Top-down control of soil fungal community composition by a globally distributed keystone consumer. *Ecology* 94, 2518–2528. doi: 10.1890/13-0197.1

D'Alelio, D., Libralato, S., Wyatt, T., and d'Alcalà, M. R. (2016). Ecological-network models link diversity, structure and function in the plankton food-web. *Sci. Rep.* 6, 21806. doi: 10.1038/srep21806

de Visser, S. N., Freymann, B. P., and Olff, H. (2011). The Serengeti food web: empirical quantification and analysis of topological changes under increasing human impact. *J. Of Anim. Ecol.* 80, 484–494. doi: 10.1111/j.1365-2656.2010.01787.x

Dobson, A. P. (2009). Food-web structure and ecosystem services: insights from the Serengeti. *Philos. Trans. R. Soc. London Ser. B* 364, 1665–1682. doi: 10.1098/rstb.2008.0287

Dobson, A. P., Lafferty, K. D., Kuris, A. M., Hechinger, R. F., and Jetz, W. (2008). Homage to Linnaeus: How many parasites? How many hosts? *PNAS* 105, 11482–11489. doi: 10.1073/pnas.0803232105

Farjon, A. (2008). *A natural history of conifers*. Portland, OR: Timber Press.

Fine, P. V., Mesones, I., and Coley, P. D. (2004). Herbivores promote habitat specialization by trees in Amazonian forests. *Science* 305, 663–665. doi: 10.1126/science.1098982

Franke, M. A. (2000). *Yellowstone in the Afterglow* (Mammoth Hot Springs, Wyoming: Yellowstone National Park).

Galetti, M., Guevara, R., Côrtes, M. C., Fadini, R., Von Matter, S., Leite, A. B., et al. (2013). Functional extinction of birds drives rapid evolutionary changes in seed size. *Science* 340, 1086–1090. doi: 10.1126/science.1233774

García-Callejas, D., Molowny-Horas, R., and Araújo, M. B. (2018). Multiple interactions networks: towards more realistic descriptions of the web of life. *OIKOS* 127, 5–22. doi: 10.1111/oik.04428

Gardner, M. R., and Ashby, W. R. (1970). Connectance of large dynamic (cybernetic) systems: critical values for stability. *Nature* 228 (5273), 784.

Garrick, D. E., Hall, J. W., Dobson, A., Damania, R., Grafton, R. Q., Hope, R., et al. (2017). Valuing water for sustainable development. *Science* 358, 1003–1005. doi: 10.1126/science.aao4942

Gervasi, D. D., and Schiestl, F. P. (2017). Real-time divergent evolution in plants driven by pollinators. *Nat. Commun.* 8, 14691. doi: 10.1038/ncomms14691

Gibbs, T., Levin, S. A., and Levine, J. M. (2022). Coexistence in diverse communities with higher-order interactions. *Proc. Natl. Acad. Sci.* 119, e2205063119. doi: 10.1073/pnas.2205063119

Gilbert, G. S., and Hubbell, S. P. (1996). Plant diseases and the conservation of tropical forests. *BioSCience* 46, 98–106. doi: 10.2307/1312812

Godoy, O., Bartomeus, I., Rohr, R. P., and Saavedra, S. (2018). Towards the integration of niche and network theories. *Trends In Ecol. Evol.* 33, 287–300. doi: 10.1016/j.tree.2018.01.007

Grilli, J., Barabás, G., Michalska-Smith, M. J., and Allesina, S. (2017). Higher-order interactions stabilize dynamics in competitive network models. *Nature* 548, 210–213. doi: 10.1038/nature23273

Grilli, J., Rogers, T., and Allesina, S. (2016). Modularity and stability in ecological communities*Nature Communications* Vol. 7 (1), 12031.

Grubb, P. J. (1977). The maintenance of species-richness in plant communities: the importance of the regeneration niche. *Biol. Rev.* 52, 107–145. doi: 10.1111/j.1469-185X.1977.tb01347.x

Gruner, D. S., Smith, J. E., Seabloom, E. W., Sandin, S. A., Ngai, J. T., Hillebrand, H., et al. (2008). A cross-system synthesis of consumer and nutrient resource control on producer biomass. *Ecol. Lett.* 11, 740–755. doi: 10.1111/j.1461-0248.2008.01192.x

Guimaraes, J. P.R. (2020). The structure of ecological networks across levels of organization. *Annu. Rev. Ecology Evolution Systematics* 51, 433–460. doi: 10.1146/annurev-ecolsys-012220-120819

Hardoim, P. R., Van Overbeek, L. S., Berg, G., Pirttilä, A. M., Compant, S., Campisano, A., et al. (2015). The hidden world within plants: ecological and evolutionary considerations for defining functioning of microbial endophytes. *Microbiol. Mol. Biol. Rev.* 79, 293–320. doi: 10.1128/MMBR.00050-14

Hawkins, H.-J., Cargill, R. I., Van Nuland, M. E., Hagen, S. C., Field, K. J., Sheldrake, M., et al. (2023). Mycorrhizal mycelium as a global carbon pool. *Curr. Biol.* 33, R560–R573. doi: 10.1016/j.cub.2023.02.027

Herrera, C. M., De Vega, C., Canto, A., and Pozo, M. I. (2009). Yeasts in floral nectar: a quantitative survey. *Annals of botany* 103 (9), 1415-1423.

Herre, H. (1961). The age of Welwitschia bainesii. *South Afr. J. Bot.* 27, 139-140.

Higgins, S., Bond, W.-J., and Trollope, W.-S.-W. (2000). Fire, resprouting and variability: A recipe for grass-tree coexistence in savanna. *J. Of Ecol.* 88, 213–229. doi: 10.1046/j.1365-2745.2000.00435.x

Hillebrand, H., Gruner, D. S., Borer, E. T., Bracken, M. E., Cleland, E. E., Elser, J. J., et al. (2007). Consumer versus resource control of producer diversity depends on ecosystem type and producer community structure. *Proc. Natl. Acad. Sci.* 104, 10904–10909. doi: 10.1073/pnas.0701918104

Holdo, R. M., Sinclair, A. R. E., Dobson, A. P., Metzger, K. L., Bolker, B., and Holt, R. D. (2009). A disease-mediated trophic cascade in the Serengeti and its implications for ecosystem C. *PloS Biol.* 7 (9), 1-12. e1000210. doi: 10.1371/journal.pbio.1000210

Howe, H. F., and Smallwood, J. (1982). Ecology of seed dispersal. *Annu. Rev. Of Ecol. And Systematics* 13, 201–228. doi: 10.1146/annurev.es.13.110182.001221

Hubbell, S. (2001). *The Unified Theory of Biodiversity and Biogeography* (Princeton: Princeton University Press).

Hutchinson, G. E. (1961). The paradox of the plankton. *Am. Nat.* 95, 137–145. doi: 10.1086/282171

Hutchinson, M. C., Dobson, A. P., and Pringle, R. M. (2022). Dietary abundance distributions: Dominance and diversity in vertebrate diets. *Ecol. Lett.* 25, 992–1008. doi: 10.1111/ele.13948

Janzen, D. H. (1971). Seed predation by animals. *Annu. Rev. Of Ecol. And Systematics* 2, 465–492. doi: 10.1146/annurev.es.02.110171.002341

Jones, J. D., and Dangl, J. L. (2006). The plant immune system. *Nature* 444 (7117), 323–329.

Jones, E. I., Afkhami, M. E., Akçay, E., Bronstein, J. L., Bshary, R., Frederickson, M. E., et al. (2015). Cheaters must prosper: reconciling theoretical and empirical perspectives on cheating in mutualism. *Ecology letters* 18 (11), 1270-1284.

Jordano, P. (1987). Patterns of mutualistic interactions in pollination and seed dispersal: connectance, dependence asymmetries, and coevolution. *Am. Nat.* 129, 657–677. doi: 10.1086/284665

Jordano, P. (2000). "Fruits and frugivory," in *Seeds-the ecology of regeneration of plant communities*. Ed. M. Fenner (Wallingford: CABI), 125–166.

Kalyuzhny, M., Lake, J. K., Wright, S. J., and Ostling, A. M. (2023). Pervasive within-species spatial repulsion among adult tropical trees. *Science* 381, 563–568. doi: 10.1126/science.adg7021

Kini, S., Divyashree, M., Mani, M. K., and Mamatha, B. S. (2020). "Algae and cyanobacteria as a source of novel bioactive compounds for biomedical applications," in *Advances in cyanobacterial biology* (Academic Press), 173–194.

Kinnaird, M. F., O'Brien, T. G., and Suryadi, S. (1996). Population fluctuation in Sulawesi Red-knobbed Hornbills: tracking figs in space and time. *Auk* 113, 431–440. doi: 10.2307/4088909

Lafferty, K. D., Allesina, S., Arim, M., Briggs, C. J., De Leo, G., Dobson, A. P., et al. (2008). Parasites in food webs: the ultimate missing links. *Ecol. Lett.* 11, 533–546. doi: 10.1111/j.1461-0248.2008.01174.x

Lafferty, K. D., Dobson, A. P., and Kuris, A. M. (2006). Parasites dominate food web links. *PNAS* 103, 11211–11216. doi: 10.1073/pnas.0604755103

Lambert, F. R., and Marshall, A. G. (1991). Keystone characteristics of bird-dispersed *Ficus* in a Malaysian lowland rain forest. *J. Of Ecol.* 79, 793–809. doi: 10.2307/2260668

Levey, D. J. (1988a). Spatial and temporal variation in Costa RIcan fruit and fruit-eating bird abundance. *Ecol. Monogr.* 58, 251–269. doi: 10.2307/1942539

Levey, D. J. (1988b). Tropcal wet forest treefall gaps and distribution of understory birds and plants. *Ecology* 69, 1076–1089. doi: 10.2307/1941263

Lo Presti, L., Lanver, D., Schweizer, G., Tanaka, S., Liang, L., Tollot, M., et al. (2015). Fungal effectors and plant susceptibility. *Annu. Rev. Plant Biol.* 66, 513–545. doi: 10.1146/annurev-arplant-043014-114623

Loreau, M., and De Mazancourt, C. (2013). Biodiversity and ecosystem stability: a synthesis of underlying mechanisms. *Ecol. Lett.* 16, 106–115. doi: 10.1111/ele.12073

Mangan, S. A., Schnitzer, S. A., Herre, E. A., Mack, K. M., Valencia, M. C., Sanchez, E. I., et al. (2010). Negative plant-soil feedback predicts tree-species relative abundance in a tropical forest. *Nature* 466, 752. doi: 10.1038/nature09273

May, R. M. (1973). Stability and complexity in model ecosystems. *Ecology*. 54 (3), 638-641.

Mayfield, M. M., and Stouffer, D. B. (2017). Higher-order interactions capture unexplained complexity in diverse communities. *Nat. Ecol. Evol.* 1, 0062. doi: 10.1038/s41559-016-0062

McCann, K. S. (2011). *Food webs (Monographs in Population Biology-50).* (Princeton University Press).

McCann, K., Rasmussen, J. B., and Umbanhowar, J. (2005). The dynamics of spatially coupled food webs. *Ecol. Lett.* 8, 513–523. doi: 10.1111/j.1461-0248.2005.00742.x

McNaughton, S. J. (1985). Ecology of a grazing ecosystem: The Serengeti. *Ecol. Monogr.* 55, 259–294. doi: 10.2307/1942578

Mulder, C. P., Spellman, K. V., and Shaw, J. (2021). Berries in winter: A natural history of fruit retention in four species across Alaska. *Madrono* 68, 487–510. doi: 10.3120/0024-9637-68.4.487

O'Brien, T. G., Kinnaird, M. F., Dierenfeld, E. S., Conklin-Brittain, N. L., and Silver, S. C. (1998). What's so special about figs: A pantropical mineral analysis. *Nature* 392, 668. doi: 10.1038/33580

Olesen, J. M., Bascompte, J., Dupont, Y. L., Elberling, H., Rasmussen, C., and Jordano, P. (2011). Missing and forbidden links in mutualistic networks. *Proc. R. Soc. London B: Biol. Sci.* 278, 725–732. doi: 10.1098/rspb.2010.1371

Ollerton, J., Winfree, R., and Tarrant, S. (2011). How many flowering plants are pollinated by animals? *OIKOS* 120, 321–326. doi: 10.1111/j.1600-0706.2010.18644.x

Packer, A., and Clay, K. (2000). Soil pathogens and spatial patterns of seedling mortality in a temperate tree. *Nature* 404, 278–281. doi: 10.1038/35005072

Parihar, M., Rakshit, A., Meena, V. S., Gupta, V. K., Rana, K., Choudhary, M., et al. (2020). The potential of arbuscular mycorrhizal fungi in C cycling: a review. *Arch. Microbiol.* 202, 1581–1596. doi: 10.1007/s00203-020-01915-x

Petermann, J. S., Fergus, A. J., Turnbull, L. A., and Schmid, B. (2008). Janzen-Connell effects are widespread and strong enough to maintain diversity in grasslands. *Ecology* 89, 2399–2406. doi: 10.1890/07-2056.1

Pilosof, S., Porter, M. A., Pascual, M., and Kéfi, S. (2015). The multilayer nature of ecological networks. *arXiv preprint arXiv* 1511, 04453.

Pocock, M. J., Evans, D. M., and Memmott, J. J. S. (2012). The robustness and restoration of a network of ecological networks. *Science* 335, 973–977. doi: 10.1126/science.1214915

Polis, G. A. (1991). Complex trophic interactions in deserts: an empirical critique of food web theory. *Am. Nat.* 138, 123–155. doi: 10.1086/285208

Ponisio, L. C., Gaiarsa, M. P., and Kremen, C. (2017). Opportunistic attachment assembles plant–pollinator networks. *Ecol. Lett.* 20, 1261–1272. doi: 10.1111/ele.12821

Price, P. W. (2002). Resource-driven terrestrial interaction webs. *Ecol. Res.* 17, 241–247. doi: 10.1046/j.1440-1703.2002.00483.x

Pringle, R. M., Goheen, J. R., Palmer, T. M., Charles, G. K., DeFranco, E., Hohbein, R., et al. (2014). Low functional redundancy among mammalian browsers in regulating an encroaching shrub (Solanum campylacanthum) in African savannah. *Proc. R. Soc. London B: Biol. Sci.* 281, 20140390.

Pringle, R. M., Abraham, J. O., Anderson, T. M., Coverdale, T. C., Davies, A. B., Dutton, C. L., et al. (2023). Impacts of large herbivores on terrestrial ecosystems. *Fungal biology reviews* 21 (11), R584-R610.

Ram, H. M. (2016). Iconic flora of heritage significance in India. *Indian J. History Sci.* 51, 312–342.

Roberts, A. (1974). The stability of a feasible random ecosystem. *Nature* 251, 607–608. doi: 10.1038/251607a0

Robertson, A. W., Kelly, D., Ladley, J. J., and Sparrow, A. D. (1999). Effects of pollinator loss on endemic New Zealand mistletoes (Loranthaceae). *Conserv. Biol.* 13, 499–508. doi: 10.1046/j.1523-1739.1999.97471.x

Rodríguez-Pérez, J., Wiegand, K., and Ward, D. (2011). Interaction between ungulates and bruchid beetles and its effect on Acacia trees: modeling the costs and benefits of seed dispersal to plant demography. *Oecologia* 167, 97–105. doi: 10.1007/s00442-011-1964-6

Rooney, N., McCann, K., Gellner, G., and Moore, J. C. (2006). Structural asymmetry and the stability of diverse food webs. *Nature* 442, 265–269. doi: 10.1038/nature04887

Sauve, A. M., Fontaine, C., and Thébault, E. (2014). Structure–stability relationships in networks combining mutualistic and antagonistic interactions. *OIKOS* 123, 378–384. doi: 10.1111/j.1600-0706.2013.00743.x

Schleuning, M., Fründ, J., Schweiger, O., Welk, E., Albrecht, J., Albrecht, M., et al. (2016). Ecological networks are more sensitive to plant than to animal extinction under climate change. *Nat. Commun.* 7, 13965. doi: 10.1038/ncomms13965

Staniczenko, P. P., Kopp, J. C., and Allesina, S. (2013). The ghost of nestedness in ecological networks. *Nat. Commun.* 4, 1391. doi: 10.1038/ncomms2422

Staver, A. C., Archibald, S., and Levin, S. (2011). Tree cover in sub-Saharan Africa: rainfall and fire constrain forest and savanna as alternative stable states. *Ecology* 92, 1063–1072. doi: 10.1890/10-1684.1

Tang, S., Pawar, S., and Allesina, S. (2014). Correlation between interaction strengths drives stability in large ecological networks. *Ecol. Lett.* 17, 1094–1100. doi: 10.1111/ele.12312

Thébault, E., and Fontaine, C. (2010). Stability of ecological communities and the architecture of mutualistic and trophic networks. *Science* 329, 853–856. doi: 10.1126/science.1188321

Tilman, D. (1982). *Resource Competition and Community Structure (Monographs in Population Biology – 17)* (Princeton University Press).

Tilman, D. (1988). *Plant Strategies and the Dynamics and Structure of Plant Communities (Monographs in Population Biology-26).* (Princeton University Press).

Turner, M. G., Romme, W. H., Gardner, R. H., and Hargrove, W. W. (1997). Effects of fire size and pattern on early succession in Yellowstone National Park. *Ecol. Monogr.* 67, 411–433. doi: 10.1890/0012-9615(1997)067[0411:EOFSAP]2.0.CO;2

Turner, M. G., Romme, W. H., and Tinker, D. B. (2003). Surprises and lessons from the 1988 Yellowstone fires. *Front. In Ecol. And Environ.* 1, 351–358. doi: 10.1890/1540-9295(2003)001[0351:SALFTY]2.0.CO;2

Valdovinos, F. S. (2019). Mutualistic networks: moving closer to a predictive theory. *Ecol. Lett.* 22, 1517–1534. doi: 10.1111/ele.13279

Valdovinos, F. S., Hale, K. R., Dritz, S., Glaum, P. R., McCann, K. S., Simon, S. M., et al. (2022). A bioenergetic framework for aboveground terrestrial food webs. *Trends In Ecol. Evol.*

Valdovinos, F. S., and III, R. M. (2021). Niche theory for mutualism: A graphical approach to plant-pollinator network dynamics. *Am. Nat.* 197, 393–404. doi: 10.1086/712831

van Altena, C., Hemerik, L., and de Ruiter, P. C. (2016). Food web stability and weighted connectance: the complexity-stability debate revisited. *Theor. Ecol.* 9, 49–58. doi: 10.1007/s12080-015-0291-7

Vorholt, J. A. (2012). Microbial life in the phyllosphere. *Nature Reviews Microbiology* 10 (12), 828-840.

Wardle, D. A., Bardgett, R. D., Klironomos, J. N., Setala, H., van der Putten, W. H., and Wall, D. H. (2004). Ecological linkages between aboveground and belowground biota. *Science* 304, 1629–1633. doi: 10.1126/science.1094875

Frontiers in
Ecology and Evolution

Ecological and evolutionary research into our natural and anthropogenic world

This multidisciplinary journal covers the spectrum of ecological and evolutionary inquiry. It provides insights into our natural and anthropogenic world, and how it can best be managed.

Discover the latest Research Topics

See more →

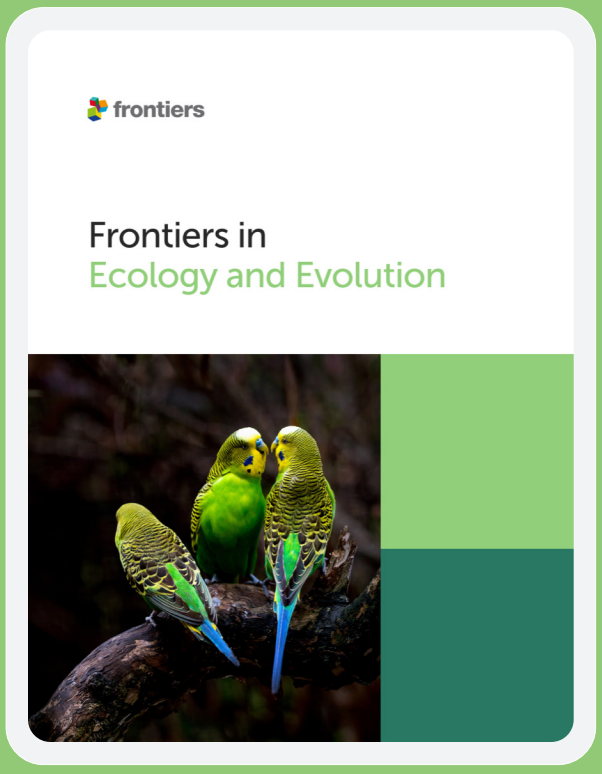

Frontiers

Avenue du Tribunal-Fédéral 34
1005 Lausanne, Switzerland
frontiersin.org

Contact us

+41 (0)21 510 17 00
frontiersin.org/about/contact